Biochemical characterisation of peroxygenase enzymes for use in the fuel industry

A thesis submitted to the University of Manchester for the degree of Doctor of Philosophy in the Faculty of Science and Engineering

2021

Alessia Andrews

Faculty of Science and Engineering

School of Natural Sciences

Table of Contents

List of tables 8

List of figures 9

Abbreviations 12

Abstract 15

Declaration 16

Copyright statement 16

Acknowledgements 17

Preface to the Journal Format Thesis 19

Author contributions 20

1 Introduction 21

1.1 Biofuels 21

1.1.1 Introduction to biofuels 21

1.1.2 Biohydrocarbons as biofuels 24

1.2 Cytochromes P450 29

1.2.1 A brief introduction 29

1.2.2 P450 reaction 30

1.2.3 General structure of cytochromes P450 32

1.2.4 Structure and spectroscopic properties of heme 35

1.2.5 Catalytic cycle 38

1.2.6 Biological diversity of redox partner systems 41

1.3 The cytochrome P450 peroxygenase family 43

1.3.1 An introduction to the peroxygenase family 43

1.3.2 Discovery of $OleT_{JE}$ and its decarboxylating abilities 44

1.3.3 $OleT_{JE}$ in biotechnology 44

1.3.4 Structure of $OleT_{JE}$ and other CYP152 enzymes 47

1.3.5 Peroxygenase catalytic cycle 51

1.4 Project aims 55
1.5 References 55
2 A unique dimeric structure of the cytochrome P450 peroxygenase from *Kocuria rhizophila* 71
2.1 Abstract 72
2.2 Introduction 72
2.3 Materials and Methods 76
2.3.1 Bioinformatics 76
2.3.2 Gene expression and general biological methods 76
2.3.2.1 P450 KR 76
2.3.2.2 Formation of the of P450 Δα35-KR deletion variant 76
2.3.2.3 TEV protease 77
2.3.2.4 Flavodoxin and flavodoxin reductase 77
2.3.3 Protein purification 78
2.3.3.1 P450 KR 78
2.3.3.2 TEV protease production 78
2.3.3.3 Production of *E. coli* flavodoxin and flavodoxin reductase 79
2.3.4 Protein quantification and determination of substrate affinity 79
2.3.5 Redox potentiometry 80
2.3.6 EPR analysis of P450 KR 81
2.3.7 *In vitro* substrate turnover of P450 KR 81
2.3.8 Nano electrospray ionisation (ESI) mass spectrometry 82
2.3.9 Analytical Ultracentrifugation (AUC) 83
2.3.10 Size Exclusion Chromatography Multi-Angle Light Scattering (SEC-MALS) 83
2.3.11 Crystallisation of KR 83
2.3.12 Data collection, structural determination and analysis 84
2.4 Results and Discussion 85

2.4.1 Expression and purification of KR 85
2.4.2 UV-visible absorption properties of P450 KR 86
2.4.3 Substrate binding studies 89
2.4.4 Heme iron redox potential of P450 KR 91
2.4.5 EPR analysis of P450 KR 95
2.4.6 Fatty acid conversion by P450 KR 96
2.4.7 Alternative oxidation methods to drive P450 KR 100
2.4.8 Structural characterisation of P450 KR 102
2.4.9 Probing the dimeric interface of P450 KR in solution 109
2.4.9.1 Size exclusion chromatography with multi-angle light scattering (SEC-MALS) 109
2.4.9.2 Analytical ultracentrifugation (AUC) 111
2.4.9.3 Nano electrospray ionisation (nano ESI) MS 113
2.5 Conclusions 116
2.6 References 118
2.7 Supplementary 127
3 Characterisation of a cytochrome P450 CYP152 peroxygenase from *Corynebacterium efficiens* 128
3.1 Abstract 129
3.2 Introduction 129
3.3 Materials and Methods 133
3.3.1 Expression of P450 CE 133
3.3.2 Mutagenesis of P450 CE 133
3.3.3 Purification of P450 CE 133
3.3.3.1 Buffer screen 133
3.3.3.2 Final Purification 134
3.3.4 UV-visible spectroscopy and protein quantification 134

3.3.5 Fatty acid binding titrations of P450 CE proteins 135
3.3.6 Fatty acid biotransformations 135
3.3.6.1 *In vitro* substrate turnover 135
3.3.6.2 Gas chromatography Mass spectrometry 136
3.3.7 Size exclusion chromatography multi-angle light scattering 136
3.3.8 Analytical Ultracentrifugation 136
3.3.9 Crystallography of P450 CE 137
3.4 Results and Discussion 137
3.4.1 Expression and purification of P450 CE 137
3.4.2 UV-visible properties of P450 CE and variants 140
3.4.3 Crystal structure of P450 CE and H186N variant 142
3.4.4 Fatty acid binding assay of P450 CE proteins 155
3.4.5 Products formed from fatty acid turnover by P450 CE and variants 159
3.4.6 Exploring the oligomeric properties of P450 CE and variants 164
3.5 Conclusions 167
3.6 References 167
3.7 Supplementary 177
4 Expression and purification of a novel CYP152 family member from *Dietzia cinnamea* 182
4.1 Abstract 183
4.2 Introduction 183
4.3 Materials and Methods 185
4.3.1 Gene identification, synthesis and cloning of P450 DC 185
4.3.2 Expression of P450 DC 186
4.3.3 Purification of P450 DC 186
4.3.4 Product analysis by GC-MS 187

4.3.5 Size Exclusion Chromatography Multi-Angle Light Scattering (SEC-MALS) 188

4.4 Results and Discussion 188

4.4.1 Expression and purification of P450 DC 188

4.4.2 Size-exclusion Size exclusion chromatography multi-angle light scattering 192

4.4.3 Spectroscopic characterisation of P450 DC 193

4.4.4 Characterisation of P450 DC reaction products 194

4.5 Conclusions 197

4.6 References 198

5 Discussion 211

5.1 Summary and conclusions 211

5.2 Future work 219

5.3 References 220

List of tables

Table 1.1 Common types of liquid fuels. 24
Table 1.2 Different reactions catalysed by cytochromes P450. 31
Table 2.1 Statistics from crystallography for the P450 KR structure. 85
Table 2.2 Determination of affinity of P450 KR against fatty acid substrates. 90
Table 2.3 Conversion of fatty acid substrates to alkene and hydroxylated products by P450 KR. 98
Table 3.1 Summary of thermo stability and aggregation of P450 CE and CYP152 members. 139
Table 3.2 Binding dissociation constants (K_d) for WT P450 CE and H186N mutant against a range of fatty acid substrates. 156
Table 3.3 Product profile and conversion of fatty acid substrates to alkene and hydroxylated products by WT P450 CE and mutant CE enzymes. 161
Table 3.4 Product profile of WT P450 CE with different concentrations of H_2O_2 and enzyme. 164
Table 5.1 Summary of products formed with CYP152 peroxygenase enzymes. 217

List of figures

Figure 1.1 Biosynthetic pathways and enzymes leading to the production of alk(a/e)nes which have been utilised in previous reports. 26
Figure 1.2 General topology of cytochromes P450. 33
Figure 1.3 Structure of the *b*-type heme. 36
Figure 1.4 General proposed catalytic cycle of cytochromes P450. 40
Figure 1.5 Three major classes of the cytochromes P450 and their redox-partner protein arrangements. 42
Figure 1.6 Structural properties of the CYP152 family. 49
Figure 1.7 Proposed cytochrome P450 catalytic cycle for peroxygenase activity and formation of terminal alkenes. 52
Figure 2.1 Proposed reaction mechanism of CYP152 peroxygenases. 75
Figure 2.2 12% SDS PAGE gel showing purity of P450 KR. 86
Figure 2.3 UV-visible spectroscopic features of P450 KR. 87
Figure 2.4 UV-vis spectrum of P450 KR with alternative tagged systems. 89
Figure 2.5 Fatty acid binding titrations with P450 KR. 91
Figure 2.6 Heme iron redox potential of substrate-free and decanoic acid-bound P450 KR. 94
Figure 2.7 EPR spectroscopic analysis of P450 KR. 96
Figure 2.8 Products of fatty acid turnover from P450 KR enzymes. 97
Figure 2.9 Oxidative decarboxylation and hydroxylation of myristic acid (C14:0) by P450 KR. 99
Figure 2.10 GC MS fragmentation of hydroxylated fatty acid products in reactions by P450 KR. 100
Figure 2.11 Products of fatty acid turnover with P450 KR enzymes using alternative routes for substrate oxidation. 102
Figure 2.12 Structure of P450 KR and superimposition with CYP152 orthologues. 103
Figure 2.13 Structural comparison of active site residues of P450 KR comparison with $OleT_{JE}$. 104
Figure 2.14 Structural comparison of heme planarity in P450 KR and P450 SPα. 105
Figure 2.15 Oligomeric structure of P450 KR. 107
Figure 2.16 Interactions stabilising the dimeric interface of P450 KR. 108

Figure 2.17 Chromatogram obtained from SEC-MALS analysis of the P450 KR protein, showing both light scattering and molar mass plots. 110
Figure 2.18 Chromatogram obtained from SEC-MALS analysis of chemically reduced P450 KR and ΔNα35-KR variant..... 111
Figure 2.19 Determination of the monomer-dimer equilibrium by sedimentation equilibrium. 112
Figure 2.20 Mass spectrometric profile of P450 KR under oxidising and reducing conditions obtained by Nano-ESI MS..... 115
Figure 2.21 Sequence alignment of Kocuria species..... 127
Figure 3.1 Proposed mechanism of CYP152 peroxygenases. 131
Figure 3.2 General reaction undertaken by CYP152 peroxygenase enzymes. 132
Figure 3.3 Final purity of P450 CE. 140
Figure 3.4 UV-visible spectroscopic features of P450 CE..... 142
Figure 3.5 Overall structure of P450 CE in complex with myristic acid. 144
Figure 3.6 Structural comparison of published CYP152 peroxygenase members. 145
Figure 3.7 hydrophobicity and charge of P450 CE surface. 146
Figure 3.8 Active site structure of P450 CE. 148
Figure 3.9 Dimeric interface of WT P450 CE. 150
Figure 3.10 Overlap of P450 CE and P450 KR. 152
Figure 3.11 Structural comparison of WT P450 CE and His186Asn variant. 153
Figure 3.12 Structure of P450 CE H186N dimeric structure. 154
Figure 3.13 Imidazole bound P450 CE His186Asn variant with phosphoglyceride. 155
Figure 3.14 UV-visible binding titrations of P450 CE. 157
Figure 3.15 UV-visible binding titrations of P450 CE H186N variant. 158
Figure 3.16 Products of fatty acid turnover from P450 CE. 162
Figure 3.17 Time dependence experiments of P450 CE with myristic acid. 163
Figure 3.18 Elution volume and molar mass determination by SEC-MALS of P450 CE and variants. 166
Figure 3.19 UV-visible absorbance of P450 CE from expression trails in E. coli cells. 177
Figure 3.20 Trace of P450 CE obtained from gel filtration step. 178
Figure 3.21 PISA interface of WT P450 CE. 181
Figure 3.22 Sequence alignment of P450 KR and P450 CE by EMBOSS Needle. 181

Figure 4.1 UV-Visible spectra of P450 DC samples obtained from different expression conditions. 188
Figure 4.2 UV-visible traces obtained from the purification of P450 DC obtained from different buffering systems. 191
Figure 4.3 Chromatogram obtained from SEC-MALS analysis of P450 DC. 192
Figure 4.4 UV-visible spectroscopic features of P450 DC. 194
Figure 4.5 Percentage conversion of fatty acids by P450 DC. 195
Figure 4.6 Time dependent conversion of myristic acid by P450 DC. 197

Abbreviations

Abs – Absorbance

Å – Ångstrom

ADO – Aldehyde deformylating oxygenase

AldO – Alditol Oxidase from Streptomyces coelicor

AUC – Analytical ultracentrifugation

BSTFA – N,O-bis(trimethylsilyl)trifluoroacetamide containing 1% trimethylchlorosilane

CO – carbon monoxide

CO_2 – carbon dioxide

CH_4 – methane

Cpd 0 – Compound 0

Cpd I – Compound I

Cpd II – Compound II

CPR – Cytochrome P450 Reductase

ΔALA – δ-aminolevulinic acid

DCM – Dicholormethane

DNAse – Deoxyribonuclease

DT – Dithionite

DTT – Dithiothreitol

EDTA – Ethylenediamineetetraacetate

E. coli – *Escherichia coli*

EPR – Electron Paramagnetic Resonance

ER – Endoplasmic Reticulum

ESI – Electrospray inionisation

FAD - Flavin Adenine Dinucleotide

FAP – fatty acid photodecarboxylase

FAME – fatty acid methyl esters

FDH – Formate Dehydrogenase

Fld – Flavodoxin

FldR – Flavodoxin reductase

FdR – Ferredoxin Reductase

FdX – Ferredoxin

FMN – Flavin Mononucleotide

FTIR – Fourier Transform Infrared Spectroscopy

GC-MS – Gas Chromotography Mass Spectrometry

GDH – Glucose Dehydrogenase

GHG – Green house gases

HS – High Spin (S = 5/2)

Int2 – Second Intermediate

IPTG – Isopropyl 1-thio-b-D-galactopyranoside

K_d – Dissociation Constant

KIE – Kinetic Isotope Effect

LS – Low Spin (S = 1/2)

µM – Micromolar

mM – Millimolar

M – Molar

mV – Millivolt

$MgCl_2$ – Magnesium chloride

MWCO – Molecular Weight Cutoff

CH_4 – Methane

NAD(P)H – Nicotinamide Adenine Dinucleotide (phosphate)

NHE – Normal Hydrogen Electrode

Ni-NTA – Nickel Nitrilotriacetic Acid

nM – Nanomolar

Ole-I – $OleT_{JE}$ Compound I

$OleT_{JE}$ – Cytochrome P450 $OleT_{JE}$ (CYP152L1) from *Jeogalicoccus* sp. 8456

P450 BM3 – Cytochrome P450 BM3 (CYP102A1) from *Bacillus megaterium*

P450 BSβ - P450 BSβ (CYP152A1) from *Bacillus subtilis*

P450 CE – P450 CE (CYP152T7) from *Corynebacterium efficiens*

P450 cam – Cytochrome P450 cam (CYP101A1) from *Pseudomonas putida*

P450 DC – P450 DC (CYP152T8) from *Dietzia cinnamea*

P450 KR – Cytochrome P450 from *Kocuria rhizophila*

P450 SPα - P450 SPα (CYP152B1) from Sphingomonas paucimobilis

PAH – polycyclic hydrocarbons

PDA – Photon Diode Array

PDH – Phosphite Dehydrogenase

PDOR – Phthalate Dioxygenase Reductase

PdR – Putidaredoxin reductase

PdX – Putidaredoxin

pKa – Isoelectric Point

PMT – Photon Multiplier Tube

ROS – Reactive Oxygen Species

TAG – Triacylglycerol

V – Volt

Abstract

The bacterial CYP152 peroxygenases are a subset of the cytochrome P450 family that have evolved to efficiently harness hydrogen peroxide as the sole oxygen and hydrogen donor during catalysis, bypassing the use of redox-partner proteins. Disocovery of P450 $OleT_{JE}$ (CYP152L1) isolated from *Jeotgalicoccus* sp. 8456 was shown to primarily functions as a fatty acid decarboxylase (C20:0 – C12:0), producing terminal alkenes. These alkenes are well suited to be implemented into the existing fuel infrastructure and provide an ideal alternative to transportation fuels, due to their 'drop in' compatibility.

This thesis describes biochemical and structural characterisation of three novel members of the CYP152 family from *Kocuria rhizophila* (P450 KR, CYP152T1), *Corynebacterium efficiens* (P450 CE, CYP152T7) and *Dietzia cinnamea* (P450 DC, CYP152T8). All three orthologues described are capable of decarboxylating and/or hydroxylating saturated fatty acids (C10:0 – C18:0), with overlapping substrate specificity towards myristic acid (C14:0). While P450 KR functions primarily as a fatty acid hydroxylase, P450 CE and DC preferentially act as fatty acid decarboxylases.

In contrast to the monomeric form of $OleT_{JE,}$ both P450 KR and P450 CE function as dimers, revealing novel dimeric interfaces in their respective crystal structures. P450 KR was crystallised and structure determined to 3.0 Å, revealing an extended N-terminal helix that protrudes from the core of the protein, and forms a "zipper-like" interaction with the adjacent monomer. These interactions appear stabilised by a disulphide linkage that contributes to protein stability. A surface disulphide linkage is also present in P450 CE in a similar position to P450 KR. However, the P450 CE structure (determined to 2.05 Å) revealed a distinct dimer interface, an additional heme molecule coordinated between two histidine residues (His186) of each monomer as seen in and stabilised by multiple hydrophobic interactions. The structure of P450 CE H186N variant (determined to 2.06 Å) lacked the extra heme group, but retained the dimer interface through the extensive hydrophobic interactions.

These data provide functional and structural insights into oligomerisation, substrate-binding and product diversity of the CYP152 family.

Declaration

No portion of the work referred to in this thesis has been submitted in support of an application for another degree or qualification of this or any other institute of learning.

Copyright statement

Acknowledgements

First of all I would like to thank my Supervisors Andy Munro and David Leys for the opportunity to do this PhD and being so supportive. A massive thank you to Kirsty, Hazel, Sarah, Harsh and Richard for always being there to answer questions, guiding me through the PhD and having a laugh or two… just generally being fab people! Also thank you to Marina and Michi for answering my 10000000 questions daily… I ask a lot of questions! Massive thanks to Derren for being a top babe, great person to cry to and proof reading my thesis!

I really couldn't have done it without the support and friendship of the MUNLOP group, past and present! The OGs, Mark (would write something nice about you but you didn't write me in to your acknowledgements <3), Charlie, Sarah and Dom… thanks for inviting me to secret steak club as a first year #foreverblessed! Thank you for introducing me to "english tapas" You guys inspired me to do a PhD in the first place. The current MUNLOPs; Irwin, James, Matt, Sian, and Sahara - you've filled the years with genuine laughs and great advice. James you have been my favourite leg rest and always there if I had a stressy wobble! Sahara, thank you for introducing me to hot pot haha… you have been a lil buddle of joy from the beginning and so glad I got have to have your lil supportive face in my final year!

One of the most amazing and memorable things that has come out of the PhD is the amazing friends I have met along the way …oh AND TRAVELLING TO AUSTRALIA! Sian you have been the most incredible travelling and eating buddy a girl could ask for! I don't think I could have surived the lab or this PhD without you <3 Thanks for doing EVERYTHING with me, genuinely think we are tweedle dum and tweedle dee running around the lab haha! Dundee to the Great Barrier Reef (sorry have i told you we've been to Australia??). You have really been a dream to work and play with. My caffeine crew (past and present), those little… well sometimes hours breaks were the best part of my day! Thank you Alec for always being avalibale for coffee (no matter what time)! Little shout out to Aoife and Emilie thankyou for always being there to cry, laugh and have treat day with! You have made the third floor even more enjoyable and definitely wouldn't have made it through without your love and support! Wish I had more space to write paragraphs about everyone… BIG shout out to (the now) Kayak Society… I couldn't have asked for more supportive, lovely and all around fabulous friends <3

I wouldn't have been able to complete this PhD without my advent way heroes. Thank you for being my surrogate family in Manchester, cooking and taking care of me. You guys showed me how great alcohol/cocktails and craft beer is, thanks to you guys I am even poorer. Beth, can't believe we spent nearly every day together and still had so much to talk about, thanks you for taking me in when I was a mere Master student and showing me your CV! Jabonbon what can I say, two peas in a pod, thanks for wearing yellow that day so we can forever be THIRD OF A BRAIN! Lucy my partner in absolute weirdness…thanks for making me look super cool… joking I am a dweeb too! Thanks for

singing Hamilton with me any time and giving the best hugs. And Ross! My other gym buddy but also my eating buddy….Big cook little cook! My wonderful housemate of a million years B! We made it through university, pandemic and now a PhD together…and still amazing!!! Thanks for dealing with my tears and screams… and cleaning up after me as I cook! You really have been a star <3

Just all in all 4.5 amazing years of loads of sweat (that's one is for you James), laughs and tears with the most incredible people by my side. Do-able but soul destroying (Andrews., 2021) xx

Preface to the Journal Format Thesis

This thesis in presented in the University of Manchester journal style of PhD thesis. This allows the incorporation of data already published and/or sections that are in a format suitable for submission for publication in a peer-reviewed journal. The structure of each chapter follows that of the journal in which it is prepared for publications, meaning a separate methods chapter is not included as they are in the individual results chapters, and heading labels for each chapter may differ. The layout of the journal format thesis is as follows; an abstract, introduction, three results chapters (papers), and a summary, conclusions and future work chapter. Each chapter contains self-contained references. The general formatting of these papers has been kept consistent throughout this thesis, along with the page numbering. The journal format thesis was introduced in the University of Manchester to help students develop their skills in writing papers for peer-reviewed submission and to be overall more relevant to scientific research. Successful scientific publications are often collaborative and therefore as part of the journal format the contributions of each co-author are stated below.

Papers included as results chapter:

Chapter 2: Andrews, C. A., Tee, K. L., Matthews, S., Pacholarz, K., Jowitt, T., Poddar, H., McLean, K. J., Girvan, H., Levy, C., Leys, D.,Munro, A.W. (2021) A unique dimeric structure of the cytochrome P450 peroxygenase from *Kocuria rhizophila. Manuscript in preparation for submission (JBC).*

Chapter 3: Andrews, C. A., Tunnicliffe, B. R., Poddar, H., Jowitt, T., McLean, K. J., Girvan, H., Levy, C., Leys, D.,Munro, A.W. (2021) Characterisation of a cytochrome P450 CYP152 peroxygenase from *Corynebacterium efficiens. Manuscript in preparation for submission (JBC).*

Chapter 4: Andrews, C. A., Tunnicliffe, B. F., Poddar, H., McLean, K. J., Girvan, H., Leys, D.,Munro, A.W. (2021). Expression and purification of a novel CYP152 family member from *Dietzia cinnamea. Awaiting further data before publishing.*

Author contributions

As PhD supervisors, Professor Andrew Munro and Professor David Leys contributed to the manuscript preparations for all papers

Chapter 2

Tee, K.L. performed redox potentiometry; prepared samples for EPR; preparation of protein from crystallography

H., Levy, C., Leys collected X-ray diffraction data at Diamond Synchotron

McLean, K.J., Girvan, H. M., performed EPR experiments and analysis

Poddar, H., assisted with refinement of the crystal structures.

Jowitt, T., assisted with AUC experiments and data processing

Pacholarz, K., assisted in nano-ESI experiments and data processing

Chapter 3

H., Levy, C., Leys collected X-ray diffraction data at Diamond Synchotron

Jowitt, T., assisted with AUC experiments and data processing

Poddar, H., assisted with bio-informatics and general work

Tunnicliffe, B. R., Poddar, H., assisted with refinement of crystal structures and preparation of figures

Chapter 4

Poddar, H., assisted with bio-informatics and general work

1 Introduction

1.1 Biofuels

1.1.1 Introduction to biofuels

Today's global demand for energy along with concerns of dwindling fossil resources and climate change, have spurred research into the development of alternatives to fossil fuels (Himmel *et al.*, 2007). Currently, fossil fuels such as petroleum, natural gas and coal are the primary energy source, accounting for 84 % of the world's consumption (British Petroleum (BP), 2018). They also play a major role in the world's energy "money" market, with an estimated 1.5 trillion dollars spent on primary energy every year (Goldemberg, 2006). Undoubtedly, we rely heavily on these fuels, which have allowed society to reach unprecedented levels of development over the past century. However, the continued heavy reliance and increasing consumption of these fuels means oil deposits can be used up by 2052, gas by 2060, and coal by 2090 (British Petroleum (BP), 2018).

It is not only the finite source that should have us looking for alternatives, but the detrimental effects that extracting, producing and burning fossil fuels have on the environment and climate change. Carbon dioxide (CO_2) is the principal product of the combustion of coal (39%), oil (31%) and natural gas (18%) and is considered to be one of the major greenhouse gases (GHGs) (Olivier and Peters, 2020). One of the major drivers of climate change is increasing GHG and CO_2 emissions from combustion of fossil fuels, which remains trapped in the earth's atmosphere for thousands of years (Alam and Tanveer, 2020). Other pollutants and GHG associated with energy related fossil fuel combustion include methane (CH_4), almost all sulphur dioxide and nitrous oxides (NxO). Also emitted are polycyclic hydrocarbons (PAH) and volatile chemicals that can form ground level ozone (IEA (2016), Energy and Air Pollution, IEA, Paris https://www.iea.org/reports/energy-and-air-pollution). All are associated with multiple adverse health effects. Another issue that arises is the uneven geographical distribution of fossil fuel reserves which, in some cases, are located in socio-politically unstable regions and are the origin of multiple political and economic issues worldwide (O'Sullivan and Sandalow, 2017).

Although fossil fuels still dominate the market, other renewables have been developed and are currently in use. These include solar (electricity), wind (electricity), geothermal

(heating and electricity), hydropower (electricity), and biomass (heating, electricity and transportation) (*Total Energy - U.S. Energy Information Administration (EIA)*). During the last decade there has been an enormous interest in the commercial production and usage of liquid biofuels as promising substitutes for fossil fuels. Bioethanol and biodiesel are currently the most commercially used biofuels on the market. They have been introduced on a large scale in several countries (for example Brazil, USA and some EU countries). Bioethanol and biodiesel are projected to be one of the dominating renewable biofuels in the transportation sector in the next 20 years (Galbe, Wallberg and Zacchi, 2019). At present, bioethanol is derived from fermentation of crop-based biomass, such as corn starch, sugar cane, wheat and lignocellulose using *Saccharomyces cerevisiae*, and is often classed as first-generation bioethanol (Lee and Lavoie, 2013). Bioethanol is a highly oxygenated fuel, which exhibits clean burning characteristics, such as reduction in GHG emission, particulate matter and low vapour pressure (Nanda *et al.*, 2018).

Biodiesel is the second most abundant renewable fuel made on an industrial scale and can be produced from animal fats as well as vegetable and plant oils (especially rapeseed oil and soybean oil) (Alam and Tanveer, 2020). Biodiesel is formed from the transesterification of triglycerides with short chain alcohols to produce fatty acid methyl esters (FAMES) and glycerol, which must be removed through high-cost purification steps (Chongkhong *et al.*, 2007; Naik *et al.*, 2010). Biodiesel is non-toxic and reduces some of the pollutants that are produced from burning of diesel, although the production of NO_x increases (Hoekman and Robbins, 2012).

Second- and third-generation biofuels are not yet used for production on an industrial scale and are still considered to be in the early stages of research. Second generation biofuels can be derived from feedstocks not limited by non-edible lignocellulosic biomass, such as wood chip, agricultural residues and municipal solid waste. The prices of these sources are significantly cheaper than oils, corn and sugar cane. However, the production of these fuels is not yet cost effective and generally more complex to convert (Lee and Lavoie, 2013). Third generation biofuels are derived from algae biomass and are considered viable alternative energy resources that are devoid of the major drawbacks of first- and second-generation biofuels (Chowdhury and Loganathan, 2019). Microalgae, which can grow rapidly and convert solar energy to chemical energy

via CO_2 fixation, are now considered a promising oil source for making biodiesel (Chen *et al.*, 2011). A major benefit is the oil production capacity produce 58,700 L per hectare, which is one to two orders of magnitude higher than other energy crops (Chisti, 2007). Depending on the species, microalgae produce several different kinds of lipids, hydrocarbons and other complex oils (Banerjee *et al.*, 2002; Metzger and Largeau, 2005). To compete economically with fossil and first-generation fuels, production costs of microalgae biodiesel needs to be decreased with requirements of subsidies and market interventions.

As it stands, first generation bioethanol and biodiesel can provide some energy security, although, biomass cannot realistically sustain future energy demands and are far from the ideal alternative fuel candidates. The hygroscopic and corrosive properties of ethanol limit its incorporation into the existing fuel, storage, transportation and engine infrastructure (Peralta-Yahya and Keasling, 2010). The corrosive nature of ethanol limits its ability to be blended in high concentrations with the current spark ignition engines (Atsumi and Liao, 2008), which can only tolerate low concentration blends (between 5-15%) with conventional petrol (E5-E15) (Serrano-Ruiz, Ramos-Fernández and Sepúlveda-Escribano, 2012). Furthermore, despite its high-octane number (in comparison to petrol), ethanol contains ~30 % less energy per volume than petrol, and thus can reduce fuel economy and use within vehicles. Ethanol-petrol blends are prone to suffering from water contamination, and when saturation levels for this specific blend are reached, phase-separation between the water, ethanol and petrol occurs, causing damage to the engine (French and Malone, 2005). Biodiesel has similar storage, transportation and energy-density drawbacks to bioethanol (Lee *et al.*, 2008). Although biodiesel has similar physicochemical properties to that of diesel produced from crude oil, direct use of vegetable oils in compression ignition engines is problematic due to their high viscosity and low volatility and this can leave carbon deposits in the fuel injectors (Atadashi, Aroua and Aziz, 2011).

Production of first generation biofuels have been met with some scepticism. There are concerns about surrounding large-scale production and the impact on global food supply, as production of these biofuels requires a vast amount of farmland and agricultural resources, with competition of crops between food and fuel production (Lee *et al.*, 2008; Zhang, Rodriguez and Keasling, 2011). The challenge is to make a next-

generation biofuel with similar energy and combustion properties as existing fossil-based fuels on the market, to allow for minimal changes in the existing fuel infrastructure and allow compatibility with existing engine systems (Zhang, Rodriguez and Keasling, 2011). The ideal outcome would be a fuel so similar that it is able to be mixed with existing fuels, with 'drop in' compatibility for spark or compression ignition engines (Yan *et al.*, 2015). Several factors to consider when designing and producing a biofuel include; energy content, combustion quality (octane and cetane number), volatility, freezing point, odour, and toxicity (Lee *et al.*, 2008). An ideal biofuel would have similar properties to gasoline, diesel and jet fuel (properties are reviewed in **table 1.1**) (Lee *et al.*, 2008).

Table 1.1 Common types of liquid fuels.

Common types of liquid fuels			
Fuel type	**Components**	**Important properties**	**Biosynthetic alternatives**
Petrol	• C4-C12 hydrocarbons • Linear, branched, cyclic, aromatic. • Anti-knock additives	• Octane number • Energy content • Transportability	• Ethanol • *N-/iso*-butanol • Short-chain alcohols • Short-chain alkene
Diesel	• C9-C23 (typically C16) • Linear, branched, cyclic, aromatic. • Anti-freeze additives	• Cetane number • Low freezing temperature • Low vapour pressure	• Biodiesel • Fatty alcohols • Alk(a/e)nes • Linear or cyclic isoprenoids
Jet Fuel	• C8-C16 hydrocarbons • Linear, branched, cyclic, aromatic. • Anti-freeze additives	• Very-low freezing temperature • Net heat of combustion • Density	• Alk(a/e)nes • Biodiesel • Linear or cyclic isoprenoids

1.1.2 Biohydrocarbons as biofuels

Biohydrocarbons, such as fatty acids, alkenes and alkanes, are ideal alternatives to current transportation fuels. These short-, medium- or long-chained alk(a/e)ne(s) have similar chemical composition (low hygroscopicity) and physical characteristics to fossil fuels (Lee *et al.*, 2008). Hydrocarbons are intrinsically hydrophobic, overcoming the natural drawbacks of the high miscibility of ethanol in water. These hydrocarbons, such as alk(a/e)ne(s), have many advantages over petroleum because they do not contain any sulphur, sulphates and PAHs, demonstrating clean burning and therefore no SO_2 and CO emissions (Fu *et al.*, 2015). Biohydrocarbons could be integrated into the existing fuel infrastructure (storage/transportation) with no significant modifications. Unlike biodiesel and bioethanol, biohydrocarbons provide an equivalent energy-density,

with no effect on petrol mileage or engine performance (Serrano-Ruiz, Ramos-Fernández and Sepúlveda-Escribano, 2012; Yan *et al.*, 2015).

Currently there are two major strategies for production of biohydrocarbons. The first is the chemical hydrotreatment of acylglycerides, fatty acids and fatty acyl esters from vegetable oils and related feedstock to produce liquid alkanes. However, this method requires the use of an expensive metal catalyst (Pt, Pd and Ni), high temperatures and pressures. Thus, this method is highly energy intensive and not a suitable method for producing a long-term fossil fuel replacement (Serrano-Ruiz, Ramos-Fernández and Sepúlveda-Escribano, 2012; Yan *et al.*, 2015). The second method includes the *de novo* synthesis of hydrocarbons by microorganisms (Peralta-Yahya and Keasling, 2010). Advances in microbial engineering offer a huge possibility to convert renewable sources to biofuels. Some microorganisms can produce certain biofuels naturally, although most native microorganisms often suffer from low growth rates, intolerance of toxic biofuel products and incomplete carbon source usage (Zhang, Rodriguez and Keasling, 2011). In recent years it has been found that many marine cyanobacteria, eubacteria, engineered *E. coli*, endophytic fungi, engineered yeast, marine yeast, plants and insects can synthesise intracellular and extracellular hydrocarbons with different chain lengths (Fu *et al.*, 2015).

Alk(a/e)nes are an important class of hydrocarbons, used as liquid transportation fuels and as plastics. There are many reports of organisms that synthesise alkenes and alkanes naturally for protection against environmental threats, but the production levels are not ideal for direction utilisation as drop-in biofuels. The expression of some of the enzymes and pathways involved in natural production of alk(a/e)nes into heterologous microbial hosts has allowed for the production of various alk(a/e)nes (Kang and Nielsen, 2017). Thus, these alk(a/e)ne producing microorganisms have received great attention in recent years, as they offer promise as scalable and cost effective production of biofuels (see **figure 1.1**) (Zhang, Rodriguez and Keasling, 2011). Aldehyde decarbonylases (ADs) have been discovered in various organisms, including plants, insects and cyanobacteria, and can convert fatty aldehydes to the corresponding C_{n-1} alkanes with co-current production of CO_2, CO, or formate, respectively (Marsh and Waugh, 2013). There are several mechanistically distinct classes of decarbonylase. In insects, the *Drosophila* AD enzyme responsible is a cytochrome P450 (CYP4G1) and a

cytochrome P450 reductase (CPR). Expression in *Saccharomyces cerevisiae* produced long chain alkanes (C23, C25, and C27) (Qiu *et al.*, 2012). The plant decarbonylases remain the least understood class, in part because they are integral membrane proteins which are difficult to over-express. In *Arabidopsis*, the *Cer1* and *Cer3* genes encode a membrane-bound complex of the AD and acyl-CoA reductase, respectively. These expressed in yeast along with endoplasmic reticulum-localised cytochrome b_5 isoforms (CYTB5s) and long-chain acyl-CoA synthetase 1 (LACS1) saw the production of exceptionally long chain alkanes (C28, C29, and C30) with production of nonacosane C29 at 89 ng per mg of dry weight (Aarts *et al.*, 1995; Bernard *et al.*, 2012).

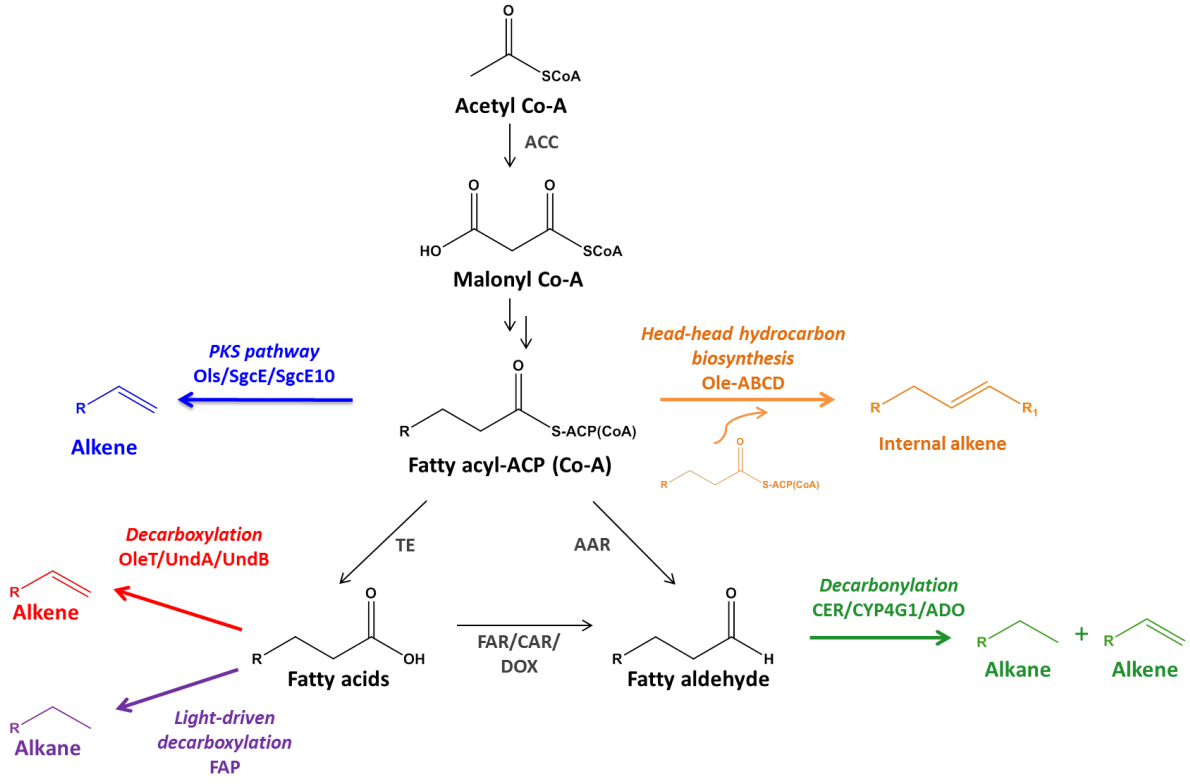

Figure 1.1 Biosynthetic pathways and enzymes leading to the production of alk(a/e)nes which have been utilised in previous reports. These include (blue) conversion of alkenes by the PKS pathway by Ols and SgcE-SgcE10; (orange) internal alkene formation by a head-to-head condensation reaction; (green) the decarbonylation by plants (CER), insects (CYP4G1) and ADO (cyanobacteria); Decarboxylation undertake by (red) OleT, UndA and UndB to produce terminal alkenes and (purple) light activated decarboxylation by FAP. Figure adapted from (Kang and Nielsen, 2017).

Many cyanobacterial strains have been identified that produce alk(a/e)nes. Due to the production of formate during the reaction, the enzyme has been renamed to aldehyde deformylating oxygenase (ADO) (Li *et al.*, 2012). The pathway utilises free fatty acids by the action of acyl-acyl carrier proteins (acyl-ACP) reductase (AAR) or by fatty acid reductase (FAR) with ADO (Schirmer *et al.*, 2010). AAR catalyses the first step of this

pathway, reducing the substrate fatty acyl-ACP/fatty acyl-coenzyme A (acyl-CoA) into the corresponding aldehyde in a NADPH-dependent manner. ADO catalyses the conversion of fatty aldehydes to C_{n-1} terminal alkanes and formate (Schirmer *et al.*, 2010; Gao *et al.*, 2020). Studies demonstrated that dioxygen is required for activity, with O_2 being incorporated into formate (Li *et al.*, 2011). One of the first engineered pathways for alkane biosynthesis consisted of an acyl-ACP reductase ORF159 from *Synechococcus elongatus* and an aldehyde decarbonylase from *Nostac punctiforme* PCC73102 constructed in *E. coli* cells. This system produced a total of 300 mg/L of alkanes and 100 mg L^{-1} of long chained alcohols (Schirmer *et al.*, 2010; Liu *et al.*, 2014; Yan *et al.*, 2015). Some variant forms of ADO, from *Prochlorococcus marinus* MIT9313, have been employed as the terminal decarbonylases to produce short chain aldehydes that are usually not encountered by the native cyanobacteria. Assembly of ADO with alternative pathways that are not dependent on the fatty acid biosynthetic pathway could produce 220 ± 3 μg L^{-1} of propane through the *atoB-TPC7-ADO* route (Menon *et al.*, 2015).

A recently discovered light-activated enzyme, fatty acid photodecarboxylase (FAP), provides a highly attractive route in the production of alkanes. FAP is found in unicellular photosynthetic green microalgae and catalyses the blue light driven decarboxylation of fatty acid substrates to generate n-alk(a/e)nes. FAP contains a flavin adenine dinucleotide (FAD) cofactor, showing preference towards long chain fatty acid substrates (C16:0 – C17:0) (Sorigué *et al.*, 2017). Expression of the microalgae *Chlorella variabilis* NC64A in *E. coli* produced C13:0 to C17:0 alk(a/e)nes. However, the purified enzyme was shown to convert saturated fatty acids to alkanes. The FAD cofactor in FAP is photo-excited, with decarboxylation initiated through electron abstraction from the fatty acid (Heyes *et al.*, 2020).

Studies of long-chain alkene biosynthesis of *Micrococcus luteus* resulted in identification of a three gene cluster (Mlut_1320_13250) encoding Ole-ABCD (*OleA, OleBC and OleD*). Heterologous expression of the three gene cluster in fatty acid-overexpressing *E. coli* was shown to produce medium chain alkenes as dominant products, predominantly 27:3 and 29:3 (no. carbon atoms: no. C=C bonds) (Beller, Goh and Keasling, 2010). The first step of the reaction is initiated by OleA. Two activated fatty acids undergo a non-decarboxylative head-to-head Claisen condensation reaction to generate a β-keto acid

(Frias *et al.*, 2011). The intermediate acid is then transferred to the OleBCD complex, where it is reduced to a β-hydroxy acid by the NADH-dependent dehydrogenase OleD (Sukovich *et al.*, 2010). The lactone synthase OleC forms a heat labile internal ester between the β-hydroxy and carboxyl group, with a water molecule released. Finally, the lactone decarboxylase OleB liberates one molecule of CO_2 and converts the internal lactone to an alkene with a *cis*-configured internal double bond produced from head-to-head connection of the two original fatty acid precursors (Beller, Goh and Keasling, 2010; Christenson *et al.*, 2017).

A gene encoding an alkene-producing multi-domain protein was identified in the cyanobacterium *Synechococcus* sp. PC7002, that synthesizes C19 alkenes (1,14-nonadecadiene and 1-nonadecene) with terminal double bonds. Overexpression of the Ols enzyme increased alkene biosynthesis by 4.2 μg/mL/OD_{730}. The *Ols* protein (olefin synthase) is homologous to type I polyketide synthases (PKS), which usually consist of 3-β-keto-acyl synthases (KS), acyltransferases (AT), acyl carrier proteins (ACP), β-keto reductases (KR), dehydratases (DH), enoyl reductases (ER), and finally a thioesterase (TE). The pathway uses an elongation-decarboxylation mechanism, with elongation of a β-keto group and reduction to a β-hydroxyl group, and then finally decarboxylation and dehydration to produce alkenes (Mendez-Perez, Begemann and Pfleger, 2011; Kang and Nielsen, 2017). Another study showed an engineered pathway of an iterative type I polyketide synthase SgcE with its cognate thioesterase (TE) SgcE10 in *E. coli,* showing overproduction of pentadecahept(a/e)ne (PDH) followed by hydrogenation to generate pentadecane. A fusion construct of SgcE-SgcE10 with fed-batch fermentation and chemical hydrogenation produced ~140 mg L^{-1} in a single alkane form (Liu *et al.*, 2015).

There are three different types of enzymes that are involved in the direct enzymatic conversion of fatty acids to terminal alkenes, $OleT_{JE}$, UndA, and UndB. UndA and UndB have been detected in members of the *Pseudomonas* genus that decarboxylate fatty acids to give terminal alkenes, similar to the activity of the $OleT_{JE}$ enzyme (Rui *et al.*, 2014). UndA is a non-heme iron oxidase that can convert medium chain fatty acids (C10:0 – C14:0) into their corresponding terminal alkenes using an oxygen-activating, non-heme iron dependent mechanism (Rui *et al.*, 2014). UndB is a membrane-bound desaturase-like enzyme that converts C10:0 – C16:0 fatty acids to their corresponding *n*-1 terminal alkenes. Although it is membrane bound, which makes it difficult to study *in*

vitro, it can be efficiently developed for whole cell transformations (Rui *et al.*, 2015). The decarboxylation pathway is exemplified by the cytochrome P450 peroxygenase $OleT_{JE}$ from *Jeotgalicoccus* sp. 8456, which decarboxylates long-chain fatty acids to produce terminal alkenes, rather than their insect CYP4G decarbonylating route (Rude *et al.*, 2011; Liu *et al.*, 2014). These peroxygenases are discussed in detail below.

1.2 Cytochromes P450

1.2.1 A brief introduction

Cytochromes P450 are a superfamily of heme-*b*-containing monooxygenases that are ubiquitously distributed throughout life (Munro, Girvan and McLean, 2007). They catalyse the scission of molecular oxygen and the subsequent insertion of one oxygen atom into the bound substrate, whilst simultaneously using the oxygen molecule for production of water. They can perform a diverse range of oxidative reactions on highly diverse substrates (Cook *et al.*, 2016). Cytochromes P450 were first noted experimentally as early as the 1950s, where preparations of mammalian liver microsomes were found to oxidise xenobiotic compounds. However, the enzyme responsible was unknown (Brodie *et al.*, 1955). It was not until 1958 that Klingenberg formally identified and named the cytochromes P450 superfamily, through studies of dithionite-reduced rat microsomes which displayed an intense absorption band at 450 nm when bubbling carbon monoxide (CO) into the P450 enzyme (Klingenberg, 1958). Following on from these studies, Omura and Sato deduced that the "carbon-monoxide binding pigment" was a heme *b*-containing P450 protein. Thus, this group of enzymes receive their name not based on their function, but instead form their unique spectral features upon binding carbon monoxide to the reduced, ferrous state of the P450 enzyme. This unique spectral feature is induced by a cysteine thiolate group forming a fifth (proximal) ligand to the heme iron, and with the distal ligand typically bound to a water ligand. The displacement of the water ligand enables the binding of the relevant substrate and a series of subsequent reactions that transform the substrate to a novel product (Omura and Sato, 1962, 1964).

In the years following their discovery, the importance and widespread nature of the reactions catalysed by cytochromes P450 became evident. One of the main functions of human P450s is the primary metabolism of drugs, steroids and xenobiotic compounds (through hydroxylation) (Estabrook, Cooper and Rosenthal, 1963; Guengerich, 2006). It

is now known that 75% of drug metabolism is mediated by P450 enzymes – with 90% of these reactions accounted for by just 5 human P450s (Guengerich, 2006).

Since confirmation of cytochrome P450 oxygenase activity, a rapid expansion of the field occurred. Through advances made in genome sequencing, many sequences have been identified throughout all five kingdoms, including eukaryotes, prokaryotes and hyperthermophilic bacteria (with the exception of *E. coli* and *Salmonella typhimurium,* which are devoid of P450 genes). The P450 superfamily is thought to be ancient, with the ancestral gene having existed more than 3.5 billion years ago (Nelson *et al.*, 1993). The genes that encode cytochromes P450 are denoted as CYPs and the P450 superfamily genes can be divided into families, and classified on their amino acid sequence, phylogenetic criteria and gene organisation (Peterson and Graham, 1998). To be considered members of the same family, P450s must have an amino acid sequence greater than 40%, while members of the same subfamily have amino acid sequence homologies greater than 55% (Nelson *et al.*, 1993; Cook *et al.*, 2016). The nomenclature system for cytochrome P450 enzymes was first proposed in 1987 and relies on the evolutionary relationships depicted in phylogenetic trees. The decision to include sequences in a tree depends largely on how it clusters on a tree, and not so much on the absolute percentage of identity. Names of new P450 genes are submitted to the committee on standardised cytochrome P450 nomenclature for naming (Nelson, 2006).

1.2.2 P450 reaction

Cytochromes P450 bind, reductively activate and catalyse the scission of molecular dioxygen that binds to the heme iron. This leads to insertion of an atom of oxygen into a substrate (frequently involving hydroxylation), whilst the other oxygen is reduced to water. The typical reaction requires the timed delivery of two electrons and two protons to the P450 heme iron (see **equation 1**) (Munro, Girvan and McLean, 2007).

$RH + O_2 + 2e^- + 2H^+ \rightarrow ROH + H_2O$ (Equation 1)

However, cytochromes P450 are not just determined by one reaction or outcome. The P450s can catalyse a diverse range of over 20 different types of reactions (see Summary **table 1.2**), ensuring they are one of nature's most versatile catalysts (Sono *et al.*, 1996). Some of the basic reactions include hydroxylation, such as N-/S-/and O-dealkylation, epoxidation and oxidative dehalogenation – to name just a few. These reactions are

usually catalysed by the highly reactive compound I, with hydrogen abstraction and oxygen rebound (discussed further in section **1.2.4**). Cytochromes P450 can undertake some more unusual reactions, for example the nitration of tryptophan in the synthesis of thaxtomin in *Streptomyces turgidiscabies*. The proposed reaction of this enzyme involves nitric oxide (NO) with a ferric-superoxide complex to form an iron peroxynitrite-like species that is capable of nitrating tryptophan (Barry *et al.*, 2012).

Table 1.2 Different reactions catalysed by cytochromes P450.

Common cytochrome P450-catalysed reactions
Hydroxylation
Alkene epoxidation/alkyne oxygenations
N-, S- and O-dealkylation
Arene epoxidation
Aromatic hydroxylation
N-hydroxylation
N-, and S-oxidations
Oxidative deamination
Oxidative dehalogenation
Dehydrogenation
Dehydration
Reductive dehalogenation
N-oxide reduction
Epoxide reduction
Reductive beta-scission of alkyl peroxides
NO reduction
Alcohol and aldehyde oxidations
Isomerization
Oxidative C-C bond cleavage

P450s catalyse the transformation of a broad range of endogenous and exogenous substrates. They contribute to the biotransformation of drugs, degradation of xenobiotics, bioactivation of carcinogens, and biosynthesis of physiologically important compounds such as steroids, fatty acids, eicosanoids, fat-soluble vitamins and bile acids. In addition, they also participate in the conversion of alkanes, terpenes, aromatic compounds and pesticides into various products (Bernhardt, 2006; Hannemann *et al.*, 2007b). Their substrates include fatty acids, steroids, prostaglandins, as well as a multitude of foreign compounds such as drugs, anaesthetics, organic solvents, ethanol, alkyl aryl hydrocarbon products, pesticides, and carcinogens (Bernhardt, 2006).

The range of chemical transformations performed by P450s is substantial and continues to grow through discovery of novel P450s and protein engineering. Due to the P450's

ability to perform regio- and stereo-selective oxidations, they have become attractive catalysts for applications in synthetic biology and the generation of high value oxy-chemicals that may not be economical to produce by traditional synthetic chemistry (Girvan and Munro, 2016). P450 BM3 from *B. megaterium* has proven a popular model system based on its catalytic self-sufficiency, its high catalytic rate, and its amenability to mutations (Munro *et al.*, 2013). Through rational design, P450 BM3 has been shown to bind the proton pump inhibitor (PPI) drug omeprazole with oxidation at the 5-methyl position, mimicking the major human metabolite of CYP2C19 (Butler *et al.*, 2013). Engineered variants of P450 BM3 were shown to catalyse the highly diastereo- and enantioselective cyclopropanation of styrenes from diazoester reagents via putative carbene transfer (Coelho *et al.*, 2013).

1.2.3 General structure of cytochromes P450

The first crystal structure of a cytochrome P450 was solved in the late 1980's for the bacterial camphor hydroxylase P450cam (CYP101A1) from *Pseudomonas putida* (Poulos, Finzel and Howard, 1987). This was then followed by the cytochrome P450 BM3 heme domain, a fatty acid hydroxylase from *B. megaterium* in 1993 (Ravichandran *et al.*, 1993). Several other P450 structures have since been solved from several different bacterial species. Currently there are over 6000 structures (and counting) deposited in the protein database, displaying P450 isoforms with various ligands/substrates bound, and displaying various conformational states (Ortiz de Montellano, 2015). What is clear is that despite low sequence similarity (10 – 30%) between members of the superfamily, the overall structure and topology of P450s are highly conserved. The typical 'CYP' fold has a general triangular prism shape, and consists of 12-13 α-helices (A, B, B' and C-L) and 5 β-sheets (1-5) (Hasemann *et al.*, 1995; Sirim *et al.*, 2010) (as shown in **figure 1.2**). Through comparative analysis it has been shown that the most highly conserved regions are those involved in the heme-binding core, which is essential for structure and function of the P450s (Hasemann *et al.*, 1995). It is a general rule that the closer to the heme, the more conserved are the structures (Sirim *et al.*, 2010).

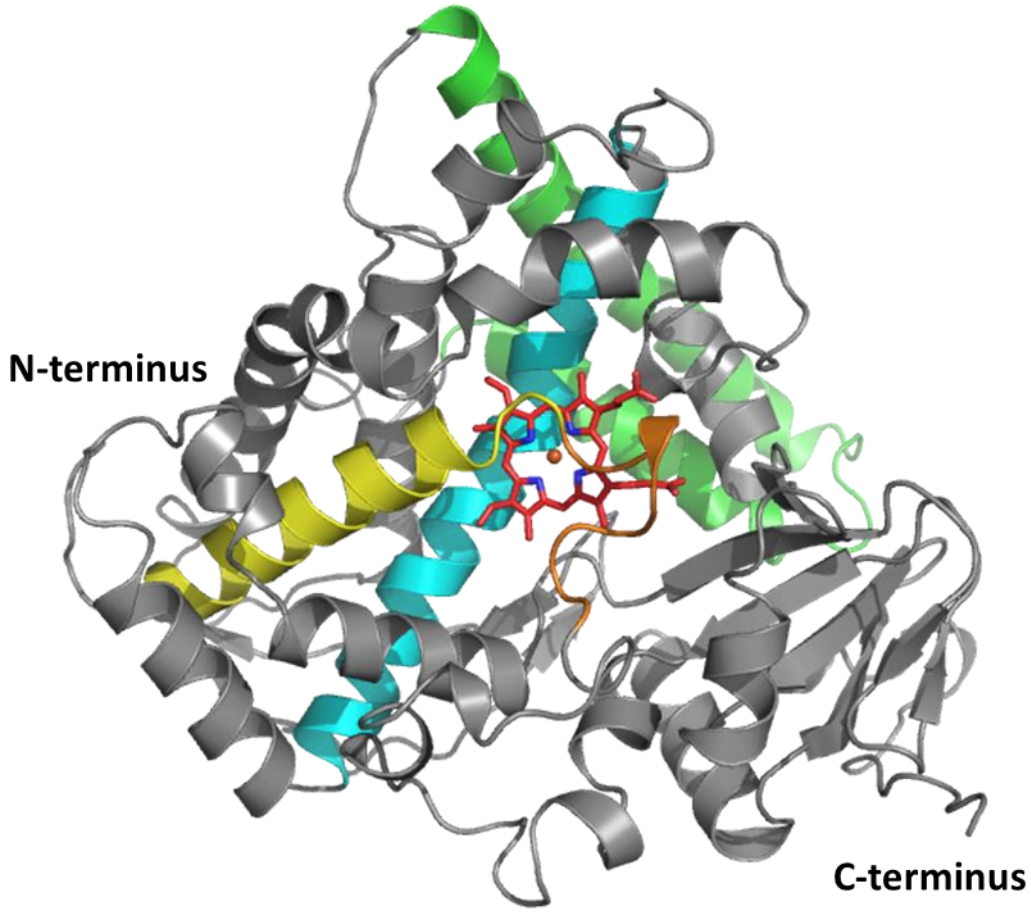

Figure 1.2 General topology of cytochromes P450. Cartoon representation of the heme domain of the fatty acid hydroxylase P450 BM3 from *B. megaterium* (CYP101A1) (PDB code 1BU7). The I-helix (cyan), F- and G-helix (green) and L-helix (yellow) are highlighted. The important meander loop region which houses the Cys-ligand and which ligates the heme is highlighted in orange. The heme-*b* prosthetic group is represented by red sticks. Helices were assigned to data presented by (Whitehouse, Bell and Wong, 2012) and nomenclature first described by (Poulos *et al*., 1987).

These conserved P450 structural cores consist of a four-helix bundle composed of three parallel α-helices (α-D, L and I) and anti-parallel α-E and helices J and K (Presnell and Cohen, 1989; Peterson and Graham, 1998; Denisov *et al.*, 2005). The prosthetic heme group is housed between the distal I-helix and the proximal L helix and is bound to the adjacent cysteine residue. The cysteine thiolate residue is completely conserved across the whole P450 superfamily, and acts as the proximal ligand to the heme iron, located in a signature heme binding loop amino acid sequence (FxxGx(H/R)xCxG). The phenylalanine, glycine and histidine/arginine residues are generally, but not absolutely, conserved in this motif (Dorner *et al.*, 2015). The region that houses the cysteine ligand is named the β-bulge. The β-bulge structurally holds the Cys ligand so that it can hydrogen bond with two neighbouring backbone amides, although geometry suggests it is only able to form one hydrogen bond at a time (Ortiz de Montellano, 2015). This

arrangement is not only solely seen in P450s; it is also present in two closely related heme-thiolate enzymes, nitric oxide synthase (NOS) and chloroperoxidase (CPO). These enzymes display folding patterns distinct from P450s and different H-binding geometry (NOS: provided by an indole ring N atom of a Thr residue). Other residues that are considered to be conserved are the glutamate and arginine in the ExxR motif in the α-K helix (Glu320 and Arg323 in P450 BM3), that has an important role in the stabilisation of the 'meander' loop region of P450 and H-bonding interactions (Hasemann *et al.*, 1995; Peterson and Graham, 1998). The 'meander' loop is a coiled motif located on the proximal face of the protein, which has a role in heme binding and stabilisation of the tertiary structure (Sirim *et al.*, 2010; Dorner *et al.*, 2015). The long α-I helix forms a wall of the heme pocket and contains the signature sequence (A/G)Gx(E/D)T. The highly conserved threonine residue is followed by an acidic residue and is positioned just over the pyrrole ring B (or III) in the active site. Sequence alignment comparisons have shown a high degree of conservation of the threonine residue and the adjacent acidic side chain (Thr252 and Asp251 in CYP101A1) (threonine can occasionally be replaced by a serine or asparagine). The threonine residue has a proposed role in dioxygen binding and is also implicated in proton transfer to the heme distal oxygen in order to generate highly reactive heme iron-oxo species that enable the progression of the P450 catalytic cycle, ultimately leading to scission of the iron-dioxygen bond and catalysis (Peterson and Graham, 1998; Yoshigae, Kent and Hollenberg, 2013; Ortiz de Montellano, 2015). In addition to this, the I-helix plays a key role in substrate recognition and binding, and therefore has an important role in regulating access to the heme prosthetic group (Li *et al.*, 2008).

Mutation of the conserved threonine in CYP101A1 to a hydrophobic residue results in a phenotype that has near normal kinetic parameters during pyridine nucleotide oxidation, but cannot efficiently cleave the O—O bond, and instead releases two electron-reduced dioxygen species in the form of hydrogen peroxide. This uncoupling of oxygen consumption from the monooxygenase reaction in the mutant results from the loss of the proton donating group from the threonine residue (Imai et al., 1989; Shimada et al., 1991). Therefore, it has been suggested that the threonine hydroxyl group participates in hydrogen bond interactions with a secondary proton donor, rather than serving this role itself (Denisov *et al.*, 2005).

To account for the diversity of P450 substrates, redox partners and chemical reactions, there are some structural variations in the positions and flexibility of secondary structural elements and the length of interconnecting loop regions (Schuler and Sligar, 2007; Munro et al., 2013). These subtle variations can be seen around the heme catalytic site and are known as substrate recognition sites (SRS) (Gotoh, 1992). The SRS are responsible for the P450s' ability to recognise and bind to a diverse range of substrates, and thus lend themselves to each P450's individual biochemical processes (Sirim et al., 2010; Munro et al., 2013). Six SRS sequences have been identified across the P450 superfamily, initially characterised through sequence alignments of novel P450s, with those of the CYP2 family and P450cam enzymes (Gotoh, 1992). Since then, structural alignments from 20 different crystal structures (including bacterial, fungal and mammalian P450s) revealed SRS regions with significant structural variation. However, there are slight variations as to where the SRS are located between CYP families. Generally, SRS 1 is found in a highly variable loop region between B- and C-helices (BC-loop). SRS 2 is found in the C-terminal end of the F-helix and SRS 3 spans the N-terminal region of the α-G and part of the FG-loop. The F- and G-helices usually undergo strong conformational changes upon substrate binding (Li and Poulos, 1997, 1999). Additionally, the FG region can be longer in eukaryotes as it likely interacts with the endoplasmic reticulum membrane (Schuler and Sligar, 2007). SRS 4 elongates over the I-helix which extends over the heme pyrrole ring B. SRS 5 is found in the amino terminus of β-(1-4) and extends over the conserved ExxR motif (Seifert and Pleiss, 2009). The β-turn at the end of the β-sheet 4 houses SR6 (Gotoh, 1992; Sirim et al., 2010; Munro et al., 2013).

1.2.4 Structure and spectroscopic properties of heme

Heme (iron-protoporphyrin) is an extremely versatile prosthetic group, found in a variety of proteins. Its physico-chemical properties serve many biological functions and are vital in aerobic life. Depending on the nature of the substituents linked to the porphyrin ring and the way the cofactor is bound to the protein matrix, different heme types have been classified and have been associated with specific functions. There are several biologically relevant types of heme (A, B, C and D) (Gilardi and Di Nardo, 2017). The *b*-type heme is most abundant and has major roles in oxygen binding and gas transport (e.g. haemoglobin, myoglobin) and complex O_2-mediated chemical catalysis

(e.g. P450s, terminal oxidases and peroxidases) (Chapman, Daff and Munro, 1997; Schneider *et al.*, 2007).

Heme *b* is an iron protoporphyrin IX ring structure that associates with proteins via non-covalent interactions. The protoporphyrin IX shown in **figure 1.3** is a hydrophobic planar molecule which consists of four pyrrole rings (I–IV) linked by methyl bridges (α, β, γ, δ) forming a tetrapyrrole ring. The structure produces four inward facing nitrogen atoms which are coordinated by a ferric (Fe^{III}) or ferrous (Fe^{II}) iron. Pyrrole I and IV carry propionate groups from which their carboxyl termini engage in electrostatic interactions with the protein environment (Poulos, Finzel and Howard, 1987; Schneider *et al.*, 2007).

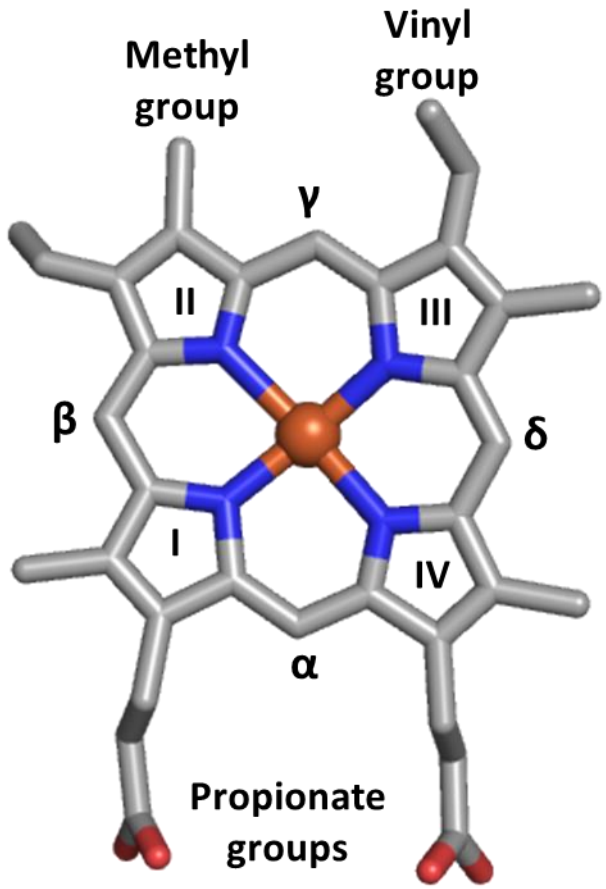

Figure 1.3 Structure of the *b*-type heme. The protoporphyrin IX ring structure contains a central iron atom that forms five coordination bonds, four to pyrrole group nitrogens and the last to the proximal thiolate ligand. In the resting state, H_2O occupies the sixth axial ligand position, but substrate binding to the protein can displace the water molecule, with the penta-coordinated state shown.

In its penta-coordinated state, the heme iron is coordinated by four of the surrounding pyrrole nitrogens as electron pair donors (in the plane of the heme) and a fifth axial thiolate ligand is bound to an evolutionally conserved cysteine in the case of the P450s).

The strong electron donation of the thiolate can facilitate the heterolysis of dioxygen that can coordinate *trans* to the thiolate ligand (Dawson, 1988; Yoshioka *et al.*, 2001). The cysteine thiolate is supported by H-bonding networks on the proximal side of the heme in the protein (Shimizu, 2012).

Iron is a transition metal with five 3d orbitals – they are partially occupied by either five (ferric) or six (ferrous) electrons (Rich and Maréchal, 2012). Under aerobic conditions, the heme iron usually presents a ferric (Fe^{III}) hexa-coordinated state (or resting state) with water as the 6th axial ligand. This is known as the low-spin (LS) state (S=1/2). In this state the five 3d electrons maximally pair. When the water molecule is displaced by substrate binding, the ferric heme iron becomes penta-coordinate and reorganisation of the iron d-orbitals occur, causing the five 3d orbitals to become maximally unpaired in the high spin (HS) state (S=5/2). The ionic radius is larger for the HS Fe^{III} than the LS Fe^{III}, with the HS Fe^{III} moving out of the plane of the porphyrin ring as the central cavity is too small (Shannon and Prewitt, 1970; Tsai *et al.*, 1970).

The electronic properties of heme make them particularly amenable to analysis by UV-visible spectroscopy, since they have strong absorption bands that are dependent on heme types and their redox, spin and ligation states. Low-spin (substrate-free) heme has a characteristic Soret absorbance (λ) at 415-417 nm, followed by α- and β-bands typically between 500-600 nm. Substrate-binding to P450s can be monitored by the concomitant transition from LS to HS using absorption difference spectra (Luthra, Denisov and Sligar, 2011).

The type I shift is associated with substrate binding to a hydrophobic pocket located near the catalytic site of the heme, which displaces the water molecule as the 6th axial ligand. The penta-coordinated heme iron shifts from LS to HS with an accompanying blue shift in Soret absorbance and is identified by a reduction of the Soret absorption band at ~417 nm and an increase in the maximum at 390 nm with an isosbestic point at 407 nm. The type I shift makes the heme more easily reduced by cytochrome P450 reductase providing electrons that drive the catalytic cycle for oxidative metabolism (Jiinig *et al.*, 1977)

The type II binding mode occurs when a substrate binds as the 6th axial ligand to the heme iron. The heme iron remains in the LS state, which makes reduction difficult. Type

II compounds usually consist of substrates that contain a sp^2 hybridised nitrogen atom as part of a heteroaromatic system where the nitrogen lone pair coordinates to the heme iron (Peng *et al.*, 2008). The spectral changes are characterized by an absorption minimum at 390-405 nm and an absorption peak at 425-435 nm (blue shift) (Schenkman, Sligar and Cinti, 1981).

1.2.5 Catalytic cycle

The catalytic cycle for cytochrome P450 has been widely reviewed, and the generally accepted mechanism was originally constructed using P450cam (CYP101A1) and P450 BM3 enzymes (CYP102A1) (see **figure 1.4**). The mechanism includes the timed delivery of two electrons that are ultimately derived from pyridine nucleotide coenzymes (NAD(P)H). Electrons are transported to the heme via one or more redox partners to other points in the catalytic cycle (Munro, Girvan and McLean, 2007). In the resting state, the ferric heme iron (Fe^{III}) is hexa-coordinated equatorially and coordinated by four pyrrole nitrogen groups, with a water molecule occupying the axial position trans to the conserved proximal thiolate ligand (Sono *et al.*, 1996). This is considered to represent the low-spin state, as the d-orbitals of the complex are split into 3 below 2 molecular orbitals (MOs). Here, they occupy the lower MO and are low-spin (LS) species (LS S=1/2), as it is more energetically favourable to spin pair then populate the upper levels (Sligar and Gunsalus, 1979). In their resting state, P450s appear in the ferric (Fe^{III}) form because of the low reduction potential of the Fe^{III}/Fe^{II} couple, usually in the range of -400 mV to -170 mV, which is maintained by the negatively charged proximal thiolate ligand (Guengerich, Ballou and Coon, 1975; Guengerich, 1983; Fantuzzi, Fairhead and Gilardi, 2004). Substrate binding in the active site pocket can displace the water molecule coordinated to the heme iron, producing a penta-coordinated ferric species (**a**), resulting in the iron being out of plane of the porphyrin (Ortiz de Montellano, 2015). The weak crystal field generated in the five coordinated heme, with only one axial ligand, becomes more likely to populate orbitals with minimum spin pairing, therefore causing re-organisation of the heme d-orbitals, with the ferric spin-state changing from (S=1/2) to a high-spin (HS) state (HS=5/2) (Sligar and Gunsalus, 1979). This type-I shift can be followed spectroscopically, with a shift in the Soret absorbance band maximum from ~418 nm to ~390 nm, where absorbance spectral features arise from $\pi \rightarrow \pi^*$ transitions of the delocalised π system of the porphyrin ring (Denisov *et al.*, 2005; Ortiz

de Montellano, 2015). In the HS state, the heme iron reduction potential becomes more positive (heme reduction potential is more oxidising and redox potential is lowered), favouring electron transfer from the redox partner to reduce it to its ferrous state (**b**). In P450cam, camphor binding can alter the redox potential of the heme iron from ~303 mV (substrate-free) to approximately -173 mV (substrate-bound) (Sligar and Gunsalus, 1976). The first electron transfer to the heme iron, in the presence of a correctly bound substrate, is an important thermodynamic regulatory mechanism, preventing the futile consumption of redox equivalents and formation of superoxide/peroxide (Ortiz de Montellano, 2015). This allows the binding of dioxygen to yield an oxy-complex (**c**), the final relatively stable intermediate in the catalytic cycle (Denisov and Sligar, 2015). The complex has dioxygen coordinated end-on to the heme iron with partial transfer of electron density from the iron to the dioxygen moiety. This structure has been determined by Schlichting *et al.*, (2000) with the hydroxylation of camphor by P450cam using cryogenic trapping techniques and rapid data collection. The binding of dioxygen also results in the change in the active site hydrogen bonding structure, suggesting a likely path for the delivery of protons to the distal atom of the bound oxygen (Carrondo *et al.*, 2007). Delivery of the second electron produces a ferric-peroxo complex (**d**). This is followed by protonation of the terminal oxygen, resulting in a hydroperoxo adduct (Compound 0). A second consecutive protonation (**e**) causes the heterolytic cleavage of the O—O bond to produce the highly reactive intermediate ferryl-oxo species, known as compound I (Cpd I), and a water molecule (**f**). This highly transient and long sought reactive intermediate was isolated and characterised by Rittle and Green (2010) through Mossbauer and EPR spectroscopy. Cpd I was formed by reacting CYP119 with *m*-chloroperoxidase acid. Cpd I is an $iron^{IV}$-oxo species with an additional oxidising equivalent delocalised over the porphyrin ring and thiolate ligand. It is thought that the Cpd I moiety is transiently stabilised by the P450 protein fold via specific positioning and orientation of the proximal thiolate ligand (Denisov and Sligar, 2015). Cpd I then abstracts a hydrogen atom from the substrate to give Compound II (Fe^{IV}-OH, Cpd II), the one electron reduced form of Cpd I, and a substrate radical (**g**). Cpd II then quickly "rebounds" with the substrate radical, with oxygen insertion into the C-H bond (**h**). The product then leaves the active site and the heme iron is restored to its resting state (**i**) (Zhang, Biggs and Mukamel, 2015).

At certain points in the catalytic cyclic, non-productive pathways can lead to the collapse of the iron-oxo intermediates. If dioxygen binding is altered it can affect the transfer of the second electron. This leads to production of the superoxide anion and the return of the enzyme to its resting state, a process known as the autoxidation shunt (Munro et al., 2007; Whitehouse et al., 2012). Cpd 0 can also collapse with the production of peroxide, referred to as the peroxide shunt. This occurs if the iron-bound oxygen is protonated due to hindered substrate binding (Denisov *et al.*, 2005). The peroxide shunt can be driven in the reverse direction, using hydrogen peroxide (H_2O_2) as an alternative route to achieve substrate oxidation, albeit rarely productive, though notably effective in the P450 peroxygenase enzyme family (Guengerich and Munro, 2013). The oxidase shunt occurs when Cpd I is oxidised to water, instead of oxygenating the substrate (Denisov *et al.*, 2005).

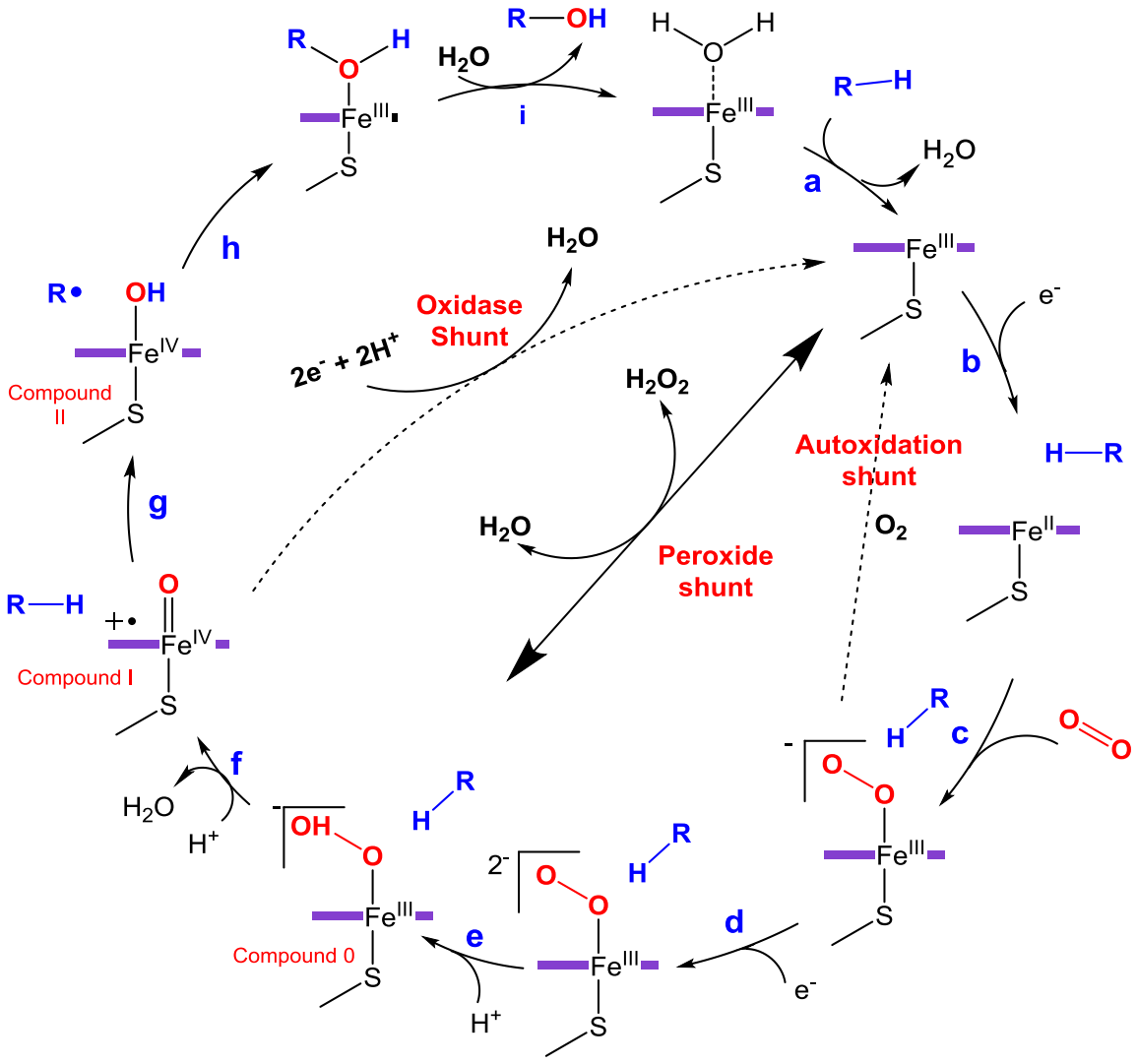

Figure 1.4 General proposed catalytic cycle of cytochromes P450. Based on (Denisov et al., 2005).

1.2.6 Biological diversity of redox partner systems

Stereotypically, cytochromes P450 require the timed consecutive delivery of two electrons to heme iron at distinct points in the catalytic cycle. In most cases, electrons are sourced from reduced pyridine nucleotides (NADPH/NADH), as discussed in **1.2.4**. However, P450s cannot normally receive electrons directly from these coenzymes and therefore, require auxiliary redox partner proteins to shuttle the electrons to the P450 heme iron (Munro, Girvan and McLean, 2007; Lamb and Waterman, 2013). To attain the diverse breadth of chemical reactions, P450s can interact with one or more redox partners to source their reducing equivalents (McLean *et al.*, 2005).

In early cytochrome P450 studies, two distinct classes of redox systems emerged (**figure 1.5**). Enzymes isolated from liver microsomal P450 were found to be integral membrane-bound proteins located in the endoplasmic reticulum and were shown to obtain their electrons from a similarly membrane-anchored FAD- and FMN-containing cytochrome P450 reductase (CPR) (Lu, Junk and Coon, 1969). The CPR enzyme consists of a FAD- and NADPH-binding domain and a FMN-domain linked by a flexible linker region. This enzyme has evolved as a fusion between ancestral proteins homologous to ferredoxin/ferredoxin reductase and bacterial flavodoxins, respectively (Smith, Tew and Wolf, 1994). This membrane-bound eukaryotic two-protein system was named as class II (Hannemann *et al.*, 2007a).

In contrast, the discovery of the first bacterial P450 system, P450cam from *P. putida* was shown to be freely soluble and interacted with two soluble redox partners. Here, electrons are shuttled to the heme via a NADH-specific FAD-containing reductase (putidaredoxin reductase) and a 2Fe-2S cluster-containing ferredoxin (putidaredoxin) (Sevrioukova, Li and Poulos, 2004; McLean *et al.*, 2005). This prokaryotic soluble system was named class I. However, this class I has been expanded to encompass some mitochondrial P450 systems from eukaryotes. Although these systems are not phylogenetically related, they all have in common a 3-protein redox system; (i) FAD-containing ferredoxin reductase, which transfers two electrons from pyridine nucleotide to the iron-sulfur cluster containing (ii) ferredoxin, which in turn shuttles the electrons to the (iii) cytochrome P450 heme iron one at a time. In bacterial P450s all three components are soluble, but in eukaryotes, only the ferredoxin is soluble in the

mitochondrial matrix, with the reductase and P450 are membrane-bound (Hannemann *et al.*, 2007a).

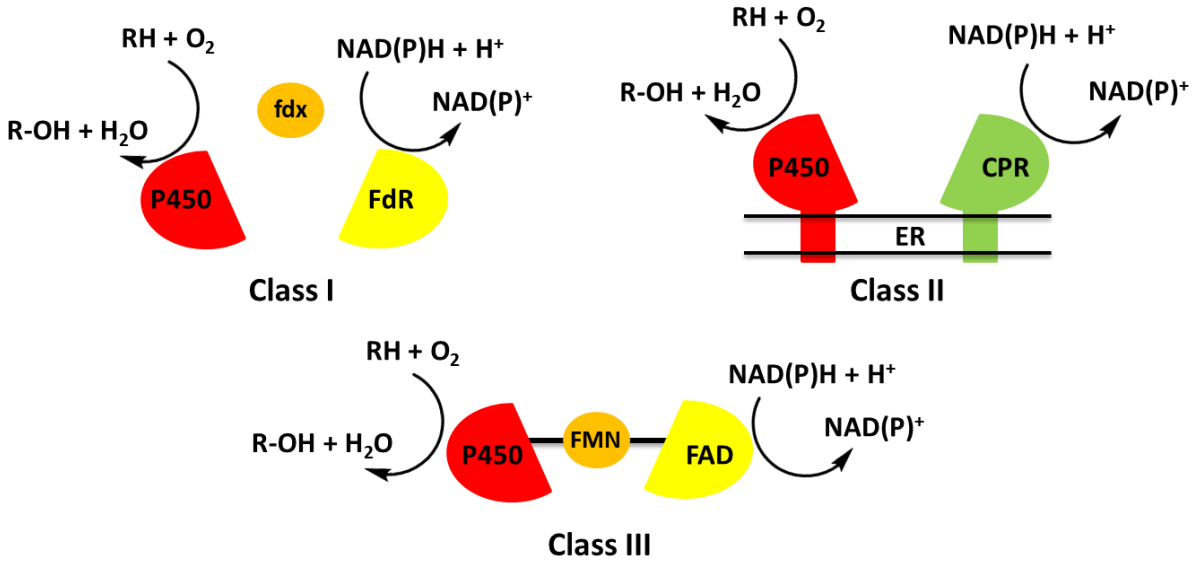

Figure 1.5 Three major classes of the cytochromes P450 and their redox-partner protein arrangements. Class I represents cytochrome P450 (shown in red) ferredoxin (Fdx) (orange) and ferredoxin reductase (FdR) (yellow) based on bacterial systems. Class II shows the mitochondrial system with the P450 (red) and the cytochrome P450 reductase (CPR) (green) tethered to the endoplasmic reticulum (ER). Class III is based on CYP101A1 from *B. megaterium* (P450 BM3). The cytochrome P450 domain is shown in red, with the flavin adenine dinucleotide (FAD) domain (yellow) and the flavin mononucleotide (FMN) domain (orange) fused in a single polypeptide. Figure adapted from (Hannemann et al., 2007a).

One of the first major outliers from the class I/II standard system came in the late 1980's with the discovery of a naturally occurring fusion protein by Armand Fulco. The unusual cytochrome P450 was isolated from the soil bacterium *Bacillus megaterium* (P450 BM3/CYP102A1) and consisted of an N-terminal P450 heme domain linked to a eukaryotic-like CPR containing FMN- and FAD-domains (Narhi and Fulco, 1986). The similarity with eukaryotic class II CYPs, in addition to the fact the enzyme is located within the cytosol as a completely soluble self-sufficient system, means that P450 BM3 has become a paradigm for researchers interested in the class II system. Interestingly, kinetic studies have shown that this fusion arrangement has produced an efficient electron transfer chain from the NADPH cofactor through the reductase onto the P450 heme, to give rise to the highest determined catalytic rate for any P450 monooxygenase at approximately 285 s^{-1} with arachidonic acid (Munro *et al.*, 1996; Noble *et al.*, 1999).

The advent of genome sequencing and the dramatic increase in discovery of P450 genes in all kingdoms of life, highlights how the P450-redox system is much more diverse than previously thought (Lamb and Waterman, 2013; Munro *et al.*, 2013). Some P450s

function without requirements for redox partners. P450nor (CYP55A1) from the fungus *Fusarium oxysporum* catalyses the reduction of two molecules of nitric oxide (NO) to form dinitrogen monoxide (N_2O), in the final step of a respiratory pathway in which nitrate/nitrite are converted to N_2O. Here, the P450 receives electrons directly from the nicotinamide adenine dinucleotide cofactor (Shoun *et al.*, 2012; Girvan and Munro, 2016). A particularly interesting group of P450 enzymes are the P450 peroxygenases that have evolved to hijack the peroxide shunt mechanism. This group of enzymes will be discussed in the next section in detail.

1.3 The cytochrome P450 peroxygenase family

1.3.1 An introduction to the peroxygenase family

In 'classic' P450 monooxygenase systems, H_2O_2 can be used as a surrogate for an $O_2/2e^-/2H^+$ system to drive P450 oxidase reactions in the absence of a redox partner, known as the peroxide shunt pathway (Lee *et al.*, 2003). The H_2O_2 can lead to the direct conversion to the ferric-hydroperoxo species (Cpd 0) intermediate, with subsequent protonation, loss of the water molecule and formation of Cpd I that oxidises the substrate. However, this pathway is rarely efficient as a means of driving catalysis, because the peroxide can lead to the oxidation of the protein and the heme prosthetic group (Guengerich and Munro, 2013). Nevertheless, a small number of P450s have evolved to exploit the peroxide shunt. A breakthrough came in this field with the discovery and characterisation of a gene encoding a cytochrome P450 fatty acid α-hydroxylase from *Sphingomonas paucimobilis* CYP152B1 (P450 SPα) and a gene from *Bacillus subtilis* CYP152A1 (P450 BSβ) (Matsunaga *et al.*, 1997, 1999). P450 SPα was shown to metabolise a range of fatty acids from C11:0 – C18:0, specifically undergoing α-hydroxylation with H_2O_2 being essential for catalysis (Matsunaga *et al.*, 1996, 2000). P450 BSβ displays significant homology towards P450 SPα with 44% sequence similarity. Unlike SPα, the recombinant P450 BSβ enzyme(s) demonstrated α- and β-hydroxylation activities, turning over myristic acid to α-hydroxy myristic acid (~40%) and β-hydroxy myristic acid (~60%). Highest turnover rates were seen in the presence of H_2O_2, and therefore it would be more appropriate to refer to P450 SPα and P450 BSβ as "peroxygenases" rather than "monooxygenases" (Matsunaga *et al.*, 1999).

1.3.2 Discovery of $OleT_{JE}$ and its decarboxylating abilities

Another breakthrough in the P450 peroxygenase field was made by Rude *et al.* (2011), who identified and characterised several new members of the CYP152 peroxygenase family that are able to synthesise terminal olefins. The authors identified *Jeotgalicoccus* as a bacterium that synthesises terminal olefins, in particular 18-methyl-1-nonadecene (most abundant) and 17-methyl-1-nonadecene. It was discovered that these olefins were derived from fatty acid biosynthesis and the key enzyme involved was a novel fatty acid decarboxylase from *Jeotgalicoccus* sp. ATCC 8456. The protein sequence of the decarboxylase was determined as a CYP152 P450 peroxygenase family member (CYP152L1), commonly known as P450 $OleT_{JE}$ due to its olefin forming abilities. P450 $OleT_{JE}$ displays 41% and 37% amino acid similarity to BSβ and SPα, respectively. However, unlike its CYP152 predecessors, $OleT_{JE}$ predominantly catalyses the oxidative decarboxylation of long chain fatty acids to produce an *n*-1 terminal alkene and a 1 carbon co-product (carbon dioxide) in the presence of H_2O_2 (Rude *et al.*, 2011).

Further studies on $OleT_{JE}$ revealed that the P450 could bind to saturated fatty acids from C10:0 – C20:0 with moderately high affinities (C20:0, K_d = 0.29 μM), determined by substrate-induced spin-state changes of the ferric heme iron. Longer chain fatty acids (C18:0 and C20:0) induced more complete conversion to the high spin state compared to shorter chains (Belcher *et al.*, 2014). However, product analysis showed that $OleT_{JE}$ activity was higher towards shorter chain fatty acids (C10:0 – C14:0), with ~97% product conversion with myristic acid (Liu *et al.*, 2014; Matthews, Belcher, *et al.*, 2017).

$OleT_{JE}$ can produce alkenes directly from fatty acids in the presence of H_2O_2 in a single-step decarboxylation. Moreover, $OleT_{JE}$ can utilise free fatty acids rather than fatty thioesters, a highly desirable attribute as microbial engineering in *E. coli* has allowed the manipulation of the composition and the level of the free fatty acid pool, which can be harnessed for biological alkene production (Howard et al., 2013; Liu et al., 2014). Given these attributes, $OleT_{JE}$ remains one of the most extensively characterised and researched members of the CYP152 family, and therefore an ideal candidate for biotechnological development.

1.3.3 $OleT_{JE}$ in biotechnology

In practice, H_2O_2 driven decarboxylation is highly advantageous as it is an inexpensive oxidant (10,000- fold cheaper than reduced nicotinamide on a molar basis) and is easily

scalable and reduces the need for auxiliary redox partners (Wise *et al.*, 2018). Efforts have been made in cell-free reaction systems to harness the peroxide shunt for non-peroxygenase P450s (Cirino and Arnold, 2003). However, H_2O_2 poses a limitation in the large-scale production of alkenes with *in vivo* bioengineering platforms (such as $OleT_{JE}$ as the catalyst) as large amounts of peroxide can be cost prohibitive and high concentrations of H_2O_2 can quickly deactivate the biocatalyst and host system (Liu *et al.*, 2014).

Since then, many efforts have been directed into improving $OleT_{JE}$ to produce a more diverse and robust biocatalyst for applications in biofuel production. This includes pushing the substrate preference towards shorter chain fatty acids, as well as making it an efficient decarboxylase without the need for high amounts of hydrogen peroxide. $OleT_{JE}$ has been leveraged with biological approaches to generate H_2O_2 in a control mannered *in situ*, using $OleT_{JE}$ fused to a H_2O_2 forming alditol oxidase (AldO) from *Streptomyces coelicolor*. AldO catalyses the oxidation of the primary alcohol moiety of alditols using molecular oxygen and forms the aldose product and H_2O_2. This allows for controlled H_2O_2 production to reduce inactivation of the enzyme due to prolonged exposure to high concentrations of H_2O_2. The fusion showed 97% turnover of myristic acid over 20 minutes (Matthews, Tee *et al.*, 2017). Other areas of research include light-driven methods to produce H_2O_2 *in situ*. This harnesses photocatalysts such as FMN to allow the reduction of O_2 to H_2O_2, with electron donors including ethylenediaminetetraacetic acid (EDTA), ascorbate or the inexpensive formate. This system allowed for the turnover of long-chain fatty acid substrates, still preferring decarboxylation, but also with hydroxylation at the Cβ-position for stearic acid (Köninger *et al.*, 2016). However, the production of alkenes enzymatically using peroxygenases *in vivo* has remained elusive. Therefore, a major goal in the field is the design of an efficient *in vivo* system for alkene generations using O_2 and redox-partner protein systems. This idea of leading the peroxygenase system back to the canonical P450 catalysis has been explored in many studies using various combinations of redox partner proteins *in vitro*.

Liu *et al.*, (2014) were first to report H_2O_2-independent activity of $OleT_{JE}$ through fusing the *Rhodococcus* reductase (RhFRED) domain from *Rhodococcus* sp. NCIMB 9784, or with *E. coli* flavodoxin (Fld) and flavodoxin reductase (FldR) redox partners. The fusion

shifted the substrate preference towards shorter chain fatty acids, displaying highest activity against lauric acid (C12:0 ~84% conversion), but was inactive towards arachidic acid (C20:0). The RhFRED-OleT fusion system displayed decreased activity towards the NAD(P)H/O_2 system than with the $OleT_{JE}$ and H_2O_2-driven system. This reinforces its evolutionary path towards peroxygenase rather than monooxygenase catalysis.

Dennig *et al.*, (2015) achieved the turnover of shorter chain fatty acids (C4:0 – C9:0) by $OleT_{JE}$ with an electron delivery system, CamA/B (putidaredoxin reductase/putidaredoxin) from *P. putida* P450cam, in combination with a NAD(P)H recycling system, with the expense of glucose, formate or phosphite**.** The production of alkene is highly dependent on the chain-length of the fatty acid substrate and the reaction temperature. The highest production of alkenes was obtained using stearic acid (C18:0), with a product titre of 0.98 gL^{-1} (TTN>2000) at room temperature. Medium chain fatty acids in the C10:0 – C16:0 region displayed higher conversions to their respective alkenes at 4°C (Dennig *et al.*, 2015).

Other efforts have included producing fusion proteins consisting of $OleT_{JE}$ and the reductase domain of P450 BM3 (BM3R) to create a catalytically self-sufficient protein, utilising NADPH and O_2, coupled with a PDH-regeneration system to eliminate the need for auxiliary redox partners. $OleT_{JE}$ and the BM3 reductase domain fusion protein was created in a single polypeptide with the aim to recreate the efficient catalytic activity of P450 BM3. $OleT_{JE}$-BM3R displayed high product titres of up 2.5 g L^{-1} (higher than CamAB systems) with 1 g of stearic acid (C18:0) successfully converted to 1-heptadecene (60% yield) (Lu *et al.*, 2018).

Further research on products of $OleT_{JE}$ revealed a plethora of other substrates arising from secondary metabolism and use of alternative substrates. Secondary metabolism of 2-hydroxy myristic acid produced 2-hydroxytetradec-2-enoic acid and tridec-1-en-1-ol. Extensive metabolism of 3-hydroxy myristic acid displayed formation of 3,4 dihydroxytetradec-2-enoic acid, revealing the ability of $OleT_{JE}$ ability to di-hydroxylate fatty acids (Matthews, Tee, *et al.*, 2017). In another study, $OleT_{JE}$ α,β-desaturase activity was identified as a dominant pathway with 2-methylbutyric acid. The α,β-desaturase activity is initiated by hydrogen atom abstraction from the Cα—H bond, which is accompanied by α-hydroxylation. Computational studies revealed that the reactivity

depends highly on substrate positioning and requires involvement with the lowest hydrogen abstraction barrier (Pickl *et al.*, 2019).

1.3.4 Structure of $OleT_{JE}$ and other CYP152 enzymes

The first of the peroxygenases to be structurally characterised was the palmitic acid-bound form of P450 BSβ, which was solved to 2.3 Å in 2003, and then the palmitic acid-bound form of P450SPα to a resolution of 1.65 Å in 2011 (Lee *et al.*, 2003; Fujishiro *et al.*, 2011). The structure of $OleT_{JE}$ was then determined by Belcher *et al.*, (2014) in both the substrate-free and arachidic acid-bound forms (C20:0), solved to 2.3 Å and 2.5 Å, respectively. Overall, these peroxygenases exhibit the typical P450 fold, containing α-helical and β-rich domains arranged in a triangular prism shape (Munro *et al.*, 2013) (**figure 1.2**). With the conserved long I-helix that extends across the entire molecule and forms part of the substrate binding pocket on the distal side of the heme. In CYP152 peroxygenases, there are two channels that connect the active site cavity to the protein surface. Channel I, or the substrate-access channel is composed of mainly hydrophobic residues (In SPα, Ile73 Leu77, Leu78, Phe169 Ala172, Ala245, Phe287, Phe288, Pro289, Leu398 and Pro399; similar positions are held in $OleT_{JE}$ and BSβ) with a small positively charged cluster at the entrance of the channel. A second, much smaller, channel (II) is present and is lined with hydrophilic residues, where crystal structures show a cluster of H-bonding water molecules along the cavity, which could be used for the transport of H_2O_2 and water during catalysis (Lee *et al.*, 2003). These two channels are housed around the B', F and G-helices.

Charge distributions of the surface of H_2O_2-driven P450 BSβ displayed some vast differences in comparison to those of other monooxygenases. Generally, peroxygenases display negatively charged acidic residues on the surface of the proximal side (heme-Cys side). Glu113, Glu216, Glu275, Glu341, Glu343, Glu358, Glu366, and Glu371 are characteristically present. In contrast, the distal side surface (substrate access channel opening) contains a positively charged basic cluster containing Lys17, Arg40, Lys44, Lys72, Arg73, Lys76, Arg179, Arg184, and Arg399 (Lee *et al.*, 2003).

However, monooxygenases usually possess a common region of positively charged residues centred over the Cys-pocket (proximal side) of each molecule (the closest approach to the heme iron). Formation of a molecular dipole allows for the redox-partner protein to dock onto the proximal face of the protein (Hasemann *et al.*, 1995).

The correct position of the redox partner facilitates proton egress towards the heme iron via a H-bonding network of waters linking the proximal side via a conserved threonine residue (Thr252) in P450cam (CYP101A1) (Stayton, Poulos and Sligar, 1989; Stayton and Sligar, 1990). In contrast peroxygenases do not utilise redox-partner proteins or electrons/protons to drive catalysis, so therefore this difference in surface potential distribution displays an evolution towards peroxygenase activity. In addition, CYP152 members appear to have undergone certain mutations which reinforce its divergence from typical P450s. In most of the cytochrome P450 superfamily there is an acid-alcohol amino acid pair close to the I-helix region on the distal side of the heme, typically Asp-Thr and Glu-Thr (P450cam Asp251 and Thr252; and P450 BM3 Glu267 and Thr268). These residues have been implicated in various roles including oxygen activation, the relay of protons to the oxo-iron species and stabilisation of the oxy-ferrous or hydroperoxy catalytic intermediates (Clark *et al.*, 2006; Whitehouse, Bell and Wong, 2012; Munro *et al.*, 2018). However, peroxygenases lack this conserved pair, and instead these are replaced by an arginine-proline pair present in the I-helix (P450 BSβ, Arg242, Pro243; SPα: Arg241, Pro242), which are located above the heme (Lee *et al.*, 2003; Fujishiro *et al.*, 2011). The arginine residue binds to the carboxylate group of the fatty acid substrate, which is placed perpendicular to the heme plane with no other direct polar contacts made between the protein and head group (Lee *et al.*, 2003). In this position, the C_α and C_β atoms of the substrate are closest to the heme iron and are primed for oxidation during P450 catalysis. In $OleT_{JE}$, Arg245 is within hydrogen bonding distance of the fatty acid substrate, with the C_α within 5.1 Å and C_β within a 5.7 Å distance, so that it is positioned near to the iron sixth coordination site (Belcher *et al.*, 2014) (see **figure 1.6B**). Studies have shown that the carboxylate group of the fatty acid serves as a general acid-base catalyst for generation of compound I using H_2O_2, pointing to a different evolutionary route taken by these enzymes to accommodate peroxide-driven catalysis (Lee *et al.*, 2003; Fujishiro *et al.*, 2011).

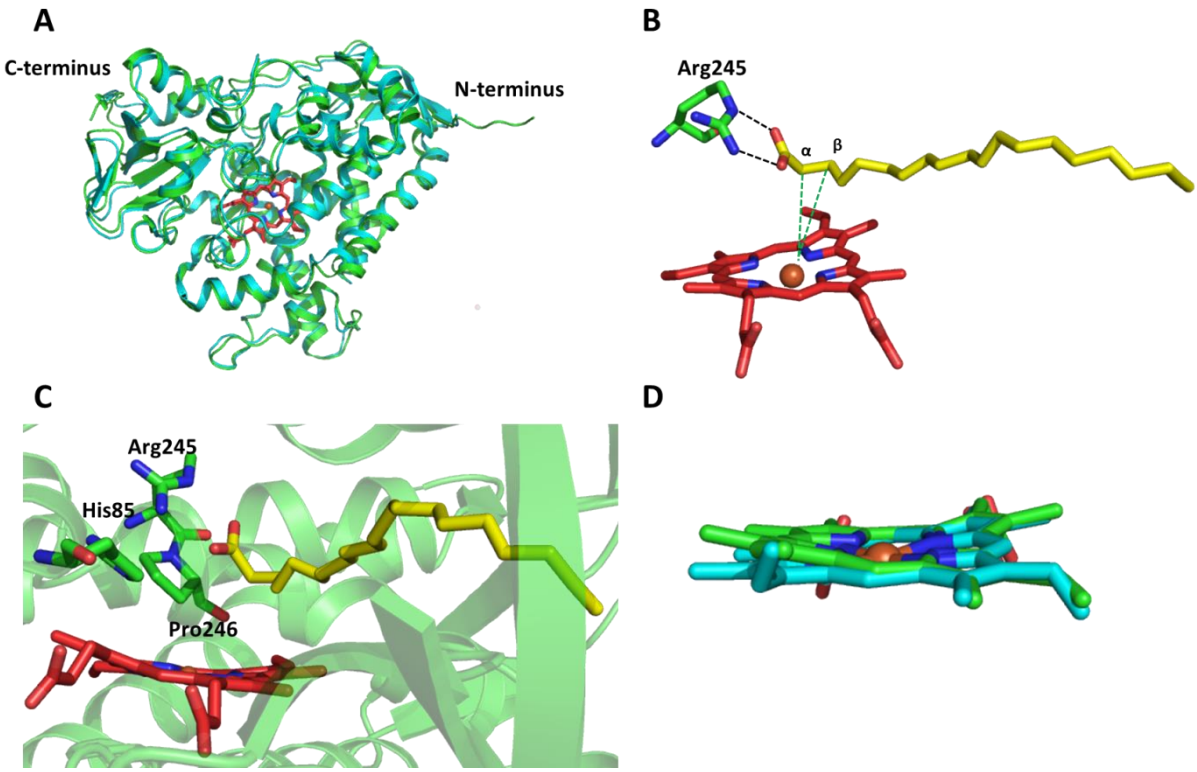

Figure 1.6 Structural properties of the CYP152 family. Panel A shows the structural superimposition of P450 OleTJE from Jeotgalicoccus (CYP152L1) (in green; PDB code 4L40) and P450 BSβ from Bacillus subtilis (CYP152A1) (in cyan; PDB code 1IZ0), with the heme represented by red sticks. Panel B shows the interaction of the bound substrate (arachidic acid, yellow sticks) to Arg245 by interactions (black lines) at the carboxylate group in $OleT_{JE}$. The green lines represent the measurements of the Cα and Cβ positions from the heme iron at 5.1 Å and Cβ 5.7 Å, respectively. Panel C shows important active site residues in OleTJE. Panel D shows an overlay of the heme molecules of $OleT_{JE}$ (green) and P450 BSβ, highlighting the disruption in the A and B pyrrole rings.

The coordination of the fatty substrate in peroxygenases and the preference towards α- and β- positions on the fatty acids is rather unique compared to other monoxygenase P450s. Other CYP members, such as CYP4, usually hydroxylate the ω-end of the fatty acid substrate (Hardwick, 2008). This is also seen in cytochrome P450 BM3 (CYP102A1) from *B. megaterium*, that catalyses the hydroxylation of ω-positions (1-3) of the fatty acid. The crystal structure of the heme domain reveals an active site channel extending from the protein surface, where you see the substrate carboxylate at the mouth of the active site (Arg47 or Tyr51) with the long fatty acid chain protruding towards the heme porphyrin (Ravichandran *et al.*, 1993; Huang *et al.*, 2007; Butler *et al.*, 2013).

The conserved phenylalanine residue (Phe393 in P450 BM3; Phe350 in P450cam) in the heme binding region is absent from the CYP152 peroxygenase family. This residue is suggested to have a key role in controlling the electronic properties of the heme system by modulating the heme reduction potential through interactions with the absolutely-

conserved heme-ligand cysteine (Ost *et al.*, 2001; Clark *et al.*, 2006). In its absence, $OleT_{JE}$ has altered thermodynamic properties, with a very positive heme iron potential (-103 ± 6 mV) compared to other typical NAD(P)H/redox partner dependent P450 systems. There is also no significant change in the redox potential in the arachidic acid substrate-bound form (-105 ± 6 mV). Several P450s use a substrate-induced increase in heme iron redox potential to facilitate electron transfer only when substrate is bound to the P450. In the peroxygenases, a potential change becomes irrelevant when H_2O_2 creates Cpd 0 directly (Belcher et al., 2014).

In $OleT_{JE}$ extensive contacts with hydrophobic amino acids (Phe291 and Phe79) anchor the substrate and provide radical stabilisation to allow for abstraction chemistry to take place (Grant, Mitchell and Makris, 2016). A water molecule has been shown to occupy a position between the imidazole moiety of His85 and the C20:0 carboxylate group. The His85 residue points towards the heme iron and was proposed as a potential proton donor to the reactive P450 Cpd I, the key species in substrate oxidation in most P450 enzymes. However, the His85 residue present in $OleT_{JE}$ appears to be replaced by a glutamine residue in P450 BSβ and SPα. The glutamine is conserved in most CYP152 members and is present in the binding channel. Interestingly, a Q85H variant of P450 BSβ showed increased product rates of 1-pentadecene and 3-hydroxy palmitic acid, and decreased rates of 2-hydroxy palmitic acid formation, suggesting this is an important residue for the catalytic mechanism (Rude *et al.*, 2011).

The structure of $OleT_{JE}$ closely resembles the structure of P450 BSβ with a root mean square deviation of 0.99 Å for 379 C_α atoms (Lee *et al.*, 2003) (**figure 1.6A**). However, there are some subtle structural differences, with most of the significant differences occurring in the FG- and C-terminal loop regions which line the fatty acid binding pocket, typically displaying many structural differences across the P450 superfamily. $OleT_{JE}$ Leu-177 in the FG-loop closes the narrow access channel to the solvent and is present both in P450 BSβ and SPα. $OleT_{JE}$ regions that are involved in fatty acid binding show high structural variance to those seen in P450 BSβ. Elongation occurs in the $OleT_{JE}$ fatty acid binding pocket to allow it to accommodate longer chain fatty acid substrates. This arises in part due to three point mutations in the β-sheet regions (BS_β; Ile-25, Leu-41 and Leu-315 changed to corresponding residues in $OleT_{JE}$; Thr-24, Ala-40 and Ala-315) which help extend the $OleT_{JE}$ substrate binding channel (Belcher *et al.*, 2014).

Another structural difference of $OleT_{JE}$ in comparison to its CYP152 members is the distortion of the A and B pyrrole groups of the heme, moving them 0.8 Å closer to the substrate than observed in BSβ (**figure 1.6D**). This heme contortion is seen in both the substrate-free and substrate-bound crystal structures of $OleT_{JE}$, ruling out a substrate binding effect. This suggests that small alterations in the P450 secondary structure underlie the changes in $OleT_{JE}$ heme planarity (Belcher *et al.*, 2014).

1.3.5 Peroxygenase catalytic cycle

To probe the peroxygenase catalytic mechanism, methods such as stopped-flow and spectroscopic approaches have been used to characterise the heme iron-oxo species involved in the decarboxylation and hydroxylation reactions. The proposed mechanism (see **figure 1.7**) starts with substrate binding within the active site (**i**) with the heme iron being oxidised by H_2O_2 utilising the peroxide shunt to give the ferric-hydroperoxo (compound 0, Cpd 0) species (**ii**). This is rapidly protonated and undergoes a dehydration reaction to form the oxo-ferryl radical cation species (Cpd I) (**iii**). The ferryl (Fe^{IV}) heme iron then abstracts a hydrogen atom from the C_α or C_β position on the fatty acid, producing a carbon radical species and ferryl (Fe^{IV})-hydroxo species (compound II) (**iv**). At this point, the reaction can split in either of two ways; substrate α- or β-hydroxylation, or decarboxylation (**v**). For the decarboxylation reaction, a proton can be abstracted from the C_β with formation of water/OH^- and a carbocation fatty acid intermediate, which readily decarboxylates, with the homolytic scission of the C-C_α bond and production of a terminal alkene and a molecule of carbon dioxide (**vi**). For the route of hydroxylation, oxygen rebound takes place, forming a hydroxylated product (Rude *et al.*, 2011; Belcher *et al.*, 2014). This proposed catalytic mechanism is unique, as P450s are not usually known for catalysing hydride abstraction chemistry or decarboxylation reactions (Grant, Hsieh and Makris, 2015).

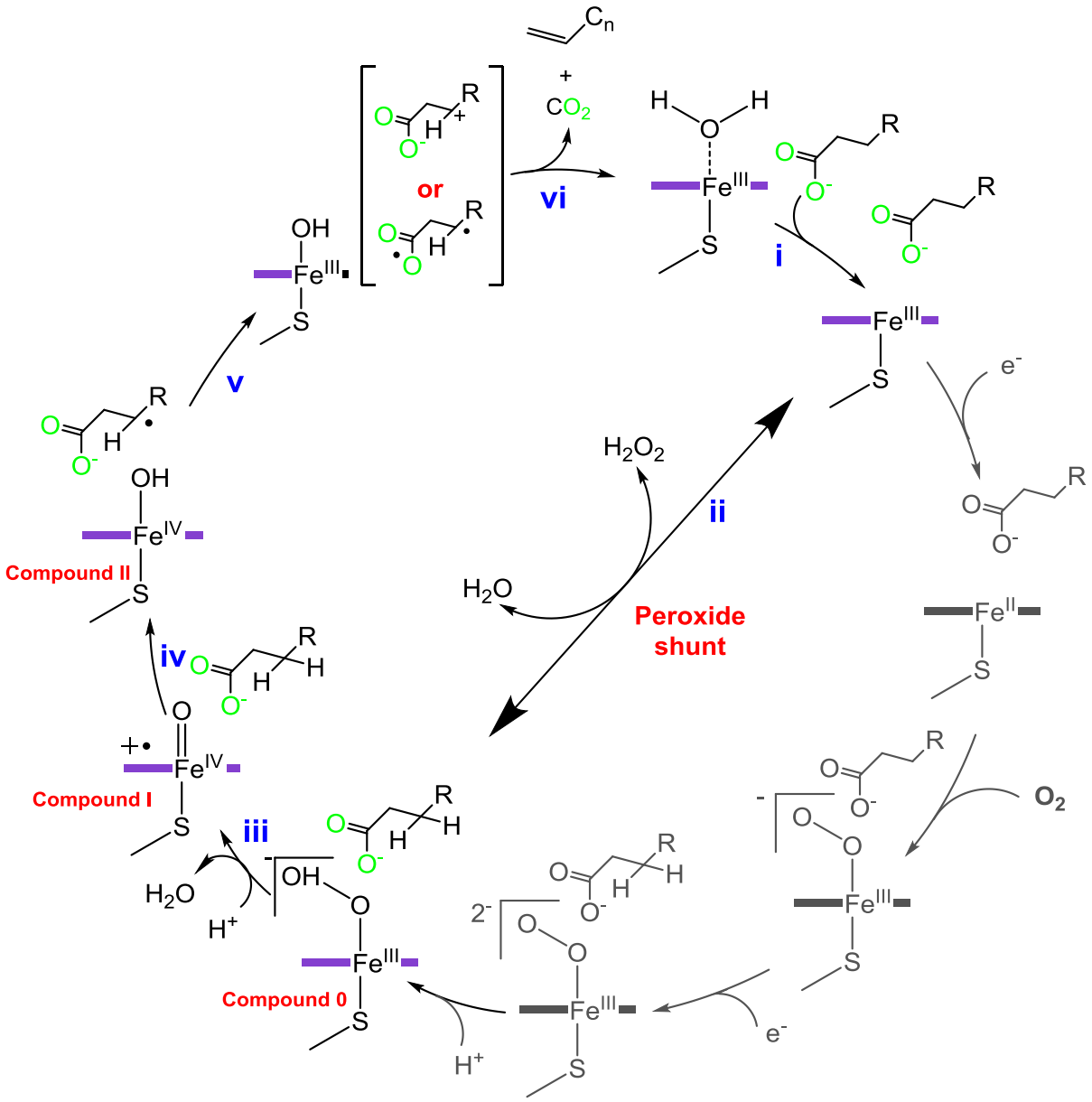

Figure 1.7 Proposed cytochrome P450 catalytic cycle for peroxygenase activity and formation of terminal alkenes. Based on figure from (Munro et al., 2018).

An important study undertaken by Grant and co-workers showed that CO_2 that is produced is derived from cleavage of the fatty acid carboxylate. During headspace FTIR experiments, addition of H_2O_2 to substrate-bound $OleT_{JE}$ resulted in the immediate formation of a doublet at 2340 and 2360 cm^{-1}, and an asymmetric stretch of CO_2. Further to this, turnover experiments using a ^{13}C labelled carboxylate head group ($CH_3(CH_2)_{18}{}^{13}COOH$) showed formation of $^{13}CO_2$ at *m/z* = 45 using headspace GCMS. The intensity of the $^{13}CO_2$ signal is ~25% of the total environment, which is significantly larger than the natural predicted isotopic abundance of ~1.1%. Further to this, the amplitude of isotopic CO_2 was unchanged with the use of $H_2{}^{18}CO_2$ (Grant, Hsieh and Makris, 2015).

They also observed the elusive reactive species, CpdI, in $OleT_{JE}$ (referred to as Ole-I), following the rapid addition of H_2O_2 to a perdeuterated arachidic substrate-OleT complex in stopped-flow studies. Within 15 ms, the high-spin substrate-protein complex (λ_{max} at 392 nm) had completely decayed, and a new intermediate with a blue-shifted Soret maximum at 370 nm, and an additional absorbance band at 690 nm was formed (Grant, Hsieh and Makris, 2015). These absorption characteristics are diagnostic of the iron(IV)-oxo π cation radical intermediate (compound I) and are almost identical to those observed by Rittle and Green (2010) with mixing studies with CYP119 and *m*-chloroperbenzoic acid. The formation of Ole-I is dependent on substrate binding and is invariant to changes in H_2O_2 concentrations. Ole-I accumulates to ~70% at 15 ms, then within 1 s, the intermediate had decayed into a species that is similar to a LS ferric species. From these data, they concluded that a logical route for decarboxylation catalysis could involve a single electron transfer to compound II or another oxidant that produces an unstable carbocation or a substrate diradical. To generate desaturation products, substrate carbocations have been used to rationalise the mechanism in which C-C bond cleavage occurs (Grant, Hsieh and Makris, 2015).

Another study by Grant et al. (2016) used a photomultiplier tube (PMT), which provides greater sensitivity to explore Ole-I turnover with protiated H_{39} arachidic acid (C20:0) substrate. Previous attempts using photodiode array studies did not detect accumulation of Ole-I due to fast reaction rates with the protiated substrate (Grant, Hsieh and Makris, 2015). H_{39}C20:0 in a single-turnover reaction with H_2O_2 was monitored at 370 nm, with the observed initial decay reaching completion within 10 ms, and reaching completion more quickly than the D_{39}-C20:0 substrate, with biphasic characteristics also observed. Reciprocal relaxation times (RRT) were obtained from these data using a two-summed exponential fit, with (fast) $1/\tau1 = 630 \pm 60\ s^{-1}$ and (slow) $1/\tau2 = 6.9 \pm 0.4\ s^{-1}$, showing that only the fast RRT demonstrates isotopic sensitivity, suggesting that the slower phase derives from a second intermediate that contributes to the 370 nm absorbance. Therefore, the fast phase cannot be extracting the H-atom.

This led to the discovery of the second ferryl intermediate (compound II) during $OleT_{JE}$ catalysis. In spectra obtained by mixing D_{39}-arachidic acid–bound $OleT_{JE}$ with a large excess of H_2O_2, the loss of Ole-I over 40 ms is accompanied by the formation of a new transient species. This species has a Soret maximum at $\lambda_{max} = 426$ nm that appears to be

red shifted and is significantly less intense than the ferric LS species (λ = 417 nm), which formed more slowly after 500 ms. A split Soret band is observed with an absorption maximum at 370 nm (Grant, Mitchell and Makris, 2016). Comparisons of these spectral features showed great similarity towards protonated thiolate F^{IV}-hydroxide complexes observed in CYP158 from *Streptomyces coelicolor* with m-CPBA, that displayed a UV-vis spectrum Soret band at 370 and 426 nm at pH 9.0 (Yosca *et al.*, 2013). There are also similarities with the heme-thiolate peroxygenase from *Agrocybe aegerita* (APO), in which an oxo ferryl intermediate displayed split Soret features of 370 and 428 nm (Wang *et al.*, 2015).

After formation of Ole-I, C-H abstraction occurs and forms the second intermediate, Cpd II (Ole-II). In this reaction Ole-II persists for hundreds of milliseconds and does not elicit oxygen rebound. Grant and co-workers proposed that the ability of $OleT_{JE}$ to produce hydroxylated products suggests that $OleT_{JE}$ can also simultaneously function as an oxidase. Bifurcation of the two pathways results in competition between ●OH rebound and the abstraction of an additional substrate electron by Ole-II. The abstraction pathway requiring the recruitment of a proton to restore Fe^{3+}-OH_2 leads to the generation of a carbocation poised for C-C_α cleavage and liberation of CO_2 (Grant, Mitchell and Makris, 2016).

1.4 Project aims

In summary, alkene-producing cytochrome P450 peroxygenases were shown to be an interesting catalyst for biotechnological applications in the production of terminal alkenes as biofuel components and fine chemicals. Therefore, the aim of this PhD project was to identify and characterise novel CYP152 enzymes that could provide a framework for robust catalysts for uses in alkene production.

The work presented in this thesis includes the further characterisation of a novel CYP152 member from *Kocuria rhizophila* which, in initial crystallisation studies, revealed a unique dimer structure, in which interlocking interactions are made by N-terminal helices towards the central domain of the monomer. From this basis, an array of biophysical characterisation and analytical methods (including analytical ultracentrifugation, SEC-MALS and nano-electrospray ionisation MS) were undertaken to probe this unique dimeric interface under different conditions. Further to this, the product profile was investigated using GC-MS.

The second goal of the project involved the identification of novel CYP152 family members from thermostable bacteria with possible alkene-producing abilities. This included the expression and purification of these enzymes; identification of appropriate substrates using UV-visible binding assays based on heme perturbations; as well as identification of products using GC-MS methods. Other techniques used included X-ray crystallography, as well as a range of other biophysical methods to explore their catalytic and structural properties of the enzymes characterised.

1.5 References

Aarts, M. G. *et al.* (1995) 'Molecular characterization of the CER1 gene of Arabidopsis involved in epicuticular wax biosynthesis and pollen fertility', *Plant Cell*. American Society of Plant Physiologists, 7(12), pp. 2115–2127. doi: 10.1105/tpc.7.12.2115.

Alam, M. S. and Tanveer, M. S. (2020) 'Conversion of biomass into biofuel: a cutting-edge technology', in *Bioreactors*. Elsevier, pp. 55–74. doi: 10.1016/b978-0-12-821264-6.00005-x.

Atadashi, I. M., Aroua, M. K. and Aziz, A. A. (2011) 'Biodiesel separation and purification: A review', *Renewable Energy*. Pergamon, pp. 437–443. doi: 10.1016/j.renene.2010.07.019.

Atsumi, S. and Liao, J. C. (2008) 'Metabolic engineering for advanced biofuels production from *Escherichia coli*', *Current Opinion in Biotechnology*, 19(5), pp. 414–419. doi: 10.1016/j.copbio.2008.08.008.

Banerjee, A. *et al.* (2002) 'Botryococcus braunii: A renewable source of hydrocarbons and other chemicals', *Critical Reviews in Biotechnology*, pp. 245–279. doi: 10.1080/07388550290789513.

Barry, S. M. *et al.* (2012) 'Cytochrome P450-catalyzed L-tryptophan nitration in thaxtomin phytotoxin biosynthesis', *Nature Chemical Biology*. Nature Publishing Group, 8(10), pp. 814–816. doi: 10.1038/nchembio.1048.

Belcher, J. *et al.* (2014) 'Structure and biochemical properties of the alkene producing cytochrome P450 OleTJE (CYP152l1) from the Jeotgalicoccus sp. 8456 bacterium', *Journal of Biological Chemistry*. American Society for Biochemistry and Molecular Biology, 289(10), pp. 6535–6550. doi: 10.1074/jbc.M113.527325.

Beller, H. R., Goh, E. B. and Keasling, J. D. (2010) 'Genes involved in long-chain alkene biosynthesis in Micrococcus luteus', *Applied and Environmental Microbiology*. American Society for Microbiology, 76(4), pp. 1212–1223. doi: 10.1128/AEM.02312-09.

Bernard, A. *et al.* (2012) 'Reconstitution of plant alkane biosynthesis in yeast demonstrates that Arabidopsis ECERIFERUM1 and ECERIFERUM3 are core components of a very-long-chain alkane synthesis complex', *Plant Cell*. American Society of Plant Biologists, 24(7), pp. 3106–3118. doi: 10.1105/tpc.112.099796.

Bernhardt, R. (2006) 'Cytochromes P450 as versatile biocatalysts', *Journal of Biotechnology*, 124(1), pp. 128–145. doi: 10.1016/j.jbiotec.2006.01.026.

British Petroleum (BP) (2018) 'Statistical Review of World Energy | Energy economics | Home', *Statistical Review of World Energy*. Available at: https://www.bp.com/en/global/corporate/energy-economics/statistical-review-of-world-energy.html (Accessed: 2 January 2021).

Brodie, B. B. *et al.* (1955) 'Detoxication of drugs and other foreign compounds by liver microsomes', *Science*, 121(3147), pp. 603–604. doi: 10.1126/science.121.3147.603.

Butler, C. F. *et al.* (2013) 'Key mutations alter the cytochrome P450 BM3 conformational

landscape and remove inherent substrate bias', *Journal of Biological Chemistry*. American Society for Biochemistry and Molecular Biology, 288(35), pp. 25387–25399. doi: 10.1074/jbc.M113.479717.

Carrondo, M. A. *et al.* (2007) 'Crystallographic evidence for dioxygen interactions with iron proteins', *Journal of Biological Inorganic Chemistry*. Springer, pp. 429–442. doi: 10.1007/s00775-007-0213-2.

Chapman, S. K., Daff, S. and Munro, A. W. (1997) 'Heme: The most versatile redox centre in biology?', in. Springer, Berlin, Heidelberg, pp. 39–70. doi: 10.1007/3-540-62870-3_2.

Chen, C. Y. *et al.* (2011) 'Cultivation, photobioreactor design and harvesting of microalgae for biodiesel production: A critical review', *Bioresource Technology*. 102(1), pp. 71–81. doi: 10.1016/j.biortech.2010.06.159.

Chisti, Y. (2007) 'Biodiesel from microalgae', *Biotechnology Advances*. Elsevier, pp. 294–306. doi: 10.1016/j.biotechadv.2007.02.001.

Chongkhong, S. *et al.* (2007) 'Biodiesel production by esterification of palm fatty acid distillate', *Biomass and Bioenergy*, 31(8), pp. 563–568. doi: 10.1016/j.biombioe.2007.03.001.

Chowdhury, H. and Loganathan, B. (2019) 'Third-generation biofuels from microalgae: a review', *Current Opinion in Green and Sustainable Chemistry*. Elsevier B.V., pp. 39–44. doi: 10.1016/j.cogsc.2019.09.003.

Christenson, J. K. *et al.* (2017) 'OleB from Bacterial Hydrocarbon Biosynthesis Is a β-Lactone Decarboxylase That Shares Key Features with Haloalkane Dehalogenases', *Biochemistry*. American Chemical Society, 56(40), pp. 5278–5287. doi: 10.1021/acs.biochem.7b00667.

Cirino, P. C. and Arnold, F. H. (2003) 'A Self-Sufficient Peroxide-Driven Hydroxylation Biocatalyst', *Angewandte Chemie International Edition*, 42(28), pp. 3299–3301. doi: 10.1002/anie.200351434.

Clark, J. P. *et al.* (2006) 'The role of Thr268 and Phe393 in cytochrome P450 BM3', *Journal of Inorganic Biochemistry*. Elsevier, 100(5–6), pp. 1075–1090. doi: 10.1016/j.jinorgbio.2005.11.020.

Coelho, P. S. *et al.* (2013) 'Olefin cyclopropanation via carbene transfer catalyzed by engineered cytochrome P450 enzymes', *Science*. American Association for the Advancement of Science, 339(6117), pp. 307–310. doi: 10.1126/science.1231434.

Cook, D. J. *et al.* (2016) 'Cytochromes P450: History, Classes, Catalytic Mechanism, and Industrial Application', in *Advances in Protein Chemistry and Structural Biology*. Academic Press Inc., pp. 105–126. doi: 10.1016/bs.apcsb.2016.07.003.

Dawson, J. H. (1988) 'Probing structure-function relations in heme-containing oxygenases and peroxidases', *Science*. American Association for the Advancement of Science, 240(4851), pp. 433–439. doi: 10.1126/science.3358128.

Denisov, I. D. and Sligar, S. G. (2015) 'Metalloproteins The long and the short of it', *Nature Chemistry*, 7, pp. 687–688. doi: 10.1053/gast.1997.v112.agast971040.

Denisov, I. G. *et al.* (2005) *Structure and chemistry of cytochrome P450*, *Chemical Reviews*. American Chemical Society. doi: 10.1021/cr0307143.

Denisov, I. G. and Sligar, S. G. (2015) 'Activation of molecular oxygen in cytochromes P450', in *Cytochrome P450: Structure, Mechanism, and Biochemistry, Fourth Edition*. Springer International Publishing, pp. 69–109. doi: 10.1007/978-3-319-12108-6_3.

Dennig, A. *et al.* (2015) 'Oxidative Decarboxylation of Short-Chain Fatty Acids to 1-Alkenes', *Angewandte Chemie - International Edition*, 54(30), pp. 8819–8822. doi: 10.1002/anie.201502925.

Dorner, M. E. *et al.* (2015) 'Comparison of intrinsic dynamics of cytochrome P450 proteins using normal mode analysis', *Protein Science*. Blackwell Publishing Ltd, 24(9), pp. 1495–1507. doi: 10.1002/pro.2737.

Estabrook, R. W., Cooper, D. Y. and Rosenthal, O. (1963) 'THE LIGHT REVERSIBLE CARBON MONOXIDE INHIBITION OF THE STEROID', *Biochemische Zeitschrift*. Biochem Z, 338, pp. 741–755. Available at: https://pubmed.ncbi.nlm.nih.gov/14087340/ (Accessed: 23 September 2020).

Fantuzzi, A., Fairhead, M. and Gilardi, G. (2004) 'Direct Electrochemistry of Immobilized Human Cytochrome P450 2E1', *Journal of the American Chemical Society*. American Chemical Society, 126(16), pp. 5040–5041. doi: 10.1021/ja049855s.

French, R. and Malone, P. (2005) 'Phase equilibria of ethanol fuel blends', in *Fluid Phase Equilibria*. Elsevier, pp. 27–40. doi: 10.1016/j.fluid.2004.09.012.

Frias, J. A. *et al.* (2011) 'Purification and characterization of OleA from Xanthomonas campestris and demonstration of a non-decarboxylative claisen condensation reaction', *Journal of Biological Chemistry*. Elsevier, 286(13), pp. 10930–10938. doi: 10.1074/jbc.M110.216127.

Fu, W. J. *et al.* (2015) 'Hydrocarbons, the advanced biofuels produced by different organisms, the evidence that alkanes in petroleum can be renewable', *Applied Microbiology and Biotechnology*. Springer Verlag, pp. 7481–7494. doi: 10.1007/s00253-015-6840-6.

Fujishiro, T. *et al.* (2011) 'Crystal structure of H_2O_2-dependent cytochrome P450 SPα with its bound fatty acid substrate: Insight into the regioselective hydroxylation of fatty acids at the α position', *Journal of Biological Chemistry*, 286(34), pp. 29941–29950. doi: 10.1074/jbc.M111.245225.

Galbe, M., Wallberg, O. and Zacchi, G. (2019) 'Techno-economic aspects of ethanol production from lignocellulosic agricultural crops and residues', in *Comprehensive Biotechnology*. Pergamon, pp. 519–531. doi: 10.1016/B978-0-444-64046-8.00380-3.

Gao, Y. *et al.* (2020) 'Structural insights into catalytic mechanism and product delivery of cyanobacterial acyl-acyl carrier protein reductase', *Nature Communications*. Nature Research, 11(1), pp. 1–11. doi: 10.1038/s41467-020-15268-y.

Gilardi, G. and Di Nardo, G. (2017) 'Heme iron centers in cytochrome P450: structure and catalytic activity', *Rendiconti Lincei*. Springer-Verlag Italia s.r.l., 28(1), pp. 159–167. doi: 10.1007/s12210-016-0565-z.

Girvan, H. M. and Munro, A. W. (2016) 'Applications of microbial cytochrome P450 enzymes in biotechnology and synthetic biology', *Current Opinion in Chemical Biology*. Elsevier Ltd, pp. 136–145. doi: 10.1016/j.cbpa.2016.02.018.

Goldemberg, J. (2006) 'The promise of clean energy', *Energy Policy*, 34(15), pp. 2185–2190. doi: 10.1016/j.enpol.2005.03.009.

Grant, J. L., Hsieh, C. H. and Makris, T. M. (2015) 'Decarboxylation of fatty acids to

terminal alkenes by cytochrome P450 compound I', *Journal of the American Chemical Society*, 137(15), pp. 4940–4943. doi: 10.1021/jacs.5b01965.

Grant, J. L., Mitchell, M. E. and Makris, T. M. (2016) 'Catalytic strategy for carbon-carbon bond scission by the cytochrome P450 OleT', *Proceedings of the National Academy of Sciences of the United States of America*, 113(36), pp. 10049–10054. doi: 10.1073/pnas.1606294113.

Guengerich, F. P. (1983) 'Oxidation-Reduction Properties of Rat Liver Cytochromes P450 and NADPH-Cytochrome P-450 Reductase Related to Catalysis in Reconstituted Systems', *Biochemistry*. American Chemical Society, 22(12), pp. 2811–2820. doi: 10.1021/bi00281a007.

Guengerich, F. P. (2006) 'Cytochrome P450s and other enzymes in drug metabolism and toxicity', *AAPS Journal*. American Association of Pharmaceutical Scientists, 8(1), pp. E101–E111. doi: 10.1208/aapsj080112.

Guengerich, F. P., Ballou, D. P. and Coon, M. J. (1975) 'Purified liver microsomal cytochrome P450. Electron accepting properties and oxidation reduction potential', *Journal of Biological Chemistry*, 250(18), pp. 7405–7414. doi: 10.1016/s0021-9258(19)40959-9.

Guengerich, F. P. and Munro, A. W. (2013) 'Unusual cytochrome P450 enzymes and reactions.', *The Journal of Biological Chemistry*. American Society for Biochemistry and Molecular Biology, 288(24), pp. 17065–73. doi: 10.1074/jbc.R113.462275.

Hannemann, F. *et al.* (2007a) 'Cytochrome P450 systems-biological variations of electron transport chains', *Biochimica et Biophysica Acta - General Subjects*. Elsevier, pp. 330–344. doi: 10.1016/j.bbagen.2006.07.017.

Hannemann, F. *et al.* (2007b) 'Cytochrome P450 systems—biological variations of electron transport chains', *Biochimica et Biophysica Acta (BBA) - General Subjects*, 1770(3), pp. 330–344. doi: 10.1016/j.bbagen.2006.07.017.

Hardwick, J. P. (2008) 'Cytochrome P450 omega hydroxylase (CYP4) function in fatty acid metabolism and metabolic diseases', *Biochemical Pharmacology*. Elsevier Inc., pp. 2263–2275. doi: 10.1016/j.bcp.2008.03.004.

Hasemann, C. A. *et al.* (1995) 'Structure and function of cytochromes P450:a comparative analysis of three crystal structures', *Structure*, 3(1), pp. 41–62. doi: 10.1016/S0969-2126(01)00134-4.

Heyes, D. J. *et al.* (2020) 'Photochemical Mechanism of Light-Driven Fatty Acid Photodecarboxylase', *ACS Catalysis*. American Chemical Society, 10(12), pp. 6691–6696. doi: 10.1021/acscatal.0c01684.

Himmel, M. E. *et al.* (2007) 'Biomass Recalcitrance: Engineering Plants and Enzymes for Biofuels Production', *Science*, 315(5813).

Hoekman, S. K. and Robbins, C. (2012) 'Review of the effects of biodiesel on NOx emissions', *Fuel Processing Technology*, 96, pp. 237–249. doi: 10.1016/j.fuproc.2011.12.036.

Howard, T. P. *et al.* (2013) 'Synthesis of customized petroleum-replica fuel molecules by targeted modification of free fatty acid pools in *Escherichia coli*', *Proceedings of the National Academy of Sciences of the United States of America*. National Academy of Sciences, 110(19), pp. 7636–7641. doi: 10.1073/pnas.1215966110.

Huang, W. C. *et al.* (2007) 'Filling a Hole in Cytochrome P450 BM3 Improves Substrate Binding and Catalytic Efficiency', *Journal of Molecular Biology*. Academic Press, 373(3), pp. 633–651. doi: 10.1016/j.jmb.2007.08.015.

Jiinig, G.-R. *et al.* (1977) 'Differentiation Between Type I and Type II Substrate Binding to Cytochrome P450 by Temperature Studies*', *CROATICA CHEMICA ACTA CCACAA*, 49(2), pp. 263–270.

Kang, M. K. and Nielsen, J. (2017) 'Biobased production of alkanes and alkenes through metabolic engineering of microorganisms', *Journal of Industrial Microbiology and Biotechnology*. Springer Verlag, pp. 613–622. doi: 10.1007/s10295-016-1814-y.

Klingenberg, M. (1958) 'Pigments of rat liver microsomes', *Archives of Biochemistry and Biophysics*, 75(2), pp. 376–386. doi: 10.1016/0003-9861(58)90436-3.

Köninger, K. *et al.* (2016) 'Light-driven enzymatic decarboxylation', *Journal of Visualized Experiments*. 2016(111), p. 53439. doi: 10.3791/53439.

Lamb, D. C. and Waterman, M. R. (2013) 'Unusual properties of the cytochrome P450 superfamily', *Philosophical Transactions of the Royal Society B: Biological Sciences*. Royal Society, 368(1612), p. 20120434. doi: 10.1098/rstb.2012.0434.

Lee, D. S. *et al.* (2003) 'Substrate recognition and molecular mechanism of fatty acid hydroxylation by cytochrome P450 from *Bacillus subtilis*: Crystallographic, spectroscopic, and mutational studies', *Journal of Biological Chemistry*. American Society for Biochemistry and Molecular Biology, 278(11), pp. 9761–9767. doi: 10.1074/jbc.M211575200.

Lee, R. A. and Lavoie, J. M. (2013) 'From first- to third-generation biofuels: Challenges of producing a commodity from a biomass of increasing complexity', *Animal Frontiers*. Oxford University Press, 3(2), pp. 6–11. doi: 10.2527/af.2013-0010.

Lee, S. K. *et al.* (2008) 'Metabolic engineering of microorganisms for biofuels production: from bugs to synthetic biology to fuels', *Current Opinion in Biotechnology*, 19(6), pp. 556–563. doi: 10.1016/j.copbio.2008.10.014.

Li, L. *et al.* (2008) 'Modes of heme binding and substrate access for cytochrome P450 CYP74A revealed by crystal structures of allene oxide synthase.', *Proceedings of the National Academy of Sciences of the United States of America*. National Academy of Sciences, 105(37), pp. 13883–8. doi: 10.1073/pnas.0804099105.

Li, N. *et al.* (2011) 'Conversion of fatty aldehydes to alka(e)nes and formate by a cyanobacterial aldehyde decarbonylase: Cryptic redox by an unusual dimetal oxygenase', *Journal of the American Chemical Society*. American Chemical Society, 133(16), pp. 6158–6161. doi: 10.1021/ja2013517.

Li, N. *et al.* (2012) 'Evidence for only oxygenative cleavage of aldehydes to alk(a/e)nes and formate by cyanobacterial aldehyde decarbonylases', *Biochemistry*. Biochemistry, 51(40), pp. 7908–7916. doi: 10.1021/bi300912n.

Liu, Q. *et al.* (2015) 'Engineering an iterative polyketide pathway in *Escherichia coli* results in single-form alkene and alkane overproduction', *Metabolic Engineering*. Academic Press Inc., 28, pp. 82–90. doi: 10.1016/j.ymben.2014.12.004.

Liu, Y. *et al.* (2014) 'Hydrogen peroxide-independent production of α-alkenes by $OleT_{JE}$

P450 fatty acid decarboxylase.', *Biotechnology for biofuels*, 7(1), p. 28. doi: 10.1186/1754-6834-7-28.

Lu, A. Y., Junk, K. W. and Coon, M. J. (1969) 'Resolution of the cytochrome P450-containing omega-hydroxylation system of liver microsomes into three components.', *Journal of Biological Chemistry*. Elsevier, 244(13), pp. 3714–3721. doi: 10.1016/s0021-9258(18)83427-5.

Lu, C. *et al.* (2018) 'An Engineered Self-Sufficient Biocatalyst Enables Scalable Production of Linear α-Olefins from Carboxylic Acids', *ACS Catalysis*, 8(7), pp. 5794–5798. doi: 10.1021/acscatal.8b01313.

Luthra, A., Denisov, I. G. and Sligar, S. G. (2011) 'Spectroscopic features of cytochrome P450 reaction intermediates', *Archives of Biochemistry and Biophysics*. NIH Public Access, pp. 26–35. doi: 10.1016/j.abb.2010.12.008.

Marsh, E. N. G. and Waugh, M. W. (2013) 'Aldehyde decarbonylases: Enigmatic enzymes of hydrocarbon biosynthesis', *ACS Catalysis*, pp. 2515–2521. doi: 10.1021/cs400637t.

Matsunaga, I. *et al.* (1996) 'Direct involvement of hydrogen peroxide in bacterial α-hydroxylation of fatty acids', *FEBS Letters*. Elsevier B.V., 386(2–3), pp. 252–254. doi: 10.1016/0014-5793(96)00451-6.

Matsunaga, I. *et al.* (1997) 'Molecular cloning and expression of fatty acid α-hydroxylase from *Sphingomonas paucimobilis*', *Journal of Biological Chemistry*. American Society for Biochemistry and Molecular Biology, 272(38), pp. 23592–23596. doi: 10.1074/jbc.272.38.23592.

Matsunaga, I. *et al.* (1999) 'Characterization of the ybdT gene product of *Bacillus subtilis*: Novel fatty acid β-hydroxylating cytochrome P450', *Lipids*. John Wiley & Sons, Ltd, 34(8), pp. 841–846. doi: 10.1007/s11745-999-0431-3.

Matsunaga, I. *et al.* (2000) 'Fatty acid-specific, regiospecific, and stereospecific hydroxylation by cytochrome P450 (CYP152B1) from *Sphingomonas paucimobilis*: Substrate structure required for α-hydroxylation', *Lipids*. American Oil Chemists Society, 35(4), pp. 365–371. doi: 10.1007/s11745-000-533-y.

Matthews, S., Belcher, J. D., *et al.* (2017) 'Catalytic determinants of alkene production by

the cytochrome P450 peroxygenase $OleT_{JE}$', *Journal of Biological Chemistry*. American Society for Biochemistry and Molecular Biology, 292(12), pp. 5128–5143. doi: 10.1074/jbc.M116.762336.

Matthews, S., Tee, K. L., *et al.* (2017) 'Production of alkenes and novel secondary products by P450 $OleT_{JE}$ using novel H_2O_2-generating fusion protein systems', *FEBS Letters*, 591(5), pp. 737–750. doi: 10.1002/1873-3468.12581.

McLean, K. J. *et al.* (2005) 'Biodiversity of cytochrome P450 redox systems', *Biochemical Society Transactions*, pp. 796–801. doi: 10.1042/BST0330796.

Mendez-Perez, D., Begemann, M. B. and Pfleger, B. F. (2011) 'Modular synthase-encoding gene involved in α-olefin biosynthesis in *Synechococcus* sp. strain pcC 7002', *Applied and Environmental Microbiology*. American Society for Microbiology, 77(12), pp. 4264–4267. doi: 10.1128/AEM.00467-11.

Menon, N. *et al.* (2015) 'A microbial platform for renewable propane synthesis based on a fermentative butanol pathway', *Biotechnology for Biofuels*. BioMed Central Ltd., 8(1), p. 61. doi: 10.1186/s13068-015-0231-1.

Metzger, P. and Largeau, C. (2005) '*Botryococcus braunii*: A rich source for hydrocarbons and related ether lipids', *Applied Microbiology and Biotechnology*. pp. 486–496. doi: 10.1007/s00253-004-1779-z.

Ortiz de Montellano, P. (2015) *Cytochrome P450: Structure, mechanism, and biochemistry, fourth edition*, *Cytochrome P450: Structure, Mechanism, and Biochemistry, Fourth Edition*. Springer International Publishing. doi: 10.1007/978-3-319-12108-6.

Munro, A. W. *et al.* (1996) 'Probing electron transfer in flavocytochrome P-450 BM3 and its component domains', *European Journal of Biochemistry*. Blackwell Publishing Ltd, 239(2), pp. 403–409. doi: 10.1111/j.1432-1033.1996.0403u.x.

Munro, A. W. *et al.* (2013) 'What makes a P450 tick?', *Trends in Biochemical Sciences*, 38(3), pp. 140–150. doi: 10.1016/j.tibs.2012.11.006.

Munro, A. W. *et al.* (2018) 'Structure and function of the cytochrome P450 peroxygenase enzymes', *Biochemical Society Transactions*. Portland Press Ltd, pp. 183–196. doi: 10.1042/BST20170218.

Munro, A. W., Girvan, H. M. and McLean, K. J. (2007) 'Variations on a (t)heme--novel mechanisms, redox partners and catalytic functions in the cytochrome P450 superfamily.', *Natural Product Reports*, 24(3), pp. 585–609. doi: 10.1039/b604190f.

Naik, S. N. *et al.* (2010) 'Production of first and second generation biofuels: A comprehensive review', *Renewable and Sustainable Energy Reviews*, pp. 578–597. doi: 10.1016/j.rser.2009.10.003.

Nanda, S. *et al.* (2018) 'A broad introduction to first-, second-, and third-generation biofuels', in *Recent Advancements in Biofuels and Bioenergy Utilization*. Springer Singapore, pp. 1–25. doi: 10.1007/978-981-13-1307-3_1.

Narhi, L. O. and Fulco, A. J. (1986) 'Characterization of a catalytically self-sufficient 119,000-dalton cytochrome P-450 monooxygenase induced by barbiturates in *Bacillus megaterium*.', *The Journal of biological chemistry*, 261(16), pp. 7160–9. Available at: http://www.ncbi.nlm.nih.gov/pubmed/3086309 (Accessed: 29 December 2016).

Nelson, D. R. *et al.* (1993) 'The P450 Superfamily: Update on New Sequences, Gene Mapping, Accession Numbers, Early Trivial Names of Enzymes, and Nomenclature', *DNA and Cell Biology*. Mary Ann Liebert, Inc., Publishers Pp, 12(1), pp. 1–51. doi: 10.1089/dna.1993.12.1.

Nelson, D. R. (2006) 'Cytochrome P450 nomenclature, 2004.', *Methods in molecular biology (Clifton, N.J.)*. Methods Mol Biol, 320, pp. 1–10. doi: 10.1385/1-59259-998-2:1.

Noble, M. A. *et al.* (1999) 'Roles of key active-site residues in flavocytochrome P450 BM3', *Biochemical Journal*. Portland Press Ltd, 339(2), pp. 371–379. doi: 10.1042/0264-6021:3390371.

O'Sullivan, M. and Sandalow, D. (2017) *The Geopolitics of Renewable Energy*.

Olivier, J. G. J. and Peters, J. A. H. W. (2020) *TRENDS IN GLOBAL CO2 AND TOTAL GREENHOUSE GAS EMISSIONS 2019 Report*. Available at: https://www.pbl.nl/sites/default/files/downloads/pbl-2020-trends-in-global- (Accessed: 2 January 2021).

Omura, T. and Sato, R. (1962) 'A new cytochrome in liver microsomes.', *The Journal of Biological Chemistry*, 237, pp. 1375–1376. Available at:

http://www.ncbi.nlm.nih.gov/pubmed/14482007 (Accessed: 27 November 2016).

Omura, T. and Sato, R. (1964) 'The carbon monoxide-bindng pigent of liver microsomes. I. Evidence for its hemoprotein nature.', *The Journal of biological chemistry*, 239(7), pp. 2370–8. Available at: http://www.ncbi.nlm.nih.gov/pubmed/14209972%5Cnhttp://www.ncbi.nlm.nih.gov/pubmed/14209971 (Accessed: 30 December 2016).

Ost, T. W. B. *et al.* (2001) 'Phenylalanine 393 exerts thermodynamic control over the heme of flavocytochrome P450 BM3', *Biochemistry*. American Chemical Society, 40(45), pp. 13421–13429. doi: 10.1021/bi010716m.

Peng, C. C. *et al.* (2008) 'Cytochrome P450 2C9 type II binding studies on quinoline-4-carboxamide analogues', *Journal of Medicinal Chemistry*. NIH Public Access, 51(24), pp. 8000–8011. doi: 10.1021/jm8011257.

Peralta-Yahya, P. P. and Keasling, J. D. (2010) 'Advanced biofuel production in microbes', *Biotechnology Journal*. WILEY-VCH Verlag, pp. 147–162. doi: 10.1002/biot.200900220.

Peterson, J. A. and Graham, S. E. (1998) 'A close family resemblance: the importance of structure in understanding cytochromes P450', *Structure*, 6(9), pp. 1079–1085. doi: 10.1016/S0969-2126(98)00109-9.

Pickl, M. *et al.* (2019) 'Mechanistic Studies of Fatty Acid Activation by CYP152 Peroxygenases Reveal Unexpected Desaturase Activity', *ACS Catalysis*. American Chemical Society, 9(1), pp. 565–577. doi: 10.1021/acscatal.8b03733.

Poulos, T. L., Finzel, B. C. and Howard, A. J. (1987) 'High-resolution crystal structure of cytochrome P450cam', *Journal of Molecular Biology*, 195(3), pp. 687–700. doi: 10.1016/0022-2836(87)90190-2.

Presnell, S. R. and Cohen, F. E. (1989) 'Topological distribution of four-alpha-helix bundles.', *Proceedings of the National Academy of Sciences of the United States of America*. 86(17), pp. 6592–6596. doi: 10.1073/pnas.86.17.6592.

Qiu, Y. *et al.* (2012) 'An insect-specific P450 oxidative decarbonylase for cuticular hydrocarbon biosynthesis', *Proceedings of the National Academy of Sciences of the United States of America*. 109(37), pp. 14858–14863. doi: 10.1073/pnas.1208650109.

Ravichandran, K. G. *et al.* (1993) 'Crystal structure of hemoprotein domain of P450 BM3, a prototype for microsomal P450's, *Science*. American Association for the Advancement of Science, 261(5122), pp. 731–736. doi: 10.1126/science.8342039.

Rich, P. R. and Maréchal, A. (2012) 'Electron transfer chains: Structures, mechanisms and energy coupling', in *Comprehensive Biophysics*. Elsevier Inc., pp. 72–93. doi: 10.1016/B978-0-12-374920-8.00806-7.

Rittle, J. and Green, M. T. (2010) 'Cytochrome P450 compound I: Capture, characterization, and C-H bond activation kinetics', *Science*, 330(6006), pp. 933–937. doi: 10.1126/science.1193478.

Rude, M. A. *et al.* (2011) 'Terminal olefin (1-alkene) biosynthesis by a novel P450 fatty acid decarboxylase from *Jeotgalicoccus* species', *Applied and Environmental Microbiology*. American Society for Microbiology, 77(5), pp. 1718–1727. doi: 10.1128/AEM.02580-10.

Rui, Z. *et al.* (2014) 'Microbial biosynthesis of medium-chain 1-alkenes by a nonheme iron oxidase', *Proceedings of the National Academy of Sciences of the United States of America*. 111(51), pp. 18237–18242. doi: 10.1073/pnas.1419701112.

Rui, Z. *et al.* (2015) 'Discovery of a Family of Desaturase-Like Enzymes for 1-Alkene Biosynthesis', *ACS Catalysis*. American Chemical Society, 5(12), pp. 7091–7094. doi: 10.1021/acscatal.5b01842.

Schenkman, J. B., Sligar, S. G. and Cinti, D. L. (1981) 'Substrate interaction with cytochrome P450', *Pharmacology and Therapeutics*. Pergamon, 12(1), pp. 43–71. doi: 10.1016/0163-7258(81)90075-9.

Schirmer, A. *et al.* (2010) 'Microbial biosynthesis of alkanes', *Schirmer, A. et al. (2010) 'Microbial biosynthesis of alkanes', Science, 329(5991), pp. 559–562. doi: 10.1126/science.1187936.*

Schlichting, I. *et al.* (2000) 'The catalytic pathway of cytochrome P450cam at atomic resolution', *Science*. American Association for the Advancement of Science, 287(5458), pp. 1615–1622. doi: 10.1126/science.287.5458.1615.

Schneider, S. *et al.* (2007) 'Diversity and conservation of interactions for binding heme in

b-type heme proteins', *Natural Product Reports*. The Royal Society of Chemistry, pp. 621–630. doi: 10.1039/b604186h.

Serrano-Ruiz, J. C., Ramos-Fernández, E. V. and Sepúlveda-Escribano, A. (2012) 'From biodiesel and bioethanol to liquid hydrocarbon fuels: new hydrotreating and advanced microbial technologies', *Energy & Environmental Science*, 5(2), p. 5638. doi: 10.1039/c1ee02418c.

Sevrioukova, I. F., Li, H. and Poulos, T. L. (2004) 'Crystal Structure of Putidaredoxin Reductase from Pseudomonas putida, the Final Structural Component of the Cytochrome P450cam Monooxygenase', *Journal of Molecular Biology*, 336(4), pp. 889–902. doi: 10.1016/j.jmb.2003.12.067.

Shannon, R. D. and Prewitt, C. T. (1970) 'Revised values of effective ionic radii', *Acta Crystallographica Section B Structural Crystallography and Crystal Chemistry*. International Union of Crystallography (IUCr), 26(7), pp. 1046–1048. doi: 10.1107/s0567740870003576.

Shimizu, T. (2012) 'Binding of cysteine thiolate to the Fe(III) heme complex is critical for the function of heme sensor proteins', in *Journal of Inorganic Biochemistry*. Elsevier, pp. 171–177. doi: 10.1016/j.jinorgbio.2011.08.018.

Shoun, H. *et al.* (2012) 'Fungal denitrification and nitric oxide reductase cytochrome P450nor', *Philosophical Transactions of the Royal Society B: Biological Sciences*. Royal Society, pp. 1186–1194. doi: 10.1098/rstb.2011.0335.

Sirim, D. *et al.* (2010) 'Prediction and analysis of the modular structure of cytochrome P450 monooxygenases', *BMC Structural Biology*. BioMed Central, 10(1), p. 34. doi: 10.1186/1472-6807-10-34.

Sligar, S. G. and Gunsalus, I. C. (1976) 'A thermodynamic model of regulation: modulation of redox equilibria in camphor monoxygenase', *Proceedings of the National Academy of Sciences of the United States of America*. 73(4), pp. 1078–1082. doi: 10.1073/pnas.73.4.1078.

Sligar, S. G. and Gunsalus, I. C. (1979) 'Proton Coupling in the Cytochrome P450 Spin and Redox Equilibria', *Biochemistry*. American Chemical Society, 18(11), pp. 2290–2295. doi:

10.1021/bi00578a024.

Smith, G. C. M., Tew, D. G. and Wolf, C. R. (1994) 'Dissection of NADPH-cytochrome P450 oxidoreductase into distinct functional domains', *Proceedings of the National Academy of Sciences of the United States of America*. 91(18), pp. 8710–8714. doi: 10.1073/pnas.91.18.8710.

Sono, M. *et al.* (1996) 'Heme-Containing Oxygenases', *Chemical Reviews*. American Chemical Society, 96(7), pp. 2841–2888. doi: 10.1021/cr9500500.

Sorigué, D. *et al.* (2017) 'An algal photoenzyme converts fatty acids to hydrocarbons', *Science*. American Association for the Advancement of Science, 357(6354), pp. 903–907. doi: 10.1126/science.aan6349.

Stayton, P. S., Poulos, T. L. and Sligar, S. G. (1989) 'Putidaredoxin Competitively Inhibits Cytochrome b_5-Cytochrome P450cam Association: A Proposed Molecular Model for a Cytochrome P450cam Electron-Transfer Complex', *Biochemistry*. American Chemical Society, 28(20), pp. 8201–8205. doi: 10.1021/bi00446a035.

Stayton, P. S. and Sligar, S. G. (1990) 'The Cytochrome P450cam Binding Surface As Defined by Site-Directed Mutagenesis and Electrostatic Modeling', *Biochemistry*. Biochemistry, 29(32), pp. 7381–7386. doi: 10.1021/bi00484a005.

Sukovich, D. J. *et al.* (2010) 'Widespread head-to-head hydrocarbon biosynthesis in bacteria and role of OleA', *Applied and Environmental Microbiology*. 76(12), pp. 3850–3862. doi: 10.1128/AEM.00436-10.

Total Energy - U.S. Energy Information Administration (EIA) (no date). Available at: https://www.eia.gov/totalenergy/ (Accessed: 23 January 2021).

Tsai, R. *et al.* (1970) 'Spin-state changes in cytochrome P450cam on binding of specific substrates.', *Proceedings of the National Academy of Sciences of the United States of America*, 66(4), pp. 1157–1163. doi: 10.1073/pnas.66.4.1157.

Wang, X. *et al.* (2015) 'Heme-thiolate ferryl of aromatic peroxygenase is basic and reactive', *Proceedings of the National Academy of Sciences of the United States of America*. National Academy of Sciences, 112(12), pp. 3686–3691. doi: 10.1073/pnas.1503340112.

Whitehouse, C. J. C., Bell, S. G. and Wong, L. L. (2012) 'P450BM3 (CYP102A1): Connecting the dots', *Chemical Society Reviews*, 41(3), pp. 1218–1260. doi: 10.1039/c1cs15192d.

Wise, C. E. *et al.* (2018) 'Dioxygen Activation by the Biofuel-Generating Cytochrome P450 OleT', *ACS Catalysis*. American Chemical Society, 8(10), pp. 9342–9352. doi: 10.1021/acscatal.8b02631.

Yan, J. *et al.* (2015) 'Assembly of lipase and P450 fatty acid decarboxylase to constitute a novel biosynthetic pathway for production of 1-alkenes from renewable triacylglycerols and oils.', *Biotechnology for biofuels*. BioMed Central, 8(1), p. 34. doi: 10.1186/s13068-015-0219-x.

Yosca, T. H. *et al.* (2013) 'Iron(IV)hydroxide pKa and the role of thiolate ligation in C-H bond activation by cytochrome P450', *Science*. American Association for the Advancement of Science, 342(6160), pp. 825–829. doi: 10.1126/science.1244373.

Yoshigae, Y., Kent, U. M. and Hollenberg, P. F. (2013) 'Role of the highly conserved threonine in cytochrome P450 2E1: prevention of H_2O_2-induced inactivation during electron transfer.', *Biochemistry*. NIH Public Access, 52(27), pp. 4636–47. doi: 10.1021/bi4004843.

Yoshioka, S. *et al.* (2001) 'Proximal cysteine residue is essential for the enzymatic activities of cytochrome P450cam', *European Journal of Biochemistry*. Blackwell Publishing Ltd., 268(2), pp. 252–259. doi: 10.1046/j.1432-1033.2001.01872.x.

Zhang, F., Rodriguez, S. and Keasling, J. D. (2011) 'Metabolic engineering of microbial pathways for advanced biofuels production', *Current Opinion in Biotechnology*, pp. 775–783. doi: 10.1016/j.copbio.2011.04.024.

Zhang, Y., Biggs, J. D. and Mukamel, S. (2015) 'Characterizing the Intermediates Compound i and II in the Cytochrome P450 Catalytic Cycle with Nonlinear X-ray Spectroscopy: A Simulation Study', *ChemPhysChem*. WILEY-VCH Verlag, 16(9), pp. 2006–2014. doi: 10.1002/cphc.201500064.

2 A unique dimeric structure of the cytochrome P450 peroxygenase from *Kocuria rhizophila*

Alessia C. Andrews[1], Sarah Mathews[1], Kan Lan Tee[1], Harshwardhan Poddar[1], Kirsty J. McLean[3], Hazel M. Girvan[3], Tom Jowitt[2], Kamilla Pocholarz[1], Colin W. Levy[1], David Leys[1], and Andrew W. Munro[1]*

[1]Manchester Institute of Biotechnology, Faculty of Life Sciences, University of Manchester, 131 Princess Street, Manchester M1 7DN, UK.

[2]Micheal Smith Building, Faculty of biology medicine health, University of Manchester, Dover St, Manchester, M13 9PT, UK

[3]Department of Biological and Geographical Sciences, School of Applied Sciences, University of Huddersfield, Queensgate, Huddersfield, HD1 3DH, UK

2.1 Abstract

Peroxygenases are a distinct class of the P450 superfamily, which have evolved to use hydrogen peroxide to drive catalysis, bypassing the requirement for redox partner proteins and expensive cofactors. On account of their natural alkene producing abilities, members of this P450 group are of significant interest to the petrochemical and fine chemical industry. Here we present the biochemical and structural characterisation of a novel biotechnologically important CYP152 peroxygenase from the bacterium *Kocuria rhizophila* (CYP152T1, or P450 KR). Substrate turnover reactions and subsequent metabolite analysis have affirmed the versatile abilities of P450 KR. Primarily, P450 KR functions as a mid-chain length fatty acid (C10:0 – C18:0) decarboxylase generating C_{n-1} terminal alkenes. In addition, P450 can serve as a hydroxylase, producing to 2-hydroxy and 3-hydroxy hydroxylated fatty acids. Further studies have also revealed that the use of alternative substrates and novel oxidation methods can lead to a more varied peroxygenase product profiles. Via extensive crystallographic and biophysical analysis, the novel dimeric structure of KR has been revealed. An extended N-terminal helix from one monomer forms "zipper"-like interactions with the corresponding helix on the partner monomer. These interactions are stabilised by disulphide bonds formed between two cysteine residues located at the base of the N-terminal helix and in an adjacent beta sheet element within the same monomer. These unusual structural interactions are unprecedented for a P450 enzyme.

2.2 Introduction

Cytochromes P450 (P450 or CYP) are a superfamily of heme-*b*-containing enzymes found throughout nature (Munro, Girvan and McLean, 2007). They have been described as "nature's most versatile catalyst" in light of the vast range of chemical reactions that they catalyse (Coon, 2005). These include hydroxylation, demethylation, isomerisation, epoxidation C-C cleavage and sulfoxidation (Guengerich and Munro, 2013); as well as some more exotic reactions, including cyclopropanation and Kemp elimination (redox-mediated conversion of 5-nitro-benzisoxazole-4-nitrophenol) catalysed by engineered P450 enzymes (Wang *et al.*, 2014; Li *et al.*, 2017).

Most P450 catalyse the reductive scission of dioxygen bound to the heme iron, relying on the delivery of two electrons acquired from pyridine nucleotide coenzymes (e.g., NADH or NAD(P)H). The electrons are then transported to the heme at discrete points in

the catalytic cycle by one or more redox partners (Munro, Girvan and McLean, 2007). The first electron reduces the ferric substrate bound state to the ferrous state, with subsequent binding of O_2. The second electron delivery leads to the production of the ferric peroxy form. Two successive protonation's then occur to produce the hydroperoxo-ferric intermediate (compound 0, Cpd 0), and heterolysis of the O—O bond and formation of compound I (Cpd I, Fe^{IV}=O porphyrin radical cation), the highly reactive ferryl iron oxo species (Rittle and Green, 2010). In a typical P450-mediated reaction (e.g. fatty acid hydroxylation, as catalysed by the well-studied *Bacillus megaterium* P450 BM3 enzyme) Cpd I abstracts a hydrogen atom from a substrate CH group to give compound II (Cpd II, a Fe^{IV}=OH state) and a substrate radical (Munro *et al.*, 2002). Cpd II reacts with the substrate radical by rebounding the hydroxyl group to generate a hydroxylated product (Denisov *et al.*, 2005). However, the type of reaction and type of product formed is highly dependent on the P450 involved and the nature of the substrate. To attain the diverse breadth of chemical reactions, P450s can also interact with one or more redox partners to source their reducing equivalents (McLean *et al.*, 2005).

A vast majority of P450s rely on NAD(P)H-dependent redox partner systems. In bacterial and some eukaryotic mitochondrial systems, the P450 typically interacts with a soluble FAD-dependent NAD(P)H-specific ferredoxin reductase and a 2Fe-2S cluster-containing ferredoxin (or a flavodoxin in some cases). Eukaryotic systems, such as mammalian liver cells, rely on an integral membrane-bound cytochrome P450 reductase (CPR), a fusion evolving from 2Fe-2S ferredoxin with a ferredoxin reductase, where ferredoxin binding was lost in favour of FMN binding (Hannemann *et al.*, 2007). However, recent years has seen the discovery of many distinct types of P450 that do not fall into class I/II. One of the first major outliers was identified as highly efficient fusion protein from P450 BM3 from *Bacillus megaterium* (CYP101A1) that has eukaryotic-like CPR fused to the C-terminus of the P450 heme domain (Munro *et al.*, 2002).

An alternative route to driving P450 catalysis is to use the "peroxide shunt" mechanism, in which hydrogen peroxide (H_2O_2) or an organic peroxide (e.g. cumene hydroperoxide) is used to convert the ferric substrate-bound P450 directly to the ferric hydroperoxo (Fe^{III}-OOH) state, known as Compound 0 (Cpd 0) (Shoji and Watanabe, 2014). Generally, this route is rarely efficient and can lead to oxidative modifications of the heme and the

protein, leading to loss of P450 activity. However, a specific class of bacterial P450s, known as the peroxygenase family, have been recognised to effectively push H_2O_2-driven substrate oxidation (Matsunaga *et al.*, 1996).

A breakthrough came in this field with the discovery and characterisation of *Sphingomonas paucimobilis* P450 SPα (CYP152B1) and *Bacillus subtilis* P450 BSβ (CYP152A1), which were initially shown to catalyse hydroxylation of fatty acid substrates either exclusively at the α-position, or both α- and β-positions, respectively (Matsunaga *et al.*, 1997, 1999). Later studies by Rude *et al*. identified CYP152 peroxygenase family members from other bacteria, including *Kocuria rhizophila, Microbacterium populi, and Jeotgalicoccus sp.* Each of the CYP152 P450s from these organisms were capable of catalysing the oxidative decarboxylation of palmitic acid (C16:0) to 1-pentadecene, in addition to hydroxylating at the α and/or β positions (Rude *et al.*, 2011).

The discovery of terminal alkene producing abilities in various members of the CYP152 family has driven further research in this area with respect to potential exploitation of these enzymes for advanced biofuel production. One of the notable members in this group is the *Jeotgalicoccus* sp. $OleT_{JE}$ (CYP152L1) P450, which is a particular efficient peroxygenase in terms of alkene production and catalyses oxidative decarboxylation of fatty acids from C10:0 – C20:0. This leads to generation of C_{n-1} terminal alkenes as the major product, with small amounts of α- and β- hydroxylated products (Rude *et al.*, 2011; Liu *et al.*, 2014).

Stopped flow experiments by Makris and co-workers, revealed transient formation of the reactive Fe^{IV}=O porphyrin cation radical (Cpd I), with addition of hydrogen peroxide to a $OleT_{JE}$-arachidic acid complex. A kinetic isotope effect for Cpd I decay suggests that it abstracts a substrate hydrogen atom with the formation of a substrate radical and the Fe^{IV}-OH compound II. Subsequent studies identified an unusually long-lived Cpd II species that is directly produced from substrate C-H abstraction, following the decay of the Cpd I intermediate (Grant, Hsieh and Makris, 2015). A proposed mechanism for decarboxylation (**figure 2.1**) involves the $OleT_{JE}$ Cpd II abstracting a substrate electron to yield a carbocation intermediate poised for C—C_α cleavage to yield a terminal alkene and CO_2 (Grant, Mitchell and Makris, 2016b).

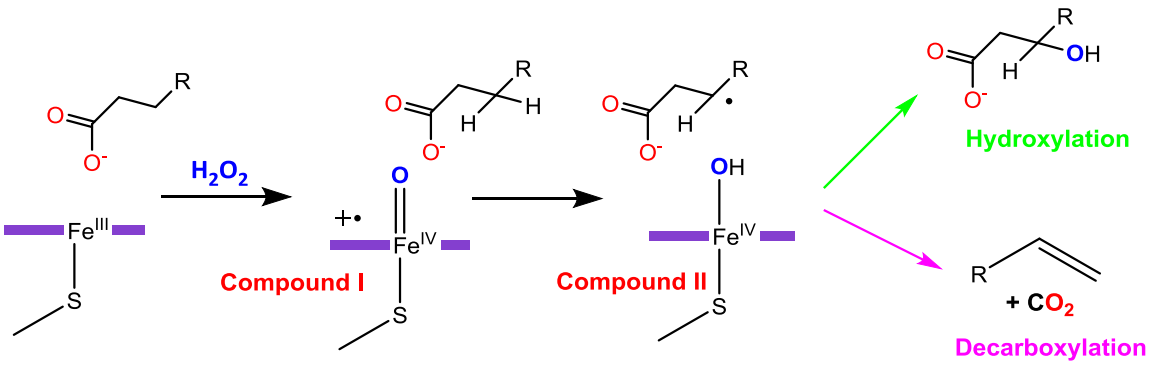

Figure 2.1 Proposed reaction mechanism of CYP152 peroxygenases. Direct conversion to transient ferric hydroperoxo species, Compound 0 (not shown) by H_2O_2 with the dehydrated to the ferryl-oxo porphyrin species (Compound I), abstraction of a hydrogen atom yields Compound II and a substrate radical. Here, the reactions can bifurcate producing hydroxylated fatty acids via oxygen rebound or decarboxylation via a second H-atom of the Cβ carbon.

Studies on P450 peroxygenases such as $OleT_{JE}$, have proved productive in identifying a biocatalyst capable of generating alkenes. The bio-catalytic conversion from the fatty acid pathway to alkenes can provide a renewable resource for both fuels and industrial chemicals. To date, there have been number of attempts at engineering a genetically tractable organism, such as *E. coli* or *Saccharomyces cerevisiae*, for this purpose. These include (i) use of a *Streptomyces* Type I polyketide synthase (SgcE) and its cognate thioesterase (TE). SgcE10 was expressed in *E. coli* to overproduce pentadecaheptane, followed by its hydrogenation to form pentadecane (Liu *et al.*, 2015); (ii) utilisation of a two-step pathway from cyanobacteria; consisting of an acyl ACP reductase (AAR) with a aldehyde deformylating oxygenase (ADO) which convert fatty acyls to alkanes (Schirmer *et al.*, 2010; Li *et al.*, 2012), or insect P450 CYP4G1 (and CPR) oxidative decarbonylasez, producing long chain alkanes (Qiu *et al.*, 2012); and a three gene cluster from *Micrococcus luteus* producing long chain alkenes with internal double bonds produced from head-to-head condensation of two fatty acyl-coenzyme A molecules (Beller, Goh and Keasling, 2010; Christenson *et al.*, 2017).

However, among these pathways, the step catalysed by CYP152 family member $OleT_{JE}$ provides the simplest one, with a one-step decarboxylation, utilising free fatty acids instead of fatty acid thioesters, which is advantageous as the abundance of free fatty acids in the metabolic pathway can be manipulated in *E. coli* (Liu *et al.*, 2012). In view of the potential industrial applications of $OleT_{JE}$, we have aimed to identify other homologues from the CYP152 peroxygenase family. Here, we present the first report of the expression, enzymatic characterisation, and structural analysis of a P450

peroxygenase from the soil bacterium *Kocuria rhizophila* (named P450 KR, CYP152T1), which shows 30% similarity to $OleT_{JE.}$ P450 KR CYP152T1 determined by Nelson, DR (2009) (The Cytochrome P450 Homepage. Human Genomics 4, 59-65). The enzyme has a novel N-terminal extension that is shown to facilitate the dimerisation of this P450 through interactions made with the same polypeptide region in the opposite monomer. This is the first report of a P450 forming this unusual dimeric interaction.

2.3 Materials and Methods

2.3.1 Bioinformatics

The amino acid sequence of $OleT_{JE}$ and P450 KR was used to search for related P450 peroxygenase enzymes from other bacteria (Rude *et al.*, 2011). Protein alignments and sequence identity data were obtained using the NCBI BLAST program and standard parameters (https://blast.ncbi.nlm.nih.gov/Blast.cgi).

2.3.2 Gene expression and general biological methods

2.3.2.1 P450 KR

The gene encoding P450 KR from *Kocuria rhizophila* was codon optimised and synthesised for expression in *E. coli* (Thermo Fisher Scientific, Bremen, Germany) and cloned into the pET24b vector using NdeI and EcoRI restriction sites, incorporating a TEV cleavage site and a N-terminal polyhistidine tag (6-His). The pET24b-P450 KR plasmids were transformed into *E. coli* C41 (DE3) competent cells. Bacteria were grown in 1 L 2xYT cultures with 50 µg mL^{-1} kanamycin, and with agitation at 180 rpm at 37°C until OD_{600} of 0.6-0.8 was reached. The temperature was reduced to 25°C, 450 µM of δ-aminolevulinic acid (Δ-ALA) was added and gene expression was induced with 1 mM IPTG. Cells were grown for a further 20 hours. Cells were harvested by centrifugation at 6880 x *g* at 4°C in a JLA-8.1000 rotor using an Avanti J-26 XP centrifuge. Cell pellets were washed in PBS buffer (10 mM Na_2HPO_4, 1.8 mM KH_2PO_4, 2.7 mM KCl, 137 mM NaCl, pH 7.4), centrifuged again and stored at -20°C.

2.3.2.2 Formation of the of P450 Δα35-KR deletion variant

A variant of KR that had a N-terminal helix deletion (with removal of 35 residues from the N-terminal α-helix) was created by site directed mutagenesis using the Q5 site-directed mutagenesis kit (as per manufacturer's instructions). The oligonucleotide primers used to create the 35 residue deletion were: Forward: 5'-

TCCCTGGAAGTACAGATTTTCGCGG-3', Reverse: 5'-AGCGATTCCGGTTGCCC-3'. The PCR samples were then mixed with 2X KLD reaction mixture and 10X KLD enzyme mix containing kinase, DNA ligase and DpnI enzymes. The reaction was mixed for 5 mins at room temperature. The mixture was then transformed using NEB 5-α *E. coli* cells. The transformation protocol was as described in (Orkin, 1990). Expression of Δα35-KR variant was as WT P450 KR in **2.3.2.1**.

2.3.2.3 TEV protease

The pRK793 plasmid was a gift from David Waugh (Addgene plasmid # 8827). It encodes the catalytic domain of the tobacco etch virus (TEV) protease with a N-terminal His-tag and a C-terminal polyarginine tag and was cloned into the pMal-C2 vector using SacI and BamHI restriction sites (Kapust *et al.*, 2001). The pRK793 plasmid was transformed into *E. coli* C41 (DE3) cells and these were grown in 1 L 2xYT cultures with 50 μg mL^{-1} carbenicillin with agitation at 180 rpm at 37°C until an OD_{600} of ~0.5 was reached. The temperature was reduced to 18°C and gene expression was induced with 100 μM IPTG. Cells were grown for a further 24 hours. Cells were collected as described above.

2.3.2.4 Flavodoxin and flavodoxin reductase

The genes for *E. coli* flavodoxin (Fld) and flavodoxin reductase (FldR) were cloned into the pET16b vector using restriction sites (NcoI and BamHI for FldR). The pET16b-Fld plasmid was transformed into JM109 competent cells, and bacteria were grown in 1 L LB cultures with 50 μg mL^{-1} ampicillin, and with agitation at 180 rpm at 37 ^{o}C until an OD_{600} of 0.8-0.9. Cultures were supplemented with 5 mg L^{-1} of riboflavin and gene expression was induced with 100 μM IPTG. Cells were then grown for a further 6 hours. Cells were collected by centrifugation at 6880 g at 4°C in a JLA-8.1000 rotor using an Avanti J-26 XP centrifuge and stored at -20^{o}C. The pET16b-FldR plasmid was transformed into HMS174 DE3 cells. Bacteria were grown in 1 L LB cultures with 50 μg mL^{-1} ampicillin and with agitation at 180 rpm at 37^{o}C until an OD_{600} of 0.8-0.9 was reached. Gene expression was induced with 100 μM IPTG. Cells were grown for a further 3 hours before being collected by the same method as used for Fld.

2.3.3 Protein purification

2.3.3.1 P450 KR

P450 KR over-expressing cells were weighed and resuspended in buffer A (100 mM KPi, 750 mM NaCl, 10% glycerol, pH 8.0), with the addition of SigmaFAST Protease Inhibitor Cocktail Tablets (EDTA-free), 10 µg mL^{-1} DNase and 10 µg mL^{-1} lysozyme, along with a ~100 mg of $MgCl_2$ and 20 mM imidazole. Cells were lysed by sonication on ice using a Bandelin Sonopuls sonicator for 45 minutes (10 s on, with 50 s off intervals) at 40% amplitude. The cell homogenate was then centrifuged at 235,000 x g for 45 minutes using a Ti45 rotor. The supernatant was filtered using a Sartorius Minisart NML Syringe filter (0.45 µM)

Nickel-iminodiacetic acid (Ni-IDA) chromatographic medium (Generon, Maidenhead, UK) was equilibrated with 20 mM imidazole contained in Buffer A and incubated with the supernatant (10 mL per 100 g cell pellet) for 1 hour at 4°C. The material was then packed onto a column and washed with 10 column volumes (CV) of 40 mM imidazole in buffer A, subsequently with another 10 CV of 60 mM imidazole in buffer A, with the flow-through collected. P450 KR was eluted with 300 mM imidazole in buffer A. Imidazole was removed from the sample using a PD-10 desalting column (GE Healthcare) isocratically with buffer A. The His-tag was then removed from P450 KR by incubating the protein fraction with TEV protease (2:5 molar ratio, respectively) overnight at 4°C. The protein solution was then loaded onto a Ni-IDA column that had been pre-equilibrated with buffer A. His-tag free protein was eluted using 20 mM imidazole in buffer A. P450 KR was concentrated using a Vivaspin (30,000 MWCO; GE Healthcare). Subsequently, a further gel filtration purification step was done using a Superdex 200 16/600 column (GE Healthcare) pre-equilibrated with buffer A. P450 KR was then flash frozen in liquid nitrogen and stored at -80°C.

2.3.3.2 TEV protease production

TEV protease expressing cells were resuspended in buffer B (0.1 M KPi, 0.75 M NaCl, 20 % glycerol (pH:0)) with the addition of 20 mM imidazole, 10 µg mL^{-1} DNase, ~100mg $MgCl_2$, 10 µg mL^{-1} RNAse and 10 µg mL^{-1} lysozyme, along with SigmaFAST Protease Inhibitor Cocktail Tablets (EDTA-free) (1 per 100 mL) and 1% 2-mercaptoethanol. Cells were lysed by sonication on ice using a Bandelin Sonoplus sonicator for 45 minutes (10 s on, with 50 s off intervals) at 40% amplitude. The supernatant was separated from the

cellular debris using a similar method to that described above. The supernatant was filtered using a Sartorius Minisart NML Syringe filter (0.45 µM). Ni-IDA chromatographic medium (Generon, Maidenhead, UK) was equilibrated in 20 mM imidazole in Buffer B and incubated with the supernatant (10 mL per 100 g cell pellet) and then incubated for 1-2 hours at 4°C. The material was then packed into a column and the resin was washed with 10 CV of 20 mM imidazole in buffer B and 10 CV of 50 mM imidazole in buffer B. TEV protease was then eluted in 250 mM imidazole in buffer B. The fractions were checked for purity and integrity by SDS-PAGE.

2.3.3.3 Production of *E. coli* flavodoxin and flavodoxin reductase

Fld and FldR expressing cells were resuspended in buffer C (50 mM KPi, pH 5.0) and buffer D (50 mM Tris, 1 mM EDTA, pH 7.2), respectively. SigmaFAST Protease Inhibitor Cocktail Tablets (EDTA-free) (1 per 100 mL) were added along with 10 µg mL^{-1} DNase and ~100 mg $MgCl_2$. Cells were lysed using a Cell Disrupter (Bio-Rad) at 17 Kpsi. The protein-containing supernatant was collected and separated from the cellular debris by the method described in section **2.3.3.1**. Fld and FldR were loaded onto a Q-Sepharose Hiprep Q XL 10/16 column attached to an AKTA pure protein purification system at 4°C. The column was charged with a high-salt buffer (Fld: Buffer E, 50 mM KPi, 1 M KCl pH 5.0) and FldR (Buffer F: 50 mM Tris, 1 mM EDTA, 1 M KCl, pH 7.2). The column was then re-equilibrated using the respective no salt buffers (Fld: buffer C, FldR: buffer D). Protein was eluted using a linear gradient from 0-1 M KCl over 15 CV. Fractions from purification were checked for quantity/purity by resolution on an SDS-PAGE gel. FldR was exchanged into buffer D, through a PD-10 desalting column (GE Healthcare, UK), before being loaded onto a Resource Q (GE Healthcare, UK) column attached to the AKTA pure at 4 ^{o}C. The column was charged with buffer F, and then re-equilibrated using buffer D. Protein was eluted using a linear gradient from 0-1 M KCl over 15 CV. Fld and FldR were concentrated using a Vivaspin concentrator (10,000 MWCO) and flash frozen in liquid nitrogen with storage at -80°C. Concentrations of Fld and FldR were determined using extinction coefficients (Fld ε_{446} = 8.25 mM^{-1} cm^{-1}; FldR ε_{456} = 7.1 mM^{-1} cm^{-1}) (McIver *et al.*, 1998; Leadbeater *et al.*, 2000).

2.3.4 Protein quantification and determination of substrate affinity

The extinction coefficient of P450 KR was determined by pyridine hemochromagen assay as discussed in (Barr and Guo, 2015), obtaining ε_{424} 75 mM^{-1} cm^{-1}. Determination

and quantification of protein integrity (i.e., retention of a cysteine thiolate proximal ligand) and its concentration was determined by generating a ferrous-CO adduct. The P450 KR heme iron was reduced with sodium dithionite, and CO gas was bubbled slowly into the solution for 30 minutes to generate the characteristic Fe^{II}-CO P450 complex. A Cary UV-Vis spectrophotometer was used to measure the spectral shift from ~418 nm (ferrous) to 448 nm (Fe^{II}-CO) and the concentration of P450 in the samples was determined using the method of Omura & Sato (1962).

UV-Visible binding titrations were done to determine the dissociation constants (K_d values) for a range of saturated fatty acids binding to P450 KR. Upon binding a substrate, the P450 heme iron undergoes a spectral shift from low-spin (424 nm) to high-spin (~390 nm), which can be followed by UV-Vis spectroscopy. Titrations were carried out in a 1 cm path-length quartz cuvette at 25°C using 4-6 µM protein. All fatty acid substrates used (C8:0 – C18:0) were dissolved in ethanol. Optimisation of reaction mixtures ensured that the total volume of substrate (and thus solvent carrier) was below 5% of the total volume in the cuvette. Spectra were recorded between 800-300 nm for the substrate-free enzyme and following each 0.1 µL addition of fatty acid substrate using a Hamilton microlitre syringe. Titrations were carried out until no further heme spectral changes occurred.

Data analysis and fitting were undertaken using OriginPro software (OriginLab). Data were analysed by subtracting the spectrum for the ligand-free protein from each of the fatty acid-bound spectra post substrate addition in order to generate a set of difference spectra for each substrate. From these, the maximum and minimum wavelengths were identified. The overall absorbance change was calculated by determining $\Delta(A_{peak} - A_{trough})$ using the same wavelength pair throughout, and these data were then plotted against the relevant ligand concentration to determine dissociation constant (K_d) values. Data were fitted using the relevant equation. For substrates with sigmoidal dependence of absorbance change on substrate concentration, the Hill equation was used ($\Theta = [L]^n / K_D + [L]^n$) where the number of bound ligands *n* is the Hill coefficient (Prinz, 2010).

2.3.5 Redox potentiometry

Midpoint potentials for the P450 KR heme Fe^{III}/Fe^{II} redox couple were determined by spectroelectrochemical redox titrations at 25 °C inside an anaerobic glove box (Belle Technology, Weymouth UK), under a nitrogen atmosphere with O_2 levels maintained

below 3 ppm. All solutions were deoxygenated by sparging with nitrogen gas. All titrations were performed using ~10 µM P450 KR in buffer A. For substrate-bound P450 KR, decanoic acid (C10:0, 400 mM stock in ethanol) was added until no further conversion of the heme iron to a high-spin state was observed (~4 mM decanoic acid). Mediators were added to expedite electronic equilibration in the system (2 µM phenazine methosulfate, 7 µM 2-hydroxy-1,4-naphthoquinone, 0.3 µM methyl viologen, and 1 µM benzyl viologen) to mediate in the range from +100 to −480 mV vs. the normal hydrogen electrode (NHE). Midpoint potentials were determined by fitting heme absorbance versus applied potential data using the Nernst equation (Dutton, 1978; Daff *et al.*, 1997).

2.3.6 EPR analysis of P450 KR

Continuous wave X-band electron paramagnetic resonance (EPR) spectra of the P450 KR heme were obtained at 10 K using a Bruker ELEXSYS E500 EPR spectrometer equipped with an ER 4122SHQ Super High Q cavity. Temperature was controlled using an Oxford Instruments ESR900 cryostat connected to an ITC 503 temperature controller. Microwave power was 0.5 milliwatts, modulation frequency was 100 KHz, and the modulation amplitude was 5 G. EPR spectra were collected from P450 KR (285 µM) in the substrate-free form and using near-saturating amounts of lauric acid (~1 mM) and myristic acid (~0.7 mM), and with 5 mM decanoic acid. All samples were prepared in buffer A with the EPR spectrum of buffer A recorded and subtracted from the EPR spectra for P450 KR samples in the same buffer. EPR spectra were also collected under the same conditions for P450 KR samples (360 µM) bound to imidazole (250 mM) and to 4-phenylimidazole (5 mM).

2.3.7 *In vitro* substrate turnover of P450 KR

All reactions contained 1 µM KR enzyme, 500 µM fatty acid substrate (C10:00, C12:00, C14:00 and C16:00) with a final volume of 0.5 mL in buffer A (0.1 M KPi, 0.75 M NaCl, 10 % glycerol (pH 8.0)). Hydrogen peroxide driven reactions also contained 500 µM H_2O_2. Two redox-dependent reactions used either 20 µM *E. coli* flavodoxin (Fld) and 5 µM flavodoxin reductase (FldR), or 20 µM ferredoxin (spFdx) from *Spinacia oleracea* (spinach) and 5 µM of FldR. Both redox-dependent samples also contained a NADPH regeneration system consisting of 0.5 mM NADPH, 0.5 mM $NADP^+$, 10 mM glucose-6-phosphate (G-6-P), and G6P dehydrogenase (1.5 units per reaction).

All reactions were incubated at 27^{o}C for 30 minutes with shaking at 700 rpm. Reactions were stopped using 40 µL of 37% HCl. Internal standards (different chain lengths) were added (50 µM *n*-1 alkene, 50 µM fatty acid, 25 µM 2-OH fatty acid, and 25 µM 3-OH fatty acid). Reactions were extracted using equal quantities of dichloromethane (DCM). The DCM layer was removed and dried using anhydrous $MgSO_4$, and mixed with equal volumes of *N*,*O*-*bis*(trimethylsilyl)trifluoroacetamide (BSTFA) containing 1% trimethylchlorosilane (TMCS), and incubated at 60^{o}C for 45 minutes to derivatise the fatty acids.

Directly after derivatisation, 1 µL of the sample was injected onto a 5975 series MSD coupled to a 7890 GC system, installed with a VF5 ht 5% phenyl-methyl column (30 m, 0.25 mm, 0.25 µm). The front inlet was set at 250^{o}C, and a split ratio of 10:1 was used. The column flow was set at 1.2 mL min^{-1}, and the oven was held at 40^{o}C for 1 min before being ramped at 10^{o}C min^{-1} until a temperature of 250^{o}C was reached. Ramping was then increased to 100^{o}C min^{-1} until a temperature of 350^{o}C was reached, and this condition was held for 2 minutes. The solvent delay was set at 2.5 minutes. Electron ionization was used, and m/z ratios of 40–500 were recorded at 5 Hz and at 230^{o}C. Quantification of products formed were estimated using external standard calibration curves and internal standards.

2.3.8 Nano electrospray ionisation (ESI) mass spectrometry

KR was exchanged into 500 mM ammonium acetate buffer (pH 6.8) using a P2 Desalting column (GE Healthcare) for the oxidised sample. For the reduced sample, KR was exchanged into 500 mM ammonium acetate and 1 mM DTT (pH 6.8) also using a P2 Desalting column (GE Healthcare). MS and ion mobility (IM)-MS data were acquired on the Synapt G2S HDMS (Waters, Manchester, UK). NanoESI capillaries were prepared in-house from thin-walled borosilicate capillaries (inner diameter 0.9 mm, outer diameter 1.2 mm, World Precision Instruments, Stevenage, UK) using a Flaming/Brown P-1000 micropipette puller (Sutter Instrument Company, Novato, CA, USA). A positive voltage was applied to the solution via a platinum wire (Goodfellow Cambridge Ltd, Huntington, UK) inserted into the capillary. The following source conditions were applied: capillary voltage ~1.4 kV, sampling cone 60-200 V, source temperature 60°C. The pressure of the backing region was 7.5 mbar. For the IM, the helium cell and the IMS gas flows were 180 and 90 mL/min, respectively, the IMS wave velocity was 400 m/s, and the IMS wave

height was 35 V. Nitrogen was the carrier gas. Data were acquired and analysed using MassLynx software (Waters, Manchester, UK).

2.3.9 Analytical Ultracentrifugation (AUC)

KR was exchanged into buffer B (0.1 M Tris-HCl, 0.75 M NaCl, (pH 8.0)) and buffer B with 1 mM Tris(2-carboxyethyl)phosphine (TCEP), and diluted to concentrations of 1, 2, 4, 9, 17 and 25 µM before being loaded into a six-sector Epon charcoal-filled centrepiece equipped with quartz windows for sedimentation equilibrium analysis. Sedimentation velocity AUC experiments were performed using an XL-A ultracentrifuge (Beckman Instruments) with an An-50 Ti rotor at 133 000 x *g* at 20˚C. In this case samples were loaded into two-sector centrepieces with quartz glass windows. The sedimentation boundaries were monitored every 90 seconds using wavelengths 420 nm, 440 nm and 480 nm. Analysis of the data for sedimentation velocity was performed using Sedfit (Brown and Schuck, 2006). Analysis of the data from sedimentation equilibrium was carried out using Heteroanalysis. Vbar was set to 0.74 ml/g using extinction coefficients of 2.285E+5 and 4.88E+4. Analysis of self-association was performed using both the average mass from a single ideal species model and from a monomer-dimer model and fitted using Logistic5 in OriginPro.

2.3.10 Size Exclusion Chromatography Multi-Angle Light Scattering (SEC-MALS)

The oligomeric state of P450 KR was assessed using SEC-MALS. Purified samples (0.5 mL) were loaded onto a Superdex 200 (GE Healthcare) at 0.75 mL min^{-1} with a constant flow of buffer B (0.1 M KPi, 0.75 M NaCl, pH 8.0), and the samples were passed through a Wyatt Heleos II EOS 18-angle laser photometer coupled to a Wyatt Optilab rEX refractive index detector. Data analysis was performed (Hydrodynamic radii and molecular mass measurements were analysed) using ASTRA 6 software (Wyatt Technologies).

2.3.11 Crystallisation of KR

The purified P450 KR was concentrated to 10 mg ml^{-1}, using Vivaspin concentrators (30,000 MWCO). Commercial screens (SG1TM Screen, JCSG-plus™, Morpheus® II, PACT premier™ from Molecular Dimensions) were used to set up crystallisation trials in sitting drop plates. A nanodispenser (Mosquito TTP Labtech) was used to set up drops of 400 nL volume, in a ratio of 1:1 (protein:reservoir) and these were left to equilibrate at 4°C. Crystals appeared in the following condition: 0.17 M ammonium sulphate, 25.5% PEG

4000, and 15% glycerol (JCSG plus HT-96 condition D9). Crystals were frozen by directly plunging into liquid nitrogen.

2.3.12 Data collection, structural determination and analysis

Diffraction data were collected on the IO3 beamline at the Diamond Synchrotron. Data scaling and merging were performed using XDS (Kabsch, 2010) and Aimless (Evans and Murshudov, 2013). The protein crystallised in the C2 space group with 3 monomers making up the asymmetric unit and a solvent content of ~48% (Matthew's coefficient 2.38).

Molecular replacement was performed using PHASER (McCoy *et al.*, 2007) from the CCP4 ('The CCP4 suite: Programs for protein crystallography', 1994) software suite. The previously solved crystal structure of $OleT_{JE}$ from a *Jeotgalicoccus* sp. (PDB 4L54) was used as a search model (Belcher *et al.*, 2014). Iterative cycles of refinement in REFMAC5 (Vagin *et al.*, 2004) together with manual model building in COOT (Emsley *et al.*, 2010), were used to improve the structures. Final cycles of refinement were performed in Phenix Refine (Adams *et al.*, 2010). The final statistics for the structure are given in **table 2.1**.

Structure analysis and figure preparation were performed using PyMOL (Schrödinger, 2015). Calculation of Cα-backbone RMSD values and superposition was carried out using the protein structure comparison service Fold at the European Bioinformatics Institute (PDBeFold) (Krissinel and Henrick, 2004).

Table 2.1 Statistics from crystallography for the P450 KR structure.

Data collection	
Space group	C2
Cell dimensions	
a, b, c (Å)	130.5, 147.3, 90.0
a, b, g (°)	90.0, 127.1, 120.0
Resolution range (Å)	29.55 – 3.03
R_{merge}	0.09 (0.61)*
I / sI	10.5 (1.7)
Completeness (%)	99.3 (95.7)
Redundancy	3.4 (3.4)
Refinement	
Resolution (Å)	29.5 – 3.0
No. reflections	26385
R_{work} / R_{free}	22.2 / 25.6
No. of residues	
Protein	1148
Water	---
Ligand	3 Heme
B-Factors (Å^2)	
Protein	66.3
Ligand	46.2
R.m.s. deviations	
Bond lengths (Å)	0.003
Bond angles (°)	0.640
Ramachandran	
Favoured (%)	95.8
Allowed (%)	3.8
Outlier (%)	0.4

2.4 Results and Discussion

2.4.1 Expression and purification of KR

Protein expression in *E. coli* resulted in cell pellets and extracts that were red in colour, suggesting successful heme incorporation into the protein. During the development of the purification process, we noticed the precipitation of P450 KR in low salt buffer, an observation similar to that made for $OleT_{JE}$ studied by Belcher *et al.*, (2014). Subsequently, only high salt buffers were used with P450 KR (buffer A: 0.1 M KPi, 0.75 M KCl, 10 % glycerol, pH 8:0). Purification was achieved through a three-step chromatographic process, involving an initial Ni-IDA affinity chromatography step, removal of His-tag and size exclusion chromatography, with samples being use for crystallography and biophysical characterisation. P450 KR expresses well, with 5 g of cell pellet yielding ~100 mg of purified protein (**figure 2.2**).

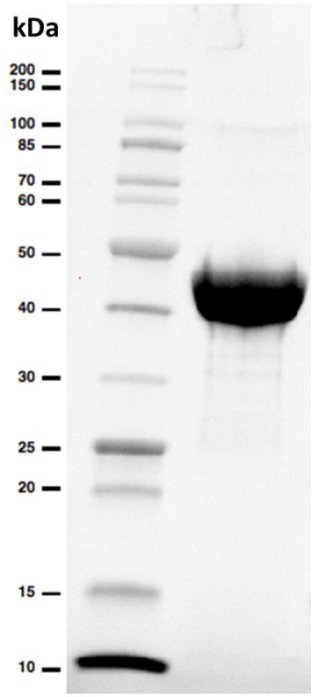

Figure 2.2 12% SDS PAGE gel showing purity of P450 KR. The first lane shows the markers of indicated sizes (NEB unstained protein standard). Purified non-tagged P450 KR is in lane 2, and shows protein isolated from *E. coli*, following Ni-IDA chromatography, his-tag removal through TEV protease cleavage, reverse Ni-IDA chromatography, and a subsequent gel filtration.

2.4.2 UV-visible absorption properties of P450 KR

Purified, tag-free P450 KR was analysed by UV-visible spectroscopy to establish the characteristics of the heme prosthetic group. **Figure 2.3** shows the characteristic absorption spectra of the pure P450 KR in its oxidised (Fe^{III}), sodium dithionite-reduced (Fe^{II}), ferrous-CO bound (Fe^{II}-CO), and ferric-nitric oxide bound (Fe^{III}-NO) form. The enzyme was eluted from the column in a low-spin ferric state, with major Soret absorption features at 424 nm and smaller α- and β-band features at ~576 nm and ~541 nm, respectively. The β-band is more pronounced, while the α-band is weaker and appears more as a shoulder on the β-band. These absorption features have been red-shifted compared to those for typical low-spin CYP152 members and other bacterial cytochrome P450s: e.g. OleT decarboxylase from *Jeotgalicoccus* (CYP152L1) with major absorption features at 418, 566 and 535 nm; *Bacillus megaterium* fatty acid hydroxylase P450 BM3 (CYP102A1) heme domain at 418, 535 and 568 nm; the *Mycobacterium tuberculosis* cyclodipeptide C-C bond forming (CYP121A1) at 416.5, 538 and 568 nm; and the camphor hydroxylase P450cam from *Pseudomonas putida* at 417 nm, 537 nm and 570 nm (McLean *et al.*, 2002; Girvan *et al.*, 2004; Murugan and Mazumdar, 2005; Belcher *et al.*, 2014). The shift of the main Soret band absorbance to longer wavelengths

(a P450 type II spectral shift) is usually indicative of a replacement of the distal water molecule (the sixth ligand to the heme iron) with a stronger ligand, including nitrogen-containing compounds such as imidazole. In view of the unusual red-shifted Soret spectroscopic feature and the use of imidazole during Ni-IDA affinity chromatography, the affinity of P450 KR for imidazole was investigated. Dialysis of the purified P450 KR in imidazole-free buffer failed to shift the absorption maximum of the P450 KR heme, suggesting that either imidazole binds extremely tightly to the P450 KR heme iron, or that an endogenous ligand (potentially the imidazole side chain of a histidine residue) occupies the distal position on the heme iron.

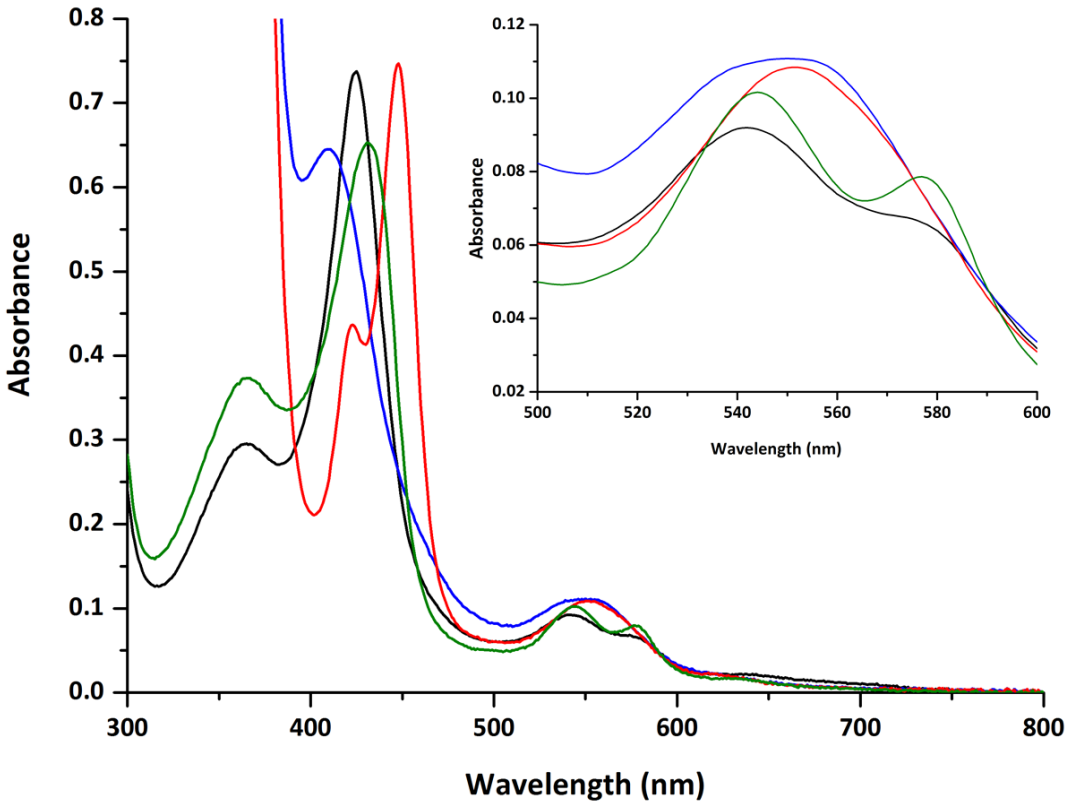

Figure 2.3 UV-visible spectroscopic features of P450 KR. UV-visible absorption spectra for P450 KR (~4.5 µM) are shown for the substrate-free ferric state (black) with Soret maximum at ~424 nm, sodium dithionite reduced ferrous state (blue), with Soret shifting to ~418 nm and the ferrous-CO bound complex (red) with diagnostic peak at 448 nm, and NO-bound complex (green) with Soret absorbance at 430 nm. Inset shows magnification of the Q-band region.

Imidazole is usually a weak inhibitor of P450s. For instance, the *M. tuberculosis* sterol demethylase CYP51B1 and the orphan *M. tuberculosis* P450 CYP144A1 have K_d values for imidazole of 11.7 ± 0.9 mM and 3.0 ± 0.7 mM, respectively (McLean *et al.*, 2006; Driscoll *et al.*, 2011). However, imidazole does bind to the Royal Demolition Explosive (RDX) degrading XplA (CYP177A1), with a K_d of 1.6 ± 0.1 µM (Sabbadin *et al.*, 2009).

However, in this case, the structural organisation of the XplA distal pocket enables a near-ideal geometry of the heme iron coordination, as well as an extended active site water-mediated hydrogen bonding network to the non-coordinating nitrogen atom of the imidazole (Sabbadin *et al.*, 2009; Bui *et al.*, 2012).

Due to uncertainty of the unusual Soret absorbance, we first investigated the binding of imidazole to low spin P450 KR, but there was negligible difference in the heme spectrum. To obtain an estimate of affinity for imidazole, a titration was instead done using a decanoic acid-bound form of P450 KR, resulting in an apparent binding constant ($K_{d\ (app)}$) of 2.2 ± 0.1 mM. Assuming competitive binding and with knowledge of the K_d for the binding of decanoic acid to P450 KR (1.69 ± 0.04 mM) (**table 2.2**) and the quantity of substrate added (4.8 mM), a "true" P450 KR imidazole K_d was determined as 445 ± 35 μM. This data suggests that P450 KR binds imidazole and that the unusually red-shifted P450 KR Soret feature at 424 nm likely does not result from distal ligation of the heme iron by imidazole retained from the Ni-IDA purification step.

For verification that endogenous heme iron coordination produces the unusual 424 nm Soret feature in P450 KR, we expressed and purified P450 KR using the Strep-tag/Step-Tactin system in the absence of any exogenous imidazole during purification. **Figure 2.4** shows Strep-Tactin-purified P450 KR enzyme in its ferric resting state has UV-visible absorption features similar to those observed in the Ni-IDA-purified P450 KR, with the Soret peak at 424 nm and the α- and β-bands at ~575 nm and ~542 nm. These data confirm that imidazole does not play a role and suggest that there may be an endogenous distal ligand that is causing the spectral peak at 424nm rather than an exogenous ligand binding to the protein.

The P450 KR heme iron is readily reduced by sodium dithionite to give a Soret band of diminished intensity that is blue shifted to 410 nm, with a broadened merged peak in the alpha/beta (Q-band) region at ~555 nm, consistent with the retention of cysteine thiolate proximal coordination to the ferrous heme iron. Addition of carbon monoxide produced a characteristic P450 Fe^{II}-CO heme spectrum, with the Soret band shifted to 448 nm and a merged Q-band feature at 550 nm (**figure 2.3**). A smaller peak at ~423 nm likely indicates a small amount of the P420 form likely arising from cysteine thiol-coordination in a proportion of the P450 KR Fe^{II}-CO complex (Perera *et al.*, 2003). The

NO-bound P450 KR also exhibits spectral features typical of other P450-NO adducts, with an asymmetric Soret peak at 431 nm and α- and β-bands with enhanced intensity at 577 nm and 544 nm. Using the method of Berry and Trumpower, (1987) an extinction coefficient of ε_{424} = 75.5 mM^{-1} cm^{-1} was established for the purified, substrate-free ferric form of P450 KR.

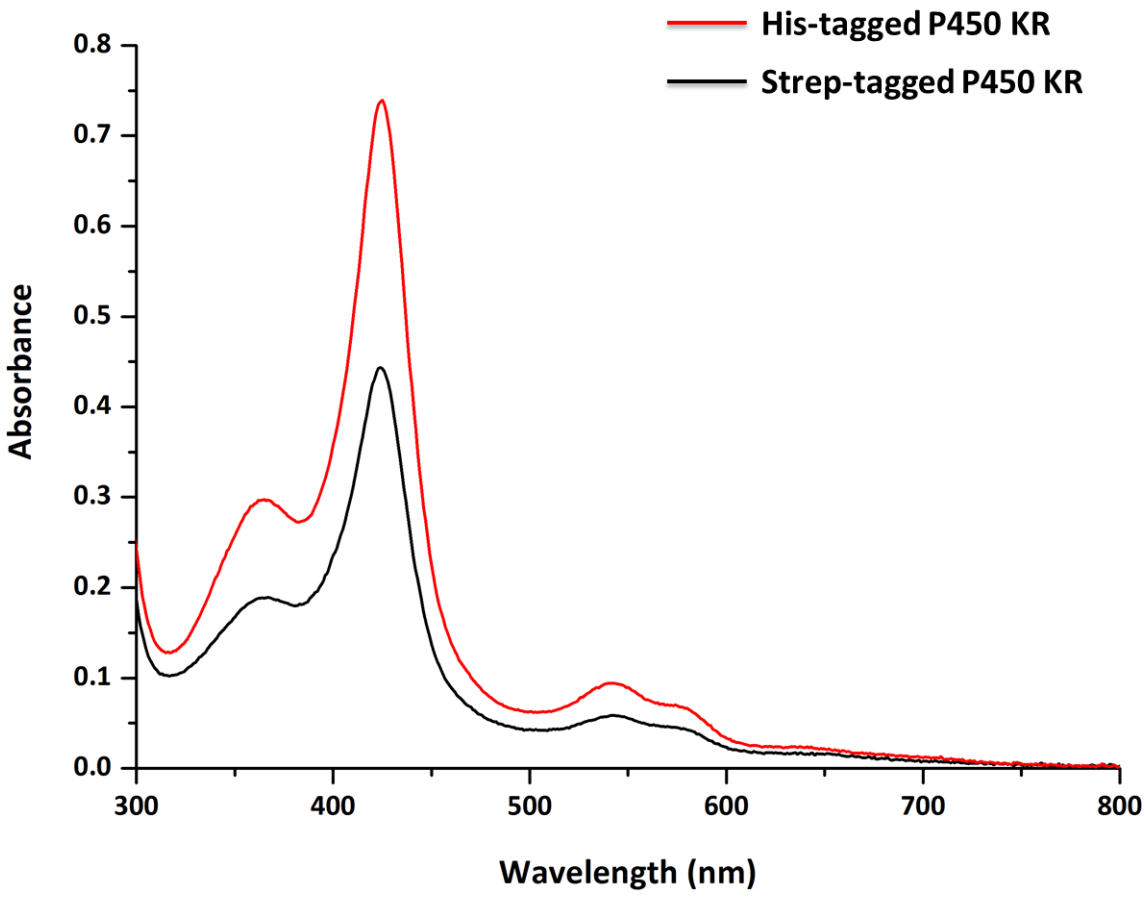

Figure 2.4 UV-vis spectrum of P450 KR with alternative tagged systems. P450 KR purified with a N-terminal polyhistidine tag (~9 μM) with a Soret absorbance at 424 nm (red) and P450 expressed with a strep-tag (~5 μM) with also a Soret absorbance at 424 nm (black).

2.4.3 Substrate binding studies

The binding of a substrate to P450 enzymes is often associated with the alteration in the spin state of the ferric heme iron, usually through displacing the weakly bound 6th water ligand, which induces a shift from the low spin (LS) state of the ferric iron to the high-spin (HS) state. A range of saturated fatty acid substrates with varied chain lengths were investigated for the binding to P450 KR, and all were found to induce a LS-to-HS heme iron transition, with the Soret band shifting from 424 nm to 397 nm. The K_d values for fatty acid binding to P450 KR and the extent of spin-state shift induced by substrates tested are shown in **table 2.2**, and **figure 2.5**, respectively. The shorter chain substrates

give a more extensive heme shift, with substrates such as C10:0, C12:0 and C14:0 displaying 100 – 90% shifts. Although the shortest fatty acid chain length tested C8:0 (7.27 ± 0.17 mM) displayed the weakest affinity towards KR, the affinity increased significantly as the chain length of the substrate increased (1.95 ± 0.09 μM for C18).

Table 2.2 Determination of affinity of P450 KR against fatty acid substrates. All data were fit using the Hill equation, *n* represents the number of binding sites.

Fatty acid substrate	Dissociation constant (K_d)	High spin heme (%)
C8:0 (octanoic acid)	7.27 ± 0.17 mM (*n* = 1.43 ± 0.04)	100
C10:0 (decanoic acid)	1.69 ± 0.04 mM (*n*= 1.94 ± 0.08)	93
C12:0 (lauric acid)	71.07 ± 0.83 μM (*n*= 2.49 ± 0.07)	92
C14:0 (myristic acid)	17.35 ± 0.25 μM (*n*= 2.28 ± 0.07)	90
C16:0 (palmitic acid)	3.33 ± 0.11 μM (*n*= 2.32 ± 0.19)	55
C18:0 (stearic acid)	1.95 ± 0.09 μM (*n*= 2.13 ± 0.26)	16

The level of the HS state decreases as the chain length increases, C16:0 (palmitic acid, 55 %) and C18:0 (stearic acid, 16%) (shown in **figure 2.5C**). The extent of the spin-state shift induced by saturated fatty acids is not dissimilar to that observed for the alkene producing peroxygenase $OleT_{JE}$ (27 – 84%). However, $OleT_{JE}$ displays the greatest spin-state shift for the long-chain fatty acids (C20:0, arachidic acid), whilst KR exhibits an extensive spin-state shift upon binding to shorter chain fatty acids (C10:0 – C14:0) (Belcher *et al.*, 2014). The K_d values for P450 KR for the fatty acids tested differ by >3 orders of magnitude (7.27 mM for decanoic acid to 1.95 μM for stearic acid). Under similar assay conditions, the K_d range for $OleT_{JE}$ is less extensive (from 2.3 μM with arachidic acid to 59.2 μM with lauric acid). These data suggest that P450 KR is a more selective enzyme compared to $OleT_{JE}$, although its general affinity for fatty acid substrates is slightly lower compared to $OleT_{JE}$. The relatively low affinity of P450 KR for fatty acids seems to suggest that these are not its natural substrates. The genus *Kocuria* also includes phenol-degrading strains, which might mean that it prefers aromatic substrates. However, trials with potential substrates (see **figure 2.5D**) including hydrocinnamic acid, indole-3-propanol, alpha-methylcinnamic acid and 4-(methyl-thio)-

benzoic acid did not exhibit any significant HS accumulation nor enzymatic turnover with the P450 KR enzyme.

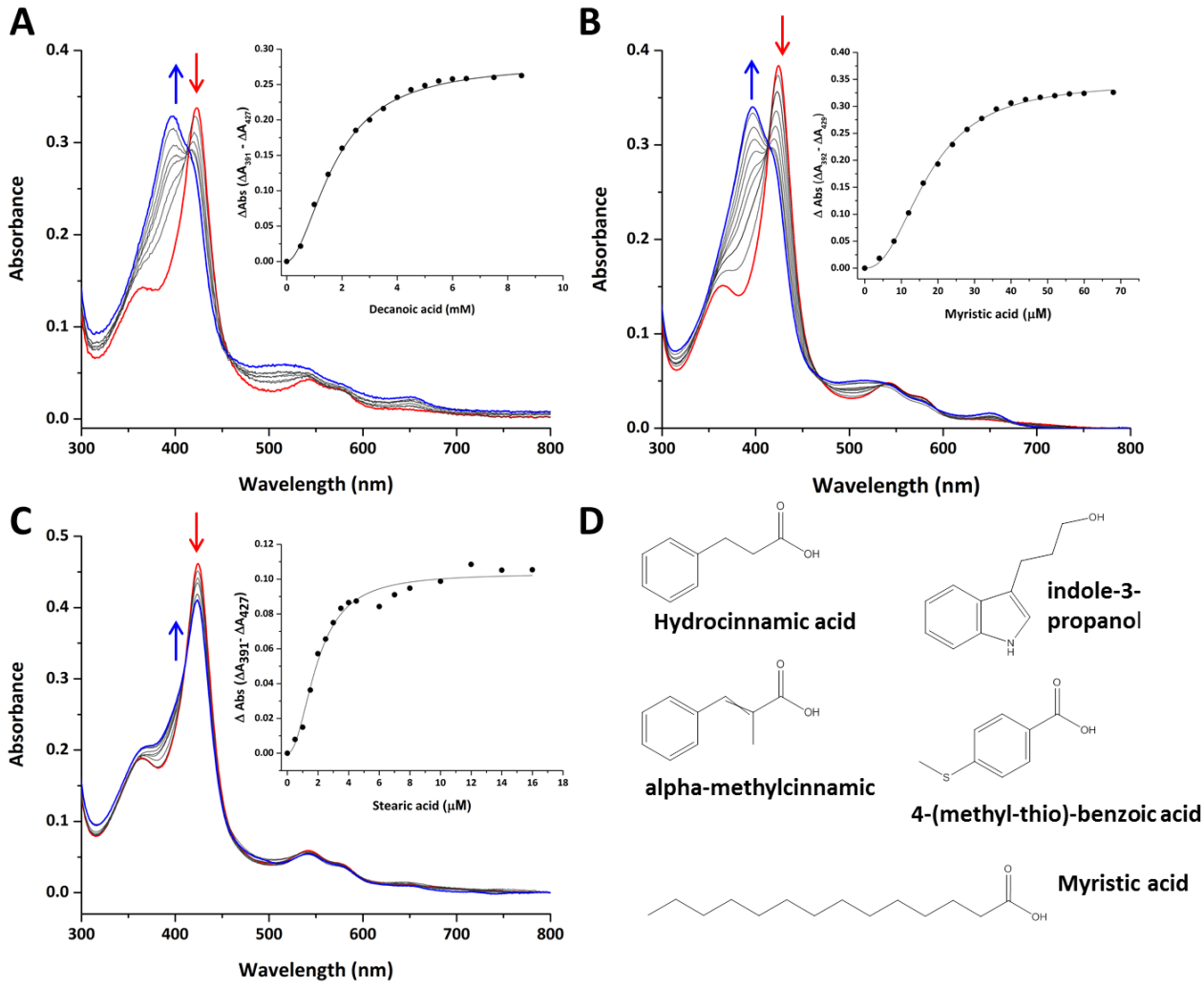

Figure 2.5 Fatty acid binding titrations with P450 KR. Panel A shows the UV-visible (UV-vis) spectral binding titration of P450 KR (~4.7 μM) with decanoic acid (C10:0). Low-spin (LS) ferric KR (substrate-free) is shown in red with a Soret absorbance at 424 nm. The addition of substrate causes a significant shift to the high spin (HS) state (blue line) at ~397 nm. Insert shows the induced absorbance changes versus decanoic acid concentration, fitted to the Hill equation to yield a K_d of 1.69 ± 0.04 mM. Panel B shows the UV-vis spectrum of KR with myristic acid (C14:0), illustrating the conversion of LS ferric KR (~5.1 μM) (424 nm) to a HS heme form (397 nm). Insert shows the induced absorbance changes versus [myristic acid], fitted to the Hill equation to yield a K_d of 17.35 ± 0.25 μM. Panel C shows the UV-vis spectral binding titration of KR (~5 μM) with stearic acid (C18:0). LS heme (424nm) shifts slightly to HS-heme (397 nm) with addition of substrate. Insert shows the induced absorbance change versus [stearic acid], fitted to the Hill equation to yield a Kd of 1.95 ± 0.09 μM. Panel D shows example of alternative substrates used in binding and turnover studies with P450 KR.

2.4.4 Heme iron redox potential of P450 KR

Oxidation-reduction (redox) potentiometry can be used to understand the energetics of biological electron-transfer process and the reactions coupled to electron transfer and determine redox potential of proteins (Dutton, 1978). For most soluble bacterial

systems, binding of a fatty acid substrate in the active site along with dehydration of water as the 6th axial ligand and the induced spin state shift of the ferric heme iron is correlated to increase in redox potential, which permits electron flow to the heme iron (Daff *et al.*, 1997; Das, Grinkova and Sligar, 2007). **Figure 2.6** shows spectra from spectroelectrochemical titrations of both substrate-free and decanoic acid-bound forms of P450 KR, illustrating progressive conversion of the ferric enzyme to the ferrous state upon addition of dithionite reductant. Substrate-free P450 KR (**figure 2.6A**) has ferric Fe^{III} Soret maximum at 424 nm with the dithionite reduced state, the ferrous Fe^{II} form absorbing maximally at 408 nm with a slightly lower Soret intensity, and α- and β-bands merging into a single peak at 550 nm. These data are consistent with retention of cysteine thiolate proximal coordination of the heme iron in the ferrous state of substrate-free P450 KR (Sligar and Gunsalus, 1976; Daff *et al.*, 1997). The decanoic acid-bound P450 KR (**figure 2.6B**) in its ferric state is predominantly in the HS state, with a Soret peak at 398 nm and a shoulder at ~415 nm for the LS component. Following reduction by dithionite, the Soret peak is shifted to 424 nm with a shoulder at ~398 nm. The spectral features in the Q-band region are distinct from those seen in the spectrum for substrate-free, ferric P450 KR (**figure 2.3**) and from those for the reduced, substrate-bound P450 KR. The asymmetric Q-band feature has a peak at 558 nm, with a pronounced shoulder at ~530 nm. These spectral data are consistent with the reduced, substrate-bound P450 KR having a mixture of cysteine thiol-/thiolate-coordination of the ferrous heme iron. The reduction of the decanoic acid-bound P450 KR is further confirmed by the abolition of the HS ferric heme iron-to-cysteine thiolate charge-transfer (CT) band at ~650 nm at the end of the reductive titration.

A shift in the heme iron spin-state equilibrium from LS to HS is often associated with development of a substantially more positive ferric heme iron potential, which facilitates efficient electron transfer from the redox partner to the P450 heme. Examples include P450 BM3 (-429 to -289 mV upon arachidonic acid binding) (Daff *et al.*, 1997). Additionally P450cam (-300 to -170 mV upon camphor binding), This change in electron potential now allows electron flow from the redox-partner, putidaredoxin with potential of -235 mV (Wilson, Tsibris and Gunsalus, 1973; Sligar and Gunsalus, 1976). However, spectroelectrochemical titrations with the determination of the midpoint potentials for the Fe^{III}/ Fe^{II} heme iron couples versus the normal hydrogen electrode (NHE)

demonstrated both the substrate-free (-129 ± 3 mV vs. NHE) and decanoic acid-bound (-149 ± 4 mV vs. NHE) forms of P450 KR revealed quite similar midpoint potentials. Although the heme iron potential is slightly more negative in decanoic acid-bound P450 KR. There is no substantial increase in heme iron potential associated with the accumulation of the HS ferric form. This is unlike redox-partner dependent cytochrome P450s which rely on electron flow to push the catalytic cycle. For example P450 cam which shows a camphor-dependent increase in redox potential of the heme iron from -303 to -270 mV (substrate-free) to -173 to -163 mV (camphor-bound) (Sligar and Gunsalus, 1976). This change in electron potential now allows electron flow from the redox-partner, putidaredoxin with potential of -235 mV (Wilson, Tsibris and Gunsalus, 1973).

While the P450 KR heme iron potential values are more positive compared to those for most other bacterial P450s, they are similar to those for the alkene-producing P450 $OleT_{JE}$ (-103 ± 6 mV for the substrate-free enzyme and -105 ± 6 mV for the arachidic acid-bound enzyme) (Belcher *et al.*, 2014). The similarity in the redox properties of the heme irons in these peroxygenase P450s is consistent with their performing the same types of reaction (albeit with some differences in their fatty acid substrate specificity profile). As was postulated for $OleT_{JE}$, lack of a major change in heme iron potential on binding decanoic acid substrate to P450 KR may be due to the proximity of the negatively charged substrate carboxylate group to the heme, counteracting any positive shift in potential resulting from accumulation of HS ferric heme iron.

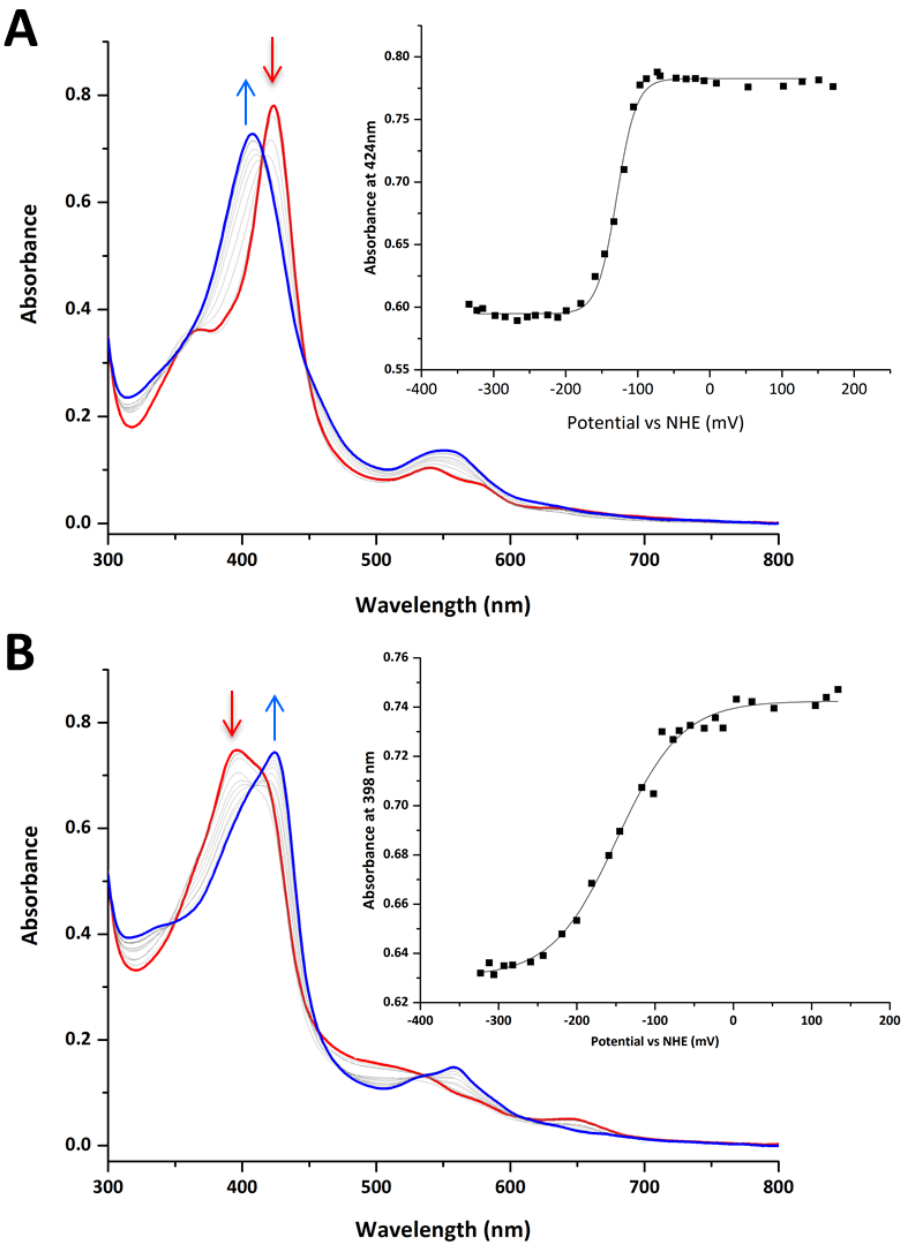

Figure 2.6 Heme iron redox potential of substrate-free and decanoic acid-bound P450 KR. Panel A shows the spectroelectrochemical redox titration of P450 KR (~10 µM). The UV-vis spectrum of KR is shown in oxidised substrate-free form with Soret absorbance at 424 nm (red), with the titration of sodium dithionite, with the final reduced form shown with a Soret 408 nm (blue), and the characteristic single Q-band feature at 550 nm. The inset shows the plot of absorbance at Soret peak (424 nm) versus the applied potential corrected for the normal hydrogen electrode (NHE). Data were fitted using the Nernst equation to give a midpoint potential of E°' = -129 ± 3 mV. Panel B shows the redox titration of P450 KR (~10 µM) in the substrate (decanoic acid) bound species with a Soret absorbance at 398 nm (red), with the reduced form at ~424 nm (blue). The insert shows the plot of absorbance at Soret peak (398 nm) versus the applied potential corrected for the NHE. Data were fitted using the Nernst equation to give a midpoint potential of E^0 = -149 ± 4 mV. The arrows indicate the direction of changes in absorbance during the reductive part of the titrations.

2.4.5 EPR analysis of P450 KR

Electron paramagnetic resonance (EPR) was used to probe the environment of the heme prosthetic group and coordination states upon substrate binding. EPR spectra were collected for substrate-free P450 KR and then in complex with decanoic acid, lauric acid and myristic acid (**figure 2.7**). Substrate-free P450 KR exhibits a major set of LS ferric heme *g*-values at g_z = 2.55, g_y = 2.26, and g_z = 1.85. There is a minor proportion of a second species with g_z = 2.72, possibly due to two different conformations of the sixth ligand. These *g*-values are distinct from those typically observed for LS microbial P450s, e.g. P450 BM3 (2.42/2.26/1.92) (Miles *et al.*, 1992) and P450cam (2.45/2.26/1.91) (Dawson, Anderssons and Sono, 1982). The spectral features of substrate-free P450 KR appear consistent with a nitrogen donor (or other strong donor) as the 6th heme ligand. These data were identical whether using enzyme His-tagged or Strep-tagged (absolutely no imidazole within samples). The g_z values observed (2.55 [major], 2.72 [minor]) are comparable to those for imidazole adducts of P450 BM3 (2.61/2.25/1.83) (McKnight *et al.*, 1993) and P450cam (2.56, 2.27, 1.87) (Lipscomb, 1980).

EPR spectra of substrate-bound forms of P450 KR display significant differences to that for the substrate-free form. The spectra are more heterogeneous and composed of 3-4 different LS species (**figure 2.7B-D**). In addition, there is a slight enhancement of the HS signal in each case, with small degree of splitting of the HS g_z signal in the case of decanoic acid (8.19/7.88) and lauric acid (8.16/7.80) complexes. These data suggest fatty acid binding results in a more complex mixture of heme coordination states compared to substrate-free P450 KR. This behaviour is different to that observed for $OleT_{JE}$, where the substrate-free form exhibits considerable heterogeneity with approximately five different LS species, and the arachidic acid-bound $OleT_{JE}$ has a single major LS form (2.46/2.25/1.89), in addition to a substantial HS rhombic S = 5/2 signal from two major pentacoordinate species (Schirmer *et al.*, 2010; Belcher *et al.*, 2014). A more complex mixture of species for P450 KR in the substrate-bound form may result from substrate-mediated disruption of active site water networks with displacement of the distal water ligand, enabling greater local protein flexibility that allows the P450 KR heme to explore different conformational and coordination states.

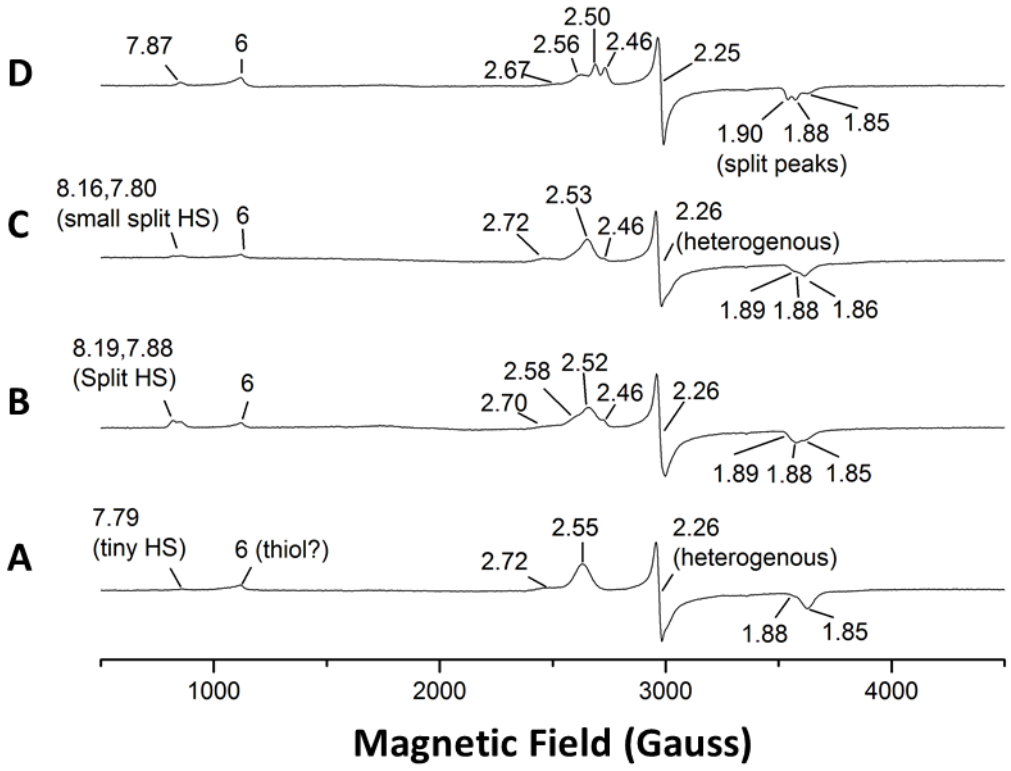

Figure 2.7 EPR spectroscopic analysis of P450 KR. X-band continuous wave EPR spectra are shown for A) P450 KR in substrate-free form, B) P450 KR with decanoic acid (C10:0), C) P450 KR with lauric acid (C12:0), and D) P450 KR with myristic acid (C14:0). The P450 KR concentration is 285 µM for substrate-free enzyme, and ~1 mM lauric acid, ~0.7 mM myristic acid and 5 mM decanoic acid added for near saturating conditions (as described in materials and methods).

2.4.6 Fatty acid conversion by P450 KR

Bioconversion of saturated fatty acids by P450 KR using H_2O_2 resulted in the generation of *n*-1 terminal alkenes, as well as α/(2)-hydroxylated and β/(3)-hydroxylated fatty acids, as determined by GC-MS analysis (**figures 2.8 – 2.10**). **Table 2.3** shows the percentage of products obtained for P450 KR-dependent turnover of fatty acids (C10:0 – C18:0). Turnover was observed for all fatty acid chain lengths tested, with the highest overall conversion of P450 KR with myristic acid (C14:0) (~89%) (**figure 2.8**). These data incorporate a ~36% conversion to 1-tridecene, ~5 % conversion to 2-OH myristic acid, and a 48% conversion to 3-OH myristic acid. Overall turnover efficiency and alkene formation reduces for both shorter chain and longer chain substrates either side of myristic acid. Stearic acid displayed the lowest overall turnover with ~6% despite displaying relatively tight binding (K_d 1.95 ± 0.09 µM). This could arise from decreased solubility of the substrate and/or higher affinity for the alkenes or hydroxylated products formed in the active site (Grant, Hsieh and Makris, 2015b; Matthews, Belcher,

et al., 2017). Despite decanoic acid displaying almost full conversion to the HS state (**figure 2.5**), it displays relatively low substrate conversion (~22 %) with 1-nonene ~8%, 2-OH 3% and 3-OH 11% (**figure 2.8**). This could arise due to P450 KR more hydrophilic nature (in comparison to $OleT_{JE}$) where the shorter chain fatty acids are withheld in the active site due to active site structural interactions.

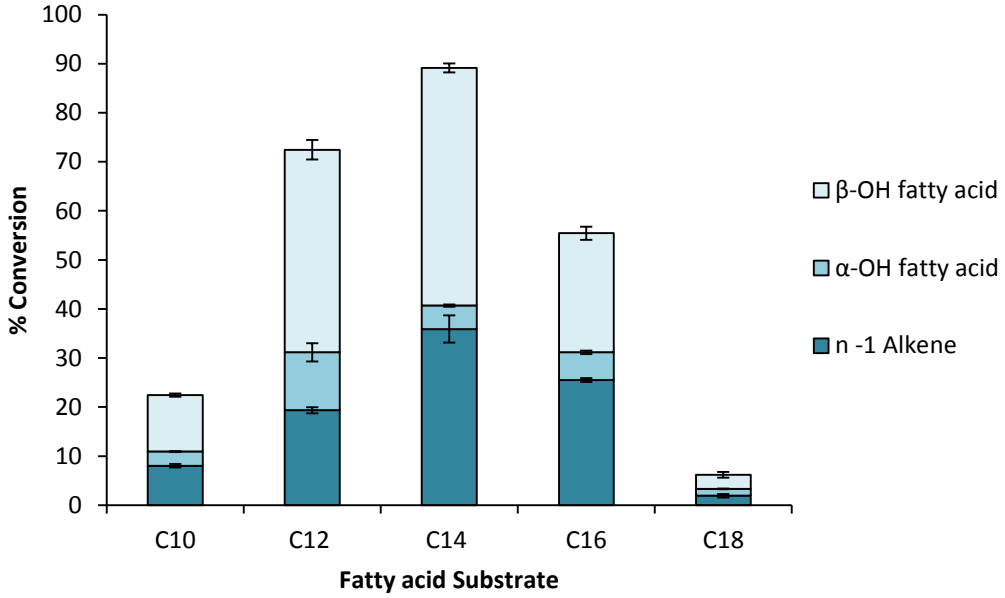

Figure 2.8 Products of fatty acid turnover from P450 KR enzymes. The bar chart shows the yields of different alkenes (n-1) (dark blue), α-hydroxy fatty acids (medium blue) and β-hydroxy fatty acids (light blue) resulting in catalytic turnover by P450 KR with saturated fatty acid substrates from C10:00- C18:00, as described in the Experimental procedures section. Data shown are the averages of three sets of experiments, with error bars shown.

$OleT_{JE}$ under similar assay conditions shows higher activity rates towards the shorter chain length fatty acids (C10:0-C14:0), with almost complete oxidation of myristic acid (C14:0) producing 72% 1-tridecene with minor quantities of C_{α}-OH FA and 25% conversion to C_{β}-OH FA (Liu *et al.*, 2014). $OleT_{JE}$ predominantly functions as a decarboxylase, with the formation of alkenes as the main reaction route for all fatty acid chain lengths (C10:0 – C20:0) tested. Turnover studies using arachidic acid (C20:0) and $OleT_{JE}$, only 1-nonadecene was detected, with negligible amounts of the hydroxylated product formed. However, KR seems to favour the hydroxylation catalytic pathway, with the α-OH and β-OH fatty acid products making up a large proportion of the total products. The ratios of products are consistent throughout the different chain lengths tested. The 3-OH fatty acid product makes up around 50 % of total turnover, and the

alkene ~ 30 – 35%. The pattern of β-hydroxylated products being more prevalent than α-hydroxylated products is also observed in $OleT_{JE}$ (Matthews, Belcher, *et al.*, 2017).

Table 2.3 Conversion of fatty acid substrates to alkene and hydroxylated products by P450 KR. P450 KR enzyme was used to catalyse H_2O_2-dependent decarboxylation and hydroxylation of saturated fatty acid substrates (C10:0 – C18:0) as described in *Materials and methods*. The mean percentage conversion of each fatty acid substrate to their respective (i) n-1 terminal alkene, (ii) 2-OH fatty acids and (iii) 3-OH fatty acids are shown.

Fatty acid substrate	*n*-1 terminal alkene (%)	2-OH fatty acid (%)	3-OH fatty acid (%)	Total conversion (%)
Decanoic acid (C10:0)	8.03 ± 0.36	2.91 ± 0.11	11.52 ± 0.33	22.46
Lauric acid (C12:0)	19.35 ± 0.64	11.81 ± 1.87	41.29 ± 2.20	72.45
Myristic acid (C14:0)	35.92 ±2.77	4.78 ± 0.24	48.42 ± 0.92	89.12
Palmitic acid (C16:0)	13.96 ± 1.59	7.65 ± 0.79	18.91 ± 1.82	40.52
Stearic acid (C18:0)	1.92 ± 0.37	1.40 ± 0.07	2.88 ± 0.58	6.20

A closer inspection of the turnover of myristic acid towards hydroxylated products saw a small distribution of peaks following the retention time of the peaks relating to the α- and β- hydroxylated products. **Figure 2.9** and **2.10** shows the representation of the mass fragments of hydroxylation of myristic acid. These demonstrate that P450 KR is able to hydroxylate further down the fatty acid chain in the γ- (4), δ- (5) and ε- (6) positions on myristic acid (**figure 2.10**). In the case for Lauric acid (C12:0) the hydroxylation products extend further down the fatty acid chain with the δ-(5), ε- (6), ζ- (7) positions, suggesting multiple binding modes of P450 KR active site. Palmitic acid we observe hydroxylation in the δ-position. For the shortest (C10:0) and longest chain (C18:0) we do not observe hydroxylation beyond the Cα and Cβ positions, this is could be due to the lower conversion rates. This extensive hydroxylation is also seen in CYP152 peroxygenase from *Methylobacterium populi* that also demonstrates γ-, δ- and ε- hydroxylated products for C12:0 – C18:0 fatty acids, resulting in up to 25% of total products (Amaya, Rutland and Makris, 2016). P450 KR is the second CYP152 enzyme that is able to produce these distal oxidations.

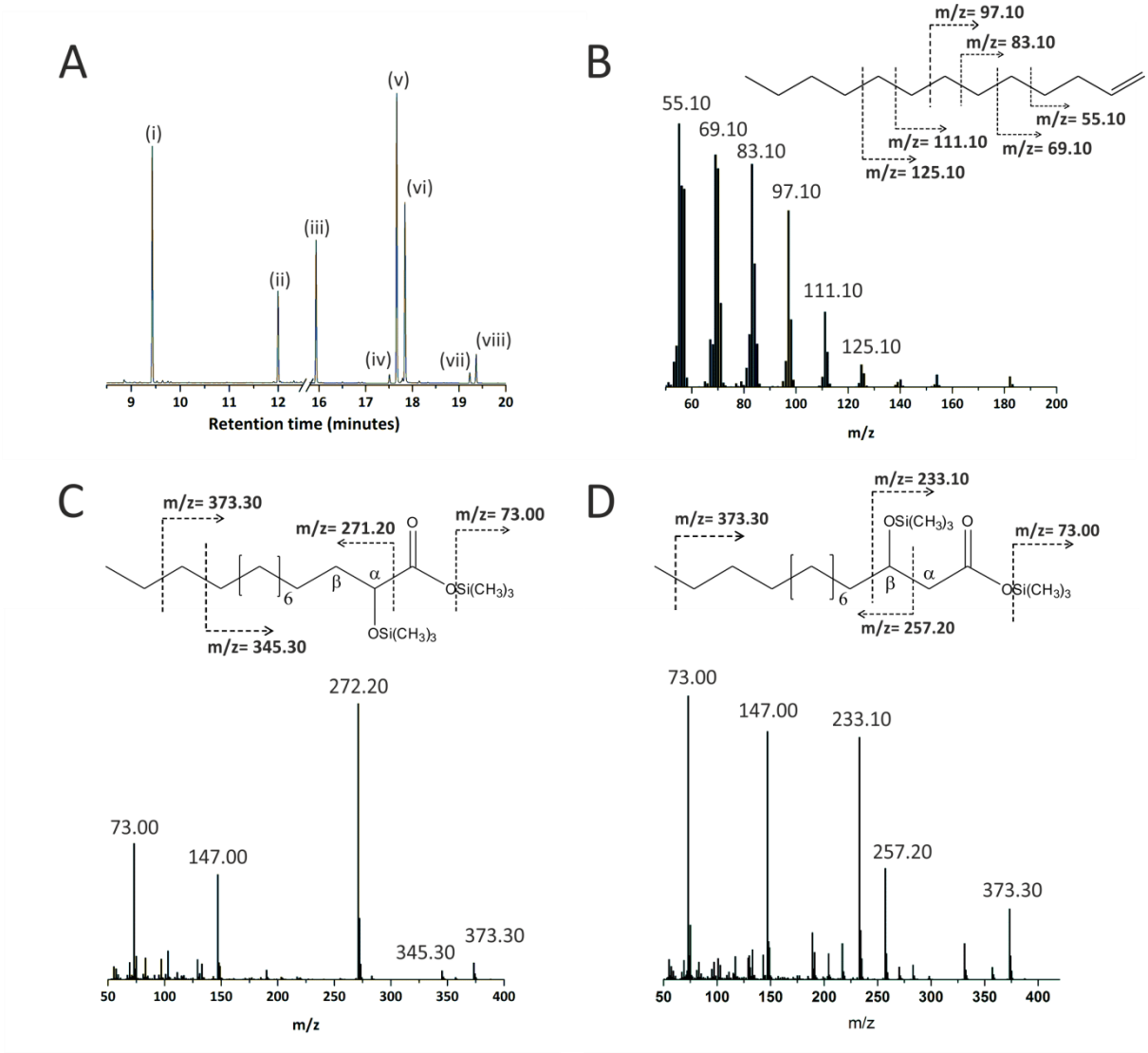

Figure 2.9 Oxidative decarboxylation and hydroxylation of myristic acid (C14:0) by P450 KR. Panel A displays the chromatogram obtained from H_2O_2-dependent turnover of myristic acid by P450 KR. Shown here are (i) 1-tridecene, (ii) 1-pentadecene (internal standard), (iii) myristic acid, (iv) α-hydroxy myristic acid, (v) β-hydroxy myristic acid, (vi) palmitic acid (internal standard), (vii) α-hydroxy palmitic acid (internal standard) and (viii) β-hydroxy palmitic acid (internal standard) and their retention times. Panel B, C and D show the ion count (mass to charge ratio (m/z) of the 3 major products produced by P450 KR with 500 µM myristic acid, with 1-tridecene, α-hydroxy myristic acid and β-hydroxy myristic acid, respectively. The inserts show the chemical structure of the compounds with fragmentation pattern (represented by the dashed arrows) to their respective m/z values.

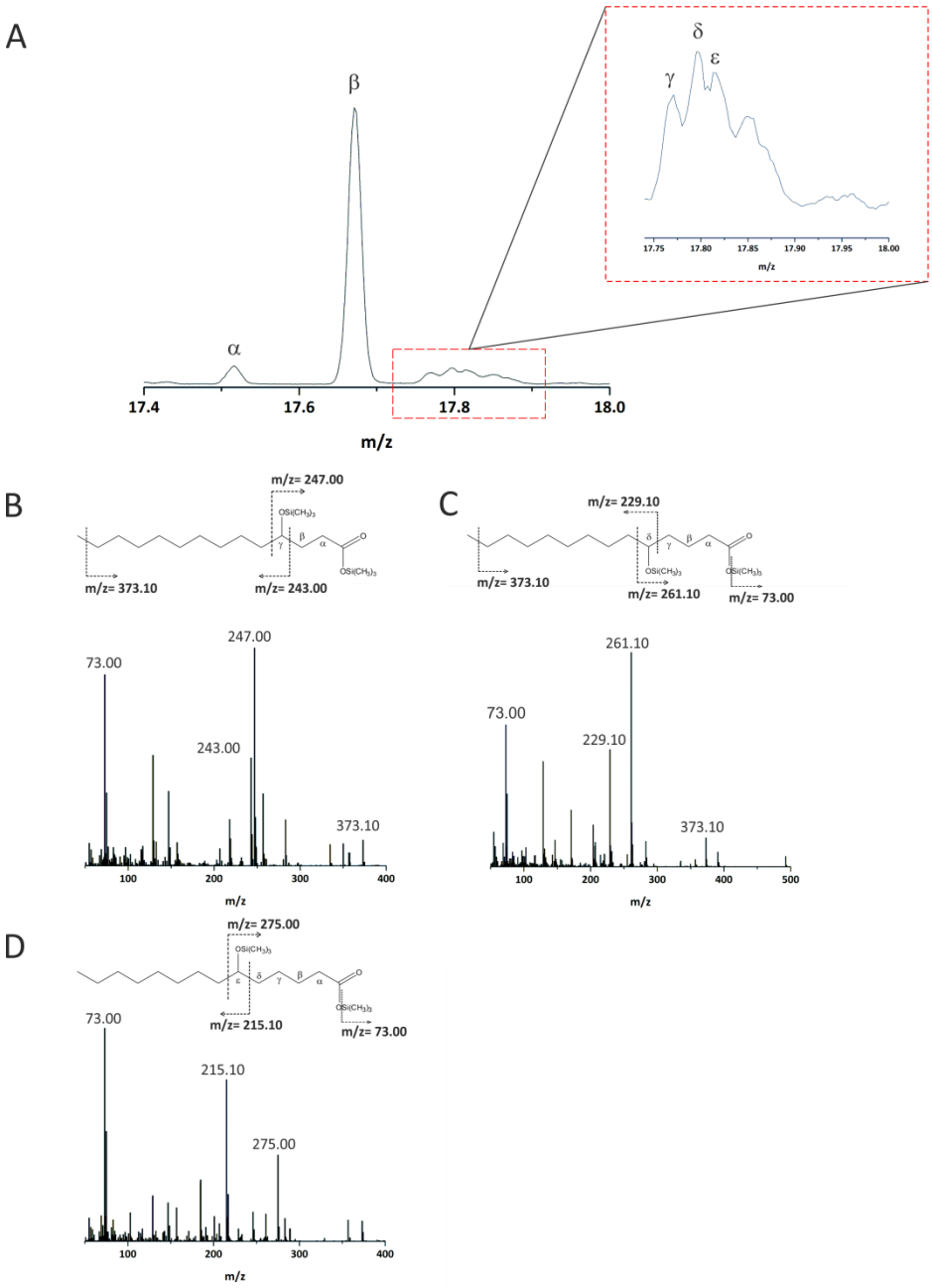

Figure 2.10 GC MS fragmentation of hydroxylated fatty acid products in reactions by P450 KR. Panel A Chromatogram obtained from H_2O_2 dependent turnover of myristic acid with P450 KR. Panel B, C and D represents the mass fragment patterns (mass to charge ratio m/z) of γ-(4), δ-(5) and ε-(6) hydroxyl myristic acid products with their major fragment ions highlighted.

2.4.7 Alternative oxidation methods to drive P450 KR

The use of H_2O_2 to initiate catalysis has been seen as a desirable attribute for leveraging key industrial transformations. H_2O_2 provides an alternative inexpensive oxidant (in comparison to NAD(P)H and redox partner proteins). However, high concentrations of the oxidant can cause inhibitory effects on the protein, such as excess oxidation of the heme and protein side chains (Wise *et al.*, 2018). To overcome this, we employed the electron-transfer components from *E. coli,* flavodoxin (Fld) and flavodoxin reductase

(FldR), and *Spinacia oleracea* ferredoxin (SpFdx) as alternative methods to drive substrate oxidation in P450 KR (**figure 2.11**). The percentage conversion of decarboxylation of C10:0, C12:0 and C14:0 fatty acid substrates were increased in both Fld/FldR and SpFdx/fldR systems. We observe an 11% increase of 1-tridecene formation with use of the SpFdx/FldR system with myristic acid, with a decrease of the β-OH FA. These data also suggest that overall turnover of decanoic acid and lauric acid increased by approximately 14% and 22%, respectively.

There have been a number of reports that show NAD(P)H-surrogate redox partners can support alkene formation with $OleT_{JE}$ and CYP152 orthologues *in vitro*. Efforts have also been explored with putidaredoxin and putidaredoxin reductase (CamAB) from P450cam with $OleT_{JE}$ that has shown to increase turnover number and obtain turnover for short-chain fatty acids (C4:0-C8:0) for the first time (Dennig *et al.*, 2015). Genetic fusions between $OleT_{JE}$ and RhFRED or the reductase domain of P450 BM3 have also shown to increase alkene formation, with the latter fusion producing 209.2 mg L^{-1} h^{-1} (Liu *et al.*, 2014; Lu *et al.*, 2018). However, a study by Wise *et al*. presented data that suggested that CYP152 family members such as $OleT_{JE}$ are unlikely to work in a redox-dependent manner (using the canonical CYP catalytic cycle), instead use of these enzymatic system stems from the adventitious production of hydrogen peroxide. This occurs through autooxidation from the oxy-ferrous complex, the redox donor, or from pyridine nucleotide itself (Wise *et al.*, 2018). From this we could suggest that increased rate of fatty acid turnover in P450 KR with redox-partner proteins could be the result sustained slow H_2O_2 release, providing a less oxidising environment for the protein and/or heme than a single spike/addition of H_2O_2. Other systems have included $OleT_{JE}$ fusion with H_2O_2-forming alditol oxidase (AldO) from *Streptomyces coelicolor* (oxidises polyols including glycerol) enabling control over activity over a prolonged period (Matthews, Tee, *et al.*, 2017a).

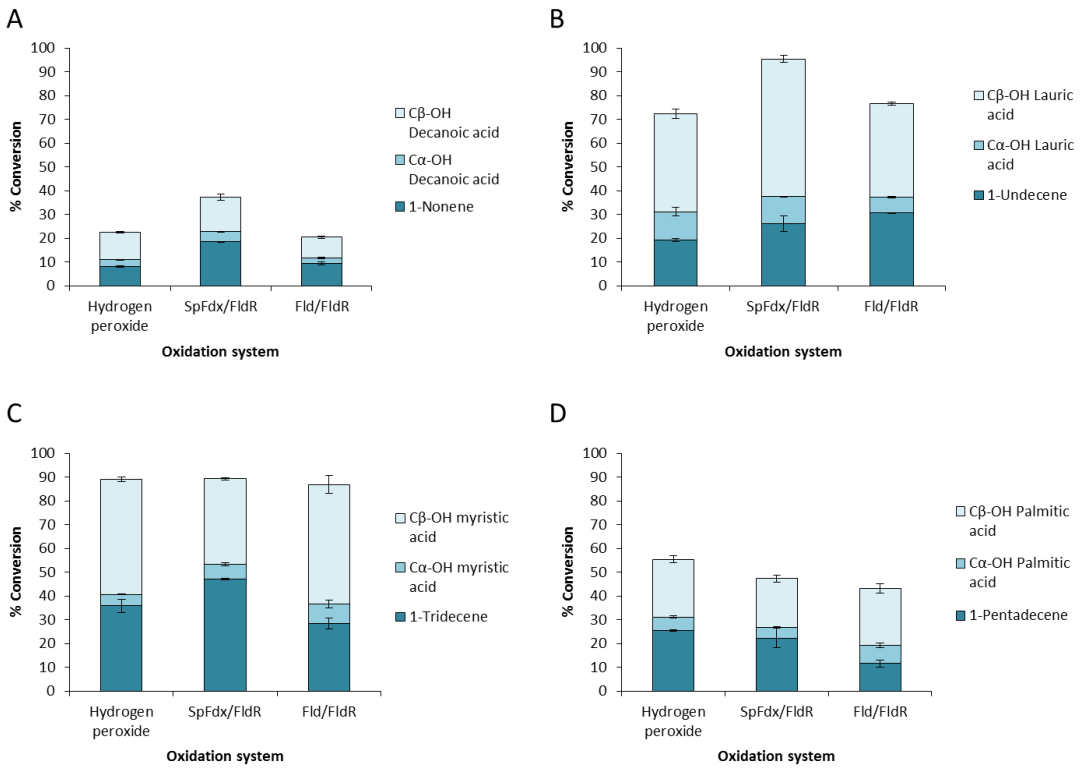

Figure 2.11 Products of fatty acid turnover with P450 KR enzymes using alternative routes for substrate oxidation. The bar charts shows the yield of *n*-1 alkenes, α-hydroxy fatty acids and β-hydroxy fatty acids resulting from catalytic turnover by: H_2O_2, spinach ferredoxin (SpFdx) and flavodoxin reductase from E.coli(FldR), and flavodoxin (Fld) and flavodoxin reductase from E.coli. Panel A shows the products formed from C10:0 substrate (decanoic acid). Panel B shows the products from C12:0 substrate of (lauric acid). Panel C shows the products formed from C14:0 substrate (myristic acid). Panel D shows the product formed from C16:0 substrate (palmitic acid).

2.4.8 Structural characterisation of P450 KR

Diffraction quality crystals appeared in a single condition and diffraction data was collected on a single crystal with the structure solved to 3.0 Å resolution. Three monomers were found to be present in the asymmetric unit of the solved structure.

Overall P450 KR displays the typical P450 fold consisting mainly of α-helices and β-sheets, resembling a triangular prism shape (Poulos, Finzel and Howard, 1987). The I-helix runs the length of the molecule on the distal side of the heme which is buried within the protein and ligated by completely conserved cysteine residue (Cys376). The overall structure of P450 KR largely resembles that of $OleT_{JE}$ the well-studied peroxygenase from the CYP152 family, despite amino acid sequence similarity of ~30% (Belcher *et al.*, 2014). Superimposition of P450 KR with CYP152 family members is shown in **figure 2.12** with root mean square deviation's (RMSD) of only 1.66 Å for 343 C_α atoms for $OleT_{JE}$, 1.73 Å for 308 C_α atoms P450 SPα and 1.80 Å for 328 C_α atoms P450 BSβ.

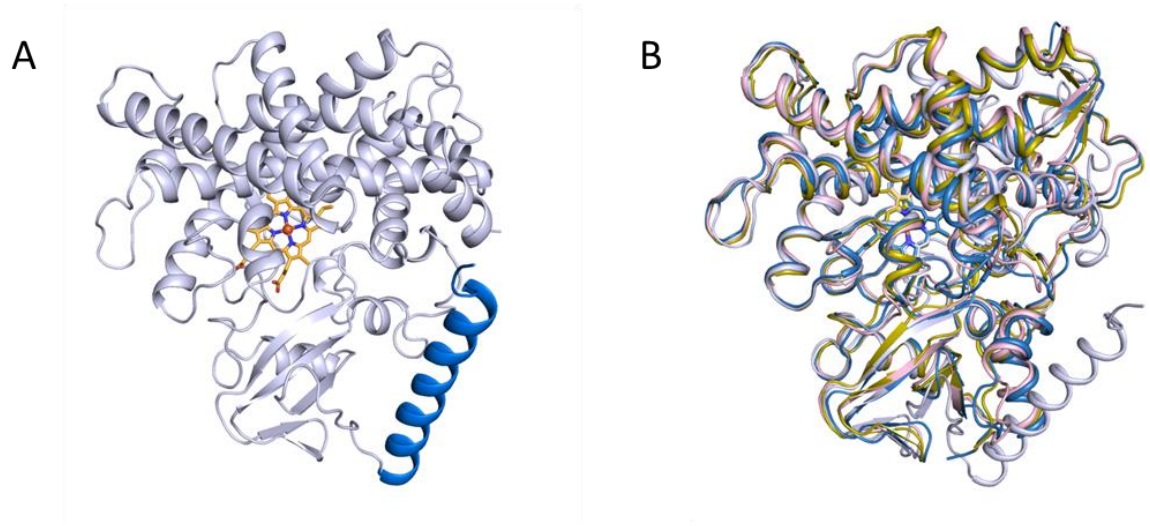

Figure 2.12 Structure of P450 KR and superimposition with CYP152 orthologues. Panel A shows the cartoon representation of the monomeric structure of KR (in grey), with the N-terminal α-helix highlighted in blue. Panel B shows the superimposed structure of P450 KR with different CYP152 peroxygenases; KR (grey), $OleT_{JE}$ (PDB: 4L40, blue), P450 Bsβ (PDB: 1IZ0, pink) and P450 SPα (PDB: 3AWM, yellow).

The structure of P450 KR displays two channels that connect the protein surface to the heme active site. The larger channel (channel I) is used as an access channel of fatty acid substrates and contains hydrophobic residues, which would provide suitable interactions for the alkyl fatty acid chain. A conserved arginine residue (Arg244) in the I-helix is placed perpendicular to the heme in the active site in P450 KR. In $OleT_{JE}$, the equivalent Arg245 residue binds to the carboxylate head group of the fatty acid, allowing the correct positioning of the Cα and Cβ carbons (5.1 and 5.7 Å, respectively) for oxidation (Belcher *et al.*, 2014). The conserved Arg residue is typically followed by proline in the I-helix in the CYP152 family. The P450 KR Arg244/Pro245 residues are conserved in $OleT_{JE}$ (Arg245/Pro246) and replace the "acid-alcohol" pair that is conserved in nearly all monooxygenase P450s that are required for protonation of the iron-oxo species in the P450 catalytic cycle (Raag *et al.*, 1991). This major structural change is an evolutionary adaptation consistent with the peroxygenase mechanism in these P450s (i.e. H_2O_2 interacts with the ferric heme iron converts it to a ferric-hydroperoxo Cpd 0 species that is readily protonated and then undergoes dehydration to form Cpd I).

We see in other CYP152 family members that they major products alter between organism (e.g. P450 SPα CYP152B1 from *S. paucimobilis* makes (C6:0- C18:0) α-FA; and P450 K6 CYP152K6 from *Bacillus methanolicus* makes 3-OH dodecanoic acid)

(Gandomkar *et al.*, 2018; Girvan *et al.*, 2018). Therefore, it is likely that the substrate-binding pocket and the orientation are important to guide the reaction to the desired products. Computational work (using a combination of density functional theory and quantum mechanics/molecular mechanics methods) done by Reinhard *et al.*, (2020) explored mutations in the active site of $OleT_{JE}$ to push shorter-chain substrates towards the majority of the alkene product. *In silica* results presented a double mutant Asn242Arg/Arg245Asn, which would effectively move the position of the substrate within the active site (salt bridge of carboxylate group of the substrate and Arg residue). Due to the similarity of $OleT_{JE}$ and KR, this mutation would be interesting to explore P450 KR catalysis with shorter chain fatty acids along with driving KR catalysis towards alkene formation.

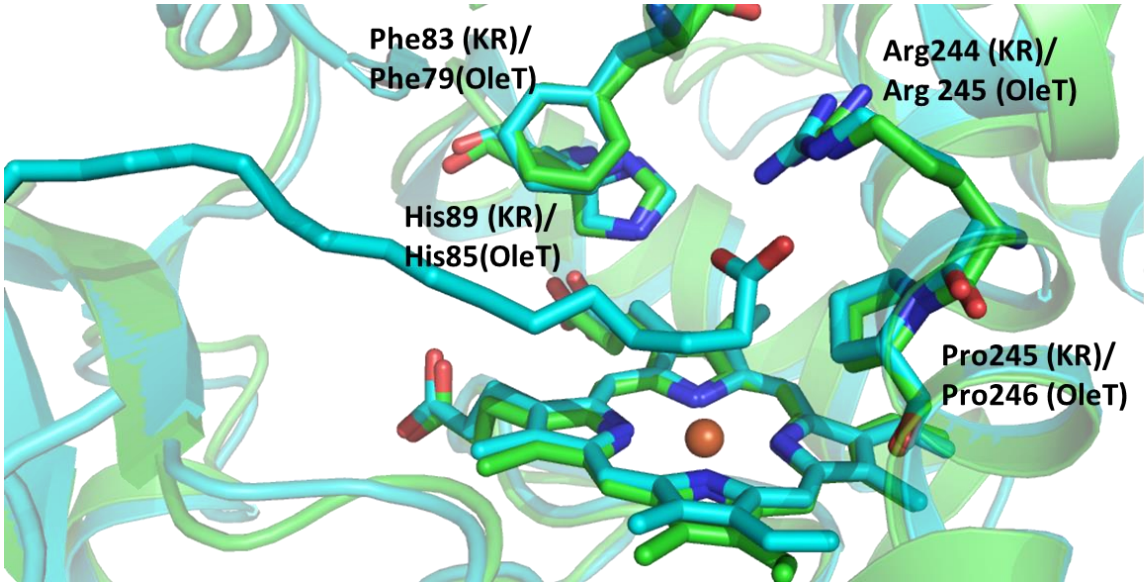

Figure 2.13 Structural comparison of active site residues of P450 KR comparison with $OleT_{JE}$. The superimposition of P450 KR (green) and $OleT_{JE}$ (PDB code: 4L40, blue). Key active site residues and their positions in respective to each other are highlighted. $OleT_{JE}$ substrate (arachidic acid) is represented by blue sticks.

Similar to $OleT_{JE}$, the P450 KR active site retains the important histidine at position 89 (position 85 for $OleT_{JE}$), within the active site (see **figure 2.13**). This histidine residue imidazole side chain points into the active site directly towards the heme iron. This is a notable difference in comparison to other CYP152 family members, where a semi-conserved glutamine residue is found in a similar position in P450 BSβ and SPα (Rude *et al.*, 2011). It was suggested that a histidine may be important for fatty acid decarboxylation. In an experiment undertaken by Rude et al., glutamine 85 in P450 BSβ was replaced with a histidine, resulting in a Q85H variant with increased rates of 1-

pentedecene and β-hydroxy palmitic acid production (Rude *et al.*, 2011). However a H85Q variant in $OleT_{JE}$ did not diminish alkene formation, instead it generated a very similar product profile as WT $OleT_{JE}$ with *n*-1 alkenes being the dominant product. However, the mutant did display diminished HS heme accumulation, which is a consistent property witnessed in P450 BSβ and SPα (Lee *et al.*, 2003; Fujishiro *et al.*, 2011; Matthews, Belcher, *et al.*, 2017). This suggests that the histidine, as postulated before, is not crucial for proton transfer to the reactive species in the catalytic cycle and alkene production (or alternative pathways may exists) (Matthews, Belcher, *et al.*, 2017). The His residue in KR lies 5.9 Å away from the heme iron in the crystal structure, but we could speculate that protein dynamic may bring this residue closer into the active site resulting in the red-shifted 424 nm absorbance. Mutagenesis of this residue could provide some clarity on the unusual Soret absorbance.

The P450 KR heme group displays a minor distorted planarity (**figure 2.14**), with the III and IV pyrrole ring groups, kinking up into the active site by ~12°. This distortion of the heme is also seen in $OleT_{JE}$ but not with P450 SPα nor BSβ (Belcher *et al.*, 2014). Heme distortion has been observed in many different divergent P450's across the larger superfamily, but the full implications of this have yet to be fully resolved. However, the majority of CYP152 enzymes seem to retain a more rigid heme structure, perhaps as a result of their evolution to utilize H_2O_2 and the importance of their active site residues for substrate alignment for their catalytic function(s).

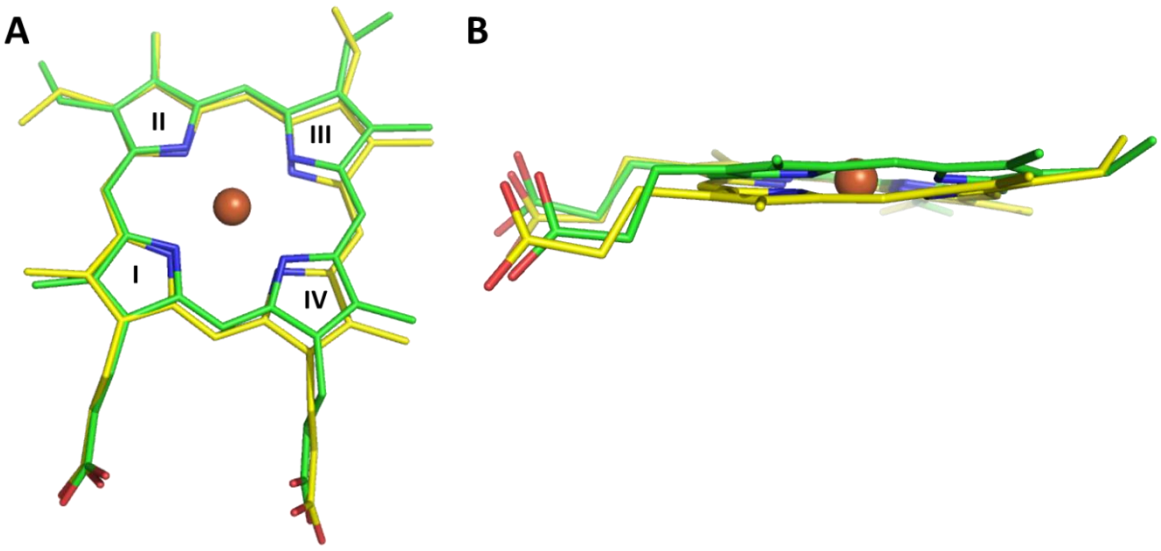

Figure 2.14 Structural comparison of heme planarity in P450 KR and P450 SPα. Panel A shows the structure of the heme in P450 KR (green) and P450 SPα (PDB code: 3AWM, yellow), with pyrrole rings

labelled. Panel B highlights the distortion in of P450 KR III and IV pyrrole rings in comparison to fellow CYP152 members.

In addition to the substrate access channel I, a second smaller channel that is observed with access to the active site, both channels are separated by B' helix. This channel is present in other H_2O_2 dependant peroxygenase enzymes such as $OleT_{JE}$ and P450 BSβ and SPα, which is thought to functions as a channel for the transportation in for H_2O_2 and exit of H_2O out of the active site cavity during the reaction (Lee *et al.*, 2003; Fujishiro *et al.*, 2011).

Despite the similarities between P450 KR and $OleT_{JE}$, there are some striking differences in both the N- and C-termini of the structures. In the $OleT_{JE}$ structure, the N-terminal region largely consists of small α-helices and β-sheets in a compact conformation. Whereas, in the P450 KR structure the N-terminal region forms a long α-helix (~40 residues) which protrudes out away from the main helical domain of the P450 enzyme (shown in blue in **figure 2.15**). The C-terminal region also terminates in a short α-helical segment that lies relatively close to the N-terminal helix. The C-terminal loop region which lines the fatty acid binding pocket in the $OleT_{JE}$ structure is absent in P450 KR. Also, the FG-loop (with general roles in substrate binding dynamics, forming part of the roof of substrate binding cavities amongst many P450s) appears to be shorter in the P450 KR structure and slightly removed from the pocket, and the density for some of the residues in this loop is ill defined (which is typical for this mobile region). Due to these differences, the P450 KR binding pocket appears to be more solvent accessible. Despite these differences in tertiary structure, the P450 KR active site is remarkably similar to that of $OleT_{JE}$.

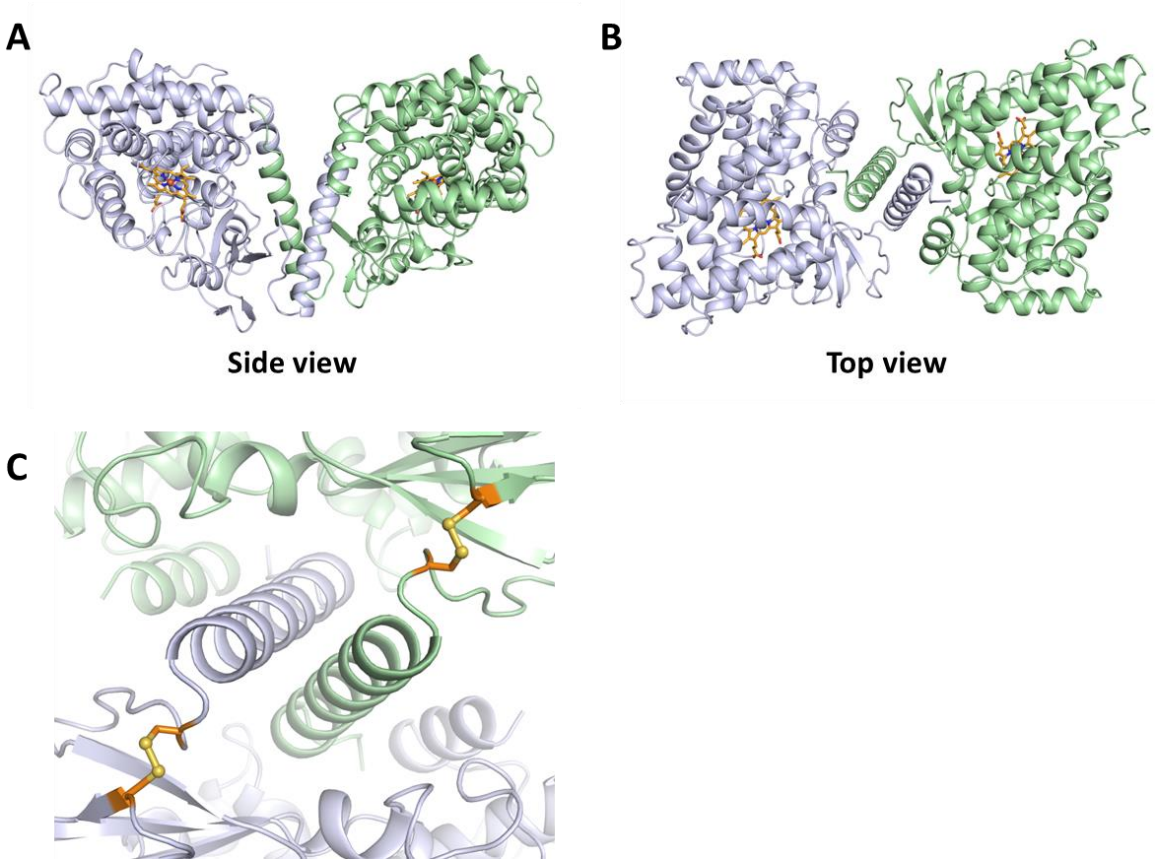

Figure 2.15 Oligomeric structure of P450 KR. Panel A and B shows cartoon representation of the dimeric structure of P450 KR, with each monomer (green and grey) shown. The heme molecule is represented by orange sticks and the centre of the molecule. Panel C highlights a disulphide bond made by cysteine residue present in the loop at the base of the N-terminal helix (Cys39) forms a disulphide bridge with another cysteine present in the central domain region (Cys317). The interaction appears to be instrumental in locking the helices in a conformational which promotes dimerisation

Closer inspection of the crystal packing reveals interesting interactions between the symmetry related elements. It appears that the enzyme crystallises as a tightly packed hexamer where three monomers form the asymmetric unit. Together with symmetry elements it forms a compact spherical unit. Interestingly, the elongated N-terminal helices, unique to P450 KR, from the adjoining monomers are found to make pseudo zipper-like interactions (**figure 2.16**). These helices cross over and make interactions with the residues from the central domain of the neighboring monomer. Most notably, hydrogen bonding interactions are made by Arg21, Tyr24, and Arg32 with Phe303, Asp331 and Thr337 respectively. Ser35 present at the end of the N-terminal helix makes hydrogen bonds with the equivalent serine from the other monomer. Unlike leucine/serine zippers, where the residues in the helices are arranged in a particular order and are involved in stabilising the structure, the pseudo zipper-like configuration observed in P450 KR appears to be serendipitous in nature. A cysteine (Cys39) residue located in the loop at the base of the N-terminal helix forms a disulfide bridge with

Cys317 present in the central domain of the same monomer (**figure 2.15**). This strong interaction appears to lock the helix in a conformation, which promotes dimerisation with the neighboring monomer. Examples of such interactions are rare, especially in the P450 family of enzymes, and this makes the P450 KR structure unique and adds to the structural diversity of cytochrome P450s in general.

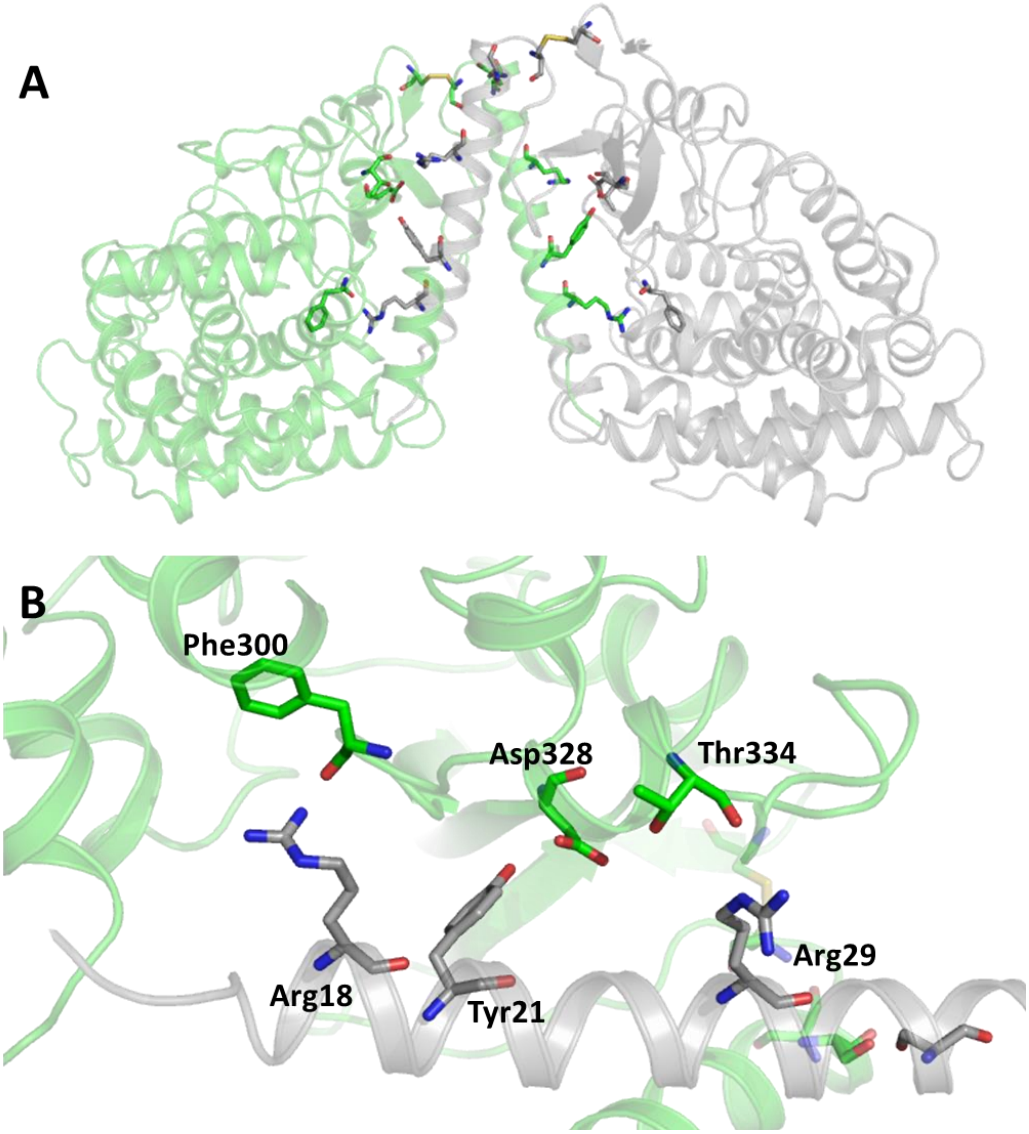

Figure 2.16 Interactions stabilising the dimeric interface of P450 KR. Panel A shows the overall structure of the dimer with the residues forming H-bonds highlighted and shown with sticks, as well as the disulphide bond shown in yellow sticks. Panel B shows a magnified view, of the N-terminal helix of one monomer (grey) interacting with a central domain of the second monomer (green), with H-bonding between Phe300 and Arg48, Asp328 and Tyr21, Thr344 and Arg29.

This novel structural arrangement reported here is unique to date in the P450 enzyme superfamily. The propensity for formation of the N-terminal helix likely results from the structural ordering of the helix as a result of stabilising effects mediated through the formation of a disulphide bridge at the end of this helix. The helices then self-interact to

form the interface that enables P450 KR dimerization. These data raise interesting questions in relation to roles of the N-terminal sequences in prokaryotic P450s and whether they may function more widely in self-interactions, or even form interactions with other cellular proteins. Additionally whether they had an evolutionally role in transmembrane association, as in in Saccharomyces cerevisiae CYP51A1 (Monk *et al.*, 2014). Although this unique N-terminal structural feature is unique in structurally characterised cytochrome P450s, a carbohydrate esterase family 7 (CE7) enzyme from *Thermotoga maritima*, which catalyses the deacetylation of acetyl esters of a broad range of alcohols shows a conserved N-terminal extension that distinguishes from the hydrolase fold. CE7 crystallises in a hexameric structure made up of trimer of dimers, with the N-terminal region interacting with the neighbouring protein segment via H-bonds with the N-terminal helix gating the active site. Removal of the helix causes a sharp decrease in temperature for activity and has been postulated that the N-terminus plays a crucial role maintaining the conformation stability of the protein (Singh *et al.*, 2017).

Turnover studies done at high P450 KR concentration (10 -20 μM) demonstrate that the enzyme binds fatty acids in the dimeric form (dimer dissociation constant discussed in section **2.4.3**), and the enzyme is clearly also functional in fatty acid decarboxylation/hydroxylation in this state. X-ray crystallographic studies of a set of P450 peroxygenases has confirmed their strong structural conservation, suggesting that those P450s with conserved cysteine residues corresponding to P450 KR Cys39 and Cys317 will likely be positioned well to form disulphide bonds, and potentially to dimerise. However, another important avenue of investigation will be to create chimeric bacterial P450s to establish whether the N-terminal sequence of P450 KR (including Cys39) can be used to drive dimerization of other prokaryotic P450s and to improve enzyme stability.

2.4.9 Probing the dimeric interface of P450 KR in solution

2.4.9.1 Size exclusion chromatography with multi-angle light scattering (SEC-MALS)

To ascertain whether the homodimer observed in the crystal structure is present in solution, P450 KR oligomeric state was explored by size exclusion chromatography coupled with multi-angle light scattering (SEC-MALS). SEC-MALS harnesses dynamic light scattering to provide structural information on protein integrity, indicating

oligomerisation states and the molecular masses associated with them. Importantly it gives an accurate degree of homogeneity via the dispersity of the protein (Sahin and Roberts, 2012). **Figure 2.17** shows the chromatograms of P450 KR obtained by SEC-MALS. P450 KR is eluted in a very broad peak spanning 4 mLs with the fraction containing two oligomeric states of KR in a monomer-dimer equilibrium. The major central peak represents 93.7% of the total protein and has an average MW of 55.4 ± 6 kDa, consistent with the estimated MW of the monomeric form. MALS was also able to detect formation of the dimer, with a MW of 98.9 ± 5.8 kDa and representing ~6.3% of the total mass fraction. The monomeric state could predominately be seen due to local dilution on the SEC, which may cause a concentration dependent dissociation of the dimer.

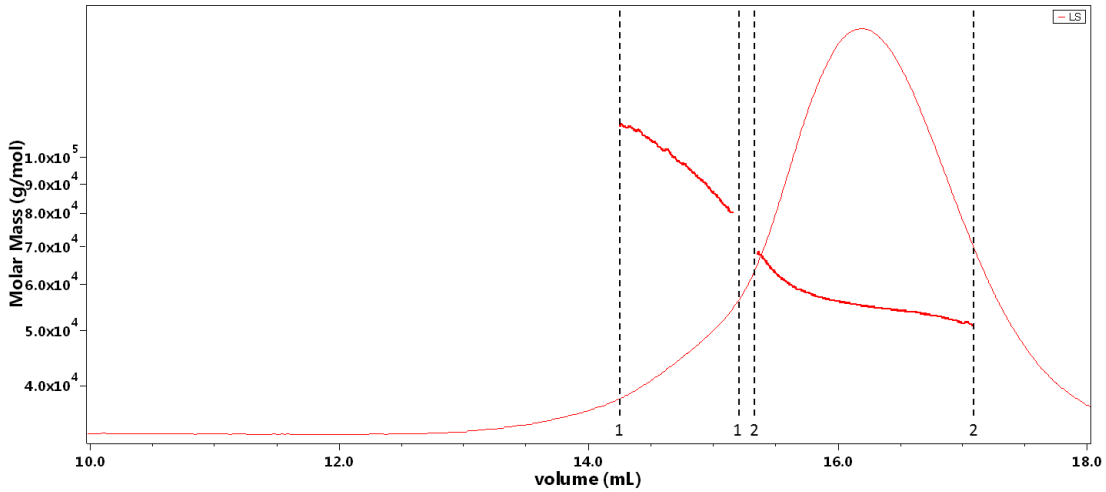

Figure 2.17 Chromatogram obtained from SEC-MALS analysis of the P450 KR protein, showing both light scattering and molar mass plots. The molecular weight average of peak 1 is 94.3 (± 5.7%) making up 6.5 % of the mass fraction. The molecular weight average of Peak 2 is 55.7 (± 6.0%) making up 93.5 % of the mass fraction. Samples run a superdex 200 GE healthcare column.

To further explore the role of the disulphide linkage at the base of dimer-forming N-terminal helix, the oligomeric-state of P450 KR with the addition of a reducing agent was assessed via SEC-MALS. Data is shown in **figure 2.18** with the addition the reducing agent TCEP. A shift in the MW to the monomeric form occurs, with a MW of 53.7 KDa (± 0.8%) with the peak eluting later than oxidised KR and making up 100% of the mass total fraction. Addition of TCEP to the protein sample causes cleavage of outer disulphide bonds, by nucleophilic attack, following with the release of oxidised phosphine and the cysteine residues becoming protonated. Therefore, it is assumed cleavage of the important dimer-inducing disulphide bond at the base of the N-terminal helix. In order

to gain further insight into the role of the N-terminal extension, a variant of P450 KR was designed that lacked the N-terminal helix but kept the stabilising disulphide bond present as the base of the helix. The variant was expressed and purified. However, there was a significant decrease in the total protein produced under the same conditions as the WT P450 KR. SEC-MALS was undertaken on the ΔNα35-KR variant, a single homogenous peak was obtained that had a MW 47.6 (±2.1%) kDa, referring to the monomeric form of the enzyme and confirming loss of the N-terminal helix. No dimer formation was observed in the sample. These data suggests that the dimeric interaction in solution occurs via this extended N-terminal helix with stabilisation occurring via the disulphide bond. When either one is interrupted we see the removal of the dimer and formation of the monomer.

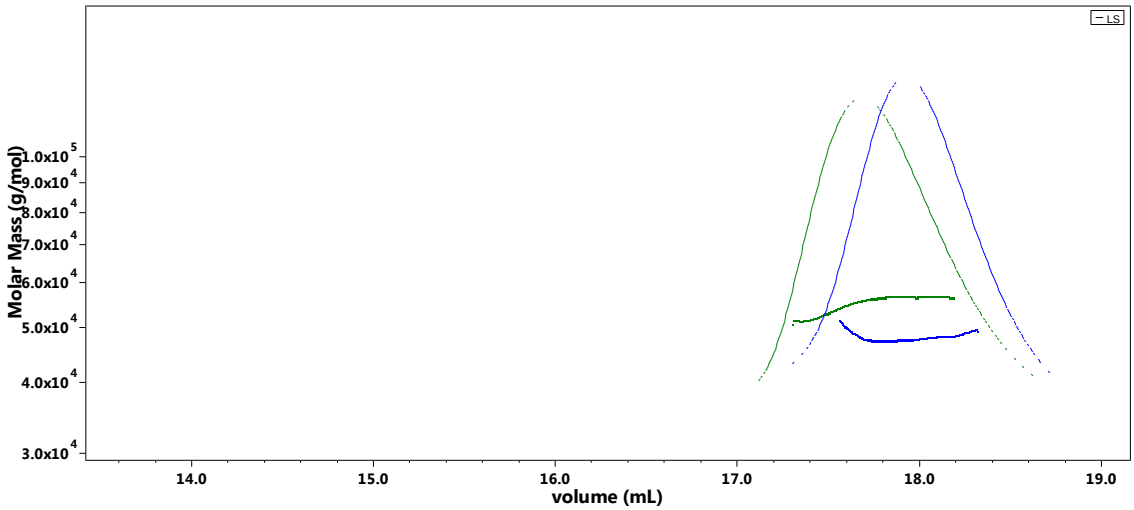

Figure 2.18 Chromatogram obtained from SEC-MALS analysis of chemically reduced P450 KR and ΔNα35-KR variant. SEC-MALS chromatogram shows both the light scattering and average molar mass. P450 KR that has been chemically reduced by 1 mM TCEP is shown in dark green with a molecular weight average 53.7 KDa (± 0.8%), ΔNα35-KR variant with average molecular weight of 47.6 (± 2.1%) kDa. Samples were run on a Superdex 6 GE healthcare column.

2.4.9.2 Analytical ultracentrifugation (AUC)

Sedimentation analytical ultracentrifugation (AUC) is a powerful tool for determining size and shape of macromolecules in their native state under biologically relevant conditions, by utilising absorbance, interference and fluorescence techniques. Experiments rely on the principle property of mass and the fundamental laws of gravitation, as mass redistributes in a gravitational field until the gravitational potential energy exactly balances the chemical potential energy at each radial position. During equilibrium sedimentation experiments, we determine the concentration distribution after equilibrium is reached allowing for thermodynamic information about MW,

stoichiometry's, and association constants (Howlett, Minton and Rivas, 2006; Cole *et al.*, 2008).

Experiments were carried in oxidising and reducing environments, with the addition of 1 mM of the reducing agent TCEP (**figure 2.19**). Equilibrium sedimentation experiments require hours to days to acquire scans (concentration distributions). Therefore, due to the length of the experiment (24 hours), KR was buffer exchanged from KPi into a Tris buffer to compliment TCEP longevity. Stability data was obtained for P450 KR in each buffer condition, with substantial changes between buffers. Under oxidising conditions, the dimer dissociation constant is 8.6 ± 0.7 µM. The experimental conditions with the addition of the reducing agent TCEP, we see no dimer formation of P450 KR, with a monomeric species seen even at concentrations where KR should be in a dimeric state with a monomeric mass of 51.2 kDa. Once again providing evidence that disulphide bond plays an important role in either the stabilisation of the dimer or formation itself.

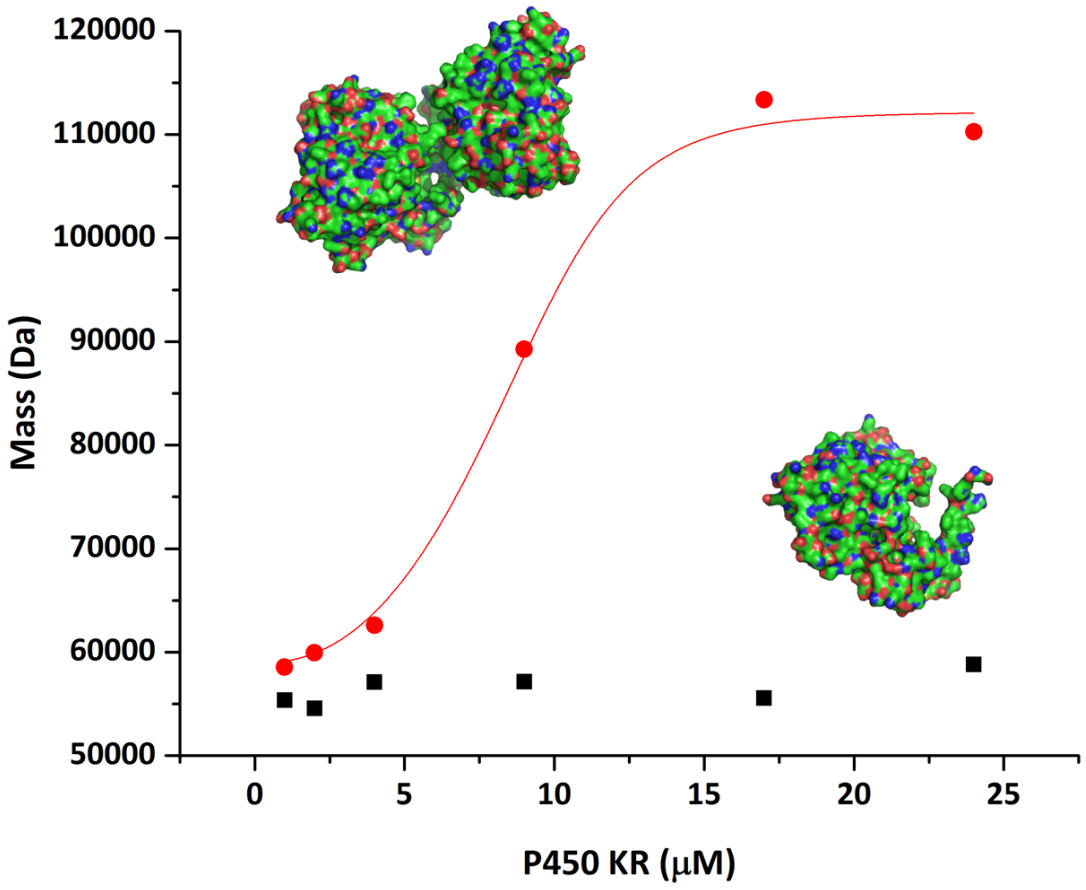

Figure 2.19 Determination of the monomer-dimer equilibrium by sedimentation equilibrium. The dimer dissociation constant for P450 KR under oxidising conditions was determined as 8.6 ± 0.7 µM (red plot). Data were fitted to Logistic5. P450 KR under reducing conditions (1 mM TCEP) does not display a monomer-dimer equilibrium, remaining in the monomeric state.

2.4.9.3 Nano electrospray ionisation (nano ESI) MS

Soft ionisation mass spectrometry (MS) techniques, such as nano electrospray ionisation (nano ESI) MS, are complimentary to traditional biophysical techniques (e.g. crystallography), as they enable investigation of the tertiary and quaternary structures. The nano ESI technique allows non-ionic interactions, such as retention of cofactors and ligands (that would usually be removed under other ionisation conditions) to be maintained in the gas phase with high control of parameters such as pH and ionic strength to maintain native folds. Typical for MS, nano-ESI-MS is incompatible with non-volatile purification buffers (such as Tris and potassium phosphate); therefore, KR was exchanged into aqueous volatile buffer, ammonium acetate (AmAc) to allow the sample to be electrosprayed. Differing concentrations of AmAc were tested, and lower concentrations (50-300 mM) resulted in precipitation of KR due to low ionic strength causing destabilisation of KR. Therefore, a concentration of 500 mM AmAc was selected to maintain the strong ionic properties that KR requires in a buffer system.

Nano-ESI MS was performed on P450 KR in its native "oxidised form" and produced a deconvoluted exact mass of 47804.83 Da. The calculated molecular weight of P450 KR is 47047.43 Da (apo-protein), addition of the heme group (molar mass: 616.49) (MW: 47663.92 Da). For P450 KR in its native "oxidised" state we observe distinct charge states (+12 to +18). During the ESI process, proteins are frequently observed in multiple charge states (Hamdy and Julian, 2012). Typically, the smaller the distribution of charge states indicates that the protein is close to its native fold, and therefore by definition should have a stable compact core sequestered from the solvent (Clemmer and Jarrold, 1997; Bernstein *et al.*, 2004). Hence, this relatively small distribution of charge states indicates that P450 KR is close to its native conformation. Reduction of the P450 KR sample using 2 mM DTT, shows an exact mass of 47, 806.99 Da as seen in **figure 2.20**. This 2 Da mass difference observed between the "oxidised" and the DTT reduced sample confers protonation of the two cysteines residues and therefore confirms breakage of the disulphide bond.

A significant difference was observed in MS data upon addition of the reducing agent, DTT (2 mM). We observe a dramatic increase of charge states from (+41 to +12). As we have hypothesised, the disulfide linkage between the two cysteine residues on the same monomer is vital to lock the N-terminal helix into a position to promote dimerization.

Therefore, destabilisation of this bond, and thus the dimeric interface, could cause KR to lose its native fold and become partially unfolded, allowing it to accommodate more charge on the protein surface and giving rise to the increased charge state distribution (Hamdy and Julian, 2012). In addition, the DTT-reduced P450 KR sample contained a second species. Following deconvolution, the mass corresponded to KR in the apo form (without the prosthetic heme group). We can also see an increase corresponding to free-heme in the spectra (present at 616). Therefore, we can postulate that chemically reducing the disulfide bond between Cys39 and Cys317 destabilises the dimeric interface and decreases the stability of P450 KR. The dimeric form of P450 KR is likely a naturally occurring conformation and has an importance in the integrity of the structure of KR.

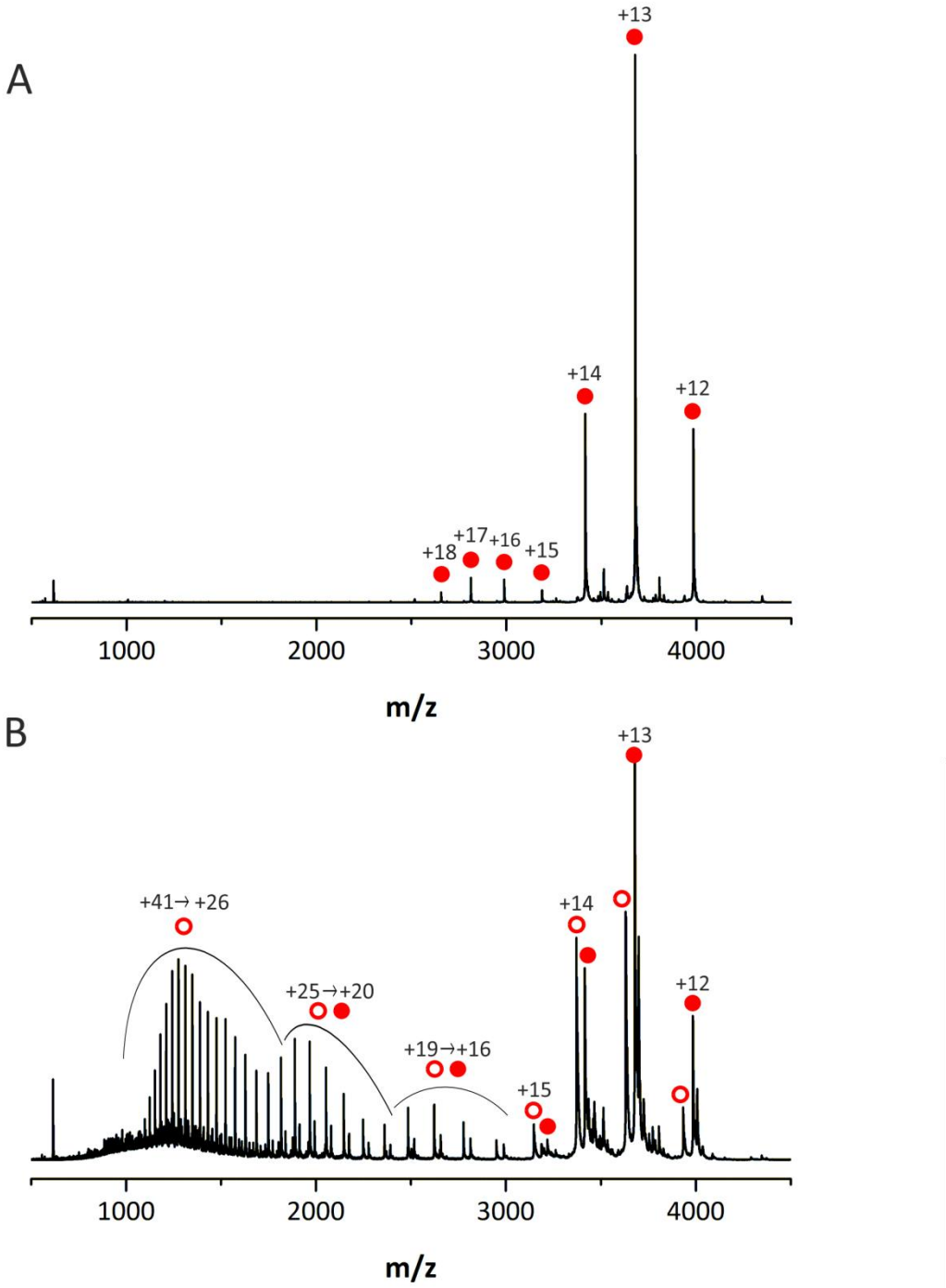

Figure 2.20 Mass spectrometric profile of P450 KR under oxidising and reducing conditions obtained by Nano-ESI MS. Panel A shows oxidised P450 KR that was prepared in 500 mM ammonium acetate. Panel B shows reduced (2 mM DTT) KR in same buffer conditions. Protein was ionised via ESI in non-denaturing conditions. The data shows the distinct protein charge states and are represented above each relating peak. The red circles represent P450 KR containing the heme prosthetic group; the red circles with white circles in the centre represent apo-KR (heme absent). Deconvoluted mass of P450 KR and P450 KR DTT-reduced was determined to be 47,804.83 Da and of 47, 806.99 Da, respectively.

2.5 Conclusions

In this paper we present the first structural and biochemical characterisation of P450 KR from the soil bacterium, *K. rhizophila*. P450 KR (CYP152T1) displayed ~30% similarity to the biotechnologically relevant P450 $OleT_{JE}$ from a *Jeotgalicoccus sp.* P450 KR is able to catalyse the turnover of fatty acids to terminal alkenes as well as alpha- and beta-hydroxylated products. This enzyme is part of the ever-growing and interesting group of CYP152 enzymes that have evolved to by bypass the need for redox-partner system (in most bacterial P450 is driven by NAD(P)H-dependent ferredoxin reductase and ferredoxin) and efficiently use hydrogen peroxide as the sole oxygen and hydride donor to produce compound 0 (McLean *et al.*, 2015). These CYP152 enzymes have efficiently evolved to function without the enzymatic delivery of protons, and h away from using the conserved acid–alcohol amino acid pair ((e.g. Asp251 and Thr252 in *Pseudomonas putida* camphor hydroxylase P450cam (CYP101A1)) that is used to relay protons to the heme iron. Instead the CYP152 family members hold a carboxylate-binding site exemplified by Arginine-proline pair (P450 BSβ: Arg242 and Pro243; $OleT_{JE}$: Arg245 and Pro246), which points to a different evolutionary route to accommodate hydrogen peroxide driven catalysis (Fujishiro *et al.*, 2011; Belcher *et al.*, 2014; Munro *et al.*, 2018).

P450 KR was shown to self-associate, forming a dimer-like association in solution (SEC-MALS and AUC data). Despite KR having a similar size (428 amino acids) to $OleT_{JE}$ and other CYP152 family members, its crystal structure revealed a unique dimeric structural organisation. The N-terminal region of P450 KR forms an unusual helical segment that interacts with the corresponding helical section of another monomer to produce a zipper-like dimeric interface. The interaction appears to be stabilised by a disulphide bond formed by two cysteine residues in the same monomer, the Cys39 which is at the base of the N-terminal alpha-helix and Cys317 which is present in the central domain. Reduction of the disulphide linkage leads to the formation of monomeric protein. This is further confirmed by production of a P450 KR variant that lacked the N-terminal region, displayed instability and the disability to make dimeric interactions. Indeed, showing that this disulphide bond linkage is instrumental in locking the N-terminal helix in a position to allow for dimerization to occur.

Further examination was done relating to the disulphide bond and the corresponding amino acid pairs in P450 KR, Cys39 and Cys317. These amino acids observed in *Kocuria*

rhizophila in a GCPV sequence motif are found to be conserved in both positions in various *Kocuria* spp. These include a number of related *K. rhizophila* strains, including *K. salsica*, *Kocuria* sp. HMSC066H03 and *K. varians*. P450s from these species have >90% amino acid sequence identity to P450 KR. However, cysteines corresponding to Cys39 are absent in *K. marina*, *Kocuria* sp. ICS0012 and *K. indica* (which all share a GCPI sequence motif in the region corresponding to *K. rhizophila* Cys-317), where percentage sequence identity drops to 82-83% with P450 KR compared to >90% in the other *Kocuria* spp. This cysteine is also absent in various apparent P450 KR orthologues in *Corynebacteria* spp., *Dietzia* spp. and in *Mycobacterium abscessus* subsp. *abscessus*. Both cysteines are absent in orthologues from various *Microbacter* and *Dermacoccus* spp., and in *Tessaracoccus massiliensis*, although the cysteine pair is retained in orthologues from *Rothia nasimurium*, *M. abscessus* subsp. bolleti, *Corynebacterium mycetoides*, *C. lipophiloflavum* and *C. lipophiloflavum* DSM44291 (which share 54-56% identity to P450 KR). Thus, there are potentially a number of other peroxygenase P450s in which a similar disulphide bridge could form (see supplementary **figure 2.21** for alignment)

P450 KR presents an unusual sub-class of CYP152 peroxygenase enzymes that displays unique oligomerisation properties and has the potential to be used as an industrial catalyst in alkene and hydroxy fatty acid production

2.6 References

Adams, P. D. *et al.* (2010) 'PHENIX: A comprehensive Python-based system for macromolecular structure solution', *Acta Crystallographica Section D: Biological Crystallography*. Acta Crystallogr D Biol Crystallogr, 66(2), pp. 213–221. doi: 10.1107/S0907444909052925.

Amaya, J. A., Rutland, C. D. and Makris, T. M. (2016) 'Mixed regiospecificity compromises alkene synthesis by a cytochrome P450 peroxygenase from Methylobacterium populi', *Journal of Inorganic Biochemistry*. Elsevier Inc., 158, pp. 11–16. doi: 10.1016/j.jinorgbio.2016.02.031.

Atsumi, S. and Liao, J. C. (2008) 'Metabolic engineering for advanced biofuels production from Escherichia coli', *Current Opinion in Biotechnology*, 19(5), pp. 414–419. doi: 10.1016/j.copbio.2008.08.008.

Barr, I. and Guo, F. (2015) 'Pyridine Hemochromagen Assay for Determining the Concentration of Heme in Purified Protein Solutions', *BIO-PROTOCOL*. Bio-Protocol, LLC, 5(18). doi: 10.21769/bioprotoc.1594.

Belcher, J. *et al.* (2014) 'Structure and biochemical properties of the alkene producing cytochrome p450 OleTJE (CYP152l1) from the jeotgalicoccus sp. 8456 bacterium', *Journal of Biological Chemistry*. American Society for Biochemistry and Molecular Biology, 289(10), pp. 6535–6550. doi: 10.1074/jbc.M113.527325.

Beller, H. R., Goh, E. B. and Keasling, J. D. (2010) 'Genes involved in long-chain alkene biosynthesis in micrococcus Luteus', *Applied and Environmental Microbiology*. American Society for Microbiology, 76(4), pp. 1212–1223. doi: 10.1128/AEM.02312-09.

Bernstein, S. L. *et al.* (2004) 'α-Synuclein: Stable compact and extended monomeric structures and pH dependence of dimer formation', *Journal of the American Society for Mass Spectrometry*. Springer New York LLC, 15(10), pp. 1435–1443. doi: 10.1016/j.jasms.2004.08.003.

Berry, E. A. and Trumpower, B. L. (1987) 'Simultaneous determination of hemes a, b, and c from pyridine hemochrome spectra', *Analytical Biochemistry*. Anal Biochem, 161(1), pp. 1–15. doi: 10.1016/0003-2697(87)90643-9.

Bharadwaj, V. S. *et al.* (2018) 'Different Behaviors of a Substrate in P450 Decarboxylase and Hydroxylase Reveal Reactivity-Enabling Actors', *Scientific Reports*. Nature Publishing Group, 8(1), p. 12826. doi: 10.1038/s41598-018-31237-4.

Brown, P. H. and Schuck, P. (2006) 'Macromolecular size-and-shape distributions by sedimentation velocity analytical ultracentrifugation', *Biophysical Journal*. Biophysical Society, 90(12), pp. 4651–4661. doi: 10.1529/biophysj.106.081372.

Bui, S. H. *et al.* (2012) 'Unusual spectroscopic and ligand binding properties of the cytochrome P450-flavodoxin fusion enzyme XplA', *Journal of Biological Chemistry*. American Society for Biochemistry and Molecular Biology, 287(23), pp. 19699–19714. doi: 10.1074/jbc.M111.319202.

Christenson, J. K. *et al.* (2017) 'OleB from Bacterial Hydrocarbon Biosynthesis Is a β-Lactone Decarboxylase That Shares Key Features with Haloalkane Dehalogenases', *Biochemistry*. American Chemical Society, 56(40), pp. 5278–5287. doi: 10.1021/acs.biochem.7b00667.

Clemmer, D. E. and Jarrold, M. F. (1997) 'Ion mobility measurements and their applications to clusters and biomolecules', *Journal of Mass Spectrometry*. John Wiley & Sons, Ltd, pp. 577–592. doi: 10.1002/(SICI)1096-9888(199706)32:6<577::AID-JMS530>3.0.CO;2-4.

Cole, J. L. *et al.* (2008) 'Analytical Ultracentrifugation: Sedimentation Velocity and Sedimentation Equilibrium', *Methods in Cell Biology*, pp. 143–179. doi: 10.1016/S0091-679X(07)84006-4.

Coleman, T. *et al.* (2020) 'Structural insights into the role of the acid-alcohol pair of residues required for dioxygen activation in cytochrome P450 enzymes', *Journal of Biological Inorganic Chemistry*. Springer, 25(4), pp. 583–596. doi: 10.1007/s00775-020-01781-4.

Coon, M. J. (2005) 'Cytochrome P450: Nature's most versatile biological catalyst', *Annual Review of Pharmacology and Toxicology*, pp. 1–25. doi: 10.1146/annurev.pharmtox.45.120403.100030.

Cryle, M. J. and De Voss, J. J. (2008) 'The role of the conserved threonine in P450BM3 oxygen activation: Substrate-determined hydroxylation activity of the Thr268Ala mutant', *ChemBioChem*, 9(2), pp. 261–266. doi: 10.1002/cbic.200700537.

Daff, S. N. *et al.* (1997) 'Redox control of the catalytic cycle of flavocytochrome P-450 BM3', *Biochemistry*. Biochemistry, 36(45), pp. 13816–13823. doi: 10.1021/bi971085s.

Das, A., Grinkova, Y. V. and Sligar, S. G. (2007) 'Redox potential control by drug binding to cytochrome P450 3A4', *Journal of the American Chemical Society*. NIH Public Access, 129(45), pp. 13778–13779. doi: 10.1021/ja074864x.

Dawson, J. H., Andersson, L. A. and Sono, M. (1982) 'Spectroscopic investigations of ferric cytochrome P-450-CAM ligand complexes. Identification of the ligand trans to cysteinate in the native enzyme.', *Journal of Biological Chemistry*, 257(7), pp. 3606–3617. doi: 10.1016/s0021-9258(18)34823-3.

Dawson, J. H., Anderssons, L. A. and Sono, M. (1982) *Spectroscopic investigations of ferric cytochrome P-450-CAM ligand complexes. Identification of the ligand trans to cysteinate in the native enzyme.*, *THE JOURNAL OF BIOLOGICAL CHEMISTRY*. doi: 10.1016/S0021-9258(18)34823-3.

Denisov, I. G. *et al.* (2005) *Structure and chemistry of cytochrome P450*, *Chemical Reviews*. American Chemical Society. doi: 10.1021/cr0307143.

Dennig, A. *et al.* (2015) 'Oxidative Decarboxylation of Short-Chain Fatty Acids to 1-Alkenes', *Angewandte Chemie - International Edition*, 54(30), pp. 8819–8822. doi: 10.1002/anie.201502925.

Driscoll, M. D. *et al.* (2011) 'Expression and characterization of Mycobacterium tuberculosis CYP144: Common themes and lessons learned in the M. tuberculosis P450 enzyme family', *Biochimica et Biophysica Acta - Proteins and Proteomics*. Biochim Biophys Acta, 1814(1), pp. 76–87. doi: 10.1016/j.bbapap.2010.05.015.

Emsley, P. *et al.* (2010) 'Features and development of Coot', *Acta Crystallographica Section D: Biological Crystallography*. Acta Crystallogr D Biol Crystallogr, 66(4), pp. 486–501. doi: 10.1107/S0907444910007493.

Evans, P. R. and Murshudov, G. N. (2013) 'How good are my data and what is the resolution?', *Acta Crystallographica Section D: Biological Crystallography*. Acta Crystallogr D Biol Crystallogr, 69(7), pp. 1204–1214. doi: 10.1107/S0907444913000061.

Fu, W. J. *et al.* (2015) 'Hydrocarbons, the advanced biofuels produced by different organisms, the evidence that alkanes in petroleum can be renewable', *Applied Microbiology and Biotechnology*. Springer Verlag, pp. 7481–7494. doi: 10.1007/s00253-015-6840-6.

Fudou, R. *et al.* (2002) 'Corynebacterium efficiens sp. nov., a glutamic-acid-producing species from soil and vegetables', *International Journal of Systematic and Evolutionary Microbiology*. Microbiology Society, 52(4), pp. 1127–1131. doi: 10.1099/ijs.0.02086-0.

Fujishiro, T. *et al.* (2011) 'Crystal structure of H 2O 2-dependent cytochrome P450 SPαwith its

bound fatty acid substrate: Insight into the regioselective hydroxylation of fatty acids at the α position', *Journal of Biological Chemistry*, 286(34), pp. 29941–29950. doi: 10.1074/jbc.M111.245225.

Gandomkar, S. *et al.* (2018) 'Biocatalytic Oxidative Cascade for the Conversion of Fatty Acids into α-Ketoacids via Internal H2O2 Recycling', *Angewandte Chemie - International Edition*. Wiley-VCH Verlag, 57(2), pp. 427–430. doi: 10.1002/anie.201710227.

Girvan, H. M. *et al.* (2004) 'Flavocytochrome P450 BM3 mutant A264E undergoes substrate-dependent formation of a novel heme iron ligand set', *Journal of Biological Chemistry*. J Biol Chem, 279(22), pp. 23274–23286. doi: 10.1074/jbc.M401716200.

Girvan, H. M. *et al.* (2018) 'Structural and catalytic properties of the peroxygenase P450 enzyme CYP152K6 from Bacillus methanolicus', *Journal of Inorganic Biochemistry*. Elsevier Inc., 188, pp. 18–28. doi: 10.1016/j.jinorgbio.2018.08.002.

Girvan, H. M. and Munro, A. W. (2016) 'Applications of microbial cytochrome P450 enzymes in biotechnology and synthetic biology', *Current Opinion in Chemical Biology*. Elsevier Ltd, pp. 136–145. doi: 10.1016/j.cbpa.2016.02.018.

Good, N. E. *et al.* (1966) 'Hydrogen Ion Buffers for Biological Research', *Biochemistry*. American Chemical Society, 5(2), pp. 467–477. doi: 10.1021/bi00866a011.

Grant, J. L., Hsieh, C. H. and Makris, T. M. (2015a) 'Decarboxylation of fatty acids to terminal alkenes by cytochrome P450 compound i', *Journal of the American Chemical Society*. American Chemical Society, 137(15), pp. 4940–4943. doi: 10.1021/jacs.5b01965.

Grant, J. L., Hsieh, C. H. and Makris, T. M. (2015b) 'Decarboxylation of fatty acids to terminal alkenes by cytochrome P450 compound I', *Journal of the American Chemical Society*, 137(15), pp. 4940–4943. doi: 10.1021/jacs.5b01965.

Grant, J. L., Mitchell, M. E. and Makris, T. M. (2016a) 'Catalytic strategy for carbon-carbon bond scission by the cytochrome p450 olet', *Proceedings of the National Academy of Sciences of the United States of America*, 113(36), pp. 10049–10054. doi: 10.1073/pnas.1606294113.

Grant, J. L., Mitchell, M. E. and Makris, T. M. (2016b) 'Catalytic strategy for carbon-carbon bond scission by the cytochrome P450 OleT', *Proceedings of the National Academy of Sciences of the United States of America*, 113(36), pp. 10049–10054. doi: 10.1073/pnas.1606294113.

Guengerich, F. P. and Munro, A. W. (2013) 'Unusual cytochrome p450 enzymes and reactions.', *The Journal of biological chemistry*. American Society for Biochemistry and Molecular Biology, 288(24), pp. 17065–73. doi: 10.1074/jbc.R113.462275.

Hagemans, D. *et al.* (2015) 'A script to highlight hydrophobicity and charge on protein surfaces', *Frontiers in Molecular Biosciences*. Frontiers Media S.A., 2(OCT), p. 56. doi: 10.3389/fmolb.2015.00056.

Hamdy, O. M. and Julian, R. R. (2012) 'Reflections on charge state distributions, protein structure, and the mystical mechanism of electrospray ionization', *Journal of the American Society for Mass Spectrometry*, 23(1), pp. 1–6. doi: 10.1007/s13361-011-0284-8.

Hannemann, F. *et al.* (2007) 'Cytochrome P450 systems—biological variations of electron transport chains', *Biochimica et Biophysica Acta (BBA) - General Subjects*, 1770(3), pp. 330–344. doi: 10.1016/j.bbagen.2006.07.017.

Van Hellemond, E. W. *et al.* (2009) 'Exploring the biocatalytic scope of alditol oxidase from Streptomyces coelicolor', *Advanced Synthesis and Catalysis*, 351(10), pp. 1523–1530. doi:

10.1002/adsc.200900176.

Howlett, G. J., Minton, A. P. and Rivas, G. (2006) 'Analytical ultracentrifugation for the study of protein association and assembly', *Current Opinion in Chemical Biology*. Curr Opin Chem Biol, pp. 430–436. doi: 10.1016/j.cbpa.2006.08.017.

Hsieh, C. H. *et al.* (2017) 'The Enigmatic P450 Decarboxylase OleT Is Capable of, but Evolved to Frustrate, Oxygen Rebound Chemistry', *Biochemistry*. American Chemical Society, 56(26), pp. 3347–3357. doi: 10.1021/acs.biochem.7b00338.

Hsieh, C. H. and Makris, T. M. (2016) *Expanding the substrate scope and reactivity of cytochrome P450 OleT*, *Biochemical and Biophysical Research Communications*. doi: 10.1016/j.bbrc.2016.05.145.

Imai, Y. *et al.* (2000) 'Unique heme environment at the putative distal region of hydrogen peroxide-dependent fatty acid α-hydroxylase from Sphingomonas paucimobilis (peroxygenase P450(SPα))', *Journal of Biochemistry*, 128(2), pp. 189–194. doi: 10.1093/oxfordjournals.jbchem.a022740.

Isin, E. M. and Guengerich, F. P. (2008) 'Substrate binding to cytochromes P450', *Analytical and Bioanalytical Chemistry*. NIH Public Access, pp. 1019–1030. doi: 10.1007/s00216-008-2244-0.

Kabsch, W. (2010) 'Integration, scaling, space-group assignment and post-refinement', *Acta Crystallographica Section D: Biological Crystallography*. International Union of Crystallography, 66(2), pp. 133–144. doi: 10.1107/S0907444909047374.

Kang, M. K. and Nielsen, J. (2017) 'Biobased production of alkanes and alkenes through metabolic engineering of microorganisms', *Journal of Industrial Microbiology and Biotechnology*. Springer Verlag, pp. 613–622. doi: 10.1007/s10295-016-1814-y.

Kapust, R. B. *et al.* (2001) 'Tobacco etch virus protease: Mechanism of autolysis and rational design of stable mutants with wild-type catalytic proficiency', *Protein Engineering*. Oxford University Press, 14(12), pp. 993–1000. doi: 10.1093/protein/14.12.993.

Koerner, R. J., Goodfellow, M. and Jones, A. L. (2009) 'The genus Dietzia: A new home for some known and emerging opportunist pathogens', *FEMS Immunology and Medical Microbiology*. Oxford Academic, pp. 296–305. doi: 10.1111/j.1574-695X.2008.00513.x.

Köninger, K. *et al.* (2016) 'Light-driven enzymatic decarboxylation', *Journal of Visualized Experiments*. Journal of Visualized Experiments, 2016(111), p. 53439. doi: 10.3791/53439.

Korasick, D. A. and Tanner, J. J. (2018) 'Determination of protein oligomeric structure from small-angle X-ray scattering', *Protein Science*. Blackwell Publishing Ltd, pp. 814–824. doi: 10.1002/pro.3376.

Krissinel, E. and Henrick, K. (2004) 'Secondary-structure matching (SSM), a new tool for fast protein structure alignment in three dimensions', *Acta Crystallographica Section D: Biological Crystallography*. Acta Crystallogr D Biol Crystallogr, 60(12 I), pp. 2256–2268. doi: 10.1107/S0907444904026460.

Leadbeater, C. *et al.* (2000) 'Probing the NADPH-binding site of Escherichia coli flavodoxin oxidoreductase', *Biochemical Journal*. Portland Press Ltd, 352(2), pp. 257–266. doi: 10.1042/0264-6021:3520257.

Lee, D. S. *et al.* (2003) 'Substrate recognition and molecular mechanism of fatty acid hydroxylation by cytochrome P450 from Bacillus subtilis: Crystallographic, spectroscopic, and mutational studies', *Journal of Biological Chemistry*. American Society for Biochemistry and

Molecular Biology, 278(11), pp. 9761–9767. doi: 10.1074/jbc.M211575200.

Leslie Dutton, P. (1978) 'Redox potentiometry: Determination of midpoint potentials of oxidation-reduction components of biological electron-transfer systems', *Methods in Enzymology*. Methods Enzymol, 54(C), pp. 411–435. doi: 10.1016/S0076-6879(78)54026-3.

Li, A. *et al.* (2017) 'A redox-mediated Kemp eliminase', *Nature Communications*. Nature Publishing Group, 8(1), pp. 1–8. doi: 10.1038/ncomms14876.

Li, H. and Poulos, T. L. (1997) 'The structure of the cytochrome p450BM-3 haem domain complexed with the fatty acid substrate, palmitoleic acid', *Nature Structural Biology*. Nature Publishing Group, 4(2), pp. 140–146. doi: 10.1038/nsb0297-140.

Li, N. *et al.* (2012) 'Evidence for only oxygenative cleavage of aldehydes to alk(a/e)nes and formate by cyanobacterial aldehyde decarbonylases', *Biochemistry*. Biochemistry, 51(40), pp. 7908–7916. doi: 10.1021/bi300912n.

Liang, J. L. *et al.* (2016) 'Regulation of the alkane hydroxylase CYP153 gene in a Gram-positive alkane-degrading bacterium, Dietzia sp. strain DQ12-45-1b', *Applied and Environmental Microbiology*. American Society for Microbiology, 82(2), pp. 608–619. doi: 10.1128/AEM.02811-15.

Lipscomb, J. D. (1980) 'Electron Paramagnetic Resonance Detectable States of Cytochrome P-450Cam', *Biochemistry*. American Chemical Society, 19(15), pp. 3590–3599. doi: 10.1021/bi00556a027.

Liu, H. *et al.* (2012) 'Production of extracellular fatty acid using engineered Escherichia coli', *Microbial Cell Factories*, 11(1), p. 41. doi: 10.1186/1475-2859-11-41.

Liu, Q. *et al.* (2015) 'Engineering an iterative polyketide pathway in Escherichia coli results in single-form alkene and alkane overproduction', *Metabolic Engineering*. Academic Press Inc., 28, pp. 82–90. doi: 10.1016/j.ymben.2014.12.004.

Liu, Y. *et al.* (2014) 'Hydrogen peroxide-independent production of α-alkenes by OleTJE P450 fatty acid decarboxylase.', *Biotechnology for biofuels*, 7(1), p. 28. doi: 10.1186/1754-6834-7-28.

Lu, C. *et al.* (2018) 'An Engineered Self-Sufficient Biocatalyst Enables Scalable Production of Linear α-Olefins from Carboxylic Acids', *ACS Catalysis*, 8(7), pp. 5794–5798. doi: 10.1021/acscatal.8b01313.

Luthra, A., Denisov, I. G. and Sligar, S. G. (2011) 'Spectroscopic features of cytochrome P450 reaction intermediates', *Archives of Biochemistry and Biophysics*. NIH Public Access, pp. 26–35. doi: 10.1016/j.abb.2010.12.008.

Matsunaga, I. *et al.* (1996) 'Direct involvement of hydrogen peroxide in bacterial α-hydroxylation of fatty acid', *FEBS Letters*. Elsevier B.V., 386(2–3), pp. 252–254. doi: 10.1016/0014-5793(96)00451-6.

Matsunaga, I. *et al.* (1997) 'Molecular cloning and expression of fatty acid α-hydroxylase from Sphingomonas paucimobilis', *Journal of Biological Chemistry*. American Society for Biochemistry and Molecular Biology, 272(38), pp. 23592–23596. doi: 10.1074/jbc.272.38.23592.

Matsunaga, I. *et al.* (1999) 'Characterization of the ybdT gene product of Bacillus subtilis: Novel fatty acid β-hydroxylating cytochrome P450', *Lipids*. John Wiley & Sons, Ltd, 34(8), pp. 841–846. doi: 10.1007/s11745-999-0431-3.

Matthews, S., Belcher, J. D., *et al.* (2017) 'Catalytic determinants of alkene production by the cytochrome P450 peroxygenase OleTJE', *Journal of Biological Chemistry*. American Society for

Biochemistry and Molecular Biology, 292(12), pp. 5128–5143. doi: 10.1074/jbc.M116.762336.

Matthews, S., Tee, K. L., *et al.* (2017a) 'Production of alkenes and novel secondary products by P450 OleTJE using novel H2O2-generating fusion protein systems', *FEBS Letters*. Wiley Blackwell, 591(5), pp. 737–750. doi: 10.1002/1873-3468.12581.

Matthews, S., Tee, K. L., *et al.* (2017b) 'Production of alkenes and novel secondary products by P450 OleTJE using novel H2O2-generating fusion protein systems', *FEBS Letters*. Wiley Blackwell, 591(5), pp. 737–750. doi: 10.1002/1873-3468.12581.

Matthews, S., Tee, K. L., *et al.* (2017c) 'Production of alkenes and novel secondary products by P450 OleTJE using novel H2O2-generating fusion protein systems', *FEBS Letters*, 591(5), pp. 737–750. doi: 10.1002/1873-3468.12581.

McCoy, A. J. *et al.* (2007) 'Phaser crystallographic software', *Journal of Applied Crystallography*. International Union of Crystallography, 40(4), pp. 658–674. doi: 10.1107/S0021889807021206.

McIver, L. *et al.* (1998) 'Characterisation of flavodoxin NADP+ oxidoreductase and flavodoxin; key components of electron transfer in Escherichia coli', *European Journal of Biochemistry*. Blackwell Publishing Ltd., 257(3), pp. 577–585. doi: 10.1046/j.1432-1327.1998.2570577.x.

McKNIGHT, J. *et al.* (1993) 'Identification of charge-transfer transitions in the optical spectrum of low-spin ferric cytochrome P-450 Bacillus megaterium', *European Journal of Biochemistry*. Eur J Biochem, 213(2), pp. 683–687. doi: 10.1111/j.1432-1033.1993.tb17808.x.

McLean, K. J. *et al.* (2002) 'Expression, purification and spectroscopic characterization of the cytochrome P450 CYP121 from Mycobacterium tuberculosis', *Journal of Inorganic Biochemistry*. J Inorg Biochem, 91(4), pp. 527–541. doi: 10.1016/S0162-0134(02)00479-8.

McLean, K. J. *et al.* (2005) 'Biodiversity of cytochrome P450 redox systems', in *Biochemical Society Transactions*, pp. 796–801. doi: 10.1042/BST0330796.

McLean, K. J. *et al.* (2006) 'Biophysical characterization of the sterol demethylase P450 from Mycobacterium tuberculosis, its cognate ferredoxin, and their interactions', *Biochemistry*. Biochemistry, 45(27), pp. 8427–8443. doi: 10.1021/bi0601609.

McLean, K. J. *et al.* (2015) 'Biological diversity of cytochrome P450 redox partner systems', *Advances in Experimental Medicine and Biology*, 851, pp. 299–317. doi: 10.1007/978-3-319-16009-2_11.

Miles, J. S. *et al.* (1992) 'Domains of the catalytically self-sufficient cytochrome p-450 BM-3. Genetic construction, overexpression, purification and spectroscopic characterization', *Biochemical Journal*. Biochem J, 288(2), pp. 503–509. doi: 10.1042/bj2880503.

Monk, B. C. *et al.* (2014) 'Architecture of a single membrane spanning cytochrome P450 suggests constraints that orient the catalytic domain relative to a bilayer', *Proceedings of the National Academy of Sciences of the United States of America*. National Academy of Sciences, 111(10), pp. 3865–3870. doi: 10.1073/pnas.1324245111.

Munro, A. W. *et al.* (2002) 'P450 BM3: The very model of a modern flavocytochrome', *Trends in Biochemical Sciences*, pp. 250–257. doi: 10.1016/S0968-0004(02)02086-8.

Munro, A. W. *et al.* (2013) 'What makes a P450 tick?', *Trends in Biochemical Sciences*, 38(3), pp. 140–150. doi: 10.1016/j.tibs.2012.11.006.

Munro, A. W. *et al.* (2018) 'Structure and function of the cytochrome P450 peroxygenase enzymes', *Biochemical Society Transactions*. Portland Press Ltd, pp. 183–196. doi: 10.1042/BST20170218.

Munro, A. W., Girvan, H. M. and McLean, K. J. (2007) 'Variations on a (t)heme--novel mechanisms, redox partners and catalytic functions in the cytochrome P450 superfamily.', *Natural product reports*, 24(3), pp. 585–609. doi: 10.1039/b604190f.

Murugan, R. and Mazumdar, S. (2005) 'Structure and Redox Properties of the Haem Centre in the C357M Mutant of Cytochrome P450cam', *ChemBioChem*. John Wiley & Sons, Ltd, 6(7), pp. 1204–1211. doi: 10.1002/cbic.200400399.

Omura, T. and Sato, R. (1962) 'A new cytochrome in liver microsomes.', *The Journal of biological chemistry*, 237, pp. 1375–1376. Available at: http://www.ncbi.nlm.nih.gov/pubmed/14482007 (Accessed: 27 November 2016).

Perera, R. *et al.* (2003) 'Neutral thiol as a proximal ligand to ferrous heme iron: Implications for heme proteins that lose cysteine thiolate ligation on reduction', *Proceedings of the National Academy of Sciences of the United States of America*. National Academy of Sciences, 100(7), pp. 3641–3646. doi: 10.1073/pnas.0737142100.

Pickl, M. *et al.* (2019) 'Mechanistic Studies of Fatty Acid Activation by CYP152 Peroxygenases Reveal Unexpected Desaturase Activity', *ACS Catalysis*. American Chemical Society, 9(1), pp. 565–577. doi: 10.1021/acscatal.8b03733.

Pluschke, G. and Overath, P. (1981) 'Function of phospholipids in Escherichia coli. Influence of changes in polar head group composition on the lipid phase transition and characterization of a mutant containing only saturated phospholipid acyl chains', *Journal of Biological Chemistry*, 256(7), pp. 3207–3212. doi: 10.1016/s0021-9258(19)69590-6.

Podust, L. M. *et al.* (2001) 'Substrate recognition sites in 14α-sterol demethylase from comparative analysis of amino acid sequences and X-ray structure of Mycobacterium tuberculosis CYP51', *Journal of Inorganic Biochemistry*. Elsevier, 87(4), pp. 227–235. doi: 10.1016/S0162-0134(01)00388-9.

Poulos, T. L., Finzel, B. C. and Howard, A. J. (1987) 'High-resolution crystal structure of cytochrome P450cam', *Journal of Molecular Biology*, 195(3), pp. 687–700. doi: 10.1016/0022-2836(87)90190-2.

Presnell, S. R. and Cohen, F. E. (1989) 'Topological distribution of four-alpha-helix bundles.', *Proceedings of the National Academy of Sciences of the United States of America*. Proc Natl Acad Sci U S A, 86(17), pp. 6592–6596. doi: 10.1073/pnas.86.17.6592.

Prinz, H. (2010) 'Hill coefficients, dose–response curves and allosteric mechanisms', *Journal of Chemical Biology*. Springer, 3(1), p. 37. doi: 10.1007/S12154-009-0029-3.

Qiu, Y. *et al.* (2012) 'An insect-specific P450 oxidative decarbonylase for cuticular hydrocarbon biosynthesis', *Proceedings of the National Academy of Sciences of the United States of America*. Proc Natl Acad Sci U S A, 109(37), pp. 14858–14863. doi: 10.1073/pnas.1208650109.

Raag, R. *et al.* (1991) 'Crystal Structure of the Cytochrome P-450CAM Active Site Mutant Thr252Ala', *Biochemistry*. American Chemical Society, 30(48), pp. 11420–11429. doi: 10.1021/bi00112a008.

Reinhard, F. G. C. *et al.* (2020) 'Bioengineering of Cytochrome P450 OleTJE: How Does Substrate Positioning Affect the Product Distributions?', *Molecules (Basel, Switzerland)*. NLM (Medline), 25(11). doi: 10.3390/molecules25112675.

Rittle, J. and Green, M. T. (2010) 'Cytochrome P450 compound I: Capture, characterization, and C-H bond activation kinetics', *Science*, 330(6006), pp. 933–937. doi: 10.1126/science.1193478.

Rude, M. A. *et al.* (2011) 'Terminal olefin (1-alkene) biosynthesis by a novel P450 fatty acid decarboxylase from Jeotgalicoccus species', *Applied and Environmental Microbiology*. American Society for Microbiology, 77(5), pp. 1718–1727. doi: 10.1128/AEM.02580-10.

Sabbadin, F. *et al.* (2009) 'The 1.5-Å structure of XplA-heme, an unusual cytochrome P450 heme domain that catalyzes reductive biotransformation of royal demolition explosive', *Journal of Biological Chemistry*. American Society for Biochemistry and Molecular Biology, 284(41), pp. 28467–28475. doi: 10.1074/jbc.M109.031559.

Sahin, E. and Roberts, C. J. (2012) 'Size-exclusion chromatography with multi-angle light scattering for elucidating protein aggregation mechanisms', *Methods in Molecular Biology*, 899, pp. 403–423. doi: 10.1007/978-1-61779-921-1_25.

Sayer, P., Gouterman, M. and Connell, C. R. (1982) 'Metalloid Porphyrins and Phthalocyanines', *Accounts of Chemical Research*, 15(3), pp. 73–79. doi: 10.1021/ar00075a002.

Schirmer, A. *et al.* (2010) 'Microbial biosynthesis of alkanes', *ScienceSchirmer, A. et al. (2010) 'Microbial biosynthesis of alkanes', Science, 329(5991), pp. 559–562. doi: 10.1126/science.1187936.*, 329(5991), pp. 559–562. doi: 10.1126/science.1187936.

Schlichting, I. *et al.* (2000) 'The catalytic pathway of cytochrome P450cam at atomic resolution', *Science*. American Association for the Advancement of Science, 287(5458), pp. 1615–1622. doi: 10.1126/science.287.5458.1615.

Schrödinger, L. (2015) 'The PyMOL Molecular Graphics System, Version 2.4.0a0'. Available at: https://www.schrodinger.com/products/pymol (Accessed: 14 March 2021).

Shaw, M. K. and Ingraham, J. L. (1965) 'Fatty Acid Composition of Escherichia coli as a Possible Controlling Factor of the Minimal Growth Temperature', *Journal of Bacteriology*, 90(1), pp. 141–146. doi: 10.1128/jb.90.1.141-146.1965.

Shimada, H. *et al.* (1991) 'The Role of Threonine 252 in the Oxygen Activation by Cytochrome P-450 cam: Mechanistic Studies by Site-directed Mutagenesis', *Studies in Surface Science and Catalysis*. Elsevier, 66(C), pp. 313–319. doi: 10.1016/S0167-2991(08)62847-5.

Shoji, O. and Watanabe, Y. (2014) 'Peroxygenase reactions catalyzed by cytochromes P450', *Journal of Biological Inorganic Chemistry*. Springer Verlag, pp. 529–539. doi: 10.1007/s00775-014-1106-9.

Singh, M. K. *et al.* (2017) 'Role of an N-terminal extension in stability and catalytic activity of a hyperthermostable α/β hydrolase fold esterase', *Protein Engineering, Design and Selection*. Oxford University Press, 30(8), pp. 559–570. doi: 10.1093/protein/gzx049.

Sligar, S. G. and Gunsalus, I. C. (1976) 'A thermodynamic model of regulation: modulation of redox equilibria in camphor monoxygenase', *Proceedings of the National Academy of Sciences of the United States of America*. National Academy of Sciences, 73(4), pp. 1078–1082. doi: 10.1073/pnas.73.4.1078.

Somvanshi, P. R. and Venkatesh, K. V. (2013) 'Hill Equation', in *Encyclopedia of Systems Biology*. Springer New York, pp. 892–895. doi: 10.1007/978-1-4419-9863-7_946.

'The CCP4 suite: Programs for protein crystallography' (1994) *Acta Crystallographica Section D: Biological Crystallography*. Acta Crystallogr D Biol Crystallogr, 50(5), pp. 760–763. doi: 10.1107/S0907444994003112.

Tyson, C. A., Lipscomb, J. D. and Gunsalus, I. C. (1972) 'The role of putidaredoxin and P450 cam in methylene hydroxylation.', *Journal of Biological Chemistry*, 247(18), pp. 5777–5784. doi:

10.1016/s0021-9258(19)44826-6.

Vagin, A. A. *et al.* (2004) 'REFMAC5 dictionary: Organization of prior chemical knowledge and guidelines for its use', *Acta Crystallographica Section D: Biological Crystallography*. International Union of Crystallography, 60(12 I), pp. 2184–2195. doi: 10.1107/S0907444904023510.

Wang, C. and Wamser, C. C. (2014) 'Hyperporphyrin effects in the spectroscopy of protonated porphyrins with 4-aminophenyl and 4-pyridyl meso substituents', *Journal of Physical Chemistry A*. American Chemical Society, 118(20), pp. 3605–3615. doi: 10.1021/jp501398g.

Wang, S. *et al.* (2020) 'Directed evolution of a hydroxylase into a decarboxylase for synthesis of 1‐alkenes from fatty acids', *ACS Catalysis*. American Chemical Society, 10(24), pp. 14375–14379. doi: 10.1021/acscatal.0c04345.

Wang, Z. J. *et al.* (2014) 'Improved Cyclopropanation Activity of Histidine-Ligated Cytochrome P450 Enables the Enantioselective Formal Synthesis of Levomilnacipran', *Angewandte Chemie International Edition*. Wiley-VCH Verlag, 53(26), pp. 6810–6813. doi: 10.1002/anie.201402809.

von der Weid, I. *et al.* (2007) 'Identification and biodegradation potential of a novel strain of Dietzia cinnamea isolated from a petroleum-contaminated tropical soil', *Systematic and Applied Microbiology*. Elsevier GmbH, 30(4), pp. 331–339. doi: 10.1016/j.syapm.2006.11.001.

Wilson, G. S., Tsibris, J. C. M. and Gunsalus, I. C. (1973) 'Electrochemical studies of putidaredoxin and its selenium analog', *Journal of Biological Chemistry*. Elsevier, 248(17), pp. 6059–6061. doi: 10.1016/s0021-9258(19)43508-4.

Wise, C. E. *et al.* (2018) 'Dioxygen Activation by the Biofuel-Generating Cytochrome P450 OleT', *ACS Catalysis*. American Chemical Society, 8(10), pp. 9342–9352. doi: 10.1021/acscatal.8b02631.

Xu, H. *et al.* (2017) 'In vitro oxidative decarboxylation of free fatty acids to terminal alkenes by two new P450 peroxygenases', *Biotechnology for Biofuels*. BioMed Central Ltd., 10(1), p. 208. doi: 10.1186/s13068-017-0894-x.

Yassin, A. F., Hupfer, H. and Schaal, K. P. (2006) 'Dietzia cinnamea sp. nov., a novel species isolated from a perianal swab of a patient with a bone marrow transplant', *International Journal of Systematic and Evolutionary Microbiology*, 56(3), pp. 641–645. doi: 10.1099/ijs.0.63863-0.

2.7 Supplementary

```
marina          MTSTAGRTRPDQVLSFLRSGYLFASRVRRRTGVSPESGAPVSMNLLGKRSVLVRGEEGVD    60
ICS0012         MTSTAGRTRPDQVLSFLRSGYLFASRVRRRTGVSPESGAPVSMNLLGKRSVLVRGEEGVD    60
indica          MTSTAGRTRSDQVLSLLRSGYLFASRVRRRTGISPESGAPVSMNLLGKRSVLVRGEEGVD    60
varians         MTSQIGQTRSEQGLSLLRSGYLFASRARRRAGLSADSGCPVRMPLLGKQTVLVRGEEGVK    60
rhizophila      MTSPFGQTRSEQGPSLLRSGYLFASRARRRAGLSSDSGCPVRMPLLGKQTVLVRGEEGVK    60
HMSC066H03      MTSQFGQTRSEQGPSLLRSGYLFASRVRRRAGLSSDSGCPVRMPLLGKNTVLVRGEEGVK    60
                ***  *:** :*  *:**********.***:*:* :**.** * ****.:*********.

marina          LFYDTSRMKRHGAMPLFIRGPLFGSGAVHALDGDAHAARKNQMADMAYEDERVAQYKPFV    120
ICS0012         LFYDTSRMKRHGAMPLFIRGPLFGSGAVHALDGDAHAARKNQMADMAYEDERVAQYKPFV    120
indica          LFYDTSRMKRHGAMPLFIRGPLFGSGAVHALDGDAHAARKNQMADMAYEDERVAQYKPYV    120
varians         LFYDTSRVQRDGAMPGVVQGPLFGAGAVHGLDGEAHRVRKNQLADMAYEDERVAAYKPFL    120
rhizophila      LFYDTSRVRRDGAMPGVVQGPLFGAGAVHGLDGEAHRVRKNQLADMAYEDERVAAYKPFV    120
HMSC066H03      LFYDTSRVQRDGAMPGVVQGPLFGAGAVHGLDGEAHRTRKNQLADMAYEDERVAAYKPFV    120
                *******::*.**** .::*****:****.***:** .****:********** ***::

marina          AEELEMLIREWTSPGNVYDGTALAFGRASFRWAGIPWSRQEMDRQARRMSRLLDTFGRPA    180
ICS0012         AEELEMLIREWTSPGNVYDGTALAFGRASFRWAGIPWSRQEMDRQARRMSRLLDTFGRPA    180
indica          AEELEMLIREWTSPGNVYDGTALAFGRASFRWAGIPWSRQEMDRQARRMSRLLDTFGRPA    180
varians         AQELEDLVTRWKDGDNVYDSTAIAFGRASFRWAGIPWSTQEMDRWAHRMSRLLDTFGRPA    180
rhizophila      AEELENLVARWKDGDNVYDSTAIAFGRASFRWAGLQWGVPEMDRWARRMSRLLDTFGRPA    180
HMSC066H03      AEELEDLVARWKDGDNVYDSTAIAFGRASFRWAGLQWGVPEMDRWAHRMSRLLDTFGRPA    180
                *:*** *: .*.. .****.**:**********: *.  **** *:**************

marina          THPISWFERFRLDRTFTQLIHGVRSGTVAADPDSVLAHMARLVDENGGLVDEKTAAVELQ    240
ICS0012         THPISWFERFRLDRTFTQLIHGVRSGTVAADPDSVLAHMARLVDENGGLVDEKTAAVELQ    240
indica          THPISWFERFRLDRTFTQLIHGVRSGTVAADPDSVLAHMARLVDENGDLVDEKTAAVELQ    240
varians         THLVSRLDRIALDRRFAALIKDVRSGKVAAPEDSVLAHMAGLVDENGELVDAKTAGIELQ    240
rhizophila      THLVSRLDRIALDRRFAALIKDVRAGKVNAPEDSVLAHMAALVDEHGELVDAKTAGIELQ    240
HMSC066H03      SHVVSRLDRIALDRRFAALIKDVRAGRVRAPQDSVLEHMAGLVDEHGELVDAKTAGIELQ    240
                :* :* ::*: *** *: **:.**:* * *  **** *** ****:* *** ***.:***

marina          NLTRPNVAVARFAAFAGAALVEHPEWAARIHEASQARGGSLLDIPEAVAFAQEVRRVYPF    300
ICS0012         NLTRPNVAVARFAAFAGAALVEHPEWAARIHEASQARGGSLLDIPEAVAFAQEVRRVYPF    300
indica          NLTRPNVAVARFAAFAGAALVEHPEWAARIHEASQARGGSLLDIPEAVAFAQEVRRVYPF    300
varians         NLTRPNVAVARFAAFAATALAEHPEWIKRIRAASEQRGGTLLDVPEAVAFAQEVRRVYPF    300
rhizophila      NLTRPNVAVARFAAFAATALVEHPEWVERIRAASEQRGGTLLDVPEAVAFAQEVRRVYPF    300
HMSC066H03      NLTRPNVAVARFAAFAATALVKHPEWVERIRTASEQCGGTLLDVPEAVAFAQEVRRVYPF    300
                ***************.:**.:****  **: **:  **:***:****************

marina          VPMLPAEATADTEIKGCPIHKGQRVLIDILGTNNDPASWERAGTFDPERFMGVDDAEAIR    360
ICS0012         VPMLPAEATADTAIKGCPIHKGQRVLIDILGTNNDPASWERAGTFDPERFMGVDDAEAIR    360
indica          VPMLPAEATADTEIKGCPIHKGQRVLIDILGTNNDPASWERAGTFDPERFMGVDDAEAIR    360
varians         VPMLPAEVTTDTEIQGCPVHKGERVVLDILGTNTDPATWDRAATFDPERFLGVEDAEAIP    360
rhizophila      VPMLPAEVTQDTEIQGCPVHKGERVVLDILGTNTDPTSWDRAATFDPERFLGVEDAEAIT    360
HMSC066H03      VPMLPAELTQDTEIQGCPVHKGERVVLDILGTNTDPASWDRAATFDPERFLGVEDAEAIT    360
                ******* * ** *:***:***:**::******.**::*:**.*******:**:*****

marina          TFIPQGGAEVRTGHRCPGEKIAVTSLSAAVVALARPNVELGTDPDDLTFSWTHMLTRPAT    420
ICS0012         TFIPQGGAEVRTGHRCPGEKIAVTSLSAAVVALARPNVELGTDPDDLTFSWTHMLTRPAT    420
indica          TFIPQGGAEVRTGHRCPGEKIAVTSLSAAVVALARPNVELGTDPDDLTFSWTHMLTRPAT    420
varians         TFIPQGGADVRTGHRCPGEKIAVTSLSAAVVALCRPEVQLPSDQDDLTFSWTHMLTRPST    420
rhizophila      TFIPQGGAEVRTGHRCPGEKIAVTSLSAAVVALCRPEVQLPGDQDDLTFSWTHMLTRPVT    420
HMSC066H03      TFIPQGGADVRTGHRCPGEKIAVTSLSAAVVALCRPEVQLPSDQDDLTFSWTHMLTRPVT    420
                ********:**********************.**:*:*  * ************ *

marina          GMRVRTAH        428
ICS0012         GMRVRAAH        428
indica          GMRVRAAH        428
varians         GVRVRSA-        427
rhizophila      GVRVRTTR        428
HMSC066H03      GVRVRSTR        428
                *:***::
```

Figure 2.21 Sequence alignment of Kocuria species. Species including *K. rhizophila*, HMSC066H03 and *K. varians* hold the GCPV sequence motif (yellow) that is postulated in disulphide linkage formation.

3 Characterisation of a cytochrome P450 CYP152 peroxygenase from *Corynebacterium efficiens*

Alessia C. Andrews[1], Harshwardhan Poddar[1], Kirsty J. McLean[3], Hazel M. Girvan[3], Richard B. Tunnicliffe[1], Tom Jowitt[2], Colin W. Levy[1], David Leys[1] and Andrew W. Munro[1]

[1]Manchester Institute of Biotechnology, Faculty of Natural sciences, University of Manchester, 131 Princess Street, Manchester M1 7DN, UK

[2]Micheal Smith Building, Faculty of biology medicine health, University of Manchester, Dover St, Manchester, M13 9PT, UK

[3]Department of Biological and Geographical Sciences, School of Applied Sciences, University of Huddersfield, Queensgate, Huddersfield, HD1 3DH, UK

3.1 Abstract

The CYP152 family of cytochrome P450 bacterial peroxygenases has evolved to efficiently use hydrogen peroxide to drive decarboxylation and hydroxylation of fatty acid substrates. These peroxygenases have become an attractive catalyst to produce terminal alkenes which can be exploited in areas such as biofuels and fine chemical production. Here we present the expression and purification of a novel CYP152 member, P450 CE (CYP152T7) from the thermotolerant soil bacterium, *Corynebacterium efficiens* YS-314. P450 CE was expressed in *E. coli*, purified, and characterised using spectroscopic, analytical and structural methods. P450 CE is able to bind, decarboxylate as well as hydroxylate both the C-alpha and C-beta positions on the fatty acids with chain lengths between C10:0 and C18:0. We show highest conversion towards the alkene product for myristic acid (C14:0) with ~50% conversion to 1-tridecene (total product: ~89%, with additional conversions to 2-OH: 15% and 3-OH: 24%). Biophysical characterisation revealed the protein is dimer in solution, corroborated by the 2.05 Å crystal structure of P450 CE in complex with myristic acid. The crystal structural reveals a unique dimeric interface, in which a heme molecule is sandwiched between two monomers and mediated by interactions by His186 to the heme iron, in addition to Phe179 and the propionate group of the heme. A H186N and H186K variants were created to explore the dimeric interface, however both variants retained dimeric properties in solution. The 2.06 Å crystal structure of H186N variant displayed a similar interface stabilised my multiple hydrophobic interactions.

3.2 Introduction

In recent years, biotechnological efforts have been focused on identifying and assembling enzyme systems that are able produce high value chemicals, such as liquid and gaseous biofuels made from microbial hosts. The conversion of CO_2 either directly or through biomass into 'drop-in compatible' hydrocarbon fuels could provide ideal renewable energy alternatives (Atsumi and Liao, 2008; Rude *et al.*, 2011). A key study by Rude *et al*. highlighted a range of terminal-alkene producing microbes including *Jeotgalicoccus* sp., *Kocuria rhizophila*, *Corynebacterium efficiens*, *Methylobacterium populi* and *Bacillus clausii*. Heterologous expression of *Jeotgalicoccus* spp. ATCC 8456 OleT ($OleT_{JE}$) in *E. coli* demonstrated novel enzymatic synthesis of terminal alkenes (in

particular 18-methyl-1-nonadecene and 17-methyl-1-nonadecene), which are derived from intermediates of fatty acid biosynthesis. $OleT_{JE}$ was assigned to the cytochrome P450 (P450 or CYP) CYP152 family of peroxygenases (Rude *et al.*, 2011).

Peroxygenases have evolved to efficiently use hydrogen peroxide (H_2O_2) as the sole oxygen, electron and hydride donor. Bypassing the requirement of O_2 binding and the timed delivery of two electrons that are ultimately derived from pyridine nucleotide coenzymes (NAD(P)H). In most P450s, electrons are transported to the heme via one or more redox partners to discrete points in the catalytic cycle, resulting in production of the ferryl-oxo porphyrin radical species compound I, the major substrate oxidising species (Rittle and Green, 2010). In contrast, peroxygenases utilise H_2O_2, with direct conversion to the ferric-hydroperoxo state (compound 0), which then rapidly undergoes dehydration to form compound I. This suggests a unique catalytic peroxygenase mechanism as shown in **figure 3.1.** Therefore, due to the bacterial peroxygenases inherently soluble nature (as opposed to many microsomal P450s), and simple requirement for H_2O_2 only, suggests these could provide robust oxidative catalysts for industrial processes.

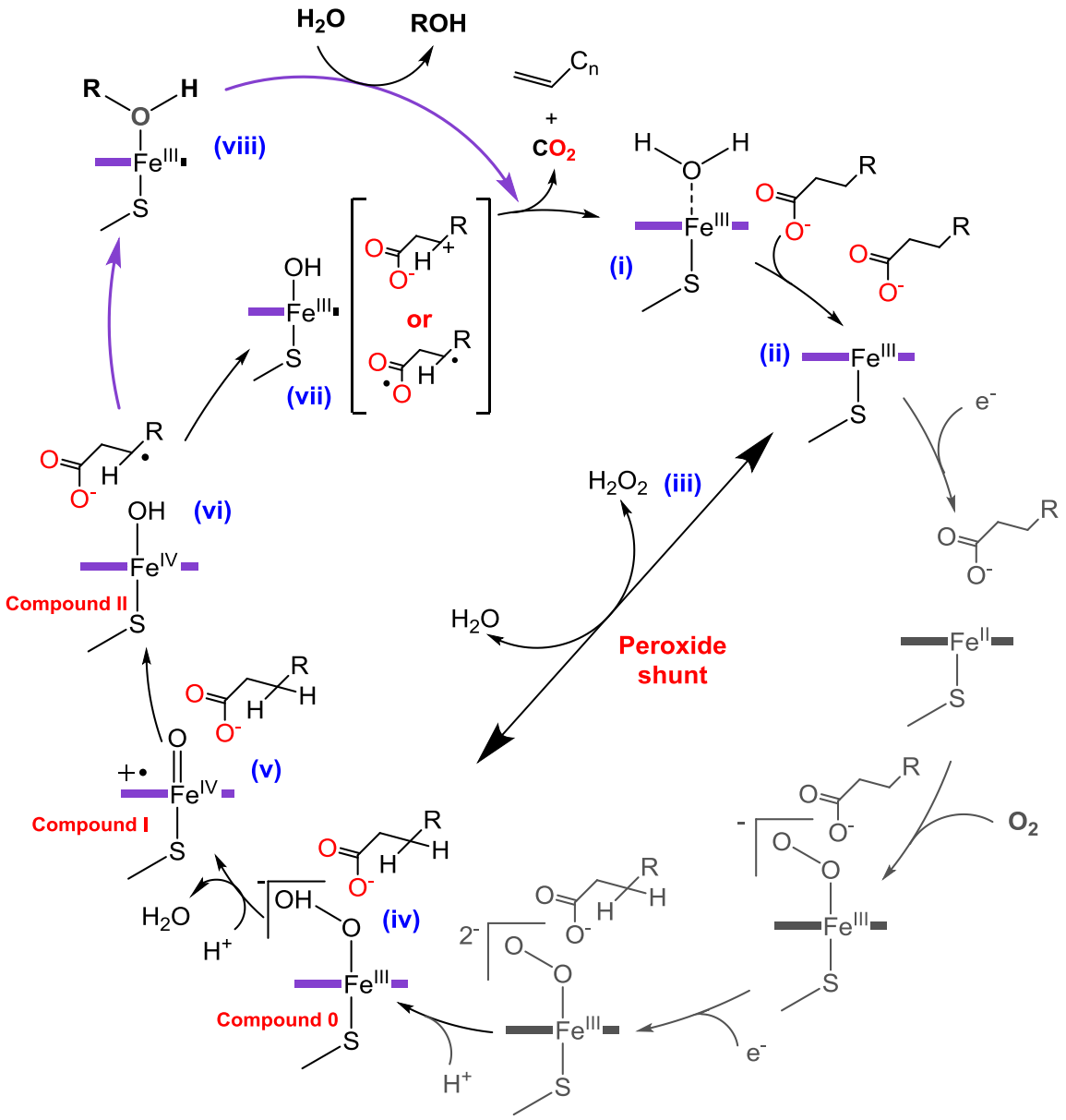

Figure 3.1 Proposed mechanism of CYP152 peroxygenases. Peroxygenases are able to carry out hydroxylation and/or decarboxylation reactions, depending on the enzyme, to produce either a terminal alkene and/or hydroxylated product, respectively. (i) the heme iron is in the resting low spin state with water coordinated as the axial ligand to the cysteine thiolate ligated heme iron; (i) binding of the substrate causes the displacement of the water molecule and causes the iron spin state shift from low spin to high spin; (iii) peroxygenases utilise the peroxide shunt pathway, that bypass electron-mediated steps (in grey), that facilitates direct conversion to compound 0 (iv) (ferric hydroperoxy species); subsequent protonation and dehydration yields the reactive ferryl oxo porphyrin species known as compound I (v); abstraction of a H-atom from the substrate with formation of a substrate radical and compound II (ferryl hydroxo species) (vi); as peroxygenases can function as mixed oxidases and decarboxylases, the catalytic cycle can bifurcate, for alkene formation Cpd II abstracts a proton from the Cβ position with formation of a carbocation intermediate or a diradical species (vii) with generation of the terminal C_{n-1} terminal alkene and a molecule of CO_2; for production of hydroxylated products oxygen rebound occurs with insertion of an –OH into the substrate (viii)

Some of the best studied CYP152 family members include *Bacillus subtilis* P450 BSβ (CYP152A1) and *Sphingomonas paucimobilis* P450 SPα (CYP152B1) (Matsunaga *et al.*, 1997, 1999). Initial studies suggest that these enzymes function as fatty acid

hydroxylases. However, Rude *et al*. subsequently demonstrated that P450 BSβ could also produce C_{n-1} terminal alkenes as well as a mixture of α-hydroxy and β-hydroxy fatty acids (**figure 3.2**). This suggests that a range of CYP152 members could undertake oxidative decarboxylation (Rude *et al.*, 2011; Matthews, Tee, *et al.*, 2017a).

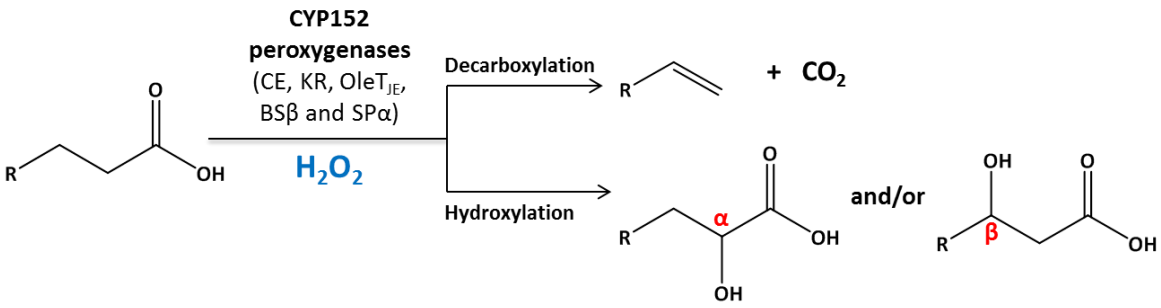

Figure 3.2 General reaction undertaken by CYP152 peroxygenase enzymes. H_2O_2 is used as a cosubstrate to drive decarboxylation of fatty acids with varying chain lengths to produce C_{n-1} terminal alkenes and carbon dioxide as a coproduct. CYP152 members can also hydroxylate fatty acids in the Cα and/or Cβ positions.

Jeotgalicoccus OleT is an efficient alkene producer, which has led to numerous studies focused on mechanistic and engineering strategies to widen substrate range and improve turnover efficiency (Bharadwaj *et al.*, 2018). OleT$_{JE}$ is able to catalyse the oxidative decarboxylation of a broad range of carboxylic acids (C4:0 – C20:0) (Dennig *et al.*, 2015; Matthews, Belcher, *et al.*, 2017). The substrate scope has been increased further with identification of α-, β-desaturase activity with branched fatty acids such as 2-methylbutyric acid (Pickl *et al.*, 2019).

The remarkable properties of OleT$_{JE}$ have led to exploration for other alkene-forming CYP152 family members. This led to the discovery of P450 KR, from *Kocuria rhizophila* (CYP152T1), that is able to decarboxylate and hydroxylate a range of fatty acid substrates (C10:0 – C18:0). The crystal structure of P450 KR demonstrated an unusual dimeric species, with an extended N-terminal helix forming a "zipper"-like interaction at the dimer interface stabilised by disulphide bonds. These unusual structural features led us onto probe homologues of P450 KR, to illustrate the extent to which these unusual features occur and link to CYP152 catalytic properties (Andrews *et al*., chapter 2).

Here we report the first expression, purification and structural characterisation of P450 CE from the thermotolerant soil bacterium, *Corynebacterium efficiens* YS-314. This enzyme displays 55% similarity with P450 KR and is a previously uncharacterised member of the CYP152 peroxygenase family.

3.3 Materials and Methods

3.3.1 Expression of P450 CE

The gene encoding P450 CE from *Corynebacterium efficiens* YS-314 was codon optimized for expression of *E. coli*, synthesised and cloned into a pET24b(+) vector, with a N-terminal polyhistidine-tag and a TEV cleavage site, under the control of a T7 polymerase promoter. P450 CE was expressed in C41 (DE3) *E. coli* cells (Lucigen). An expression trial was carried out to see the best conditions of CE production, varying concentrations of IPTG at 100 µM, 500 µM and 1 mM, the heme precursor δ-aminolevulinic acid (Δ-ALA) at 200 µM and 500 µM, and induction at either 20°C or 25°C for ~20 hours.

Freshly transformed cells were cultivated in 500 mL 2xYT broth supplemented with 50 µg mL^{-1} of kanamycin in a 2L flask at 37°C at 180 rpm. When the cell culture reached an optical density OD_{600} of 0.5, the temperature reduced to 25°C, and the cells were supplemented with 500 µM Δ-ALA. P450 CE expression was then induced with 100 µM IPTG and cells were grown for a further 20 hours. Cells were harvested by centrifugation at 6000 rpm, 4°C using a JLA-8.1000 rotor in an Avanti J-26 XP centrifuge. The cell pellet was frozen and stored at -20°C.

3.3.2 Mutagenesis of P450 CE

Rationally designed mutations H186K and H186N in P450 CE were created using the QuikChange Lightening Mutagenesis kit (Agilent) according to the published protocol. Oligonucleotide primers used were H186L Forward (Fwd): 5'-ggcacccgcttaagggaaaggccttaggctgg-3', H186L Reverse (Rvs): 5'-ccagcctaaggcctttcccttaagcgggtgcc-3', H186N Fwd: 5'-ggcacccgcttaagggaaacgccttagg-3' and H186N Rvs: 5'- cctaaggcgtttcccttaagcgggtgcc-3'. *E.coli* strain C41 (DE3) (Lucigen) was used as the expression host for CE variants, expression is as followed for WT P450 CE.

3.3.3 Purification of P450 CE

3.3.3.1 Buffer screen

Purified CE was buffer exchanged into low concentration buffer (10 mM Tris-HCl, 500 mM NaCl (pH 8.0)). Samples were then diluted to 1 mg mL^{-1} in a 1:1 with the Durham pH screen (Molecular Dimensions). Samples were loaded on UNcle (Unchained Labs) with a thermal ramp from 20 – 90°C with a ramp rate of 1°C min^{-1}. Uncle analysis software calculated the T_m using the first derivative of the ratio of fluorescence at 350 and 330

nm and T_{agg} using the onset of aggregation at 266 nm. For intrinsic fluorescence and SLS data were monitored at 266 and 473 nm.

3.3.3.2 Final Purification

Cells were thawed at 4°C and resuspended in buffer A (0.1 M Tris, 0.75 M NaCl, 10 % glycerol, pH 8.0), with 20 mM imidazole, protease inhibitor tablets (SIGMAFAST™ Protease Inhibitor Cocktail Tablets, EDTA-Free, 1 per 100 mL of suspension), 100 mg $MgCl_2$, DNase I (10 µg mL^{-1}, bovine pancreas, Sigma-Aldrich, Poole UK) and Lysosome (10 µg mL^{-1}, hen egg white, Sigma Aldrich). The cells were disrupted by sonication using 10 s bursts, at 50 s intervals and 30% amplitude for 30 mins (Bandelin SONOPULS sonicator with VS 70 T probe). The cell lysate was ultra-centrifuged (40,000 rpm, 45 min, 4 °C) using Beckman Coulter Ti45 rotor.

The supernatant was mixed with 10 mL of Ni-IDA agarose resin (Generon) pre-equilibrated using buffer A with 20 mM imidazole. The resin-protein mix was incubated for 1 hr at 4°C on a roller platform before it was transferred to an empty chromatography column. The resin with P450-CE bound was washed using 10 column volumes (CV) of buffer A with 20 mM imidazole, followed by 10 CV of buffer A with 50 mM imidazole and 5 CV of buffer A with 75 mM imidazole. P450 CE was eluted with 300 mM imidazole in buffer A. TEV protease expressed using pRK793 (a gift from David Waugh, Addgene plasmid # 8827) (Kapust *et al.*, 2001) and purified as in (Andrews *et al*., chapter 2), and was added to the eluted P450 CE in a 1:5 molar ratio (CE:TEV) and incubated overnight at 4°C on a rolling board. Cleaved P450 CE was exchanged into buffer A using a PD-10 Sephadex desalting column (GE Healthcare). The imidazole-free CE-TEV protease mixture was then applied to Ni-IDA resin pre-equilibrated with buffer A to separate the cleaved his-tag free P450 CE, from the TEV protease and uncleaved protein. The resin was washed with 5 CV of buffer A before the cleaved protein was eluted using buffer A with 20 mM imidazole. Eluted CE was concentrated by centrifugation using a Vivaspin centrifugal concentrator with 30 kDa MWCO (Generon). Concentrated protein was loaded onto a Superdex 200 pg 16/600 gel filtration column equilibrated with buffer B (0.1M Tris, 0.75 M NaCl, pH 8.0).

3.3.4 UV-visible spectroscopy and protein quantification

Analysis of the UV-visible (UV-vis) spectroscopic properties of P450 CE and CE H186N mutant were carried out using a Cary 60 UV-vis spectrophotometer (Varian, UK). For CO-

binding titrations, spectra were recorded using ~6 µM of protein in buffer A. Protein samples were reduced by sodium dithionite and carbon monoxide (CO) was introduced by slowly bubbling of the gas into the reduced protein sample. Spectra were collected every minute for an hour or until complete formation of the ferrous-CO complex was observed. The extinction coefficient of P450 KR was determined by pyridine hemochromagen assay as discussed in (Barr and Guo, 2015), obtaining ε_{424} 102 mM^{-1} cm^{-1}.

3.3.5 Fatty acid binding titrations of P450 CE proteins

Substrate binding affinity of P450 CE and the H186N mutant was assessed using UV-visible spectroscopy to determine dissociation constants (K_d values). Titrations were carried out in 1 cm path-length quartz cuvette, at 25^{o}C with 2-6 µM of protein in buffer A. Fatty acid substrates (C10:0 – C16:0) were prepared in absolute ethanol, and added to the cuvette to a maximum of <3% of total volume. Spectra were recorded between 800 – 300 nm for the substrate-free enzyme and then following stepwise additions of fatty acids that were titrated into the cuvette using 0.1-0.5 µL additions by Hamilton syringe.

Data analysis was carried out using OriginPro software (OriginLab). The difference spectra were computed by subtracting the spectrum for the ligand-free protein from each of the fatty acid-bound spectra post substrate addition. From these, the maximum (Δ_{peak}) and minimum (Δ_{trough}) wavelengths were identified. The overall absorbance change was calculated by determining $\Delta Abs(A_{peak} - A_{trough})$ using the same wavelength pair throughout, and these data were then plotted against the relevant ligand concentration to determine dissociation constant (K_d) values. Data were fitted using the relevant equation. Substrates with sigmoidal dependence of absorbance change on substrate concentration, therefore the Hill equation was used ($\Theta = [L]^n / K_D + [L]^n$) where the number of bound ligands *n* is the Hill coefficient (Somvanshi and Venkatesh, 2013).

3.3.6 Fatty acid biotransformations

3.3.6.1 *In vitro* substrate turnover

All reactions contained 1 µM CE enzyme, 500 µM fatty acid substrate (C10:0, C12:0, C14:0, C16:0 and C18:0 dissolved in ethanol) with a final volume of 0.5 mL in buffer A (0.1 M Tris, 0.75 M NaCl, 10 % glycerol pH 8.0), and were initiated following addition of

500 µM H_2O_2. Reactions were incubated at 27°C for 30 minutes with shaking at 700 rpm. For reactions with multiple additions of H_2O_2, either 1 µM or 5 µM of CE enzyme were used, following initial addition of 100 µM of H_2O_2, every 10 mins for 50 mins, and incubated for 50 minutes. Reactions were stopped using 40 µL of 37% HCl. Internal standards (of different fatty acid chain length) were added (50 µM n-1 alkene, 50 µM fatty acid, 25 µM 2-OH fatty acid, and 25 µM 3-OH fatty acid). Reactions were extracted using equal quantities of DCM. The DCM layer was removed and dried using anhydrous $MgSO_4$ and mixed with equal volumes of N,O-bis(trimethylsilyl)trifluoroacetamide (BSTFA) containing 1% trimethylchlorosilane (TMCS) and incubated at 60°C for 45 minutes to derivatise fatty acids.

3.3.6.2 Gas chromatography Mass spectrometry

Directly after derivatisation, 1 µL of the sample was injected onto a 5975 series MSD coupled to a 7890 GC system, installed with a VF5-HT 5 % phenyl-methyl column (30 m, 0.25 mm, 0.25 µm). The front inlet was set at 250^{o}C, and a split ratio of 10:1 was used. The column flow was set at 1.2 mL min^{-1}, the oven was held at 40^{o}C for 1 min before being ramped at 10^{o}C min^{-1} until 250^{o}C. Ramping was then increased to 100^{o}C min^{-1} until 350^{o}C, and held for 2 minutes. The solvent delay was set at 2.5 minutes. Electron ionization was used, with m/z ratios of 40–500 were recorded at 5 Hz and at 230^{o}C. Quantification of products formed were estimated using external standard calibration curves and internal standards.

3.3.7 Size exclusion chromatography multi-angle light scattering

Purified samples (0.5 mL) were loaded onto a Superdex 200 (GE Healthcare) at 0.75 mL min^{-1} in buffer C (0.1M Tris, 0.5M NaCl (pH 8.0)) and passed through a Wyatt Heleos II EOS 18-angle laser photometer coupled to a Wyatt Optilab rEX refractive index detector. Data analysis were performed (Hydrodynamic radii and molecular mass measurements were analysed) using Astra 6 (Wyatt Technologies).

3.3.8 Analytical Ultracentrifugation

P450 CE was gel filtered into 0.1 M Tris, 0.75 M NaCl (pH 8.0) buffer using a HiLoad 16/600 superdex 200 pg column (GE healthcare). P450 CE was then diluted to concentrations of 0.25, 0.5, 1, 2, 5, 10 and 20 µM. Samples were then loaded into a six-sector Epon charcoal-filled centrepiece equipped with quartz windows for

sedimentation equilibrium analysis. Sedimentation velocity experiments were ran as Andrews *et al*., chapter 2).

3.3.9 Crystallography of P450 CE

Purified CE in buffer B (0.1 M Tris, 0.75M NaCl, pH 8.0) and was concentrated to 13 mg/mL, using Vivaspin concentrators (30,000 MWCO). Commercial screens (Morpheus®, BCS, PACT, and JCSG) from Molecular Dimensions were used to set up crystallisation trials. For P450 CE (WT) a nano-dispenser (Mosquito TTP Labtech) was used to set up drops of 150 nL volume, in a ratio of 1:1 (protein: reservoir) and these were left to equilibrate at 4 °C. A crystal of P450 CE (presented) was found in JCSG-plus HT-96 (0.2 M Ammonium Citrate dibasic, pH 5.5, 20% PEG 3000. The P450 CE (H186N) mutant was concentrated to 17 mg/mL and drops of 200 nL (same as P450 CE WT) and found in Morpheus® 0.1M MES, 0.1M imidazole, 0.12 M ethylene glycols, 30% v/v PEG 8000 pH 6.5.

3.4 Results and Discussion

3.4.1 Expression and purification of P450 CE

Three different *E. coli* strains (BL21(DE3), C41(DE3) and ArticExpress(DE3)) were chosen for the initial expression screening. A core expression revealed C41 DE3 cells were the ideal candidate to support large-scale over-expression and purification of P450 CE. In addition, the effects of induction temperature, IPTG and δ-aminolevulinic acid (Δ-ALA) concentration on the expression of P450 CE were investigated. We found that the concentration of Δ-ALA was vital in the production of heme-containing protein, as we saw cultures that were grown with the addition of 500 µM (compared to 200 µM) Δ-ALA showed increase heme incorporation as demonstrated by a higher Soret absorbance (relative to the heme-bound protein concentration) (**see supplementary figure 3.19**). Control of the temperature of induction is essential in properly folded and monodisperse P450 CE. When CE is induced at high temps (37–28°C), we observe an increase in aggregated and misfolded protein. When induction occurs at 25–20°C, we see a reduction in aggregation and formation of a single monodisperse peak relating to that of the P450 CE dimer (**see supplementary figure 3.20**).

We tested a number of variables for the purification of P450 CE to maximise yield, reproducibility and purity. The Durham pH Screen (Molecular dimensions) was used to

identify an appropriate buffering system (taking into account pH and salt concentrations) and analysed CE proteins via Uncle (unchained labs). This technique couples fluorescence, static light scattering (SLS) and dynamic light scattering (DLS) to identify appropriate formulation properties for protein stability. This screen identified buffer systems: Tris-HCl, Bicene, Tricine and Hepes buffer solutions, with varying salt conditions. The salt concentration is important factor to consider, as other decarboxylating CYP152 members, such as P450 $OleT_{JE}$ from *Jeotgalicoccus* and P450 KR from *Kocuria rhizophila*, require a high salt concentration (~0.75 M NaCl) during purification to stabilise the protein. Indeed, both these proteins have the propensity to aggregate a low salt concentrations (Rude *et al.*, 2011; Belcher *et al.*, 2014). In contrast, P450 CE can tolerate a wider range of salt concentrations, as low as (~0.2 M NaCl), making it more of an ideal candidate for biotechnological applications, where high salt concentrations (0.75 M) are likely unfavourable.

Thermal ramp stability measurements melting temperatures (T_m) and aggregation temperature (T_{agg}) are highlighted in **table 3.1**. T_m is determined by the intrinsic fluorescence of tryptophan and tyrosine residues as the protein undergoes conformational changes as the temperature increases. T_{agg} measures the onset of protein aggregation through static light scattering (SLS) at two different wavelengths (266 and 473 nm). From the T_m distribution these conditions do not affect thermal stability, although a notable increase is seen with the addition of glycerol. SLS measured with a T_{agg} at 266 and 473 nm, which gives some information about the onset of aggregation and particle size. SLS at 266 nm usually is sensitive to changes in intensity to discern smaller particles, whereas SLS at 473 nm is useful for detection of larger aggregates. From these data, a buffering system of 0.1 M Tris-HCl (with salt concentrations depending on experiment, at pH 8.0 with the addition of 10% glycerol was chosen. P450 KR samples were expressed and purified as in (Andrews *et al*., chapter 2) and prepared in 0.1 M KPi, 0.75 M NaCl, 10% glycerol pH 8.0. $OleT_{JE}$ was expressed and purified as in (Belcher *et al.*, 2014) and prepared in 0.1 M KPi, 0.75 M NaCl, 10% glycerol pH 8.0. P450 CE displays increased thermal resistance in comparison to $OleT_{JE}$ and P450 KR. This could be attributed to *C. efficiens* thermotolerant properties, growing well at 45°C (Fudou *et al.*, 2002). From these data, a buffering system of 0.1 M Tris-HCl (with salt concentrations depending on experiment, at pH 8.0 with the addition of 10%

glycerol was chosen. Bicene/tricene was not taken forward due to the recommendation of only using these systems at low temperatures (Good *et al.*, 1966).

Table 3.1 Summary of thermo stability and aggregation of P450 CE and CYP152 members. Thermal melting (T_m) temperature and thermal aggregation (T_{agg}) measurements were made using the UNcle instrument. Protein samples were prepared to a concentration of 1 mg mL^{-1}. Data were collected by a thermal ramp from 20 – 90°C, T_{agg} data were collected using static light scattering at two wavelengths, 266 and 473 nm.

Buffer system	T_m (°C)	T_{agg} 266 (°C)	T_{agg} 473 (°C)
CE: 0.1 M Tris-HCl, 0.75 M NaCl, pH 8.0	**61.2**	**54.2**	**57.6**
+ 10% glycerol	**66.0**	**56.1**	**58.7**
CE: 0.1 M Tris-HCl, 0.25 M NaCl, pH 8.2	62.4	60.5	62.1
CE: 0.1 M Tris-HCl, 0.25 M NaCl, pH 8.7	62.4	60.6	62.2
CE: 0.1 M Hepes, 0.25 M NaCl, pH 8.0	63.6	61.6	63.1
CE: 0.1 M Tricine, 0.25 M NaCl, pH 8.5	63.7	61.2	63.3
CE: 0.1 M Bicine, 0.25 M NaCl, pH 8.2	63.4	61.2	62.8
$OleT_{JE}$: 0.1M KPi, 0.75 M NaCl, 10% glycerol pH 8.0	**48.6**	**44.5**	**42.3**
P450 KR: 0.1M KPi, 0.75 M NaCl, 10% glycerol pH 8.0	**51.3**	**47.2**	**46.1**

A three-step chromatography method was used to prepare pure P450 CE and variants. An initial Ni-IDA affinity chromatographic step in which high imidazole eluent is incubated with TEV protease to remove the histidine-tag. A reverse Ni-IDA column is then used to separate the cleaved his-tag free protein from the TEV protease and his-tag CE (as described in **section 3.3.3**). This step has proven important in separation and removal of misfolded/aggregated protein. Comparisons of AKTA chromatograms from the gel filtration procedure show that the flow-through eluent has peaks relating to a large oligomers in the void volume, whereas the P450 CE eluted from the reverse nickel affinity column with buffer A in 20 mM imidazole displays highly purified P450 CE protein in a single homogeneous peak at ~77 mLs (Superdex 200pg 16/600 GL) which suggests Mw of ~75 – 85 kDa. **Figure 3.3** shows highly purified samples of P450 CE by SDS-PAGE with a single band at ~48 kDa, with Rheinheitzahl (Rz) value (ratio of the heme 424 nm to the protein 280 nm absorbance) of ~1.2. The discrepancies in protein size could suggest that P450 CE exists as an oligomer (most likely a dimer) in solution.

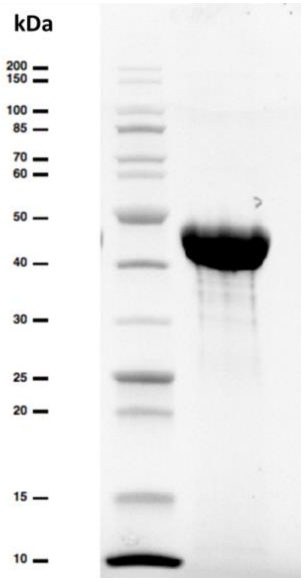

Figure 3.3 Final purity of P450 CE. Proteins are resolved on a 12 % SDS PAGE gel. The first lane shows markers of indicated size (NEB Unstained Protein standard). The second lane contains purified non-tagged P450 CE after gel filtration, with protein band matching expected molecular weight of 48 kDa.

3.4.2 UV-visible properties of P450 CE and variants

The tag-free P450 CE was analysed by UV visible spectroscopy to establish the characteristics of the heme prosthetic group. **Figure 3.4** shows the characteristic absorption spectra for P450 CE in its oxidised ferric (Fe^{III}) and sodium dithionite-reduced ferrous (Fe^{II}) forms, as well as the ferrous-carbon monoxide (CO) bound species. In the resting ferric state, P450 CE displays an unusual major Soret absorbance at 424 nm, with smaller α- and β-bands in the visible region at 575 and 539 nm, respectively. These values are very similar to the related CYP152 family member P450 KR (Soret: 424nm; Q-band features: 576nm and 541nm), in which P450 CE displays ~55% homology towards P450 KR (Andrews *et al*., chapter 2). As observed for KR, P450 CE absorption features have been red-shifted compared to those for typical CYP152 family members and other P450s in general (e.g. CYP152K6 from the methylotroph *Bacillus methanolicus* MGA3, with Soret absorbance 418 nm and smaller α- and β-bands at 568 nm and 535 nm (Girvan *et al.*, 2018); $OleT_{JE}$ decarboxylase from *Jeotgalicoccus* (CYP152L1) with major absorption features at 418, 566 and 535 nm (Belcher *et al.*, 2014); *Bacillus megaterium* fatty acid hydroxylase P450 BM3 (CYP102A1) heme domain at 418, 535 and 568 nm (Girvan *et al.*, 2004)). The red-shifted 424 nm Soret absorbance noted in P450 KR and P450 CE displays a peculiar trait of these enzymes. Characterisation of other CYP152 members have shown a subset of these enzymes e.g. CYP-MP from *Methylobacterium populi* with absorption maximum 422 nm (Amaya, Rutland and Makris, 2016). As we and

others have postulated, the spectroscopic features could arise from an endogenous distal ligand or nitrogenous amino acid positioning with the active site (Amaya, Rutland and Makris, 2016).

Upon reduction of the enzyme with sodium dithionite, the Soret band shifts to ~414 nm with diminished intensity and broadening of the Q-band visible features, with a slightly asymmetric feature present at ~540 nm. Blue shift of the Soret spectrum indicates the ferrous heme iron retains the cysteine thiolate coordination (Luthra, Denisov and Sligar, 2011). These reduced spectral maxima are similar to those features seen in P450 KR from *Koccuria rhizophila* (CYP152A1; 410 and 555 nm), for XplA from *Rhodococcus rhodochrous* which catalyses the denitration of the explosive RDX (CYP177A1; 408 and 542 nm) (Bui *et al.*, 2012), and the camphor hydroxylase P450cam from *Pseudomonas putida* (CYP101A1; 408 and 542 nm) (Tyson, Lipscomb and Gunsalus, 1972). Addition of CO under anaerobic conditions produces the characteristic P450 heme spectrum, with the Soret absorbance red-shifted to ~448 nm, and the Q-band features at ~550 nm. A small feature present as a shoulder at ~420 nm indicates a proportion of the sample (<5 %) is in the P420 form due to the presence of the cysteine-thiol coordinated form of the P450 CE Fe^{2+}-CO complex (Driscoll *et al.*, 2011; Munro *et al.*, 2013). P450 CE variants displayed the same spectroscopic properties as WT P450 CE retaining Soret absorbance at 424 nm.

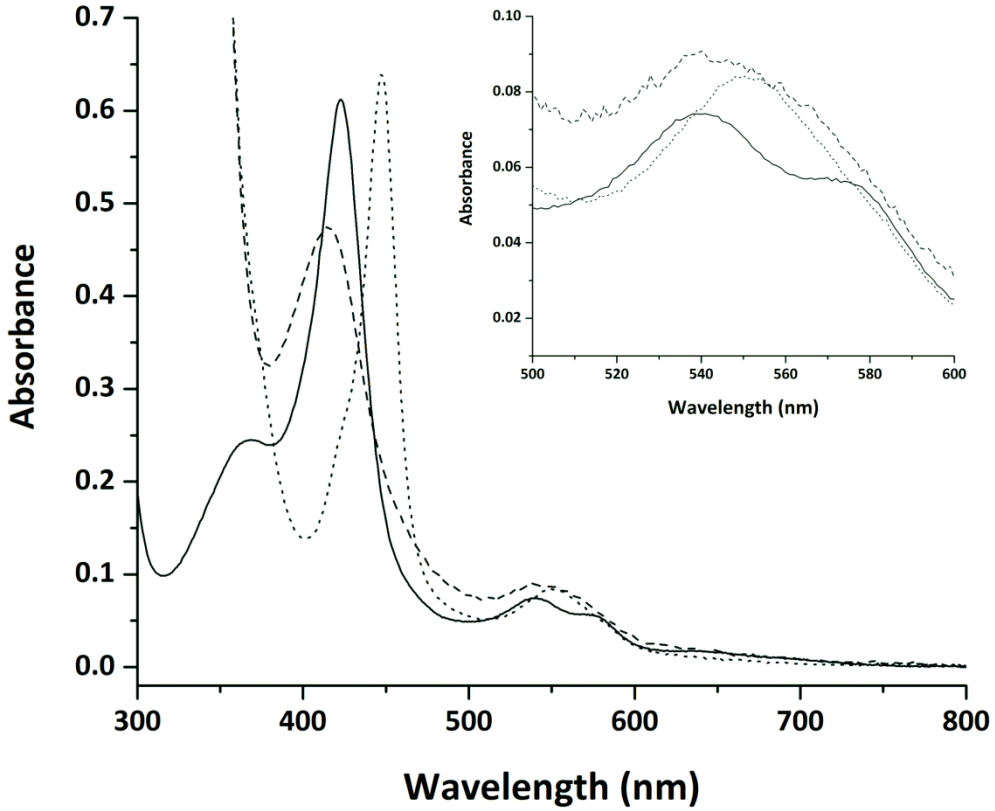

Figure 3.4 UV-visible spectroscopic features of P450 CE. UV-visible spectra of P450 CE (~6 µM) are shown for: (i) oxidised P450 CE, in its resting low spin oxidised ferric (Fe^{III}) substrate-free form (—) with a water molecule as the sixth axial ligand with Soret absorbance observed at ~424 nm and alpha- and beta- band features at 575 and ~539 nm, respectively. The sodium dithionite reduced ferrous (Fe^{II}) form (---) which displays a blue shifted Soret feature at 414 nm, with a single asymmetric Q-feature observed at 540 nm. Carbon monoxide bound, ferrous form (Fe^{II}-CO) of P450 CE (····) demonstrates a characteristic 448 nm feature accompanied by a small proportion of the thiol coordinated cytochrome P420 form, and a single asymmetric Q-band feature at ~550 nm.

3.4.3 Crystal structure of P450 CE and H186N variant

The crystal structure of WT P450 CE was determined to 2.05 Å resolution and is shown in **figure 3.5**. It exhibits the typical P450 fold, with a triangular shape (61 Å by 53 Å and 42 Å wide) with a conserved core of α-helices with the prosthetic heme group buried in the core between the distal I-helix and proximal L-helix (Presnell and Cohen, 1989; Denisov *et al.*, 2005). The heme group is bound to a conserved cysteine residue, Cys-377 in P450 CE. The long I-helix runs along the entire molecule on the distal side of the heme and makes up part of the active site. The overall protein fold closely resembles that of other CYP152 family members (with a root mean square deviation of 1.3 Å for Cα 293 atoms with $OleT_{JE}$, 1.4 Å for 320 atoms with P450 SPα and 1.4 Å for 308 atoms with P450 BSβ) (see **figure 3.6**).

The surface hydrophobicity and charge of the protein is visualised using the YRB colour scheme shown in **figure 3.7** (Hagemans *et al.*, 2015). Two distinct channels (I and II) are observed that connect to the active site cavity of the protein to the surface. On the proximal face of the protein there is a large spread of hydrophobic residues (highlighted in yellow in **figure 3.7**), that lie in and around the opening of a channel I that leads directly into the active site, reflecting the lipophilic nature of the fatty acid substrate.

Channel I has a large opening and inspection of this cavity revealed some characteristic Y-shaped fatty acid density as originally observed in P450 BM3 (Li and Poulos, 1997) and P450 SPα and BSβ BSβ (Lee *et al.*, 2003; Fujishiro *et al.*, 2011). The electron density in the cavity suggests the presence of three myristic acid (C14:0) molecules present. Interestingly, we thus observe three different binding modes for each of the myristic acid molecules in the active site (**figure 3.7 and 3.8C**), with only one myristic acid representative of the catalytic relevant binding mode (**figure 3.5**).

The carboxylate head group of this myristic acid makes strong hydrogen bonding interactions to the phylogenetically conserved arginine residue (Arg248) present in CYP152 peroxygenases, with no other direct polar contacts made between the fatty acid substrate and protein (see **figure 3.5**). The interaction between the carboxylate group and the Arg residue provides particular restraints to substrate rotation. This controls where the H-abstraction occurs as some C—H groups inaccessible, and therefore providing some control over decarboxylation and/or hydroxylation catalytic route taken (Pickl *et al.*, 2019).

This important Arg248 present in the I-helix and is placed perpendicular to the heme plane and makes up part of the active site cavity, this holds the Cα and Cβ carbons of the bound fatty acid above the heme where they are poised for catalysis (4.8 Å and 6.1 Å, respectively) (see **figure 3.5**). This is similar to $P450_{BS\beta}$ positions (Cα 5.0 Å and Cβ 6.2 Å. $P450_{BS\beta}$ mainly functions as a hydroxylase when myristic acid is used as a substrate, conversions to 1-tridecene 26%, 39% and 35% conversions to the α- and β-hydroxylated products, respectively (Wang *et al.*, 2020). P450 CE mainly functions as a decarboxylase towards myristic acid (as described in **section 3.4.4**). There are some extensive interactions made with several hydrophobic residues that line the active site pocket to help stabilise the alkyl chain of the substrate.

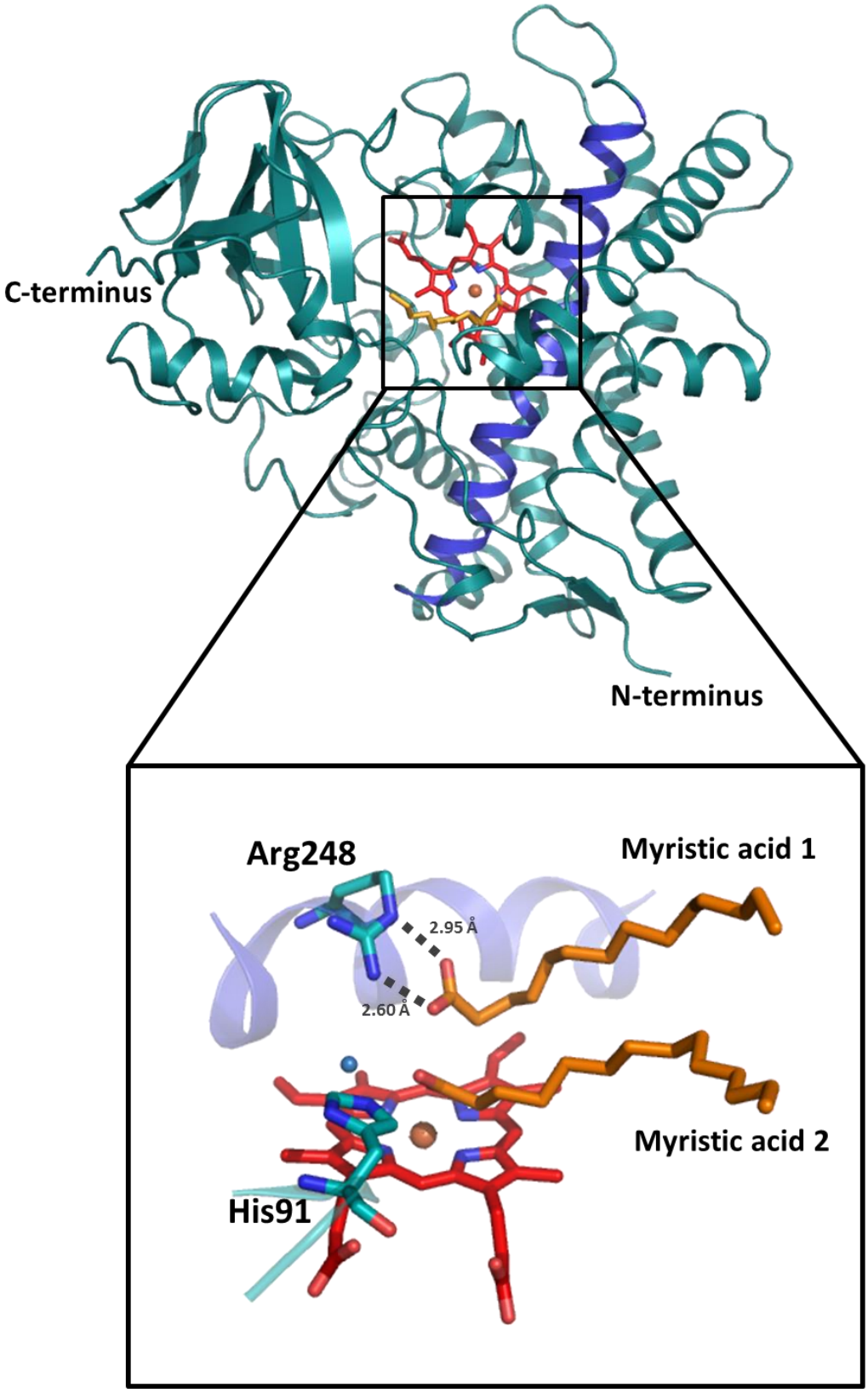

Figure 3.5 Overall structure of P450 CE in complex with myristic acid. Cartoon representation of the overall structure of P450 CE from *Corynebacterium efficiens*. The I-helix that holds the Arg248 residue is coloured in dark blue. The boxed area shows zoomed in portion of the active site with the heme represented in red sticks, the bound myristic acid molecule (detonated as myristic acid 1) and the second myristic acid molecule present in the active site (denoted as myristic acid 2) depicted by orange sticks. The dashed lines show the bonding interactions between the myristic acid and the important Argine-248 residue in angstroms (Å) and water molecule represented as a blue sphere.

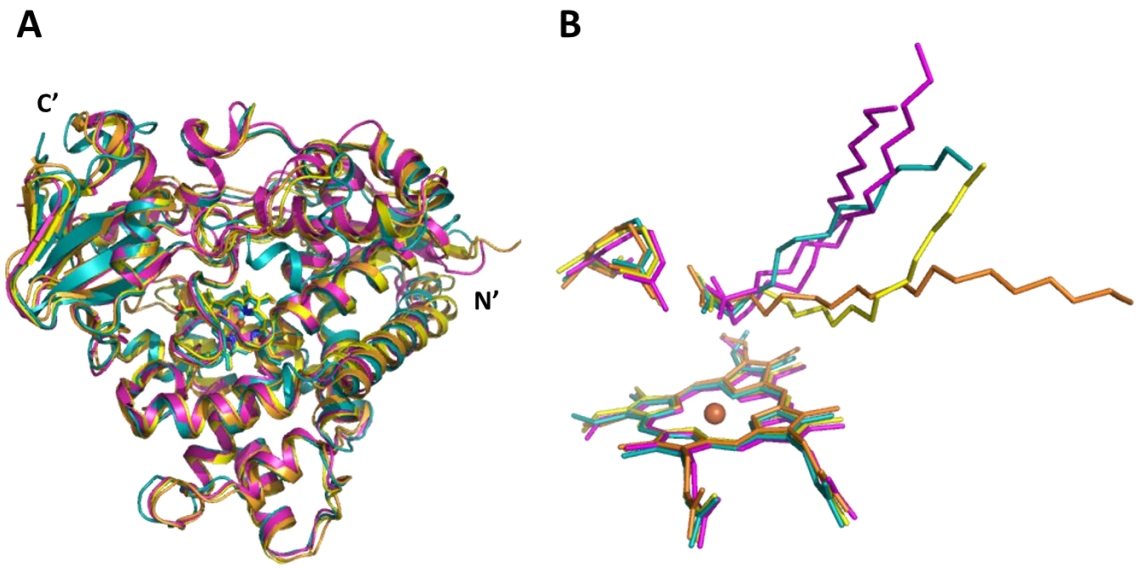

Figure 3.6 Structural comparison of published CYP152 peroxygenase members. Panel A shows the overlay of Cα carbons of P450 CE (teal), $OleT_{JE}$ (PDB: 4L40, orange), P450 SPα (PDB: 3AWM, pink) and P450 P450 BSβ (PDB: 1IZ0, yellow) with fatty acid bound in the active site. Panel B depicts a close up of the active site with the heme, arginine residue and fatty acid substrate represented by colour sticks. P450 CE shows myristic acid (C14:0), $OleT_{JE}$ arachidic acid (C20:0), P450 SPα palmitic acid (C16:0) and P450 BSβ palmitoleic acid (C16:1).

The protein that was taken forward for crystallisation was purified in the substrate-free from, with no substantial changes in the UV-visible spectrum present in low-spin Soret absorbance (λ at 424 nm). Spectral binding titrations (as discussed below in **3.4.4**) show perturbations of the Soret towards the HS state (**figure 3.14**) with addition of myristic acid.

Therefore it raises an interesting question as to whether myristic acid present was co-purified (myristic acid is prevalent metabolic product in *E. coli* cells (Shaw and Ingraham, 1965). P450 CE does display a mixed spin-state (HS λ 397 nm present) initially after the sonication and centrifugation process (**supplementary figure 3.19**). Therefore there could be some retention of the myrtistic acid from the purification process. Crystal structures of CYP152 member such as CYP152K6 from *Bacillus methanolicus* and P450 SPα co-crystallise with fatty acids (palmitic acid and myristic acid, respectively). However in both these enzymes, the addition of the fatty acid failed to produce any significant shifts to its spin-state equilibrium accompanied by a change in the UV-vis spectrum of the protein (Fujishiro *et al.*, 2011; Girvan *et al.*, 2018).

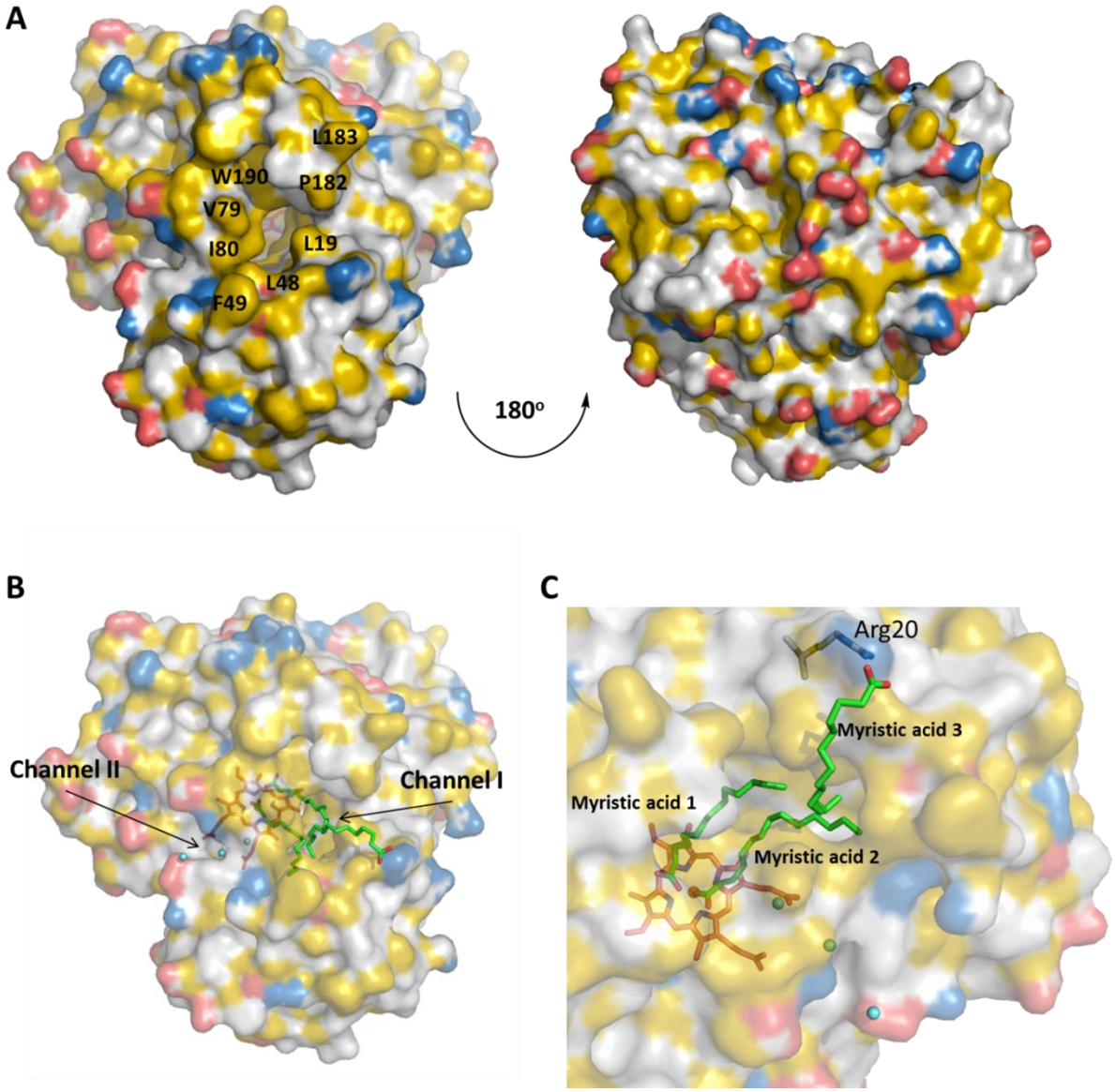

Figure 3.7 hydrophobicity and charge of P450 CE surface. Panel A shows surface highlighted by YRB, with the hydrophobic lining channel I then a 180° turn of the molecule. Panel B highlights the two channels which connect the active site to the protein surface. Channel I is involved in the binding of the fatty acid molecule in which the heme is represented by red sticks, the myristic acid molecules are represented by green sticks. Channel II is highlighted with water molecules modelled as blue sphere. Panel C shows a zoomed in version where the third myristic acid molecule is bound to the Arg20 residue on the protein surface. YRB colour scheme: yellow represents potential for hydrophobic interactions; positive charges in lysine and arginine blue and oxygen atoms in the side chains of glutamate and aspartate are red.

In addition to the myristic acid-bound to Arg428, additional density is seen in the active site that corresponds to a second fatty acid molecule in close proximity of the heme group. For the latter, the carboxylate group is not interacting with the active site arginine residue, but is ligating the iron of the heme (2.7 Å) and H-bonding to a water molecule present in the active site (**figure 3.5**).

Finally, electron density corresponding to a third fatty acid molecule was also observed, located near the opening of channel I. **Figure 3.7C** shows the third fatty acid molecule has its carboxylic acid head group interacting with an arginine residue (Arg20) on the protein surface. The omega (ω) end of the fatty acid chain is 19.6 Å away from the heme iron. Therefore, this myristic acid is highly unlikely to be involved in catalysis.

A histidine residue (His91) is present in the active site (His85 in $OleT_{JE}$), which protrudes into the active site, sandwiched between the Phe85 residue (see **figure 3.8**). His91 in CE makes an interaction with a second myristic acid molecule in the active site and is generally conserved within the CYP152 family (including $OleT_{JE}$ and P450 KR). The His residue is replaced by Glu acid in P450 BSβ, SPα and K6, which usually favour fatty acid hydroxylation (Rude *et al.*, 2011; Girvan *et al.*, 2018). This histidine residue was postulated to function as a proton donor towards the reactive iron-oxo species (Belcher et al., 2014). A study by Matthews and co-workers created a H85Q $OleT_{JE}$ mutation, which displayed preference towards the decarboxylation route and displayed a similar product profile to the WT protein. The major difference being reduced HS heme formation and weaker ability of binding towards fatty acid substrate, a property which is consistent in P450 SPα and BSβ (Imai *et al.*, 2000; Lee *et al.*, 2003; Matthews, Belcher, *et al.*, 2017).

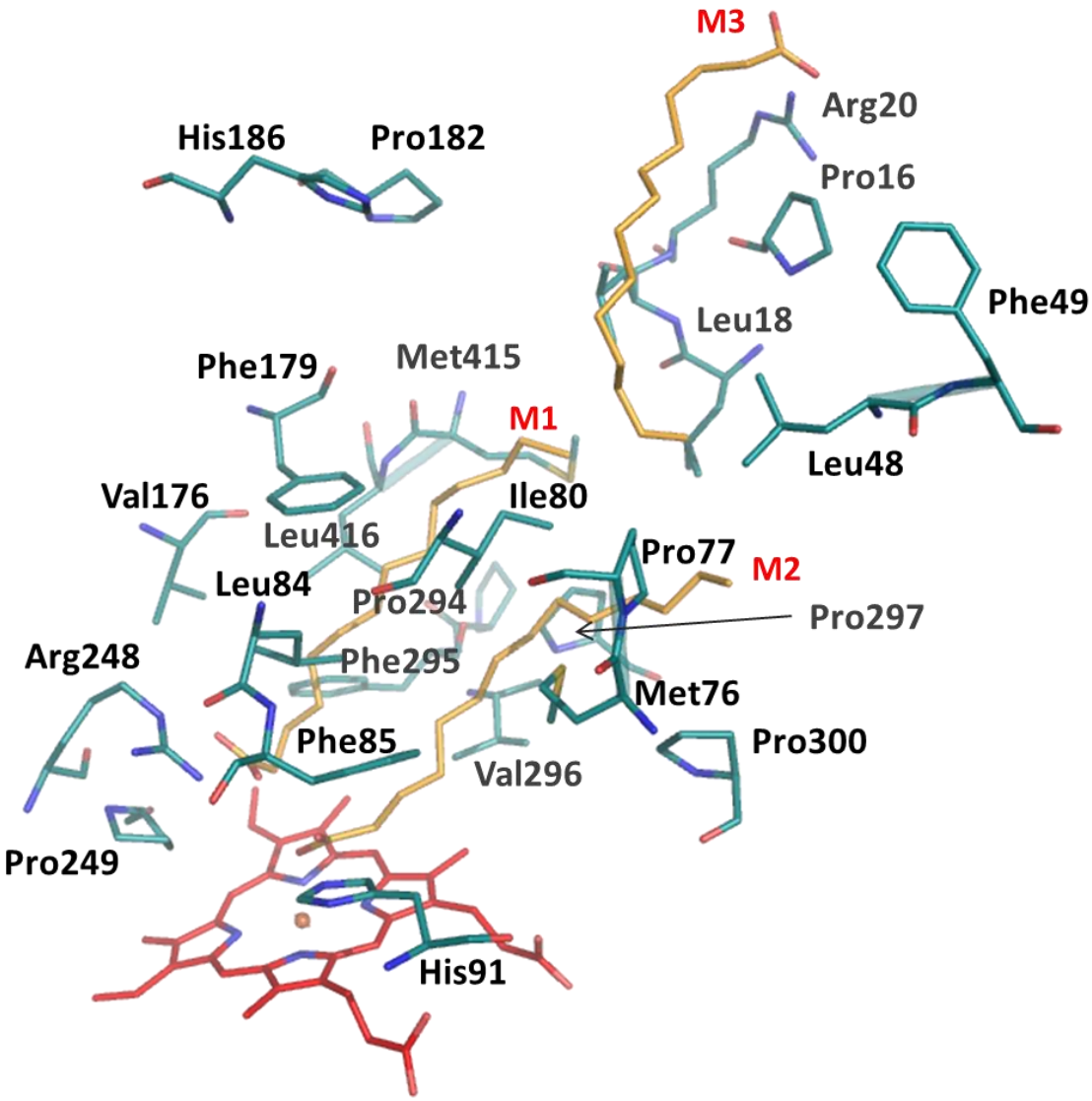

Figure 3.8 Active site structure of P450 CE. Residues involved in hydrophobic interactions and line the active site canal. Three myristic acid residues present are coloured in yellow and labelled by (M 1 – 3).

P450 CE also displays a smaller second channel (channel II), similar to other CYP152 members, that we can postulate is involved with the ingress of H_2O_2 and the egress of H_2O (Fujishiro *et al.*, 2011). The channel is lined with hydrophilic residues (e.g. Ser92/ Asp73) as well as a cluster of waters that form a H-bonding network along the cavity (see **figure 3.7B**).

A proline residue (Pro249) follows after the Arg248 and creates a kink in the I-helix, due to disruption of the local H-bonding network and therefore the helix displays a 13° kink, that has also been observed in P450 BSβ and other unrelated P450 enzymes (Podust *et al.*, 2001; Lee *et al.*, 2003). However, this Arg-Pro amino acid sequence is retained exclusively within the peroxygenase family, and is thought to have replaced the highly

conserved acid-alcohol pair (P450cam (CYP101A1) Thr252 and Asp251 and P450 BM3 Glu267 and Thr268) that is present in the I-helix near the oxygen binding groove (Schlichting *et al.*, 2000). These residues are considered critical for dioxygen activation and are highly conserved throughout redox-dependent electron transferring P450s and ensures the proper positioning of the water molecule required for catalytic turnover (Shimada *et al.*, 1991; Cryle and De Voss, 2008; Coleman *et al.*, 2020). These key differences illustrate routes how peroxygenases have diverged away from monoxygenases (Matthews, Belcher, *et al.*, 2017).

As with other members of the CYP152 family (including P450 BSβ, SPα, $OleT_{JE}$, KR and K6) we see perturbation of the II and III pyrrole ring of the heme-*b* molecule, causing the pyrrole rings to move upwards, and thought to bring these closer to the substrate bound in the active site (Belcher *et al.*, 2014). Although due to the lack of a substrate-free structure, we cannot suggest if this is altered by substrate-binding (Girvan *et al.*, 2018).

Inspection into the crystal packing reveals a dimeric structure. At the dimeric interface, we observe an additional heme molecule sandwiched between two histidine residues (His186) of each monomer as seen in **figure 3.9**. The heme is located on a crystallographic axis, and is modelling in two conformations. In addition to the heme ligation with His186 there are also interactions between the Phe179 main chain and the heme propionate group. The interface is stabilised by multiple hydrophobic interactions (noted in supplementary **figure 3.21**)

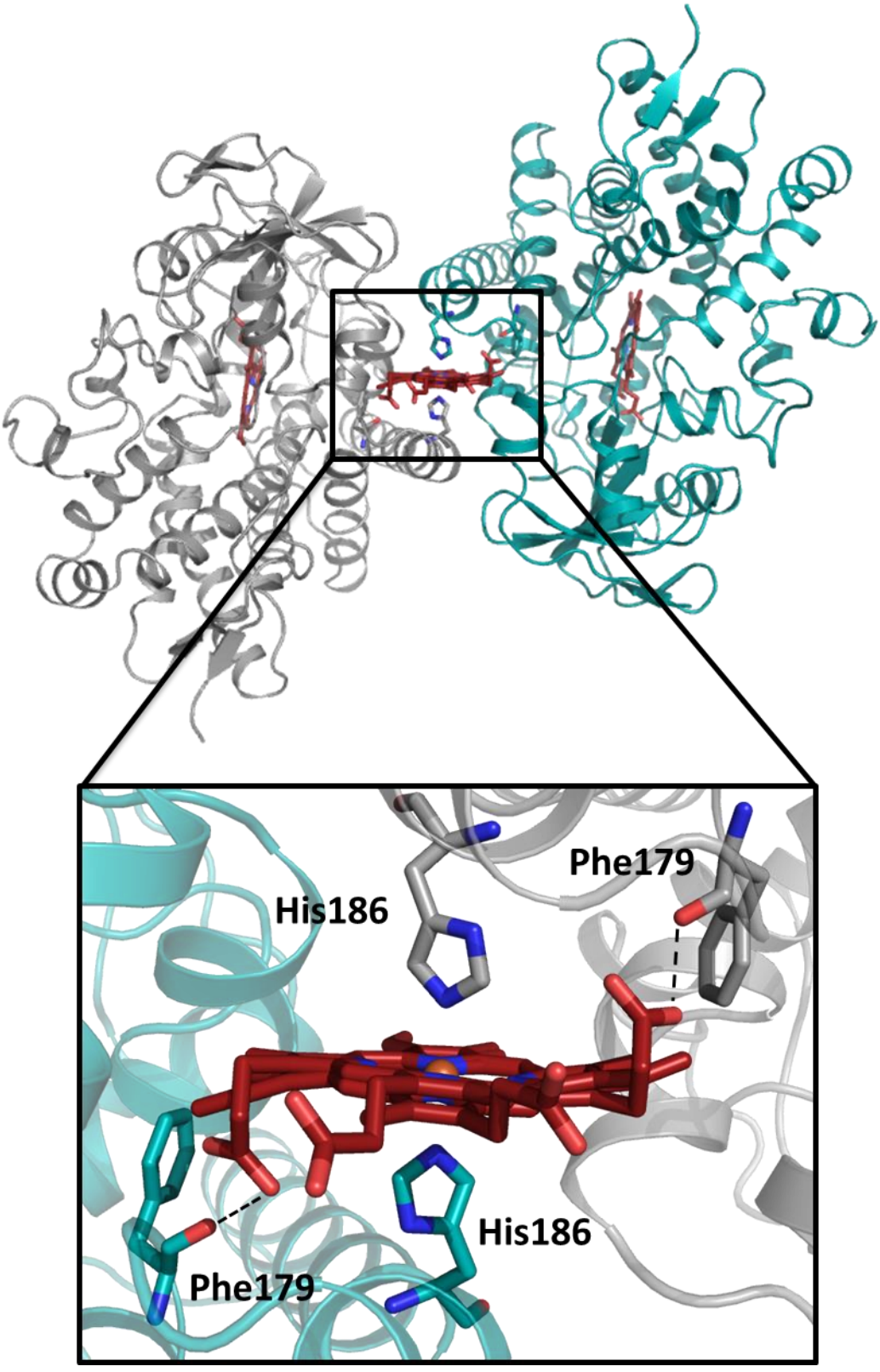

Figure 3.9 Dimeric interface of WT P450 CE. Cartoon representation of dimeric CYP152T7 from Corynebacterium efficiens (two monomers in cyan and grey). The heme is represented by red sticks. The insert shows a magnified dimeric interface, the His186 residues interact with the heme iron and the Phe179 residue H-bonds (represented by dash lines) with carboxylate groups of the heme.

Despite sequence homology, the dimeric interface of CE is very different from P450 KR. Superimposition of both structures shows the root mean square division of 1.106 Å for 343Cα atoms (**figure 3.10**). CE was originally identified form BLAST searches using P450 KR (55% sequence similarity towards each other). P450 KR has a long N-terminal terminal helix which protrudes from the core and established the dimer interface. The stabilisation of P450 KR and the dimer is assisted by a disulphide bond that occurs between a Cys39 (base of the N-terminal helix) and Cys317 (central domain of the same monomer) (Andrews *et al*., chapter 2). Sequence alignment of P450 KR and CE were done by EMBOSS Needle (supplementary **figure 3.22**). The alignment does not fully allude to P450 CE displaying a disulphide linkage in a similar sequence position as P450 KR (**figure 3.10C**). However, comparison of the two homologous structures showed that P450 CE does indeed have a disulphide bond between Cys7 and Cys312. Instead of an extended N-terminal α-helix, CE has two short helices with separated by a short linker region. However, these do not contribute to the dimer interface of P450 CE. Initial purification studies with chemical reducing agents such as TCEP caused some destabilisation of P450 resulting in aggregation. Therefore, one could postulate that as with P450 KR, the disulphide linkage is important for protein stabilisation and dimerisation, although further research is required to fully understand the role of the disulphide bond in P450 CE.

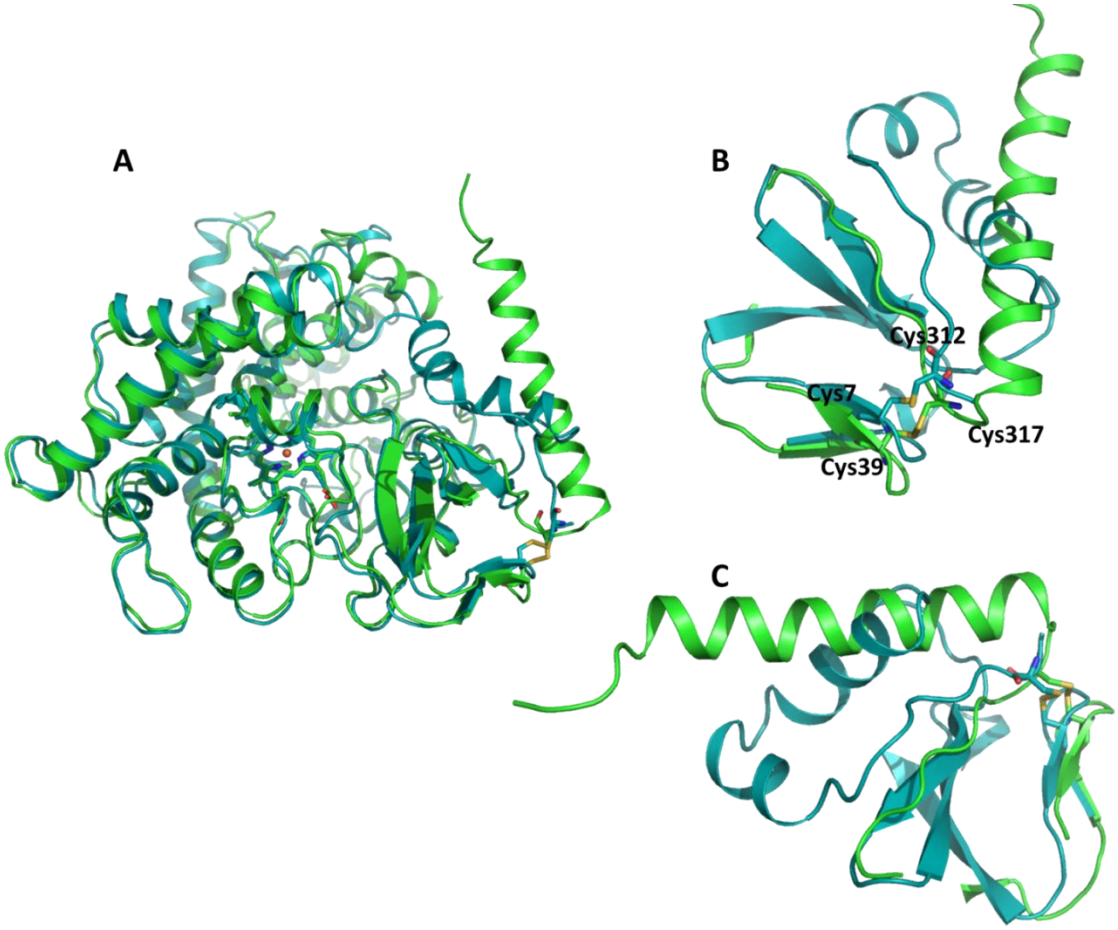

Figure 3.10 Overlap of P450 CE and P450 KR. Panel A shows the general superimposition of both structures showing a root mean square deviation of 1.106 Å (343 to 343 atoms) Cα atoms. Here P450 CE is represented by the teal cartoon and P450 KR is represented by the green cartoon. Panels B and C focus in on the N-terminal portion of both enzymes with the cysteine residues that are involved in disulphide bond formation highlighted, for P450 CE (Cys7 and Cys312) and for P450 KR (Cys39 and Cys317). The single N-terminal helix in KR extends out from the base of the disulphide linkage, with CE displaying two short helices.

To gain a better understanding of the P450 CE unique dimeric structure, mutagenesis was performed to probe the role of histidine residue 186 in heme binding and dimerisation of the protein. Two CE variants were created; H186K and H186N to disrupt the heme binding site and provide insight into the histidine role. A 2.06 Å resolution crystal structure was obtained for the H186N variant. The general structure is very similar to that of the WT CE structure, superimposition of the WT and mutant CE structures show a root mean square deviation of only 0.297 Å for 341 Cα atoms (see **figure 3.11**).

As indicated by the low RMSD values, there are minimal differences in the overall topology of the protein structure, including the main secondary elements (structural core), with notable exceptions of the α-9 helix in which houses H186N mutation (**figure**

3.13B/C). The substitution to an asparagine residue causes the helix to bend upwards, changing of the position of the loop region following the helix (**figure 3.13B/C**).

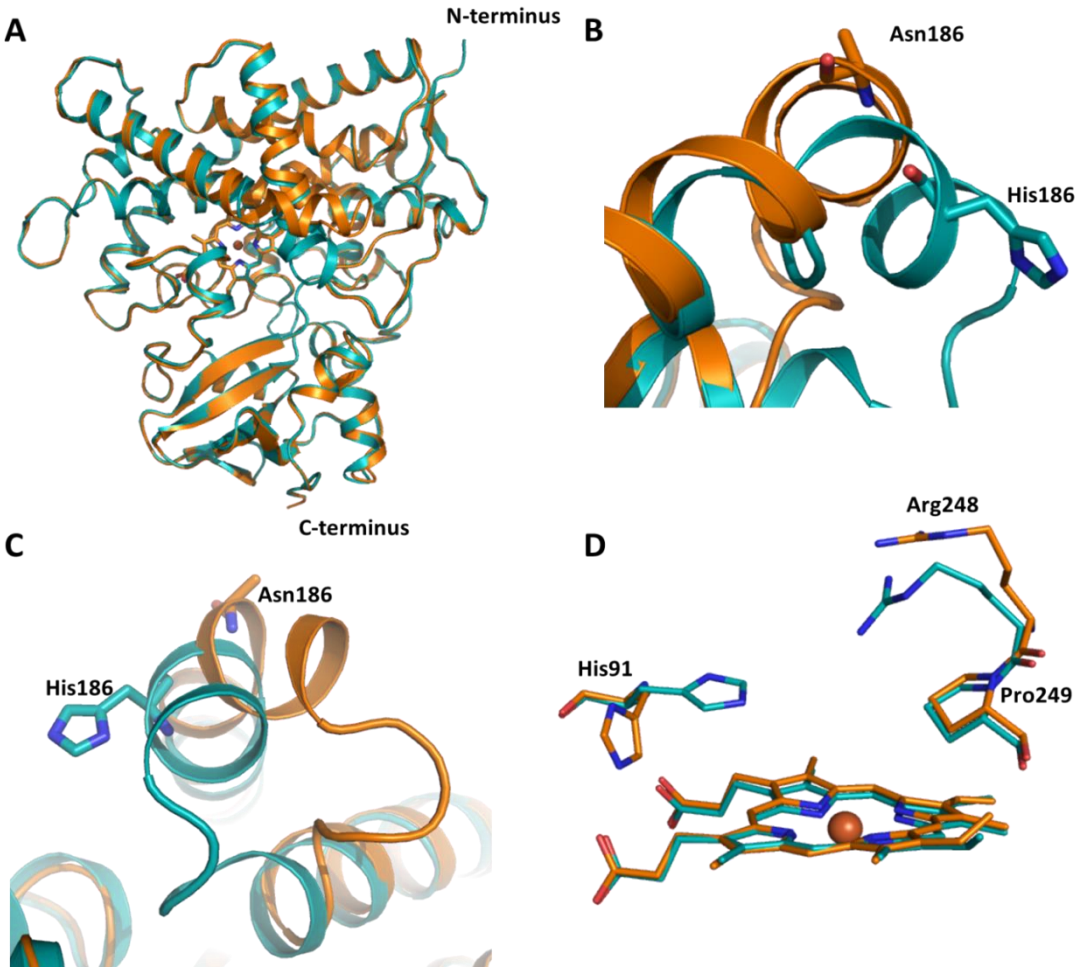

Figure 3.11 Structural comparison of WT P450 CE and His186Asn variant. Panel A shows the superimposed structures of WT P450 CE (cyan) and H186N variant (orange). The heme is represented by sticks. Panel B and C show the α-9 helix which the mutation is highlighted. Panel D shows an image of important active site residues.

Despite the potentially disruptive nature of this mutation on the P450 CE oligomeric state, the CE variant retains a dimeric status. Crystal packing reveals two copies of H186N in the asymmetric unit, which formed a putative dimer interface different to that of the WT protein. However, this interaction is unlikely to be the physiological dimer. Closer inspection reveals a symmetry related molecule makes a dimer interface similar to that observed for the WT P450 CE (**figure 3.12**). However, no heme is present at the interface and the structure is stabilised by hydrophobic interactions.

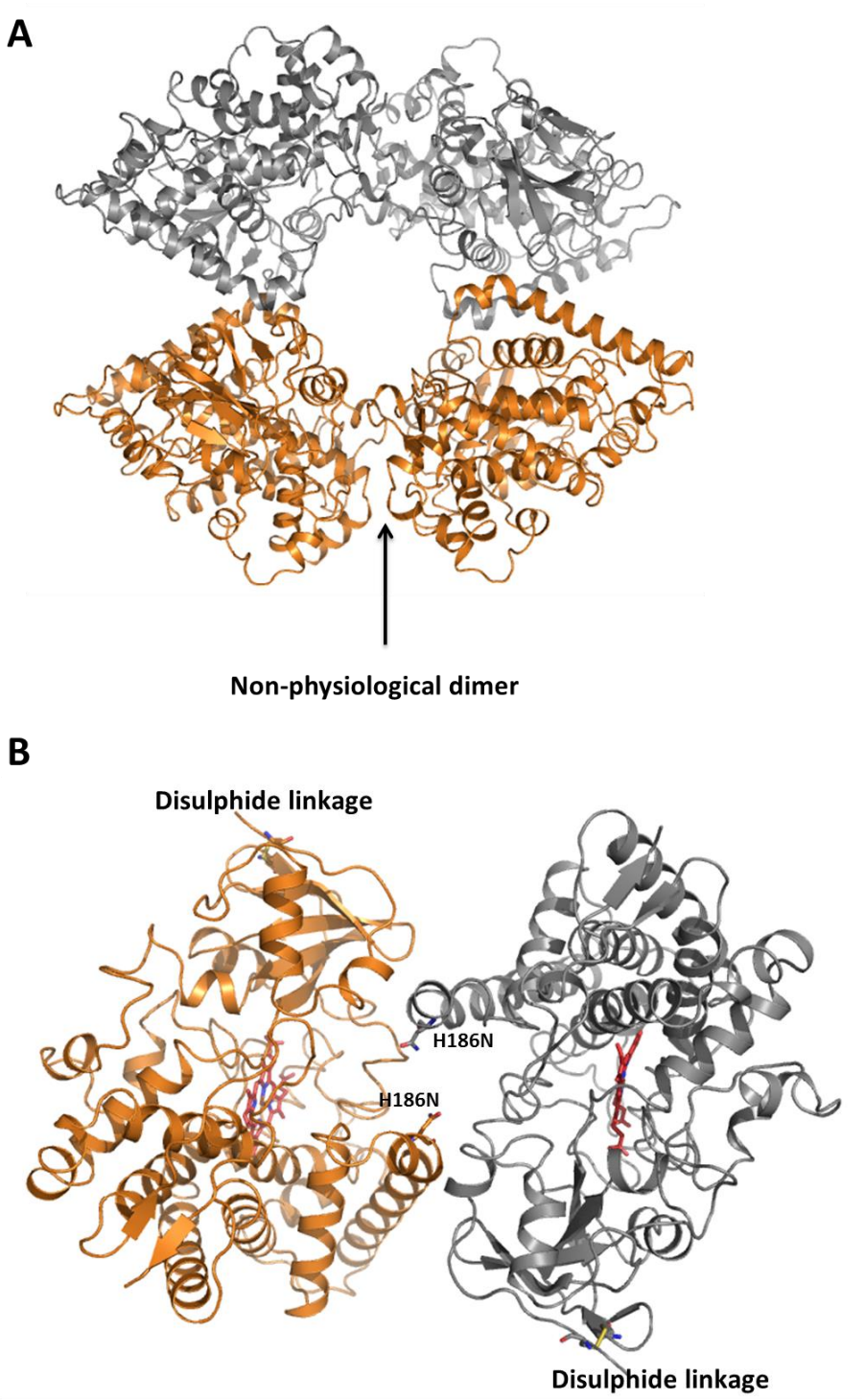

Figure 3.12 Structure of P450 CE H186N dimeric structure. Panel A shows the H186N structure with two monomers in the asymmetric unit (orange) and the symmetry related monomers (grey). Panel B highlights the dimeric structure with the position of mutation highlighted.

The disulphide bond between Cys7 and Cys312 is maintained in H186N variant, and does not interact with the interface (**figure 3.12**). An imidazole molecule is present in the active site and is bound to the heme molecule, imparted from imidazole being present in the crystallisation buffer, rather than from the purification process. A portion of extra electron density was found to be present, comprising a large Y-shaped density with two

elongated tails that extended into the substrate access channel (channel I). Due to the shape of this density, we fitted a phospholipid molecule (phosphatidylglycerol) with chain carbon chain length (16:14) that contains the two fatty acids, glycerol moiety and phosphate head group (see **figure 3.13**). This length/type of phospholipid is usually found in *E. coli* cells (Pluschke and Overath, 1981). The head-group sits on the mouth of the channel opening and does not have any direct contacts to the protein. We could postulate that this molecule has been retained through protein purification following expression in *E. coli*.

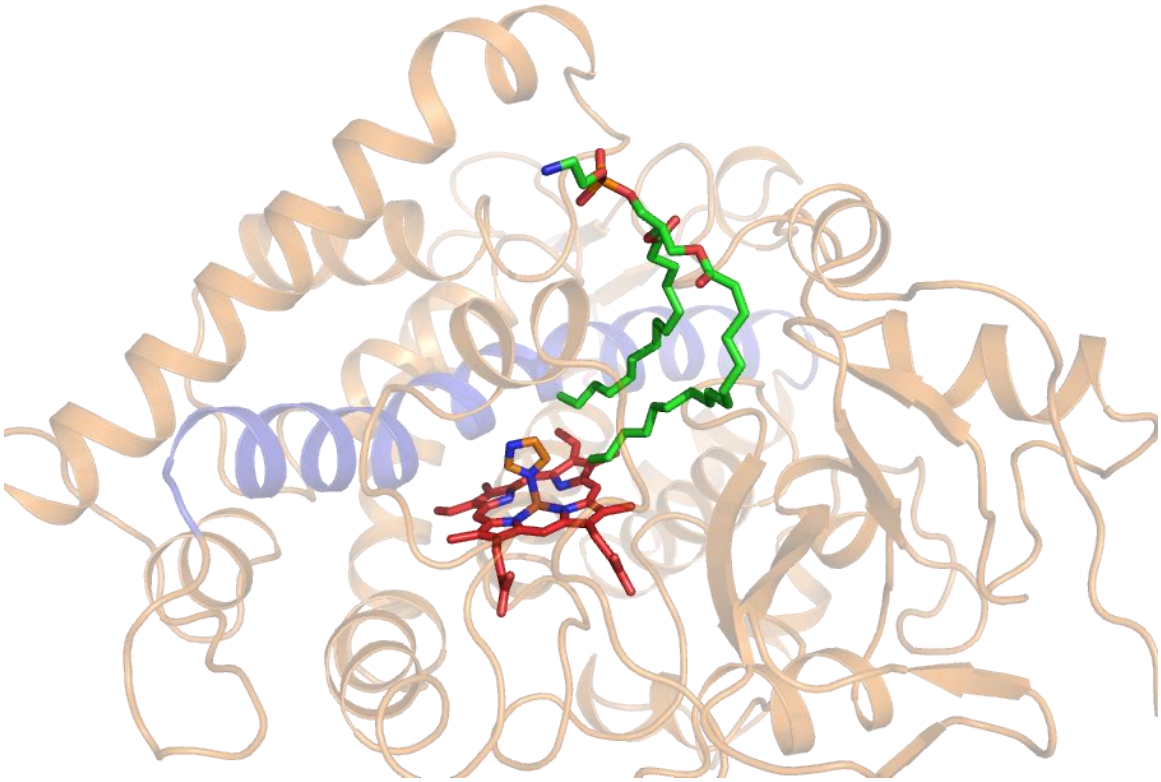

Figure 3.13 Imidazole bound P450 CE His186Asn variant with phosphoglyceride. The heme is represented by red sticks, the bound imidazole (orange) and the phosphoglyceride (green). The I-helix is highlighted in blue.

3.4.4 Fatty acid binding assay of P450 CE proteins

Substrate binding to P450 enzymes displaces the water as the 6th axial ligand to the heme iron causing reorganisation of the Fe d-orbitals electrons. This can be followed spectroscopically monitoring the changes in the Soret peak from the low spin ferric iron substrate free form to the high spin substrate at a shorter wavelength (typically 390 – 400 nm). This is typically called a type I response or blue shift (Dawson, Andersson and Sono, 1982) (Dawson, Andersson and Sono, 1982). In the case of P450 CE, and as

discussed above, the substrate free Soret band has absorbance at 424 nm, upon substrate binding this peak shifts to demonstrate the accumulation of the high spin heme with Soret absorbance at ~395 nm corresponding to the substrate bound form.

Binding dissociation constants (K_d) were determined for both WT P450 CE and the H186N variant against C10:0 – C16:0 saturated fatty acid substrates (as described in the methods in section **3.3.4**). WT P450 CE binds to all fatty acids tested and binding affinities were observed in the µM range. The K_d values are displayed in **table 3.2**. The greatest spin-shift (from LS to HS) is seen for palmitic acid (C16:0) (80%) with the tightest binding of K_d with a 28 ± 0.14 µM (**figure 3.14**). Substantial HS accumulation occurs upon the addition of lauric acid (C12:0) and myristic acid (C14:0) (62% and 59%, respectively) with relatively tight binding affinities. Binding of substrates with shorter chain lengths do not exhibit substantial conversion to the HS species (C10:0, 11% HS). In comparison, P450 KR displays more extensive high spin heme shift for shorter chain fatty acids (C10:0 – C14:0) (refer to **table 3.2**). P450 KR data obtained from Andrews *et al*., (chapter 2)).

Table 3.2 Binding dissociation constants (K_d) for WT P450 CE and H186N mutant against a range of fatty acid substrates. Data for P450 KR has also been included for comparison and is shaded in gray (Andrews et al., chapter 2). Data were fit using the Hill equation ([A]data were fit using Boltzmann, [B]data were fit using hyperbolic equation). WT CE Hill coefficients (*n*) C10:0 1.1 ± 0.1, C16:0 2.6 ± 0.1 and H186N Hill coefficients (*n*) C10:0 1.1 ± 0.1, C12:0 1.4 ± 0.1, C14:0 2.1 ± 0.1, C16:0 2.8 ± 0.2.

Fatty acid substrate	P450 CE WT		P450 CE H186N variant		P450 KR	
	K_d (µM)	HS (%)	K_d	HS (%)	K_d	HS (%)
Decanoic acid (C10:0)	120 + 21	11	2.1 ± 0.2 mM	58	1.7 ± 0.1 mM	93
Lauric acid (C12:0)	69 ± 12[A]	62	94.2 ± 3.4 µM	55	71.1 ± 0.8 µM	92
Myristic acid (C14:0)	27 ± 2[A]	59	50.4 ± 1.8 µM	59	17.4 ± 0.3 µM	90
Palmitic acid (C16:0)	28.0 ± 0.2	80	25.8 ± 0.9 µM	74	3.3 ± 0.1µM	55

P450 KR exhibits 90- 100 % conversion to the HS heme for short-medium chain fatty acids (C10:0 – C14:0) with an affinity for lauric acid (C10:0) of K_d 1.7 ± 0.04 mM. Longer chain fatty acids (C16:0 – C18:0) induce less HS accumulation (50 – 16 %) upon substrate binding within the active site (**table 3.2**). However long-chain fatty acids bind with tighter affinity resulting in reduced K_d values, the spectra obtained reaches apparent saturation. Reduced solubility of long chain fatty acids may contribute to amounts of HS. In contrast, with P450 CE the amount of conversion to high spin heme mirrors the K_d values with the higher percentages of HS conversion corresponding to lower K_d values with tighter affinity.

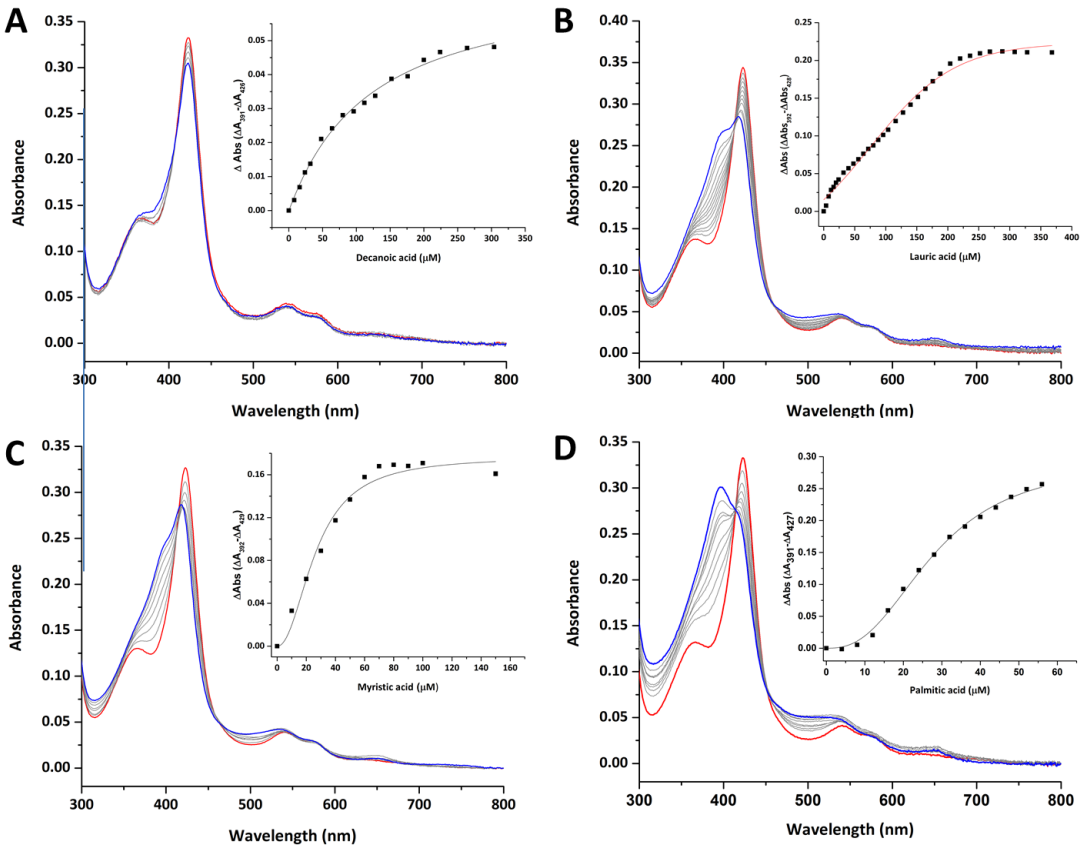

Figure 3.14 UV-visible binding titrations of P450 CE. In all cases the low spin (LS) ferric CE (substrate-free) with starting spectra at 424nm are shown in red with resultant substrate-bound high-spin (HS) at 397 nm shown in blue. Panel A binding titration of WT P450 CE with decanoic acid (C10:0). The inset shows the induced absorbance change versus [decanoic acid] and fitted using the Hill equation to give a K_d 119 ± 21 μM. Panel B, lauric acid (C12:0). Inset shows the induced absorbance change versus [Lauric acid] and best fitted using the Boltzmann equation with a K_d 68.5 ± 12.12 μM. Panel C, myristic acid (C14:0). Insert shows the induced absorbance change versus [myristic acid] and fitted using the Hill equation with a K_d 26.7 ± 2.1 μM. Panel D, palmitic acid (C16:0). Insert shows the induced absorbance change versus [palmitic acid] and fitted using the Hill equation K_d 28 ± 0.14 μM. All reactions contained ~3 μM of P450 CE.

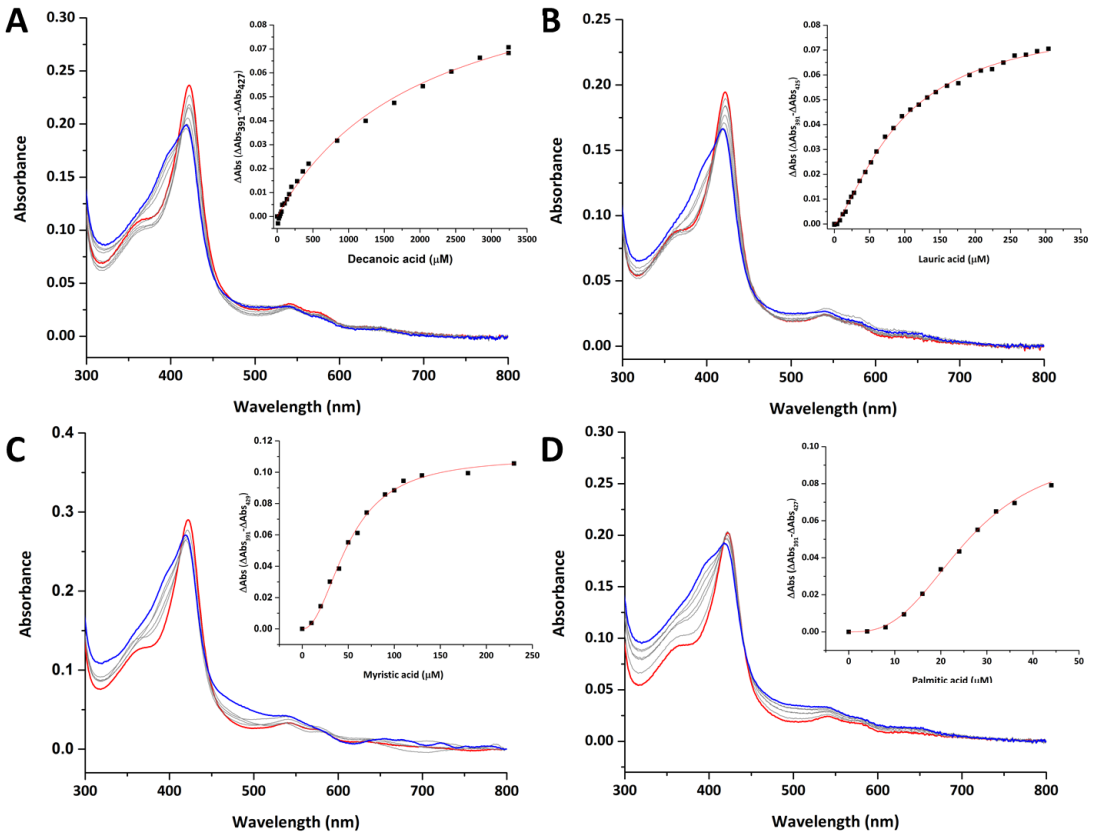

Figure 3.15 UV-visible binding titrations of P450 CE H186N variant. In all cases the low spin (LS) ferric CE (substrate-free) with starting spectra at 424nm are shown in red with resultant substrate-bound high-spin (HS) at 397 nm shown in blue. Panel A show the spectral binding titration of H186N P450 CE variant with decanoic acid (C10:0). Insert shows the induced absorbance change versus [decanoic acid] and fitted using Hyperbolic with K_d of 2.1 ± 0.2 mM. Panel B, with lauric acid (C12:0). Insert shows the induced absorbance change versus [lauric acid] and fitted using the Hill equation K_d 94.24 ± 3.40 μM. Panel C, with myristic acid (C14:0). Insert shows the induced absorbance change versus [myristic acid] and fitted using the Hill equation with a K_d 50.42 ± 1.76 μM. Panel D, palmitic acid (C16:0). Insert shows the induced absorbance change versus [palmitic acid] and fitted using the Hill equation with a K_d 25.78 ± 0.94 μM.

$OleT_{JE}$ displays tightest binding for long chain fatty acids e.g. C20:0 K_d of 4.43 ± 0.19 μM and extensive conversion to high spin (95%). The amount of HS heme decreases as fatty acid chain length decreases, with C10 displaying 35% (Matthews, Belcher, *et al.*, 2017). Going forward, assessing P450 CE ability towards the longer chain fatty acids, as well as the shorter-chain (<C10:0) that necessarily portray any spin state changes (as seen in some CYP152s) but do turn over with reasonably efficiency would be of interest.

P450 CE, KR and $OleT_{JE}$ which all display extensive HS heme accumulation upon substrate binding and have a conserved His residue in their active site cavities (His85 in $OleT_{JE}$). A H85Q $OleT_{JE}$ variant displayed diminished HS Soret shifts upon substrate binding in comparison to the WT protein. These are consistent with UV-visible binding studies obtained from other CYP152 orthologues that each contain a Gln in place of the His including P450 BSβ, P450 SPα and CYP152K6. These enzymes do not produce a shift

towards the HS state upon substrate binding (Rude *et al.*, 2011; Matthews, Belcher, *et al.*, 2017; Girvan *et al.*, 2018).

The structure of P450 CE (see **section 3.4.3**) revealed an unusual dimerisation involving an additional heme complexed with His186 (figure **3.9**). A H186N mutant (surface mutation) in P450 CE was generated to explore the role if this His186 residue in the possible dimerising properties. Spectral binding data was obtained to examine how the mutation influences fatty acid substrate binding to P450 CE (**table 3.2**). The H186N binding dissociation constants of C16:0 – C12:0 fatty acids are similar to that observed with WT CE protein. H186N displays increased accumulation of the HS species upon decanoic acid (C10:0) binding (see **figure 3.15**) but a greater binding affinity (K_d of 2.1 ± 0.2 mM).

P450 CE and the H186N mutant display some sigmoidal binding towards fatty acid e.g. WT CE palmitic acid displays n= 2.3 ± 0.1 binding sites fit by the Hill equation. Similar sigmoidal binding behaviour is also observed upon binding of palmitic acid to P450 KR with n= 2.5 ± 0.2 binding site which is consistent with P450 KR functioning as a dimer. This phenomenon is also in accordance to both WT and mutant CE homo-dimerising within solution.

3.4.5 Products formed from fatty acid turnover by P450 CE and variants

H_2O_2 mediated P450 CE turnover assays were done with a range of fatty acid substrates (C10:0 – C18:0) as described in the *Materials and Methods* section **3.3.6**. P450 CE is able to catalyse the decarboxylation and hydroxylation of saturated fatty acid substrates, converting these to the C_{n-1} terminal alkenes as well as a mixture of 2-hydroxy and 3-hydroxy fatty acids (**figure 3.16**). **Table 3.3** summarises the turnover products and yields catalysed by P450 CE and CE variants (H186N and H186K).

WT P450 CE the highest overall product turnover (~91%) is observed for lauric acid (C12:0) (alkene: 38%, 2-OH FA: 19%, 3-OH: 41%). However, for myristic acid (C14:0) the highest conversion to alkene is seen, with ~50% conversion to 1-tridecene (total product: ~89%, 2-OH: 15%, 3-OH: 24%). Interestingly the ratio of alkenes to 2-OH/3-OH products differs depending on substrate chain length. For C10:0 and C12:0 substrates the major reaction route was the hydroxylation of fatty acids, with the major product being the 3-OH FA product. Turnover of decanoic acid (C10:0) and lauric acid (C12:0) to

OH-products accounts for almost 70% and 58 % of the reaction products, respectively. As the chain length increases from C14:0 – C18:0, the decarboxylation route of catalysis becomes more prominent, with the alkene product favoured and reduced production of the mixed hydroxylated products (total product to alkene, C14:0; 56%, C16:0: ~78%, C18:0 ~77%). This is also seen with CYP152 decarboxylase $OleT_{JE}$ from *Jeotgalicoccus* for the longer chain substrates (C20:0) in which only the 1-nondecene product was detected. $OleT_{JE}$ favours the decarboxylation route, with the major product from catalysis of fatty acids (C10:0 – C20:0) to their respective terminal alkenes. Whereas in P450 KR Cα and Cβ-hydroxylation remains the prevalent route. In $OleT_{JE}$ catalysis, the 3-OH FA product is more prevalent than the 2-OH FA, which is similar to P450 CE (Matthews, Belcher, *et al.*, 2017). P450 CE displays increased accumulation of HS heme and tighter binding as fatty acid chain length increases, and the longer chain length of substrates results in more decarboxylation. We could speculate that the longer fatty acid chains bind more rigidly in the active site (through interaction with the important arginine residue). With displacement of the water molecule as the 6^{th} axial ligand (see through extensive conversion to HS λ: 397 nm) and allows for the decarboxylation route to occur through abstraction of a substrate electron by the reactive species Cpd II (Fe^{IV}–OH). The shorter chain fatty acids may bind with more mobility within the active site, favouring the ●OH rebound route, resulting in an increase of the hydroxylation products (Grant, Mitchell and Makris, 2016a).

P450 CE displays increased total product turnover of fatty acids substrates in comparison to its homologous peroxygenase family member, P450 KR. P450 KR displays decreased activity towards decanoic acid, with 22% product conversion compared to 78% for P450 CE, aswell as reduced decarboxylation activity (P450 KR: 1-nonene: 8%, 2-OH: 3% and 3-OH 13% compared with P450 CE: 1-nonene 23.6%, 2-OH: 13.3%, 3-OH: 41%). P450 CE presents as a more of an efficient decarboxylase in comparison to P450 KR for all fatty acid chain lengths tested, with a notable difference for the turnover of palmitic acid to 1-pentadecene (KR: 14% and CE: 48%) (Andrews et al., Chapter 2).

Table 3.3 Product profile and conversion of fatty acid substrates to alkene and hydroxylated products by WT P450 CE and mutant CE enzymes. WT CE and H186N and H186K protein (1 μM) with 500 μM of fatty acid substrate was used in all turnovers. H_2O_2 (500 μM) was used to drive catalysis for 30 minutes. Samples were taken in triplicate and averaged (as described in the methods section).

Substrate	P450 CE variant	Products (%)			
		C_{n-1} alkene	2-OH FA	3-OH FA	Total
C10:0	**WT**	23.6 ± 1.6	13.3 ± 0.3	41 ± 0.8	77.9
	H186N	31.7 ± 2.6	18.1 ± 1.6	50.2 ± 1.0	100.0
	H186K	25.6 ± 4.8	26.9 ± 2.3	47.5 ± 1.0	100.0
C12:0	**WT**	37.8 ± 2.9	19.4 ± 0.8	33.7 ± 1.7	90.9
	H186N	47.5 ± 0.02	11.4 ± 0.6	34.5 ± 1.5	93.4
	H186K	11 ± 1.4	13.1 ± 0.5	26.9 ± 1.9	51.0
C14:0	**WT**	50.3 ± 2.6	14.5 ± 1.4	24.1 ± 2.5	88.9
	H186N	44.5 ± 2.3	9.2 ± 0.3	26.4 ± 1.4	80.1
	H186K	28.2 ± 2.0	13.6 ± 1.6	24.6 ± 1.3	66.4
C16:0	**WT**	48.0 ± 4.3	2.8 ± 0.4	10.5 ± 0.3	61.3
	H186N	39.9 ± 0.2	3.1 ± 0.4	9.7 ± 2.1	52.7
	H186K	22.9 ± 1.6	3.1 ± 0.4	10.1 ± 1.9	36.1
C18:0	**WT**	13.7 ± 1.1	0.8 ± 0.1	3.2 ± 0.3	17.7
	H186N	14.9 ± 8.4	1.1 ± 0.4	1.5 ± 1.5	17.5
	H186K	5.9 ± 0.7	0.9 ± 0.2	2.4 ± 1.5	9.2

Turnover data was obtained for H186N and H186K variants under similar conditions for WT P450 CE. Both mutants are able to catalyse the decarboxylation and hydroxylation of fatty acids (C10:0 – C18:0) see **table 3.3**. When decanoic acid is used as the substrate, complete oxidation for both mutants occurs. H186N variant displays increase amounts of alkene, 2-OH FA and 3-OH FA for both C10:0 and C12:0 substrates. The longer chain fatty acids (C14:0 – C16:0) had a reduced efficiency of turnover of fatty acids. It poses an interesting question as to how a distal mutation from the active site has an affect on substrate binding (section **3.4.4**) and product turnover. Further work could employ directed evolution techniques to alter substrate specificity towards shorter chain fatty acids.

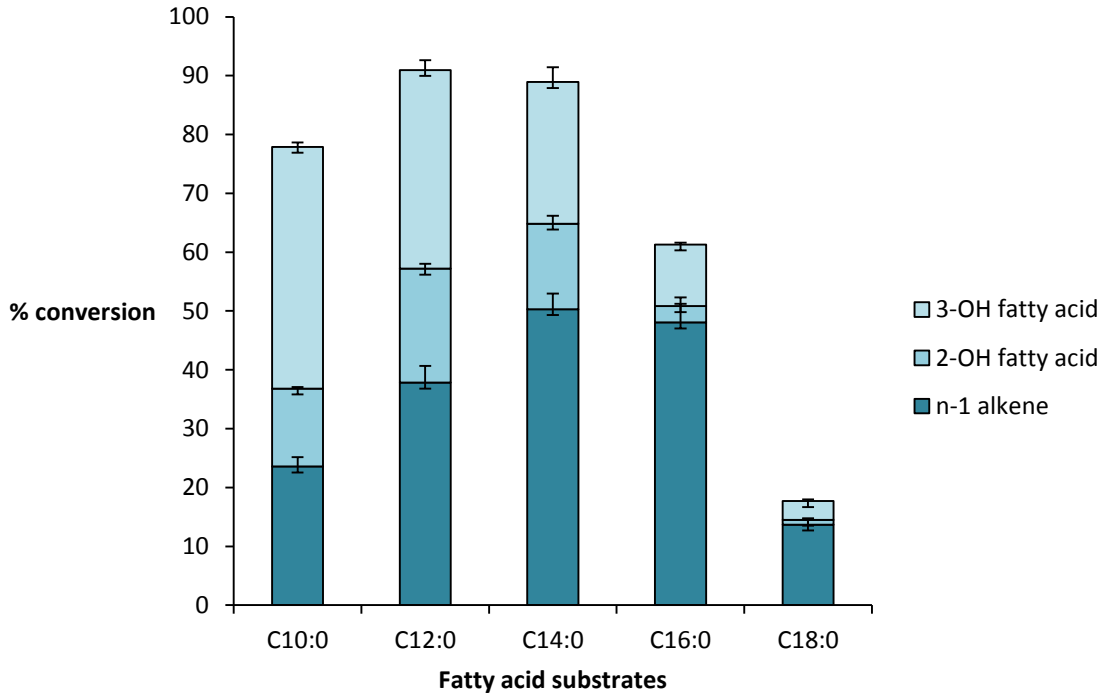

Figure 3.16 Products of fatty acid turnover from P450 CE. The bar chart shows the different yield of alkenes (dark blue), 2-hydroxyfatty acids (blue) and 3-hydroxy fatty acids (light blue). Reaction were undertaken with decanoic acid (C10:0), lauric acid (C12:0), myristic acid (C14:0), palmitic acid (C16:0) and stearic acid (C18:0). Data shown are the average of three experiments with error bars showing standard deviation between experiments.

A time-course looking at the turnover of P450 CE with myristic acid (over 2 hours) following addition of 500 µM of H_2O_2 is shown in **figure 3.17**. Near complete turnover of myristic acid is observed within 5 minutes with total turnover ~89% forming 1-tridecene 54% with 2-OH and 3-OH myristic acid 7.8% and 27 %, respectively.

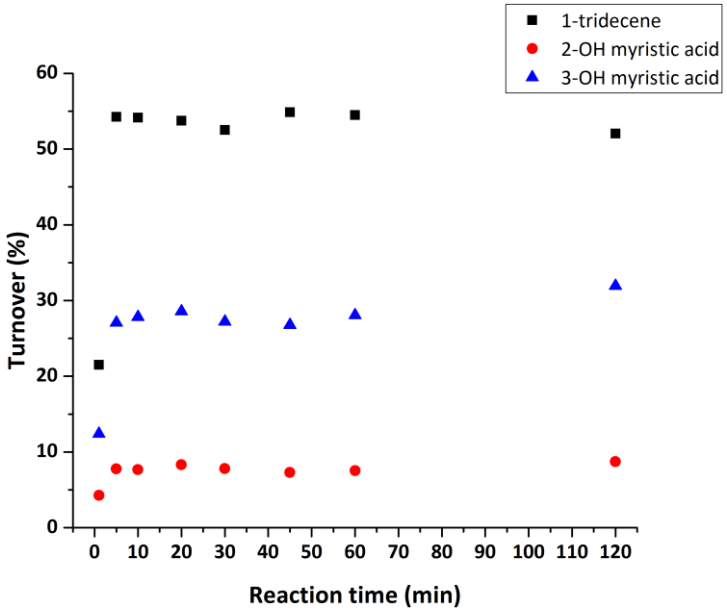

Figure 3.17 Time dependence experiments of P450 CE with myristic acid. Data obtained by GC-MS data with conversion of myristic acid is represented in % to 1-tridecene (black square), 2-hydroxy myristic acid (blue triangle) and 3-hydroxy myristic acid (red circle). Time points were collected at 1, 5, 10, 20, 30, 45 60 and 120 minutes after spiking with H_2O_2. Data were taken in triplicate.

H_2O_2 is a relatively cheap oxidant making these peroxygenases ideal tools in biotechnology. However, high concentrations can be detrimental leading to oxidation of the heme iron as well as the protein itself *in vitro,* even though these peroxygenases have evolved to efficiently utilise it to drive catalysis (Hsieh *et al.*, 2017). Initial studies were undertaken with H_2O_2-feeding at a lower level (c.f. a one-off addition of 500 µM) to explore whether this would alter the product profiles following turnover. For myristic acid turnover using 1 µM of P450 CE with additions of H_2O_2 (100 µM H_2O_2 every 10 min for 50 min), negligible changes were observed in total product turned over for initial spike of H_2O_2 compared to serial additions of peroxide (~90 % and ~93 %, respectively). However, we do see a difference in product ratios (single addition of 500 µM H_2O_2, alkene: 58%, 2-OH FA: ~7%, 3-OH FA: 25%) and (serial additions of 100 µM H_2O_2, alkene: 65%, 2-OH FA: 6%, 3-OH FA: 21%), seeing a reduction in the hydroxylated products and an increase in alkene formation. A study by Mathews *et al.,* presented a novel system expressed in *E. coli* comprising of $OleT_{JE}$ fused to H_2O_2-producing alditol oxidase (Aldo) from *Streptomyces coelicolor* (Matthews, Tee, *et al.*, 2017b). AldO oxidises polyol substrates such as glycerol, sorbitol and diols (Van Hellemond *et al.*, 2009) to produce H_2O_2. AldO-$OleT_{JE}$ fusion enzyme indicated the early formation and then decrease in concentration of 2-OH and 3-OH fatty acid (myristic acid tested). This suggests that controlling the H_2O_2 supply can minimise the oxidation inactivation of the enzyme and

prolong activity (Matthews, Tee, *et al.*, 2017b). Furthermore, the enzyme to substrate ratio was varied, with 1:500 and 1:100 (following identical conditions to the H_2O_2 cycling experiment, with serial H_2O_2 additions) (**table 3.4**). Increasing the protein concentration (from 1 µM to 5 µM) with the same concentration of myristic acid (500 µM) seems have similar product turnover percentages but reduced production of 1-tridecene and slightly increased hydroxylated products (for 1 µM, alkene: 58%, 2-OH FA: ~7% 3-OH FA: 25% and for 5 µM, alkene: 52 %, 2-OH FA: ~9%, 3-OH FA: 26%). Batch H_2O_2-feeding to 5 µM of P450 CE, shows an in ~13 % increase of 1-tridecene formation.

Table 3.4 Product profile of WT P450 CE with different concentrations of H_2O_2 and enzyme. Reactions proceeded for 50 mins. Samples were taken in triplicate.

Concentration of P450 CE (µM)	H_20_2	Products (%)			
		1-tridecene	2-OH myristic acid	3-OH myristic acid	Total
1	Spike (500 µM)	58.1 ± 0.5	7.4 ± 1.1	24.6 ± 2.0	90.1
	Serial ads. (5x 100 µM)	65.3 ± 0.9	6.5 ± 0.3	21.0 ± 1.4	92.8
5	Spike (500 µM)	52.4 ± 2.4	9.2 ± 0.5	26.2 ± 0.4	87.8
	Serial ads. (5x 100 µM)	65.8 ± 1.2	5.5 ± 0.4	17.7 ± 0.2	89.0

3.4.6 Exploring the oligomeric properties of P450 CE and variants

Size exclusion gel filtration column revealed WT P450 CE eluted with an apparent weight corresponding to a dimeric species. This led us on to further probe the oligomeric state and protein integrity of P450 CE. Analytical size-exclusion chromatography multi angle light scattering (SEC-MALS) experiments were undertaken, in which determination of molecular weight as well as protein oligomeric state and protein-protein interactions within the complex in aqueous solution can be identified.

Figure 3.18A reveals P450 CE is a dimer in solution, with a single homogenous peak eluting at ~ 15 mL exhibiting a weight average molar mass MW of 88.3 ± 5.8% kDa relating to the dimer determined by MALS. The molar mass points calculated across the whole peak at uniform towards the dimer formation, with no trailing into the monomeric form as we observe in P450 KR at low concentrations of protein (Andrews *et al*., chapter 2).

We also undertook SEC-MALS analysis of the two P450 CE variants; H186N and H186K (**figure 3.18B-C**). These two mutations were designed to probe the dimeric interface of P450 CE. In both these mutations displayed, the protein remains in a dimer formation

(no disruption of the oligomeric state of CE through these mutations which we expected to happen). CE H186N displays an observed molar mass of 95.5 ±1.8 KDa R_h 4.23 ± 0.09 nm eluting. CE H186K displays MW 93.7 ± 1.8 kDa R_h 4.17 ± 0.09 nm.

Analytical ultracentrifugation (AUC) is a technique that combines ultracentrifugation with an optical monitoring system (including absorbance, interference and fluorescence) and can study the size and shape of macromolecules in solution (Cole *et al.*, 2008). A range of protein concentrations were tested, to see if we could determine a dimer dissociation constant (K_d), however CE does not dimerise in a concentration dependent manner. For concentrations 5- 20 µM CE we see MW with reference to the dimeric form of CE (94 – 100 kDa). For concentrations below 1 µM, CE becomes unstable and has a propensity to aggregate resulting in large molecule weight species present. It seems likely that the P450 CE dimer is the most stable form, and possibly dimerises spontaneously since there is no evidence of the monomer forming. This is unlike P450 KR, which displays a concentration dependent dimer formation.

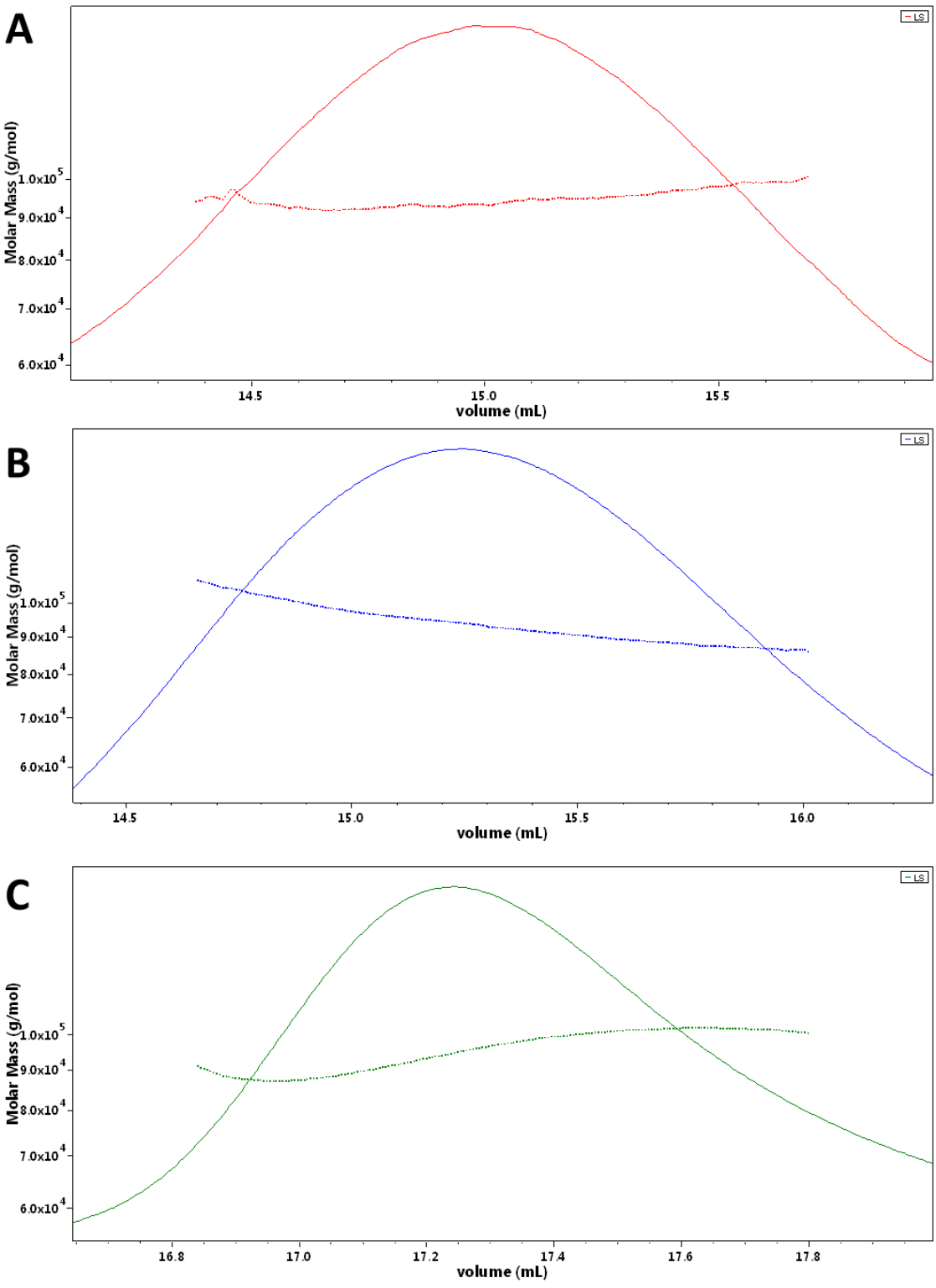

Figure 3.18 Elution volume and molar mass determination by SEC-MALS of P450 CE and variants. Lines represent light scattering with the dotted lines represent weight-average molecular mass (MW). Panel A shows trace obtained from WT P450 CE (red) elutes as dimer with a MW 88.3 ± 5.8 % kDa. Panel B H186K mutant (blue) MW 93.7 ± 1.8 kDa overlaid. Panel C shows the traces of H186N (green line) MW 95.5 ± 1.8 kDa. H186N sample was run on a Superdex6 column.

3.5 Conclusions

We present the structural, spectroscopic and catalytic characterisation of a new CYP152 peroxygenase from the thermotolerant bacterium *Corynebacterium efficiens*. P450 CE was probed as an interesting prospective biotechnological tool for production of alkenes following the characterisation of P450 KR and the decarboxylase $OleT_{JE}$. Data demonstrates that P450 CE functions as an efficient decarboxylase as well as a hydroxylase towards mid-chain fatty acid substrates. The crystal structure of P450 CE revealed a dimeric structure with a unique histidine-coordinated heme group at the interface between the two monomers. Determination of the crystal structure of H186N variant showed this mutant to be deficient in heme coordination at the protein surface; however the dimeric interface remained intact via extensive hydropobic interactions. In solution, monomeric P450 CE was not observed.

Interestingly, a disulphide linkage was found between Cys7 and Cys312 on the surface of the protein, which we believe to be important with stabilisation of the dimeric interface and overall protein integrity. This bears resemblance to the disulphide linkage between Cys39 and Cys317 in CYP152 orthlogue P450 KR – suggesting that such a linkage may be an important conserved structural feature within a subclass of these peroxygenase enzymes.

P450 CE displays tightest binding towards myristic acid (K_d 27 ± 2 μM) as well as high overall alkene titre (and overall product turnover). P450 CE displays sigmodial-like binding suggested the dimeric structure plays an important role in P450 CE catalysis.

Here we have charcterisated another example of a CYP152 member displaying unique structural features that are likely important for its function and catalysis. Therefore, further studies of CYP152 orthlogues are warranted to uncover and engineer novel enzymes for biotechnological applications and determine the extent at which this dimeric structur and disulphide-linkage is conserved across the CYP152 family.

3.6 References

Adams, P. D. *et al.* (2010) 'PHENIX: A comprehensive Python-based system for macromolecular structure solution', *Acta Crystallographica Section D: Biological Crystallography*. Acta Crystallogr D Biol Crystallogr, 66(2), pp. 213–221. doi: 10.1107/S0907444909052925.

Amaya, J. A., Rutland, C. D. and Makris, T. M. (2016) 'Mixed regiospecificity compromises alkene synthesis by a cytochrome P450 peroxygenase from Methylobacterium populi', *Journal of Inorganic Biochemistry*. Elsevier Inc., 158, pp. 11–16. doi: 10.1016/j.jinorgbio.2016.02.031.

Atsumi, S. and Liao, J. C. (2008) 'Metabolic engineering for advanced biofuels production from Escherichia coli', *Current Opinion in Biotechnology*, 19(5), pp. 414–419. doi: 10.1016/j.copbio.2008.08.008.

Barr, I. and Guo, F. (2015) 'Pyridine Hemochromagen Assay for Determining the Concentration of Heme in Purified Protein Solutions', *BIO-PROTOCOL*. Bio-Protocol, LLC, 5(18). doi: 10.21769/bioprotoc.1594.

Belcher, J. *et al.* (2014) 'Structure and biochemical properties of the alkene producing cytochrome p450 OleTJE (CYP152l1) from the jeotgalicoccus sp. 8456 bacterium', *Journal of Biological Chemistry*. American Society for Biochemistry and Molecular Biology, 289(10), pp. 6535–6550. doi: 10.1074/jbc.M113.527325.

Beller, H. R., Goh, E. B. and Keasling, J. D. (2010) 'Genes involved in long-chain alkene biosynthesis in micrococcus Luteus', *Applied and Environmental Microbiology*. American Society for Microbiology, 76(4), pp. 1212–1223. doi: 10.1128/AEM.02312-09.

Bernstein, S. L. *et al.* (2004) 'α-Synuclein: Stable compact and extended monomeric structures and pH dependence of dimer formation', *Journal of the American Society for Mass Spectrometry*. Springer New York LLC, 15(10), pp. 1435–1443. doi: 10.1016/j.jasms.2004.08.003.

Berry, E. A. and Trumpower, B. L. (1987) 'Simultaneous determination of hemes a, b, and c from pyridine hemochrome spectra', *Analytical Biochemistry*. Anal Biochem, 161(1), pp. 1–15. doi: 10.1016/0003-2697(87)90643-9.

Bharadwaj, V. S. *et al.* (2018) 'Different Behaviors of a Substrate in P450 Decarboxylase and Hydroxylase Reveal Reactivity-Enabling Actors', *Scientific Reports*. Nature Publishing Group, 8(1), p. 12826. doi: 10.1038/s41598-018-31237-4.

Brown, P. H. and Schuck, P. (2006) 'Macromolecular size-and-shape distributions by sedimentation velocity analytical ultracentrifugation', *Biophysical Journal*. Biophysical Society, 90(12), pp. 4651–4661. doi: 10.1529/biophysj.106.081372.

Bui, S. H. *et al.* (2012) 'Unusual spectroscopic and ligand binding properties of the cytochrome P450-flavodoxin fusion enzyme XplA', *Journal of Biological Chemistry*. American Society for Biochemistry and Molecular Biology, 287(23), pp. 19699–19714. doi: 10.1074/jbc.M111.319202.

Christenson, J. K. *et al.* (2017) 'OleB from Bacterial Hydrocarbon Biosynthesis Is a β-Lactone Decarboxylase That Shares Key Features with Haloalkane Dehalogenases', *Biochemistry*. American Chemical Society, 56(40), pp. 5278–5287. doi: 10.1021/acs.biochem.7b00667.

Clemmer, D. E. and Jarrold, M. F. (1997) 'Ion mobility measurements and their applications to clusters and biomolecules', *Journal of Mass Spectrometry*. John Wiley & Sons, Ltd, pp. 577–592. doi: 10.1002/(SICI)1096-9888(199706)32:6<577::AID-JMS530>3.0.CO;2-4.

Cole, J. L. *et al.* (2008) 'Analytical Ultracentrifugation: Sedimentation Velocity and Sedimentation Equilibrium', *Methods in Cell Biology*, pp. 143–179. doi: 10.1016/S0091-679X(07)84006-4.

Coleman, T. *et al.* (2020) 'Structural insights into the role of the acid-alcohol pair of residues required for dioxygen activation in cytochrome P450 enzymes', *Journal of Biological Inorganic Chemistry*. Springer, 25(4), pp. 583–596. doi: 10.1007/s00775-020-01781-4.

Coon, M. J. (2005) 'Cytochrome P450: Nature's most versatile biological catalyst', *Annual Review of Pharmacology and Toxicology*, pp. 1–25. doi: 10.1146/annurev.pharmtox.45.120403.100030.

Cryle, M. J. and De Voss, J. J. (2008) 'The role of the conserved threonine in P450BM3 oxygen activation: Substrate-determined hydroxylation activity of the Thr268Ala mutant',

ChemBioChem, 9(2), pp. 261–266. doi: 10.1002/cbic.200700537.

Daff, S. N. *et al.* (1997) 'Redox control of the catalytic cycle of flavocytochrome P-450 BM3', *Biochemistry*. Biochemistry, 36(45), pp. 13816–13823. doi: 10.1021/bi971085s.

Das, A., Grinkova, Y. V. and Sligar, S. G. (2007) 'Redox potential control by drug binding to cytochrome P450 3A4', *Journal of the American Chemical Society*. NIH Public Access, 129(45), pp. 13778–13779. doi: 10.1021/ja074864x.

Dawson, J. H., Andersson, L. A. and Sono, M. (1982) 'Spectroscopic investigations of ferric cytochrome P-450-CAM ligand complexes. Identification of the ligand trans to cysteinate in the native enzyme.', *Journal of Biological Chemistry*, 257(7), pp. 3606–3617. doi: 10.1016/s0021-9258(18)34823-3.

Dawson, J. H., Anderssons, L. A. and Sono, M. (1982) *Spectroscopic investigations of ferric cytochrome P-450-CAM ligand complexes. Identification of the ligand trans to cysteinate in the native enzyme.*, *THE JOURNAL OF BIOLOGICAL CHEMISTRY*. doi: 10.1016/S0021-9258(18)34823-3.

Denisov, I. G. *et al.* (2005) *Structure and chemistry of cytochrome P450*, *Chemical Reviews*. American Chemical Society. doi: 10.1021/cr0307143.

Dennig, A. *et al.* (2015) 'Oxidative Decarboxylation of Short-Chain Fatty Acids to 1-Alkenes', *Angewandte Chemie - International Edition*, 54(30), pp. 8819–8822. doi: 10.1002/anie.201502925.

Driscoll, M. D. *et al.* (2011) 'Expression and characterization of Mycobacterium tuberculosis CYP144: Common themes and lessons learned in the M. tuberculosis P450 enzyme family', *Biochimica et Biophysica Acta - Proteins and Proteomics*. Biochim Biophys Acta, 1814(1), pp. 76–87. doi: 10.1016/j.bbapap.2010.05.015.

Emsley, P. *et al.* (2010) 'Features and development of Coot', *Acta Crystallographica Section D: Biological Crystallography*. Acta Crystallogr D Biol Crystallogr, 66(4), pp. 486–501. doi: 10.1107/S0907444910007493.

Evans, P. R. and Murshudov, G. N. (2013) 'How good are my data and what is the resolution?', *Acta Crystallographica Section D: Biological Crystallography*. Acta Crystallogr D Biol Crystallogr, 69(7), pp. 1204–1214. doi: 10.1107/S0907444913000061.

Fu, W. J. *et al.* (2015) 'Hydrocarbons, the advanced biofuels produced by different organisms, the evidence that alkanes in petroleum can be renewable', *Applied Microbiology and Biotechnology*. Springer Verlag, pp. 7481–7494. doi: 10.1007/s00253-015-6840-6.

Fudou, R. *et al.* (2002) 'Corynebacterium efficiens sp. nov., a glutamic-acid-producing species from soil and vegetables', *International Journal of Systematic and Evolutionary Microbiology*. Microbiology Society, 52(4), pp. 1127–1131. doi: 10.1099/ijs.0.02086-0.

Fujishiro, T. *et al.* (2011) 'Crystal structure of H 2O 2-dependent cytochrome P450 SPαwith its bound fatty acid substrate: Insight into the regioselective hydroxylation of fatty acids at the α position', *Journal of Biological Chemistry*, 286(34), pp. 29941–29950. doi: 10.1074/jbc.M111.245225.

Gandomkar, S. *et al.* (2018) 'Biocatalytic Oxidative Cascade for the Conversion of Fatty Acids into α-Ketoacids via Internal H2O2 Recycling', *Angewandte Chemie - International Edition*. Wiley-VCH Verlag, 57(2), pp. 427–430. doi: 10.1002/anie.201710227.

Girvan, H. M. *et al.* (2004) 'Flavocytochrome P450 BM3 mutant A264E undergoes substrate-

dependent formation of a novel heme iron ligand set', *Journal of Biological Chemistry*. J Biol Chem, 279(22), pp. 23274–23286. doi: 10.1074/jbc.M401716200.

Girvan, H. M. *et al.* (2018) 'Structural and catalytic properties of the peroxygenase P450 enzyme CYP152K6 from Bacillus methanolicus', *Journal of Inorganic Biochemistry*. Elsevier Inc., 188, pp. 18–28. doi: 10.1016/j.jinorgbio.2018.08.002.

Girvan, H. M. and Munro, A. W. (2016) 'Applications of microbial cytochrome P450 enzymes in biotechnology and synthetic biology', *Current Opinion in Chemical Biology*. Elsevier Ltd, pp. 136–145. doi: 10.1016/j.cbpa.2016.02.018.

Good, N. E. *et al.* (1966) 'Hydrogen Ion Buffers for Biological Research', *Biochemistry*. American Chemical Society, 5(2), pp. 467–477. doi: 10.1021/bi00866a011.

Grant, J. L., Hsieh, C. H. and Makris, T. M. (2015a) 'Decarboxylation of fatty acids to terminal alkenes by cytochrome P450 compound i', *Journal of the American Chemical Society*. American Chemical Society, 137(15), pp. 4940–4943. doi: 10.1021/jacs.5b01965.

Grant, J. L., Hsieh, C. H. and Makris, T. M. (2015b) 'Decarboxylation of fatty acids to terminal alkenes by cytochrome P450 compound I', *Journal of the American Chemical Society*, 137(15), pp. 4940–4943. doi: 10.1021/jacs.5b01965.

Grant, J. L., Mitchell, M. E. and Makris, T. M. (2016a) 'Catalytic strategy for carbon-carbon bond scission by the cytochrome p450 olet', *Proceedings of the National Academy of Sciences of the United States of America*, 113(36), pp. 10049–10054. doi: 10.1073/pnas.1606294113.

Grant, J. L., Mitchell, M. E. and Makris, T. M. (2016b) 'Catalytic strategy for carbon-carbon bond scission by the cytochrome P450 OleT', *Proceedings of the National Academy of Sciences of the United States of America*, 113(36), pp. 10049–10054. doi: 10.1073/pnas.1606294113.

Guengerich, F. P. and Munro, A. W. (2013) 'Unusual cytochrome p450 enzymes and reactions.', *The Journal of biological chemistry*. American Society for Biochemistry and Molecular Biology, 288(24), pp. 17065–73. doi: 10.1074/jbc.R113.462275.

Hagemans, D. *et al.* (2015) 'A script to highlight hydrophobicity and charge on protein surfaces', *Frontiers in Molecular Biosciences*. Frontiers Media S.A., 2(OCT), p. 56. doi: 10.3389/fmolb.2015.00056.

Hamdy, O. M. and Julian, R. R. (2012) 'Reflections on charge state distributions, protein structure, and the mystical mechanism of electrospray ionization', *Journal of the American Society for Mass Spectrometry*, 23(1), pp. 1–6. doi: 10.1007/s13361-011-0284-8.

Hannemann, F. *et al.* (2007) 'Cytochrome P450 systems—biological variations of electron transport chains', *Biochimica et Biophysica Acta (BBA) - General Subjects*, 1770(3), pp. 330–344. doi: 10.1016/j.bbagen.2006.07.017.

Van Hellemond, E. W. *et al.* (2009) 'Exploring the biocatalytic scope of alditol oxidase from Streptomyces coelicolor', *Advanced Synthesis and Catalysis*, 351(10), pp. 1523–1530. doi: 10.1002/adsc.200900176.

Howlett, G. J., Minton, A. P. and Rivas, G. (2006) 'Analytical ultracentrifugation for the study of protein association and assembly', *Current Opinion in Chemical Biology*. Curr Opin Chem Biol, pp. 430–436. doi: 10.1016/j.cbpa.2006.08.017.

Hsieh, C. H. *et al.* (2017) 'The Enigmatic P450 Decarboxylase OleT Is Capable of, but Evolved to Frustrate, Oxygen Rebound Chemistry', *Biochemistry*. American Chemical Society, 56(26), pp. 3347–3357. doi: 10.1021/acs.biochem.7b00338.

Hsieh, C. H. and Makris, T. M. (2016) *Expanding the substrate scope and reactivity of cytochrome P450 OleT*, *Biochemical and Biophysical Research Communications*. doi: 10.1016/j.bbrc.2016.05.145.

Imai, Y. *et al.* (2000) 'Unique heme environment at the putative distal region of hydrogen peroxide-dependent fatty acid α-hydroxylase from Sphingomonas paucimobilis (peroxygenase P450(SPα))', *Journal of Biochemistry*, 128(2), pp. 189–194. doi: 10.1093/oxfordjournals.jbchem.a022740.

Isin, E. M. and Guengerich, F. P. (2008) 'Substrate binding to cytochromes P450', *Analytical and Bioanalytical Chemistry*. NIH Public Access, pp. 1019–1030. doi: 10.1007/s00216-008-2244-0.

Kabsch, W. (2010) 'Integration, scaling, space-group assignment and post-refinement', *Acta Crystallographica Section D: Biological Crystallography*. International Union of Crystallography, 66(2), pp. 133–144. doi: 10.1107/S0907444909047374.

Kang, M. K. and Nielsen, J. (2017) 'Biobased production of alkanes and alkenes through metabolic engineering of microorganisms', *Journal of Industrial Microbiology and Biotechnology*. Springer Verlag, pp. 613–622. doi: 10.1007/s10295-016-1814-y.

Kapust, R. B. *et al.* (2001) 'Tobacco etch virus protease: Mechanism of autolysis and rational design of stable mutants with wild-type catalytic proficiency', *Protein Engineering*. Oxford University Press, 14(12), pp. 993–1000. doi: 10.1093/protein/14.12.993.

Koerner, R. J., Goodfellow, M. and Jones, A. L. (2009) 'The genus Dietzia: A new home for some known and emerging opportunist pathogens', *FEMS Immunology and Medical Microbiology*. Oxford Academic, pp. 296–305. doi: 10.1111/j.1574-695X.2008.00513.x.

Köninger, K. *et al.* (2016) 'Light-driven enzymatic decarboxylation', *Journal of Visualized Experiments*. Journal of Visualized Experiments, 2016(111), p. 53439. doi: 10.3791/53439.

Korasick, D. A. and Tanner, J. J. (2018) 'Determination of protein oligomeric structure from small-angle X-ray scattering', *Protein Science*. Blackwell Publishing Ltd, pp. 814–824. doi: 10.1002/pro.3376.

Krissinel, E. and Henrick, K. (2004) 'Secondary-structure matching (SSM), a new tool for fast protein structure alignment in three dimensions', *Acta Crystallographica Section D: Biological Crystallography*. Acta Crystallogr D Biol Crystallogr, 60(12 I), pp. 2256–2268. doi: 10.1107/S0907444904026460.

Leadbeater, C. *et al.* (2000) 'Probing the NADPH-binding site of Escherichia coli flavodoxin oxidoreductase', *Biochemical Journal*. Portland Press Ltd, 352(2), pp. 257–266. doi: 10.1042/0264-6021:3520257.

Lee, D. S. *et al.* (2003) 'Substrate recognition and molecular mechanism of fatty acid hydroxylation by cytochrome P450 from Bacillus subtilis: Crystallographic, spectroscopic, and mutational studies', *Journal of Biological Chemistry*. American Society for Biochemistry and Molecular Biology, 278(11), pp. 9761–9767. doi: 10.1074/jbc.M211575200.

Leslie Dutton, P. (1978) 'Redox potentiometry: Determination of midpoint potentials of oxidation-reduction components of biological electron-transfer systems', *Methods in Enzymology*. Methods Enzymol, 54(C), pp. 411–435. doi: 10.1016/S0076-6879(78)54026-3.

Li, A. *et al.* (2017) 'A redox-mediated Kemp eliminase', *Nature Communications*. Nature Publishing Group, 8(1), pp. 1–8. doi: 10.1038/ncomms14876.

Li, H. and Poulos, T. L. (1997) 'The structure of the cytochrome p450BM-3 haem domain

complexed with the fatty acid substrate, palmitoleic acid', *Nature Structural Biology*. Nature Publishing Group, 4(2), pp. 140–146. doi: 10.1038/nsb0297-140.

Li, N. *et al.* (2012) 'Evidence for only oxygenative cleavage of aldehydes to alk(a/e)nes and formate by cyanobacterial aldehyde decarbonylases', *Biochemistry*. Biochemistry, 51(40), pp. 7908–7916. doi: 10.1021/bi300912n.

Liang, J. L. *et al.* (2016) 'Regulation of the alkane hydroxylase CYP153 gene in a Gram-positive alkane-degrading bacterium, Dietzia sp. strain DQ12-45-1b', *Applied and Environmental Microbiology*. American Society for Microbiology, 82(2), pp. 608–619. doi: 10.1128/AEM.02811-15.

Lipscomb, J. D. (1980) 'Electron Paramagnetic Resonance Detectable States of Cytochrome P-450Cam', *Biochemistry*. American Chemical Society, 19(15), pp. 3590–3599. doi: 10.1021/bi00556a027.

Liu, H. *et al.* (2012) 'Production of extracellular fatty acid using engineered Escherichia coli', *Microbial Cell Factories*, 11(1), p. 41. doi: 10.1186/1475-2859-11-41.

Liu, Q. *et al.* (2015) 'Engineering an iterative polyketide pathway in Escherichia coli results in single-form alkene and alkane overproduction', *Metabolic Engineering*. Academic Press Inc., 28, pp. 82–90. doi: 10.1016/j.ymben.2014.12.004.

Liu, Y. *et al.* (2014) 'Hydrogen peroxide-independent production of α-alkenes by OleTJE P450 fatty acid decarboxylase.', *Biotechnology for biofuels*, 7(1), p. 28. doi: 10.1186/1754-6834-7-28.

Lu, C. *et al.* (2018) 'An Engineered Self-Sufficient Biocatalyst Enables Scalable Production of Linear α-Olefins from Carboxylic Acids', *ACS Catalysis*, 8(7), pp. 5794–5798. doi: 10.1021/acscatal.8b01313.

Luthra, A., Denisov, I. G. and Sligar, S. G. (2011) 'Spectroscopic features of cytochrome P450 reaction intermediates', *Archives of Biochemistry and Biophysics*. NIH Public Access, pp. 26–35. doi: 10.1016/j.abb.2010.12.008.

Matsunaga, I. *et al.* (1996) 'Direct involvement of hydrogen peroxide in bacterial α-hydroxylation of fatty acid', *FEBS Letters*. Elsevier B.V., 386(2–3), pp. 252–254. doi: 10.1016/0014-5793(96)00451-6.

Matsunaga, I. *et al.* (1997) 'Molecular cloning and expression of fatty acid α-hydroxylase from Sphingomonas paucimobilis', *Journal of Biological Chemistry*. American Society for Biochemistry and Molecular Biology, 272(38), pp. 23592–23596. doi: 10.1074/jbc.272.38.23592.

Matsunaga, I. *et al.* (1999) 'Characterization of the ybdT gene product of Bacillus subtilis: Novel fatty acid β-hydroxylating cytochrome P450', *Lipids*. John Wiley & Sons, Ltd, 34(8), pp. 841–846. doi: 10.1007/s11745-999-0431-3.

Matthews, S., Belcher, J. D., *et al.* (2017) 'Catalytic determinants of alkene production by the cytochrome P450 peroxygenase OleTJE', *Journal of Biological Chemistry*. American Society for Biochemistry and Molecular Biology, 292(12), pp. 5128–5143. doi: 10.1074/jbc.M116.762336.

Matthews, S., Tee, K. L., *et al.* (2017a) 'Production of alkenes and novel secondary products by P450 OleTJE using novel H2O2-generating fusion protein systems', *FEBS Letters*. Wiley Blackwell, 591(5), pp. 737–750. doi: 10.1002/1873-3468.12581.

Matthews, S., Tee, K. L., *et al.* (2017b) 'Production of alkenes and novel secondary products by P450 OleTJE using novel H2O2-generating fusion protein systems', *FEBS Letters*. Wiley Blackwell, 591(5), pp. 737–750. doi: 10.1002/1873-3468.12581.

Matthews, S., Tee, K. L., *et al.* (2017c) 'Production of alkenes and novel secondary products by P450 OleTJE using novel H2O2-generating fusion protein systems', *FEBS Letters*, 591(5), pp. 737–750. doi: 10.1002/1873-3468.12581.

McCoy, A. J. *et al.* (2007) 'Phaser crystallographic software', *Journal of Applied Crystallography*. International Union of Crystallography, 40(4), pp. 658–674. doi: 10.1107/S0021889807021206.

McIver, L. *et al.* (1998) 'Characterisation of flavodoxin NADP+ oxidoreductase and flavodoxin; key components of electron transfer in Escherichia coli', *European Journal of Biochemistry*. Blackwell Publishing Ltd., 257(3), pp. 577–585. doi: 10.1046/j.1432-1327.1998.2570577.x.

McKNIGHT, J. *et al.* (1993) 'Identification of charge-transfer transitions in the optical spectrum of low-spin ferric cytochrome P-450 Bacillus megaterium', *European Journal of Biochemistry*. Eur J Biochem, 213(2), pp. 683–687. doi: 10.1111/j.1432-1033.1993.tb17808.x.

McLean, K. J. *et al.* (2002) 'Expression, purification and spectroscopic characterization of the cytochrome P450 CYP121 from Mycobacterium tuberculosis', *Journal of Inorganic Biochemistry*. J Inorg Biochem, 91(4), pp. 527–541. doi: 10.1016/S0162-0134(02)00479-8.

McLean, K. J. *et al.* (2005) 'Biodiversity of cytochrome P450 redox systems', in *Biochemical Society Transactions*, pp. 796–801. doi: 10.1042/BST0330796.

McLean, K. J. *et al.* (2006) 'Biophysical characterization of the sterol demethylase P450 from Mycobacterium tuberculosis, its cognate ferredoxin, and their interactions', *Biochemistry*. Biochemistry, 45(27), pp. 8427–8443. doi: 10.1021/bi0601609.

McLean, K. J. *et al.* (2015) 'Biological diversity of cytochrome P450 redox partner systems', *Advances in Experimental Medicine and Biology*, 851, pp. 299–317. doi: 10.1007/978-3-319-16009-2_11.

Miles, J. S. *et al.* (1992) 'Domains of the catalytically self-sufficient cytochrome p-450 BM-3. Genetic construction, overexpression, purification and spectroscopic characterization', *Biochemical Journal*. Biochem J, 288(2), pp. 503–509. doi: 10.1042/bj2880503.

Monk, B. C. *et al.* (2014) 'Architecture of a single membrane spanning cytochrome P450 suggests constraints that orient the catalytic domain relative to a bilayer', *Proceedings of the National Academy of Sciences of the United States of America*. National Academy of Sciences, 111(10), pp. 3865–3870. doi: 10.1073/pnas.1324245111.

Munro, A. W. *et al.* (2002) 'P450 BM3: The very model of a modern flavocytochrome', *Trends in Biochemical Sciences*, pp. 250–257. doi: 10.1016/S0968-0004(02)02086-8.

Munro, A. W. *et al.* (2013) 'What makes a P450 tick?', *Trends in Biochemical Sciences*, 38(3), pp. 140–150. doi: 10.1016/j.tibs.2012.11.006.

Munro, A. W. *et al.* (2018) 'Structure and function of the cytochrome P450 peroxygenase enzymes', *Biochemical Society Transactions*. Portland Press Ltd, pp. 183–196. doi: 10.1042/BST20170218.

Munro, A. W., Girvan, H. M. and McLean, K. J. (2007) 'Variations on a (t)heme--novel mechanisms, redox partners and catalytic functions in the cytochrome P450 superfamily.', *Natural product reports*, 24(3), pp. 585–609. doi: 10.1039/b604190f.

Murugan, R. and Mazumdar, S. (2005) 'Structure and Redox Properties of the Haem Centre in the C357M Mutant of Cytochrome P450cam', *ChemBioChem*. John Wiley & Sons, Ltd, 6(7), pp. 1204–1211. doi: 10.1002/cbic.200400399.

Omura, T. and Sato, R. (1962) 'A new cytochrome in liver microsomes.', *The Journal of biological*

chemistry, 237, pp. 1375–1376. Available at: http://www.ncbi.nlm.nih.gov/pubmed/14482007 (Accessed: 27 November 2016).

Perera, R. *et al.* (2003) 'Neutral thiol as a proximal ligand to ferrous heme iron: Implications for heme proteins that lose cysteine thiolate ligation on reduction', *Proceedings of the National Academy of Sciences of the United States of America*. National Academy of Sciences, 100(7), pp. 3641–3646. doi: 10.1073/pnas.0737142100.

Pickl, M. *et al.* (2019) 'Mechanistic Studies of Fatty Acid Activation by CYP152 Peroxygenases Reveal Unexpected Desaturase Activity', *ACS Catalysis*. American Chemical Society, 9(1), pp. 565–577. doi: 10.1021/acscatal.8b03733.

Pluschke, G. and Overath, P. (1981) 'Function of phospholipids in Escherichia coli. Influence of changes in polar head group composition on the lipid phase transition and characterization of a mutant containing only saturated phospholipid acyl chains', *Journal of Biological Chemistry*, 256(7), pp. 3207–3212. doi: 10.1016/s0021-9258(19)69590-6.

Podust, L. M. *et al.* (2001) 'Substrate recognition sites in 14α-sterol demethylase from comparative analysis of amino acid sequences and X-ray structure of Mycobacterium tuberculosis CYP51', *Journal of Inorganic Biochemistry*. Elsevier, 87(4), pp. 227–235. doi: 10.1016/S0162-0134(01)00388-9.

Poulos, T. L., Finzel, B. C. and Howard, A. J. (1987) 'High-resolution crystal structure of cytochrome P450cam', *Journal of Molecular Biology*, 195(3), pp. 687–700. doi: 10.1016/0022-2836(87)90190-2.

Presnell, S. R. and Cohen, F. E. (1989) 'Topological distribution of four-alpha-helix bundles.', *Proceedings of the National Academy of Sciences of the United States of America*. Proc Natl Acad Sci U S A, 86(17), pp. 6592–6596. doi: 10.1073/pnas.86.17.6592.

Prinz, H. (2010) 'Hill coefficients, dose–response curves and allosteric mechanisms', *Journal of Chemical Biology*. Springer, 3(1), p. 37. doi: 10.1007/S12154-009-0029-3.

Qiu, Y. *et al.* (2012) 'An insect-specific P450 oxidative decarbonylase for cuticular hydrocarbon biosynthesis', *Proceedings of the National Academy of Sciences of the United States of America*. Proc Natl Acad Sci U S A, 109(37), pp. 14858–14863. doi: 10.1073/pnas.1208650109.

Raag, R. *et al.* (1991) 'Crystal Structure of the Cytochrome P-450CAM Active Site Mutant Thr252Ala', *Biochemistry*. American Chemical Society, 30(48), pp. 11420–11429. doi: 10.1021/bi00112a008.

Reinhard, F. G. C. *et al.* (2020) 'Bioengineering of Cytochrome P450 OleTJE: How Does Substrate Positioning Affect the Product Distributions?', *Molecules (Basel, Switzerland)*. NLM (Medline), 25(11). doi: 10.3390/molecules25112675.

Rittle, J. and Green, M. T. (2010) 'Cytochrome P450 compound I: Capture, characterization, and C-H bond activation kinetics', *Science*, 330(6006), pp. 933–937. doi: 10.1126/science.1193478.

Rude, M. A. *et al.* (2011) 'Terminal olefin (1-alkene) biosynthesis by a novel P450 fatty acid decarboxylase from Jeotgalicoccus species', *Applied and Environmental Microbiology*. American Society for Microbiology, 77(5), pp. 1718–1727. doi: 10.1128/AEM.02580-10.

Sabbadin, F. *et al.* (2009) 'The 1.5-Å structure of XplA-heme, an unusual cytochrome P450 heme domain that catalyzes reductive biotransformation of royal demolition explosive', *Journal of Biological Chemistry*. American Society for Biochemistry and Molecular Biology, 284(41), pp. 28467–28475. doi: 10.1074/jbc.M109.031559.

Sahin, E. and Roberts, C. J. (2012) 'Size-exclusion chromatography with multi-angle light scattering for elucidating protein aggregation mechanisms', *Methods in Molecular Biology*, 899, pp. 403–423. doi: 10.1007/978-1-61779-921-1_25.

Sayer, P., Gouterman, M. and Connell, C. R. (1982) 'Metalloid Porphyrins and Phthalocyanines', *Accounts of Chemical Research*, 15(3), pp. 73–79. doi: 10.1021/ar00075a002.

Schirmer, A. *et al.* (2010) 'Microbial biosynthesis of alkanes', *ScienceSchirmer, A. et al. (2010) 'Microbial biosynthesis of alkanes', Science, 329(5991), pp. 559–562. doi: 10.1126/science.1187936.*, 329(5991), pp. 559–562. doi: 10.1126/science.1187936.

Schlichting, I. *et al.* (2000) 'The catalytic pathway of cytochrome P450cam at atomic resolution', *Science*. American Association for the Advancement of Science, 287(5458), pp. 1615–1622. doi: 10.1126/science.287.5458.1615.

Schrödinger, L. (2015) 'The PyMOL Molecular Graphics System, Version 2.4.0a0'. Available at: https://www.schrodinger.com/products/pymol (Accessed: 14 March 2021).

Shaw, M. K. and Ingraham, J. L. (1965) 'Fatty Acid Composition of Escherichia coli as a Possible Controlling Factor of the Minimal Growth Temperature', *Journal of Bacteriology*, 90(1), pp. 141–146. doi: 10.1128/jb.90.1.141-146.1965.

Shimada, H. *et al.* (1991) 'The Role of Threonine 252 in the Oxygen Activation by Cytochrome P-450 cam: Mechanistic Studies by Site-directed Mutagenesis', *Studies in Surface Science and Catalysis*. Elsevier, 66(C), pp. 313–319. doi: 10.1016/S0167-2991(08)62847-5.

Shoji, O. and Watanabe, Y. (2014) 'Peroxygenase reactions catalyzed by cytochromes P450', *Journal of Biological Inorganic Chemistry*. Springer Verlag, pp. 529–539. doi: 10.1007/s00775-014-1106-9.

Singh, M. K. *et al.* (2017) 'Role of an N-terminal extension in stability and catalytic activity of a hyperthermostable α/β hydrolase fold esterase', *Protein Engineering, Design and Selection*. Oxford University Press, 30(8), pp. 559–570. doi: 10.1093/protein/gzx049.

Sligar, S. G. and Gunsalus, I. C. (1976) 'A thermodynamic model of regulation: modulation of redox equilibria in camphor monoxygenase', *Proceedings of the National Academy of Sciences of the United States of America*. National Academy of Sciences, 73(4), pp. 1078–1082. doi: 10.1073/pnas.73.4.1078.

Somvanshi, P. R. and Venkatesh, K. V. (2013) 'Hill Equation', in *Encyclopedia of Systems Biology*. Springer New York, pp. 892–895. doi: 10.1007/978-1-4419-9863-7_946.

'The CCP4 suite: Programs for protein crystallography' (1994) *Acta Crystallographica Section D: Biological Crystallography*. Acta Crystallogr D Biol Crystallogr, 50(5), pp. 760–763. doi: 10.1107/S0907444994003112.

Tyson, C. A., Lipscomb, J. D. and Gunsalus, I. C. (1972) 'The role of putidaredoxin and P450 cam in methylene hydroxylation.', *Journal of Biological Chemistry*, 247(18), pp. 5777–5784. doi: 10.1016/s0021-9258(19)44826-6.

Vagin, A. A. *et al.* (2004) 'REFMAC5 dictionary: Organization of prior chemical knowledge and guidelines for its use', *Acta Crystallographica Section D: Biological Crystallography*. International Union of Crystallography, 60(12 I), pp. 2184–2195. doi: 10.1107/S0907444904023510.

Wang, C. and Wamser, C. C. (2014) 'Hyperporphyrin effects in the spectroscopy of protonated porphyrins with 4-aminophenyl and 4-pyridyl meso substituents', *Journal of Physical Chemistry A*. American Chemical Society, 118(20), pp. 3605–3615. doi: 10.1021/jp501398g.

Wang, S. *et al.* (2020) 'Directed evolution of a hydroxylase into a decarboxylase for synthesis of 1‐alkenes from fatty acids', *ACS Catalysis*. American Chemical Society, 10(24), pp. 14375–14379. doi: 10.1021/acscatal.0c04345.

Wang, Z. J. *et al.* (2014) 'Improved Cyclopropanation Activity of Histidine-Ligated Cytochrome P450 Enables the Enantioselective Formal Synthesis of Levomilnacipran', *Angewandte Chemie International Edition*. Wiley-VCH Verlag, 53(26), pp. 6810–6813. doi: 10.1002/anie.201402809.

von der Weid, I. *et al.* (2007) 'Identification and biodegradation potential of a novel strain of Dietzia cinnamea isolated from a petroleum-contaminated tropical soil', *Systematic and Applied Microbiology*. Elsevier GmbH, 30(4), pp. 331–339. doi: 10.1016/j.syapm.2006.11.001.

Wilson, G. S., Tsibris, J. C. M. and Gunsalus, I. C. (1973) 'Electrochemical studies of putidaredoxin and its selenium analog', *Journal of Biological Chemistry*. Elsevier, 248(17), pp. 6059–6061. doi: 10.1016/s0021-9258(19)43508-4.

Wise, C. E. *et al.* (2018) 'Dioxygen Activation by the Biofuel-Generating Cytochrome P450 OleT', *ACS Catalysis*. American Chemical Society, 8(10), pp. 9342–9352. doi: 10.1021/acscatal.8b02631.

Xu, H. *et al.* (2017) 'In vitro oxidative decarboxylation of free fatty acids to terminal alkenes by two new P450 peroxygenases', *Biotechnology for Biofuels*. BioMed Central Ltd., 10(1), p. 208. doi: 10.1186/s13068-017-0894-x.

Yassin, A. F., Hupfer, H. and Schaal, K. P. (2006) 'Dietzia cinnamea sp. nov., a novel species isolated from a perianal swab of a patient with a bone marrow transplant', *International Journal of Systematic and Evolutionary Microbiology*, 56(3), pp. 641–645. doi: 10.1099/ijs.0.63863-0.

3.7 Supplementary

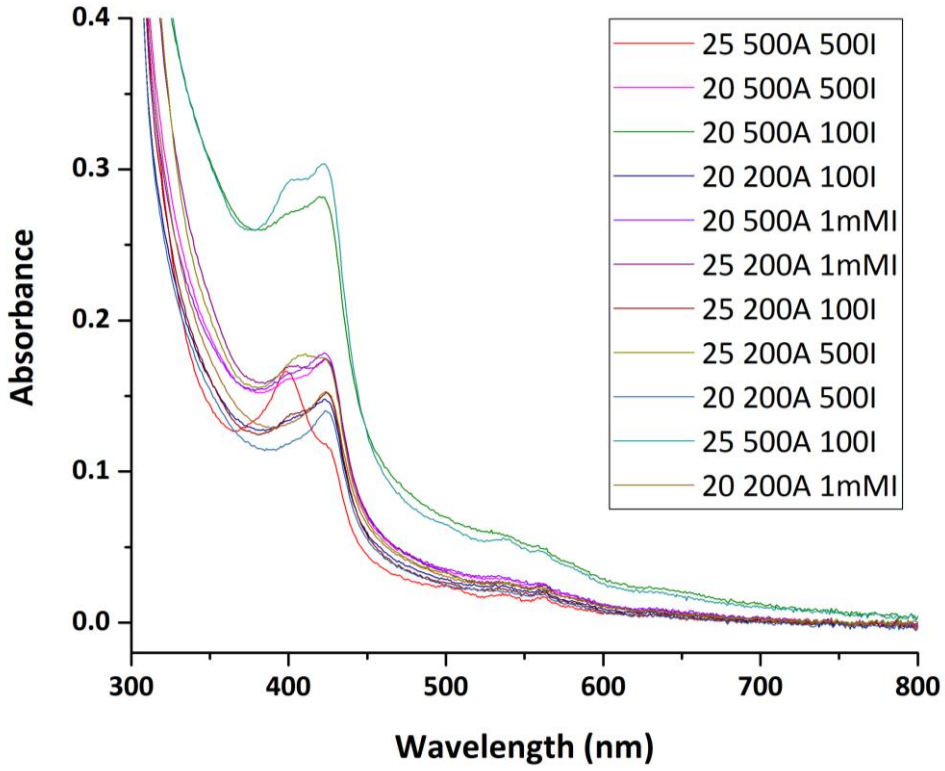

Figure 3.19 UV-visible absorbance of P450 CE from expression trails in E. coli cells. All cells were grown at 37°C until OD600nm 0.5-0.8 was reached. Temperature was reduced to either 25°C or 20°C and supplement with δ-aminolevulinic (A) at either 500 µM or 200 µM. Cells were then induced by IPTG using concentrations of either 100 µM, 500 µM or 1 mM. Cells pellets collected after 24 hours of growth, lysed and centrifuged to obtain samples.

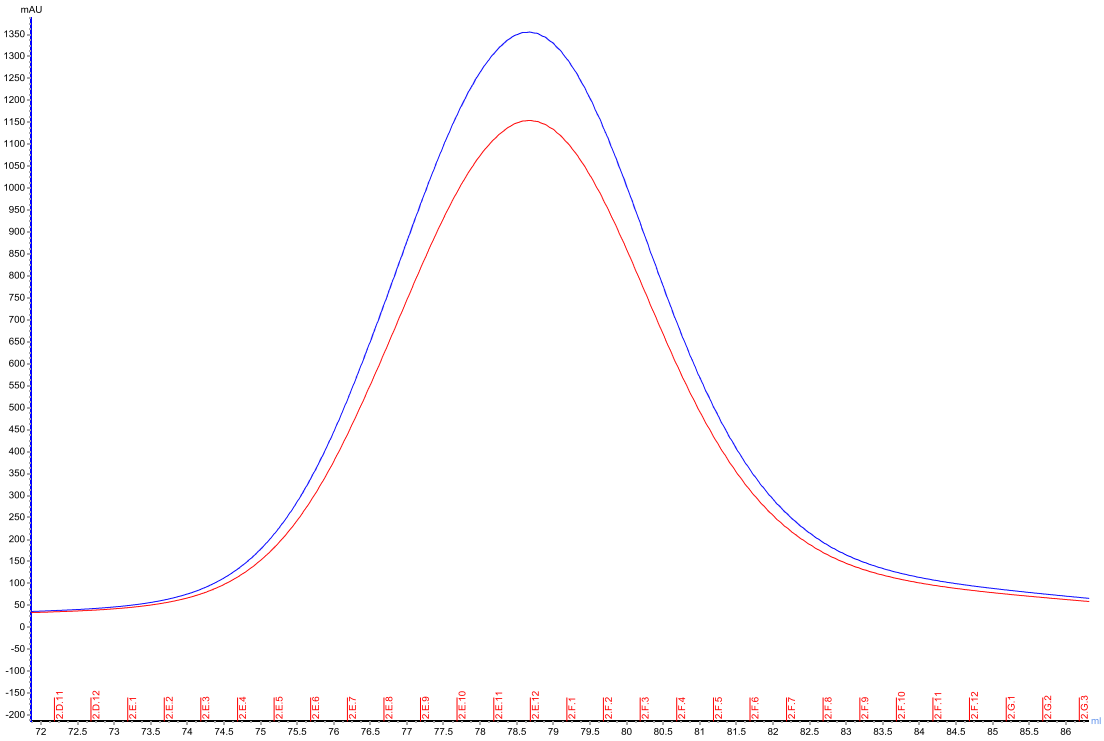

Figure 3.20 Trace of P450 CE obtained from gel filtration step. The UV-visible properties of fraction obtained from the AKTA (blue, UV 280 nm; red UV 424 nm). Superdex 200 16/600 (GE Healthcare) was used.

No disulfide bonds found
No covalent bonds found
No hydrogen bonds found
No salt bridges found

Interfacing residues (not a contact table)

XML Display level: Residues

Inaccessible residues
Solvent-accessible residues
HSDC Residues making Hydrogen/Disulphide bond, Salt bridge or Covalent link
Interfacing residues
ASA Accessible Surface Area, Å² BSA Buried Surface Area, Å² ΔG Solvation energy effect, kcal/mol |||| Buried area percentage, one bar per 10%

##	Structure 1	HSDC	ASA	BSA	ΔG
1	A:SER 5		125.12	0.00	0.00
2	A:SER 6		73.41	0.00	0.00
3	A:CYS 7		58.41	0.00	0.00
4	A:PRO 8		16.44	0.00	0.00
5	A:PHE 9		100.17	0.00	0.00
6	A:ALA 10		0.67	0.00	0.00
7	A:PRO 11		90.14	0.00	0.00
8	A:GLY 12		40.18	0.00	0.00
9	A:GLU 13		57.31	8.53 ||	0.13
10	A:GLN 14		6.61	0.00	0.00
11	A:ALA 15		22.32	12.16 ||||||	0.19
12	A:PRO 16		59.20	50.32 ||||||||	0.79
13	A:ASN 17		24.60	0.00	0.00
14	A:LEU 18		32.54	0.00	0.00
15	A:LEU 19		138.78	76.09 ||||||	1.15
16	A:ARG 20		154.54	49.30 ||||	-0.50
17	A:HIS 21		30.05	0.00	0.00
18	A:GLY 22		0.37	0.00	0.00
19	A:TYR 23		13.96	0.00	0.00
20	A:LEU 24		46.59	0.00	0.00
21	A:PHE 25		1.49	0.00	0.00
22	A:LEU 26		9.61	0.00	0.00
23	A:SER 27		37.56	0.00	0.00
24	A:ARG 28		103.89	0.00	0.00
25	A:LEU 29		1.97	0.00	0.00
26	A:ARG 30		6.65	0.00	0.00
27	A:ARG 31		185.67	0.00	0.00
28	A:LYS 32		118.83	0.00	0.00
29	A:ALA 33		21.72	0.00	0.00
30	A:GLY 34		69.25	0.00	0.00
31	A:ILE 35		36.17	0.00	0.00
32	A:SER 36		57.82	0.00	0.00
33	A:PRO 37		62.33	0.00	0.00
34	A:ASP 38		85.05	0.00	0.00
35	A:ALA 39		26.24	0.00	0.00
36	A:ASN 40		41.60	0.00	0.00
37	A:THR 41		31.44	0.00	0.00
38	A:PRO 42		2.66	0.00	0.00
39	A:LEU 43		2.34	0.00	0.00
40	A:ARG 44		61.55	0.00	0.00
41	A:SER 45		0.25	0.00	0.00
42	A:ARG 46		86.81	0.00	0.00
43	A:MET 47		11.15	0.00	0.00
44	A:LEU 48		67.95	45.29 ||||||	0.69
45	A:PHE 49		164.14	103.29 ||||||	1.63
46	A:LYS 50		99.78	22.58 |||	-0.49
47	A:PRO 51		36.46	0.00	0.00
48	A:VAL 52		0.33	0.00	0.00
49	A:THR 53		3.05	0.00	0.00
50	A:ILE 54		1.03	0.00	0.00
51	A:VAL 55		0.67	0.00	0.00
52	A:ARG 56		11.03	0.00	0.00
53	A:GLY 57		0.33	0.00	0.00
54	A:SER 58		39.49	0.00	0.00
55	A:ALA 59		46.11	0.00	0.00
56	A:GLY 60		0.00	0.00	0.00
57	A:VAL 61		11.16	0.00	0.00
58	A:GLU 62		126.26	0.00	0.00
59	A:LEU 63		3.61	0.00	0.00
60	A:PHE 64		1.96	0.00	0.00
61	A:TYR 65		27.66	0.00	0.00
62	A:ASP 66		39.79	0.00	0.00
63	A:ASN 67		100.36	0.00	0.00
64	A:ASP 68		122.38	0.00	0.00
65	A:ARG 69		57.34	0.00	0.00
66	A:MET 70		12.54	0.00	0.00
67	A:LYS 71		75.87	0.00	0.00
68	A:ARG 72		14.25	0.00	0.00
69	A:ASP 73		85.33	0.00	0.00
70	A:GLY 74		54.71	0.00	0.00
71	A:ALA 75		1.63	0.00	0.00
72	A:MET 76		27.41	0.00	0.00
73	A:PRO 77		34.81	15.25 |||||	0.24
74	A:ALA 78		45.08	7.72 ||	0.04
75	A:VAL 79		125.55	51.46 |||||	0.81
76	A:ILE 80		88.08	0.00	0.00

##	Structure 2	HSDC	ASA	BSA	ΔG
1	A:SER 5		125.12	0.00	0.00
2	A:SER 6		73.41	0.00	0.00
3	A:CYS 7		58.41	0.00	0.00
4	A:PRO 8		16.44	0.00	0.00
5	A:PHE 9		100.17	0.00	0.00
6	A:ALA 10		0.67	0.00	0.00
7	A:PRO 11		90.14	0.00	0.00
8	A:GLY 12		40.18	0.00	0.00
9	A:GLU 13		57.31	7.97 ||	0.13
10	A:GLN 14		6.61	0.00	0.00
11	A:ALA 15		22.32	12.43 ||||||	0.19
12	A:PRO 16		59.20	51.16 ||||||||	0.80
13	A:ASN 17		24.60	0.00	0.00
14	A:LEU 18		32.54	0.00	0.00
15	A:LEU 19		138.78	76.59 ||||||	1.15
16	A:ARG 20		154.54	49.17 ||||	-0.49
17	A:HIS 21		30.05	0.00	0.00
18	A:GLY 22		0.37	0.00	0.00
19	A:TYR 23		13.96	0.00	0.00
20	A:LEU 24		46.59	0.00	0.00
21	A:PHE 25		1.49	0.00	0.00
22	A:LEU 26		9.61	0.00	0.00
23	A:SER 27		37.56	0.00	0.00
24	A:ARG 28		103.89	0.00	0.00
25	A:LEU 29		1.97	0.00	0.00
26	A:ARG 30		6.65	0.00	0.00
27	A:ARG 31		185.67	0.00	0.00
28	A:LYS 32		118.83	0.00	0.00
29	A:ALA 33		21.72	0.00	0.00
30	A:GLY 34		69.25	0.00	0.00
31	A:ILE 35		36.17	0.00	0.00
32	A:SER 36		57.82	0.00	0.00
33	A:PRO 37		62.33	0.00	0.00
34	A:ASP 38		85.05	0.00	0.00
35	A:ALA 39		26.24	0.00	0.00
36	A:ASN 40		41.60	0.00	0.00
37	A:THR 41		31.44	0.00	0.00
38	A:PRO 42		2.66	0.00	0.00
39	A:LEU 43		2.34	0.00	0.00
40	A:ARG 44		61.55	0.00	0.00
41	A:SER 45		0.25	0.00	0.00
42	A:ARG 46		86.81	0.00	0.00
43	A:MET 47		11.15	0.00	0.00
44	A:LEU 48		67.95	45.43 ||||||	0.69
45	A:PHE 49		164.14	103.41 ||||||	1.62
46	A:LYS 50		99.78	22.41 |||	-0.49
47	A:PRO 51		36.46	0.00	0.00
48	A:VAL 52		0.33	0.00	0.00
49	A:THR 53		3.05	0.00	0.00
50	A:ILE 54		1.03	0.00	0.00
51	A:VAL 55		0.67	0.00	0.00
52	A:ARG 56		11.03	0.00	0.00
53	A:GLY 57		0.33	0.00	0.00
54	A:SER 58		39.49	0.00	0.00
55	A:ALA 59		46.11	0.00	0.00
56	A:GLY 60		0.00	0.00	0.00
57	A:VAL 61		11.16	0.00	0.00
58	A:GLU 62		126.26	0.00	0.00
59	A:LEU 63		3.61	0.00	0.00
60	A:PHE 64		1.96	0.00	0.00
61	A:TYR 65		27.66	0.00	0.00
62	A:ASP 66		39.79	0.00	0.00
63	A:ASN 67		100.36	0.00	0.00
64	A:ASP 68		122.38	0.00	0.00
65	A:ARG 69		57.34	0.00	0.00
66	A:MET 70		12.54	0.00	0.00
67	A:LYS 71		75.87	0.00	0.00
68	A:ARG 72		14.25	0.00	0.00
69	A:ASP 73		85.33	0.00	0.00
70	A:GLY 74		54.71	0.00	0.00
71	A:ALA 75		1.63	0.00	0.00
72	A:MET 76		27.41	0.00	0.00
73	A:PRO 77		34.81	15.24 |||||	0.24
74	A:ALA 78		45.08	7.56 ||	0.03
75	A:VAL 79		125.55	51.64 |||||	0.82
76	A:ILE 80		88.08	0.00	0.00

72	A:MET 76	27.41	0.00	0.00
73	A:PRO 77	34.81	15.25 |||||	0.24
74	A:ALA 78	45.08	7.72 ||	0.04
75	A:VAL 79	125.55	51.46 |||||	0.81
76	A:ILE 80	88.08	0.00	0.00
77	A:ARG 81	54.12	0.00	0.00
78	A:ILE 82	76.34	0.00	0.00
79	A:PRO 83	46.84	0.00	0.00
80	A:LEU 84	83.86	0.00	0.00
81	A:PHE 85	54.75	0.00	0.00
82	A:GLY 86	9.89	0.00	0.00
83	A:GLU 87	101.79	0.00	0.00
84	A:GLY 88	23.61	0.00	0.00
85	A:ALA 89	3.35	0.00	0.00
86	A:VAL 90	13.39	0.00	0.00
87	A:HIS 91	25.65	0.00	0.00
88	A:SER 92	27.67	0.00	0.00
89	A:LEU 93	25.44	0.00	0.00
90	A:ASP 94	44.77	0.00	0.00
91	A:GLY 95	59.13	0.00	0.00
92	A:GLU 96	97.05	0.00	0.00
93	A:GLU 97	77.91	0.00	0.00
94	A:HIS 98	9.03	0.00	0.00
95	A:ARG 99	101.91	0.00	0.00
96	A:LEU 100	20.29	0.00	0.00
97	A:ARG 101	17.61	0.00	0.00
98	A:LYS 102	5.25	0.00	0.00
99	A:ARG 103	92.48	0.00	0.00
100	A:GLN 104	18.17	0.00	0.00
101	A:LEU 105	4.93	0.00	0.00
102	A:ALA 106	0.00	0.00	0.00
103	A:ASP 107	60.93	0.00	0.00
104	A:VAL 108	5.85	0.00	0.00
105	A:ALA 109	4.53	0.00	0.00
106	A:TYR 110	29.64	0.00	0.00
107	A:ASP 111	54.82	0.00	0.00
108	A:ASP 112	90.80	0.00	0.00
109	A:ASP 113	103.97	0.00	0.00
110	A:LYS 114	46.57	0.00	0.00
111	A:VAL 115	19.58	0.00	0.00
112	A:ALA 116	64.64	0.00	0.00
113	A:GLU 117	95.72	0.00	0.00
114	A:PHE 118	0.16	0.00	0.00
115	A:ASP 119	40.14	0.00	0.00
116	A:ALA 120	51.14	0.00	0.00
117	A:LEU 121	23.23	0.00	0.00
118	A:VAL 122	0.00	0.00	0.00
119	A:ARG 123	75.13	0.00	0.00
120	A:ARG 124	146.97	0.00	0.00
165	A:ALA 169	0.00	0.00	0.00
166	A:HIS 170	78.11	0.00	0.00
167	A:GLN 171	17.72	0.00	0.00
168	A:MET 172	0.17	0.00	0.00
169	A:ALA 173	4.51	0.00	0.00
170	A:GLU 174	72.77	0.00	0.00
171	A:LEU 175	31.54	0.00	0.00
172	A:VAL 176	23.87	0.00	0.00
173	A:TYR 177	14.56	0.00	0.00
174	A:GLN 178	73.94	0.00	0.00
175	A:PHE 179	69.35	0.00	0.00
176	A:GLY 180	40.34	0.00	0.00
177	A:HIS 181	103.99	1.01		0.02
178	A:PRO 182	84.51	0.00	0.00
179	A:LEU 183	141.86	78.22 ||||||	1.22
180	A:LYS 184	115.38	26.08 |||	0.31
181	A:GLY 185	25.38	0.00	0.00
182	A:ASN 186	115.94	13.41 ||	-0.09
183	A:ALA 187	64.23	43.58 |||||||	0.57
184	A:LEU 188	81.36	73.00 ||||||||	1.17
185	A:GLY 189	9.33	0.00	0.00
186	A:TRP 190	160.20	99.96 |||||||	1.46
187	A:ILE 191	55.06	44.52 ||||||||	0.71
188	A:ASN 192	43.78	12.68 |||	-0.17
189	A:ARG 193	76.79	0.00	0.00
190	A:ALA 194	39.36	0.00	0.00
191	A:ARG 195	129.42	46.90 ||||	-0.72
192	A:LEU 196	2.01	0.00	0.00
193	A:ASN 197	59.31	0.00	0.00
194	A:ARG 198	138.81	0.00	0.00
195	A:TRP 199	10.24	0.00	0.00
196	A:ALA 200	0.33	0.00	0.00
197	A:LEU 201	29.64	0.00	0.00
198	A:LYS 202	85.48	0.00	0.00
199	A:LEU 203	0.17	0.00	0.00
200	A:ILE 204	0.00	0.00	0.00
201	A:ARG 205	143.46	0.00	0.00
202	A:GLN 206	44.72	0.00	0.00
203	A:ALA 207	13.23	0.00	0.00

72	A:MET 76	27.41	0.00	0.00
73	A:PRO 77	34.81	15.24 |||||	0.24
74	A:ALA 78	45.08	7.56 ||	0.03
75	A:VAL 79	125.55	51.64 |||||	0.82
76	A:ILE 80	88.08	0.00	0.00
77	A:ARG 81	54.12	0.00	0.00
78	A:ILE 82	76.34	0.00	0.00
79	A:PRO 83	46.84	0.00	0.00
80	A:LEU 84	83.86	0.00	0.00
81	A:PHE 85	54.75	0.00	0.00
82	A:GLY 86	9.89	0.00	0.00
83	A:GLU 87	101.79	0.00	0.00
84	A:GLY 88	23.61	0.00	0.00
85	A:ALA 89	3.35	0.00	0.00
86	A:VAL 90	13.39	0.00	0.00
87	A:HIS 91	25.65	0.00	0.00
88	A:SER 92	27.67	0.00	0.00
89	A:LEU 93	25.44	0.00	0.00
90	A:ASP 94	44.77	0.00	0.00
91	A:GLY 95	59.13	0.00	0.00
92	A:GLU 96	97.05	0.00	0.00
93	A:GLU 97	77.91	0.00	0.00
94	A:HIS 98	9.03	0.00	0.00
95	A:ARG 99	101.91	0.00	0.00
96	A:LEU 100	20.29	0.00	0.00
97	A:ARG 101	17.61	0.00	0.00
98	A:LYS 102	5.25	0.00	0.00
99	A:ARG 103	92.48	0.00	0.00
100	A:GLN 104	18.17	0.00	0.00
101	A:LEU 105	4.93	0.00	0.00
102	A:ALA 106	0.00	0.00	0.00
103	A:ASP 107	60.93	0.00	0.00
104	A:VAL 108	5.85	0.00	0.00
105	A:ALA 109	4.53	0.00	0.00
106	A:TYR 110	29.64	0.00	0.00
107	A:ASP 111	54.82	0.00	0.00
108	A:ASP 112	90.80	0.00	0.00
109	A:ASP 113	103.97	0.00	0.00
110	A:LYS 114	46.57	0.00	0.00
111	A:VAL 115	19.58	0.00	0.00
112	A:ALA 116	64.64	0.00	0.00
113	A:GLU 117	95.72	0.00	0.00
114	A:PHE 118	0.16	0.00	0.00
115	A:ASP 119	40.14	0.00	0.00
116	A:ALA 120	51.14	0.00	0.00
117	A:LEU 121	23.23	0.00	0.00
118	A:VAL 122	0.00	0.00	0.00
119	A:ARG 123	75.13	0.00	0.00
120	A:ARG 124	146.97	0.00	0.00
165	A:ALA 169	0.00	0.00	0.00
166	A:HIS 170	78.11	0.00	0.00
167	A:GLN 171	17.72	0.00	0.00
168	A:MET 172	0.17	0.00	0.00
169	A:ALA 173	4.51	0.00	0.00
170	A:GLU 174	72.77	0.00	0.00
171	A:LEU 175	31.54	0.00	0.00
172	A:VAL 176	23.87	0.00	0.00
173	A:TYR 177	14.56	0.00	0.00
174	A:GLN 178	73.94	0.00	0.00
175	A:PHE 179	69.35	0.00	0.00
176	A:GLY 180	40.34	0.00	0.00
177	A:HIS 181	103.99	1.01		0.02
178	A:PRO 182	84.51	0.00	0.00
179	A:LEU 183	141.86	77.84 ||||||	1.22
180	A:LYS 184	115.38	26.10 |||	0.31
181	A:GLY 185	25.38	0.00	0.00
182	A:ASN 186	115.94	13.10 ||	-0.10
183	A:ALA 187	64.23	43.22 |||||||	0.57
184	A:LEU 188	81.36	72.49 ||||||||	1.16
185	A:GLY 189	9.33	0.00	0.00
186	A:TRP 190	160.20	100.60 |||||||	1.47
187	A:ILE 191	55.06	44.19 ||||||||	0.71
188	A:ASN 192	43.78	12.38 |||	-0.17
189	A:ARG 193	76.79	0.00	0.00
190	A:ALA 194	39.36	0.00	0.00
191	A:ARG 195	129.42	47.08 ||||	-0.71
192	A:LEU 196	2.01	0.00	0.00
193	A:ASN 197	59.31	0.00	0.00
194	A:ARG 198	138.81	0.00	0.00
195	A:TRP 199	10.24	0.00	0.00
196	A:ALA 200	0.33	0.00	0.00
197	A:LEU 201	29.64	0.00	0.00
198	A:LYS 202	85.48	0.00	0.00
199	A:LEU 203	0.17	0.00	0.00
200	A:ILE 204	0.00	0.00	0.00
201	A:ARG 205	143.46	0.00	0.00
202	A:GLN 206	44.72	0.00	0.00
203	A:ALA 207	13.23	0.00	0.00

Figure 3.21 PISA interface of WT P450 CE. Residues highlighted in yellow

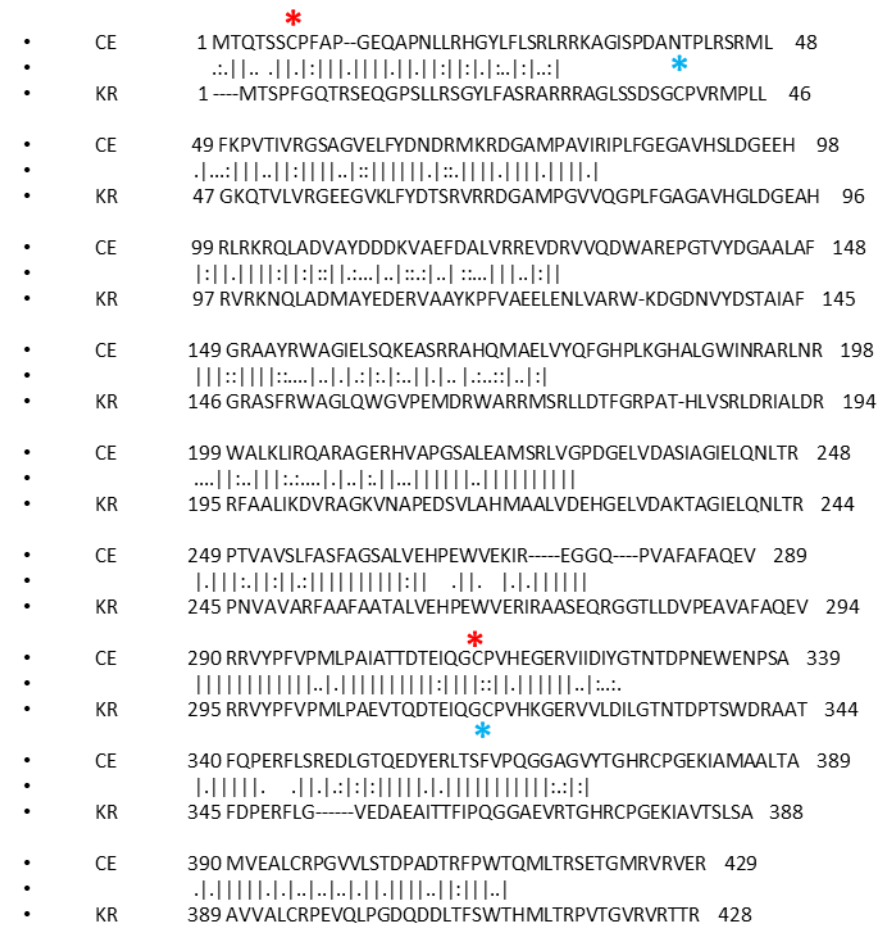

Figure 3.22 Sequence alignment of P450 KR and P450 CE by EMBOSS Needle. Asterisk highlights the cysteine residues involved in the disulphide linkage.

4 Expression and purification of a novel CYP152 family member from *Dietzia cinnamea*

Alessia C. Andrews[1], Harshwardhan Poddar[1], Kirsty J. McLean[3], Hazel M. Girvan[3], Tom Jowitt[2], David Leys[1], and Andrew W. Munro[1]*

[1]Manchester Institute of Biotechnology, Faculty of Life Sciences, University of Manchester, 131 Princess Street, Manchester M1 7DN, UK.

[2]Micheal Smith Building, Faculty of biology medicine health, University of Manchester, Dover St, Manchester, M13 9PT, UK

[3]Department of Biological and Geographical Sciences, School of Applied Sciences, University of Huddersfield, Queensgate, Huddersfield, HD1 3DH, UK

4.1 Abstract

Biohydrocarbons such as alkenes provide ideal alternatives to current transportation fuels and are compatible with the existing infrastructure. The CYP152 alkene producing peroxygenases utilise hydrogen peroxide (H_2O_2) as their sole oxygen and hydrogen donor during catalysis, evading the requirement for auxiliary redox-partner proteins and offer scope for industrial applications. Here we describe expression, purification and initial *in vitro* biochemical characterisation of a CYP152 peroxygenase from *Dietzia cinnamea*. Fatty acid turnover reactions show that P450 DC is able to function as a decarboxylase, producing C_{n-1} terminal alkenes. In addition, P450 DC also has a hydroxylase activity, yielding Cα or Cβ hydroxylated fatty acids. P450 DC displays complete conversion to product with decanoic acid (C10:0), while myristic acid (C14:0) leads to the highest alkene titre of ~52%, comparable to the CYP152T7 orthologue from *Corynebacterium efficiens*.

4.2 Introduction

Cytochromes P450 enzymes (P450s or CYPS) are able to perform regioselective oxidations along with their extreme reaction biodiversity makes them ideal biocatalysts to generate high value oxy-chemicals that are not economical to produce via synthetic chemistry routes (Girvan and Munro, 2016). Among the many P450 reactions, the formation of alkenes and hydroxylated carboxylic acids has significant interest due to the importance of hydrocarbon products in the petrochemical industry as 'drop in' biofuels. Several pathways and enzymes from different organisms have been shown to synthesize alk(a/e)nes from the fatty acid biosynthetic pathway (Kang and Nielsen, 2017). Some of the main pathways include; (i) decarbonylation of fatty aldehydes (ii) head to head hydrocarbon biosynthesis; (iii) polyketide and; (iv) decarboxylation of fatty acids (Rude *et al.*, 2011; Li *et al.*, 2012; Fu *et al.*, 2015; Liu *et al.*, 2015; Kang and Nielsen, 2017). In 2011, Rude and co-workers reported the first one step oxidative decarboxylation of fatty acids to produce *n*-1 terminal alkenes from *Jeotgalicoccus OleT* ($OleT_{JE}$). When stearic acid was used as substrate, the predominant product was 1-heptadecene (Rude *et al.*, 2011). $OleT_{JE}$ was shown to be a cytochrome P450 from the CYP152 peroxygenase family, which includes bacterial fatty acid hydroxylases such as P450 SPα (CYP152B1) from *Sphingomonas paucimobilis* and P450 BSβ (CYP152A1) from *Bacillus subtilis* (Matsunaga *et al.*, 1999; Lee *et al.*, 2003). Since its discovery, $OleT_{JE}$ has been highly characterised and shown to decarboxylate a wide range of fatty acids (C12:0

– C20:0 region), predominantly producing C_{n-1} terminal alkenes and small amounts of hydroxylated fatty acid products in the Cα and Cβ positions (Belcher *et al.*, 2014). Recent studies have been trying to harness the natural alkene-producing abilities of $OleT_{JE}$ for biotechnological purposes in both academia and industry.

Indeed, $OleT_{JE}$ could support a sustainable viable platform for biosynthetic production of alkenes from biologically abundant feedstocks such as free fatty acids (Xu *et al.*, 2017). Therefore, a huge effort has been placed making $OleT_{JE}$ a biotechnological tool for chemical productions and research has focused on optimising $OleT_{JE}$ catalysis by understanding its catalytic cycle mechanism and its product output.

This has included making $OleT_{JE}$ more viable for applications *in vivo*, by leveraging $OleT_{JE}$ with alternative catalytic systems including redox partner systems and NAD(P)H to support alkene formation (Liu *et al.*, 2014; Dennig *et al.*, 2015). Examples include fusion of OleT with P450 reductase domain RhFRED from *Rhodococcus* species and using *E.coli* redox partner protein flavodoxin/flavodoxin reductase (Liu *et al.*, 2014). Additionally fusion between bacterial reductase domain of P450 BM3 from *Bacillus megaterium* (CYP102A1) to form a alkene-producing self-sufficient fusion protein (Lu *et al.*, 2018). However, the use of these methods require the addition of expensive pyridine nucleotide cofactors (NAD(P)H) that would have to be taken into account if these processes were to be scaled up to produce alkenes at industrial levels. As such, additional methods to generate H_2O_2 *in situ*, allowing for the controlled release of H_2O_2 to circumvent catalyst and heme inactivation by excess oxidant have been explored (Amaya, Rutland and Makris, 2016). These include light dependent H_2O_2 generating systems harnessing FMN as a photocatalyst (Köninger *et al.*, 2016). Other methods have included harnessing a $OleT_{JE}$ fusion system with alditol oxidase from *Streptomyces coelicolor*, which oxidises polyols (glycerol) generating H_2O_2 as a coproduct as a means to support alkene formation (Matthews, Tee, *et al.*, 2017c). Ongoing research expansion of the substrate scope of $OleT_{JE}$ is also of great interest including; shortening the substrate (C4:0 – C10:0 region) length, production of styrene, aromatic carboxylic acid , dienes, dionic acids and dicarboxylic acids (Dennig *et al.*, 2015; Hsieh and Makris, 2016; Matthews, Tee, *et al.*, 2017b; Pickl *et al.*, 2019).

Mechanistically, the vast majority of P450s achieve substrate oxidation by the reductive scission of O_2 bound to the heme iron, with the timed delivery of electrons at discrete

points in the catalytic cycle (Munro, Girvan and McLean, 2007). The electrons are usually supplied by cofactors NADH and/or NADPH, which transfer electrons by hydride transfer to the flavin cofactor (FAD/FMN) within a P450 redox-partner protein for generation of the active intermediate compound I (Rittle and Green, 2010). Compound I (Cpd I) is the ferryl iron oxo Fe^{IV}=O species with additional porphyrin π delocalisation, or its ferryl radical resonance form Fe^{IV}-OH Compound II (Cpd II), are attributed to the extensive monooxygenation reactions with ability to functionalise unactivated C—H bonds (McLean *et al.*, 2015).

However, the peroxygenase CYP152 family have structurally and functionally evolved to evade the requirement for O_2 and redox-partner proteins, by virtue of the peroxide shunt mechanism. In the substrate-bound state, hydrogen peroxide (H_2O_2) causes direct conversion to the ferric hydroperoxo species, Compound 0 (Cpd 0) evading the necessary electrons and proton required by the typical canonical P450 cycle (Grant, Hsieh and Makris, 2015a).

In an interest to explore the CYP152 family for decarboxylases, a whole host of peroxygenases are being discovered and characterised to expand the enzyme inventory for broader biotechnological applications. Particularly the search for biocatalysts that are capable of utilising short- medium chain fatty acids which have potential as liquid biofuels and biolubricants (Xu *et al.*, 2017). In this study, we highlight initial characterisation of a novel peroxygenase - CYP152T8 from *Dietzia cinnamea* (P450 DC).

4.3 Materials and Methods

4.3.1 Gene identification, synthesis and cloning of P450 DC

The CYP152T8 gene encoding for the *Dietzia cinnamea* cytochrome P450 (NCBI reference WP_063971857.1) (P450 DC) was identified using a protein BLAST searched with amino acid sequence of the P450 KR (CYP152T1) from *Kocuria rhizophila.* The formal title was assigned by Prof. David Nelson according to the level of similarity of CYP152T8 amino acid sequence with other members of the CYP152 P450 peroxygenase family.

The gene for P450 DC was codon optimised for usage for *E. coli* and cloned into a pET24b(+) vector, using EcoR1 and NdeI restriction sites. The construct was designed to

contain an N-terminal 6x polyhistidine-tag and a TEV protease cleavage site between the CYP152T8 gene and the his-tag, under the control of a T7 polymerase promoter.

4.3.2 Expression of P450 DC

Competent *E. coli* cell strains C41 (DE3) and BL21 (DE3) were transformed with the CYP152T8 pET24b(+) construct to test for P450 DC protein expression and protein solubility. The conditions of growth then differed with (i) growth media (LB, TB, 2xYT), (ii) Isopropyl β- d-1-thiogalactopyranoside (IPTG) concentration (ii) δ-aminolevulinic acid (Δ-ALA) (involved in the rate limiting step of heme synthesis) and (iii) incubation temperature after induction. Single colonies were grown overnight in LB media. A second culture was inoculated from the overnight culture and grown until mid-log phase. This was then used to inoculate 500 mL cultures of LB, autoinduction (AI) LB, TB, AI TB, 2xYT and 2xYT AI. Cells were grown at 37°C with shaking at 190 rpm. For autoinduction media δ-aminolevulinic acid (Δ-ALA) was added at the beginning of growth (when the cells were added). Before OD_{600nm} ~0.5-0.8 was reached the temperature was reduced to either (25°C or 20°C). Cultures that required IPTG induction were first inoculated with Δ-ALA (200 µM and 500 µM) then with IPTG (1 mM, 500 µM and 100 µM). Cells were grown for a further 20 hours. The cells were harvested by centrifugation at 6880 *x* g rpm at 4°C for 10 min using a Beckman-Coulter Avanti J-26 XP centrifuge with a JLA-8.1000 rotor.

4.3.3 Purification of P450 DC

P450 DC overexpressing cells were weighed and re-suspended in buffer A with 20 mM imidazole (0.1M Tris, 0.3 M NaCl, 10% glycerol, pH 8.2), with the addition of 20 µg mL^{-1} DNAase, 20 µg mL^{-1} lysozyme, SigmaFAST Protease Inhibitor Cocktail Tablets (EDTA-free) (1 per 100 mL) and ~100 mg of $MgCl_2$. Cells were lysed by 2 passes through a cell disrupter homogeniser (10,000 Kpi at 4°C). The homogenate was then ultracentrifuged at 40,000 rpm, 4°C for 30 min using a JA 45.5 rotor (Beckman). The supernatant was removed and filtered using a Sartorius Minisart NML Syringe filter (0.45 µM). The sample was then incubated for 1 hour with Ni-IDA chromatographic median (Generon, Maidenhead UK) on a rolling table at 4°C, then poured into a column with the P450 DC-bound median collected. The beads were then washed was 10 column volumes (CV) of buffer A with 20 mM imidazole, then 10 CV each of buffer A with 50 mM imidazole and 75 mM imidazole to remove weakly bound contaminants. P450 DC was eluted by buffer

A with 300 mM imidazole. The sample was then desalted to remove the imidazole using a PD-10 desalting column (GE Healthcare) isocratically with buffer A. P450 DC was incubated with TEV protease (1:5 molar ratio, respectively) overnight at 4°C. The imidazole-free digested DC sample was then loaded onto a Ni-IDA column that had been pre-equilibrated with buffer A. The column was then washed with 5 CV of buffer A and tag-free protein was eluted with buffer A with 20 mM imidazole. Samples of pure tag-free P450 DC were concentrated using a Vivaspin (10,000 MWCO, GE Healthcare). A final gel filtration step was undertaken using a Superdex 200 10/300 column (GE Healthcare) pre equilibrated with buffer A. P450 DC was flash frozen in liquid nitrogen and stored at -80°C.

4.3.4 Product analysis by GC-MS

Fatty acid substrate turnover was carried out in buffer A in a total volume of 500 uLcontaining 1 µM or 5 µM P450 DC with 500 µM fatty acid substrate (C10:0 – C18:0) dissolved ethanol. Reactions were initiated by the addition of 500 µM of H_2O_2, proceded for 30 min at 27°C and stopped by the addition of 40 µL of 37% HCl. Additional time-dependent reactions were stopped at 1, 5, 10, 20 and 45 minutes. Internal standards (different chain lengths) were added (containing 50 µM *n*-1 alkene, 50 µM fatty acid, 25 µM 2-OH fatty acid, and 25 µM 3-OH fatty acid). Products were extracted using equal volumes of dichloromethane (DCM), and any residual aqueous material removed by anhydrous magnesium sulfate.

N,O-Bis(trimethylsilyl)trifluoroacetamide (BSTFA) with 1% trimethylchlorosilane (TMCS) was added in equal quantities to samples and incubated at 60°C for 45 min. Directly after derivatisation, 1 µL of the sample was injected onto a 5975 series MSD coupled to a 7890 GC system, installed with a VF5 ht 5% phenyl-methyl column (30 m, 0.25 mm, 0.25 µm). The front inlet was set at 250°C, and a split ratio of 10:1 was used. The column flow was set at 1.2 mL min^{-1}, and the oven was held at 40°C for 1 min before being ramped at 10°C min^{-1} until a temperature of 250°C was reached. Ramping was then increased to 100°C min^{-1} until a temperature of 350°C was reached, and this condition was held for 2 minutes. The solvent delay was set at 2.5 min. Electron ionization was used, and m/z ratios of 40–500 were recorded at 5 Hz and at 230°C. Quantification of products formed were estimated using external standard calibration curves and internal standards.

4.3.5 Size Exclusion Chromatography Multi-Angle Light Scattering (SEC-MALS)

The oligomeric state of P450 DC was assessed using SEC-MALS. Purified samples (5 mg mL^{-1}) were loaded onto a Superdex 200/6 (GE Healthcare) at 0.75 mL min^{-1} with a constant flow of buffer A minus glycerol, and the samples were passed through a Wyatt DAWN Heleos II EOS 18-angle laser photometer coupled to a Wyatt Optilab rEX refractive index detector. Data analysis was performed (Hydrodynamic radii and molecular mass measurements were analysed) using Astra 6 (Wyatt Technologies).

4.4 Results and Discussion

4.4.1 Expression and purification of P450 DC

Following cloning of the CYP152T8 gene into C41 (DE3) *E. coli* cells. Different expression conditions were tested for increased protein solubility and stability. Initial expression condition systems consisted of 2xYT as the growth medium with different concentrations of ΔALA and IPTG, with induction temperatures at either 20°C or 25°C. Following initial cell lysis and supernatant centrifugation, the UV-vis spectrum of protein samples was used to assess heme incorporation and protein concentration (**figure 4.1)**.

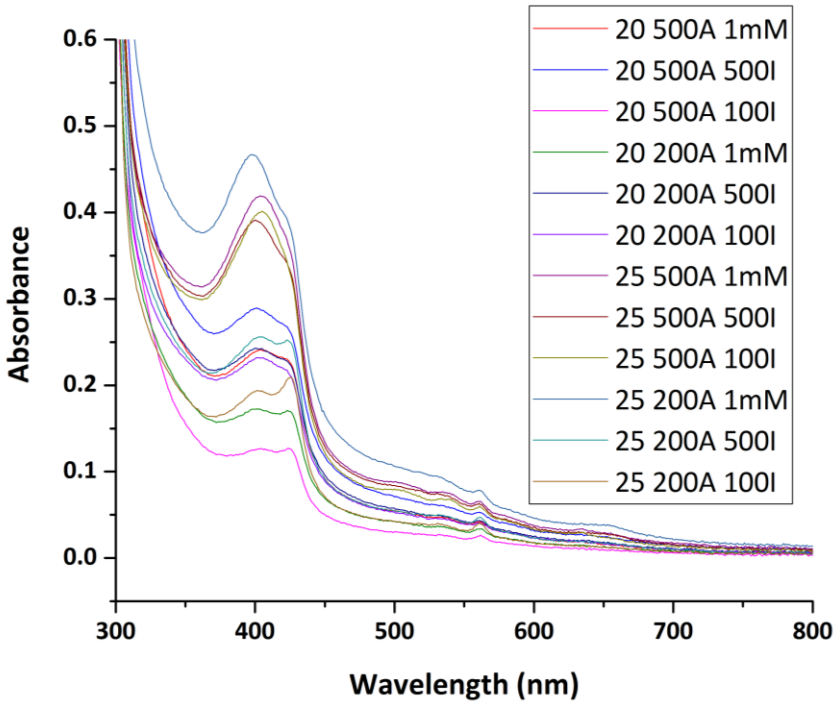

Figure 4.1 UV-Visible spectra of P450 DC samples obtained from different expression conditions. Samples were taken from different expression conditions of P450 DC with the change in temperature after induction (20 or 25°C), concentration of the heme additive δ-aminolevulinic acid (Δ-ALA, A) (200 or 500 µM) and concentration of IPTG (100, 500 µM or 1 mM). After 24 hours of growth, samples were centrifuged, and pellets collected. Sample concentrations were normalised before running on the spectrophotometer.

It was observed that the unpurified P450 DC obtained from these samples is either in a mixed spin state (mixture of some low-spin (LS) species and high-spin (HS) species), corresponding with Soret maximums at 424 nm (LS) and 396 nm (HS). Substrate binding in the active site usually displaces the 6^{th} axial water ligand to the heme iron resulting in a substrate-induced type I red-shift resulting in an absorbance peak ~396 nm (Isin and Guengerich, 2008). It is postulated that the observed mixed spin species relates to a proportion of fatty acid-like molecule bound P450 DC that originated from the *E. coli* cells (Pluschke and Overath, 1981).

Dramatic differences in Soret absorbance was observed across the conditions tested. The conditions yielding maximal amounts of soluble heme-containing protein were (i) 20°C after induction, 500 µM ΔALA and 500 µM IPTG; (ii) 25°C, 500 µM ΔALA and 1mM IPTG; (iii) 25°C, 500 µM ΔALA and 100 µM IPTG; (iv) 25°C, 500 µM ΔALA and 500 µM IPTG. This suggests that ΔALA concentration is vital for efficient production of heme-bound P450 DC along with manual induction rather than the more gradual induction from auto-induction media. The expression condition; P450 DC 500 µM ΔALA and 500 µM IPTG with the temperature reduced to 20°C after induction, was taken forward to support large scale purification. The cell pellet and extracts obtained from expression were tinged red suggesting successful heme incorporation.

During the development of the purification process the propensity of P450 DC to aggregate in high salt buffers (NaCl < 0.7 M) was observed. This is unlike other CYP152 members such as $OleT_{JE}$ and its closest homologue P450 KR, which both require high iconic strength to stabilise these enzymes (Rude *et al.*, 2011; Belcher *et al.*, 2014). Salt concentrations between 200 – 300 mM were optimal (data from initial crystallographic screens, data not shown) suggesting P450 DC could be a potential catalyst that could evade the high salt concentrations required by $OleT_{JE}$ and KR, and might thus be favoured in biotechnological applications.

The effect of differing buffer systems upon the stability of P450 DC was also explored. Four buffering systems were chosen; 0.1 M Tris (pH 8.2), 0.1M Hepes (pH 8.3), 50 mM MES (pH 6.2) and 50 mM Bicene (pH 8.2), all with 0.3 M NaCl and 10% glycerol. Initial purifications using Tris and Hepes buffers showed promising results, so they were taken forward for purification.

The final gel filtration step for P450 DC in the Tris and Hepes buffer systems are shown in **figure 4.2**. The UV-visible trace obtained from the ÄKTApure with the red line representing UV absorbance at 280 nm and the blue represents UV at 424 nm. The purification of P450 DC in 0.1 M Hepes, 0.3 M NaCl and 10 % glyercol (pH 8.3) is shown in **figure 4.2A**.

Three elution peaks were observed, the first peak (i) (1 mL) relates to elution in the void volume suggesting large aggregates, with R*z* (A_{424}/A_{280} nm) value close to 0.5, which suggests low purity and/or reduced heme incorporation. Then two subsequent peaks (ii) and (iii) likely correspond with the elution of P450 DC in the dimer and monomeric form, respectively. The insert shows the SDS-page gel obtained from purification, with P450 DC appearing as a single band at ~50 kDa.

Purification of P450 DC in the Tris buffering system is shown in **figure 4.2B**. A soluble aggregation peak eluting in the void volume is again observed, then a second asymmetric peak that could relate to the MW of the P450 DC dimer. It is interesting to observe the difference in oligomerisation states between both buffer that differ in 0.1 pH point. The Tris purified samples were taken forward for further experiments.

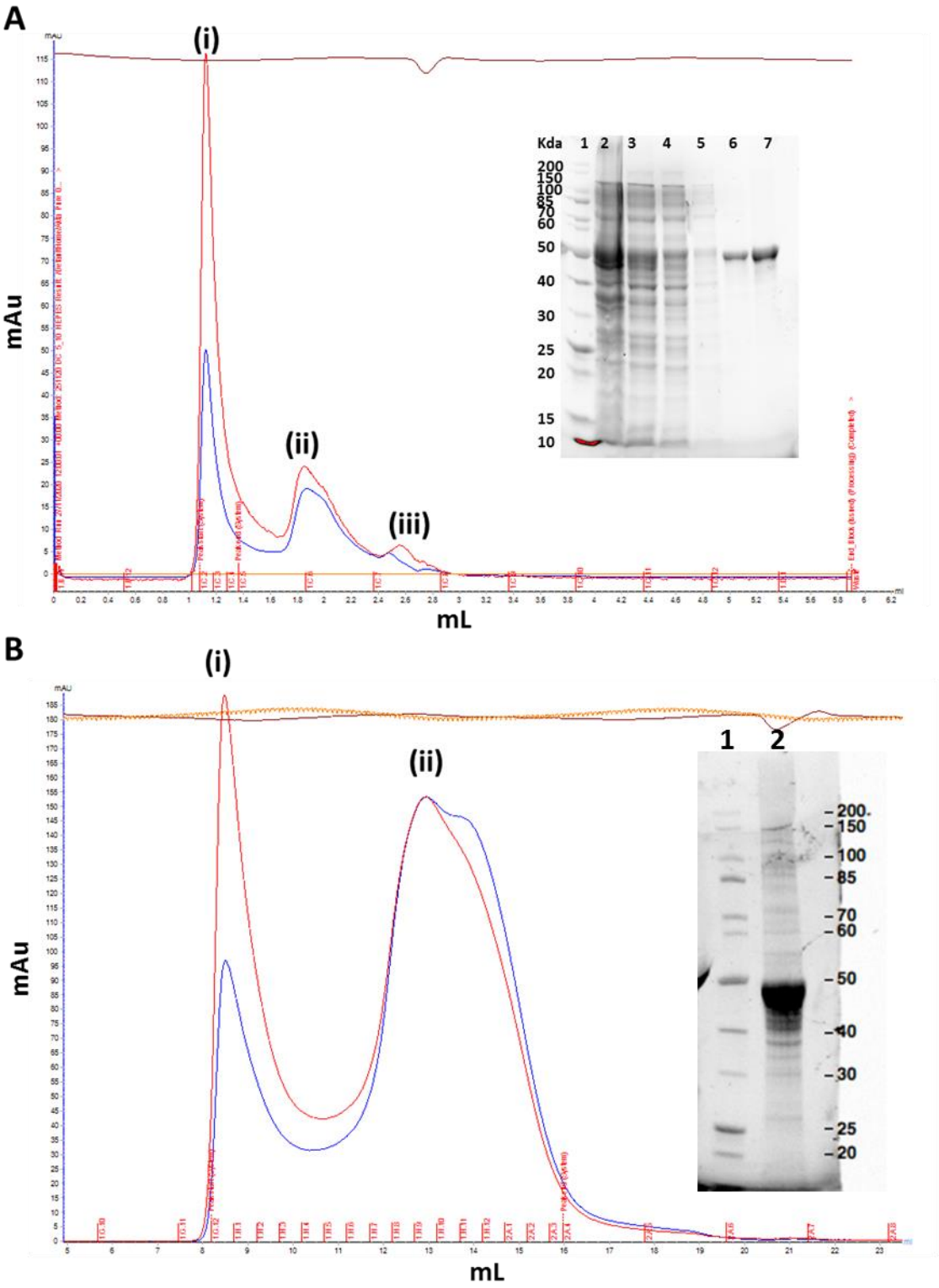

Figure 4.2 UV-visible traces obtained from the purification of P450 DC obtained from different buffering systems. Panel A shows the ÄKTA trace obtained from gel filtration final purification step of P450 DC in 0.1 M Hepes, 0.3 M NaCl, 10% glycerol (pH 8.3). The red line represents UV at 280 nm and the blue like represents UV at 424 nm. The insert shows the SDS-PAGE gel following the initial Ni-IDA chromatography steps, P450 DC elutes at 300 mM imidazole in lanes 6 and 7, and proteins are resolved on a 12 % SDS PAGE gel. The first lane shows markers of indicated size (NEB Unstained Protein standard). Panel B shows ÄKTA trace of final gel purification step of P450 DC in 0.1 M Tris, 0.3 M NaCl, 10% glycerol (pH 8.2). Insert shows final purity of P450 DC with Rz values of ~1.

4.4.2 Size-exclusion Size exclusion chromatography multi-angle light scattering

A subset of the CYP152 family including P450 KR and P450 CE form dimers in solution experiments and crystallography (Andrews et al., Chapter 2, Chapter 3). To assess stability, protein integrity and oligomeric state(s) of P450 DC, size exclusion chromatography coupled to multi-angle light scattering (SEC-MALS) was performed in Tris-buffer system. SEC-MALS data obtained is shown in **figure 4.3.** We observe multiple peaks obtained with larger aggregates eluting first. A peak at ~15 mLs has an estimated molecular weight 144.8 (± 9.1%) kDa, the estimated MW from EXPASY 48 kDa suggesting maybe that the enzyme could be a trimer.

To further understand the oligomeric state, small angle X-ray scattering (SAXS) and analytical ultracentrifugation (AUC) techniques were also performed on P450 DC protein samples. However the samples displayed soluble aggregates making it difficult to obtain viable data. However, these soluble aggregates are still catalytic active displaying high decarboxylation and hydroxylation activities. Further work is required is required in understanding the oligomerisation underpinning stability of P450 CE.

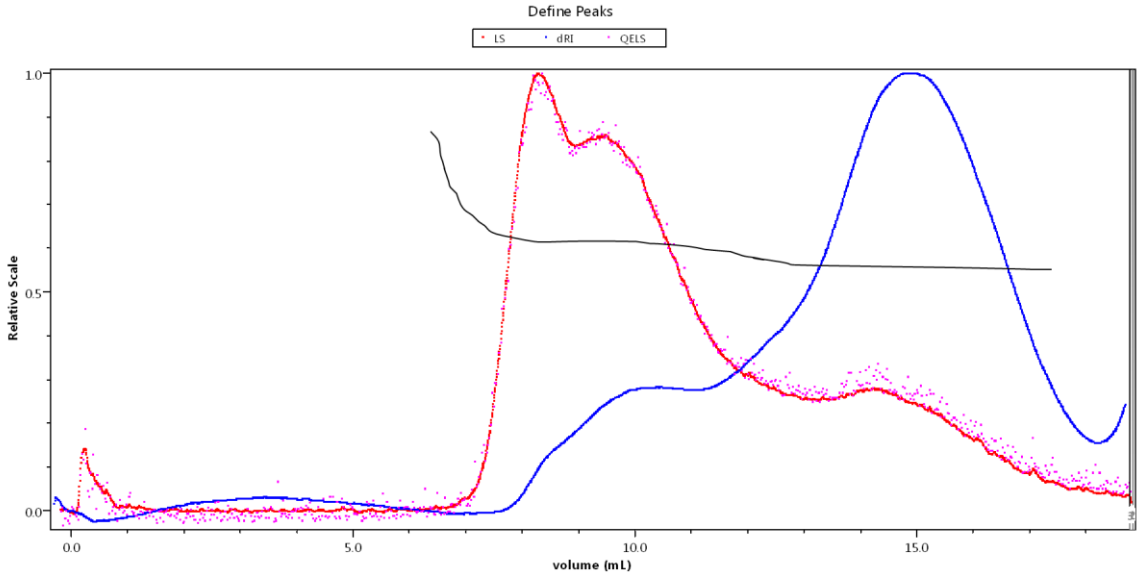

Figure 4.3 Chromatogram obtained from SEC-MALS analysis of P450 DC. The red lines represent the QELS and light scattering, the blue represents UV at 280 nm. The black like represents the mean molar mass across the sample, with a MW of 144.8 (± 9.1%) kDa.

4.4.3 Spectroscopic characterisation of P450 DC

In **figure 4.4**, resting ferric (Fe^{III}) state, purified P450 DC has a Soret absorbance (λ) at ~421 nm, with the smaller α and β bands visible at 541 nm and 578 nm, respectively. DC thus displays a red-shifted Soret absorbance compared to the majority of other bacterial cytochromes P450, such as CYP152 member $OleT_{JE,}$ which has major absorption features at 418, 566 nm and 535 nm (Belcher *et al.*, 2014), and the P450cam camphor hydroxylase from *Pseudomonas putida* (417 nm, 537 nm and 570 nm) (Murugan and Mazumdar, 2005). However, a new subset of characterised members of the CYP152 family display this unique red-shifted Soret absorbance, including P450 KR from *Koccuria rhizophilla* (424, 576 and 541 nm) and P450 CE from *Corynebacterium efficiens* (424, 575 and 539 nm) (Andrews et al., chapter 2 and chapter 3). CYP-MP from *Methylobacterium populi* (422, 545 and 575 nm) (Amaya, Rutland and Makris, 2016), as well as newly characterised CYP-Sm46Δ29 which displayed absorbance's (424, 571and 540 nm) (Xu *et al.*, 2017). For all these, including P450 DC, we observe a more prominent α-band and a weaker β-band. In previous work (Andrews et al, chapters 2) it has been shown that this red-shifted Soret peak is not due to the presence of imidazole ligating to the heme iron but seems a common factor within this emerging and growing subset of CYP152 peroxygenases. An additional spectral feature is present at 360 nm, which is characteristic of a hyperporphyrin species, which can be attributed to metal-to-porphyrin charge transfer transitions or upon protonation/deprotonation of the porphyrin rings (Sayer, Gouterman and Connell, 1982; Wang and Wamser, 2014). Similar hyperporphyrin characteristics is observed in CYP-MP and the authors postulated that the spectral feature at 360 nm is indicative of an altered coordination environment around the heme iron, possibly deriving from binding an alternative axial ligand (Amaya, Rutland and Makris, 2016). Reduction of P450 DC to the ferrous form (Fe^{II}) form by addition of sodium dithionite produced a reduced intensity Soret absorbance at 421 nm, with the Q-bands (the α and β bands) merging to form an asymmetric single peak at ~550 nm. The shift in the Soret peak upon heme iron reduction does not seem as pronounced (blue shifted) as those observed for P450 KR (418 nm) and P450 CE (414 nm). Addition of carbon monoxide under anaerobic conditions sees the formation of the ferrous-CO complex displayed the characteristics P450 spectrum, with red-shifted Soret absorbance at 447 nm, and Q-band features at ~553 nm. The spectrum exhibits a large

contribution of the P420 nm form, due to protonation of the cysteine-thiolate coordinated heme (Perera *et al.*, 2003).

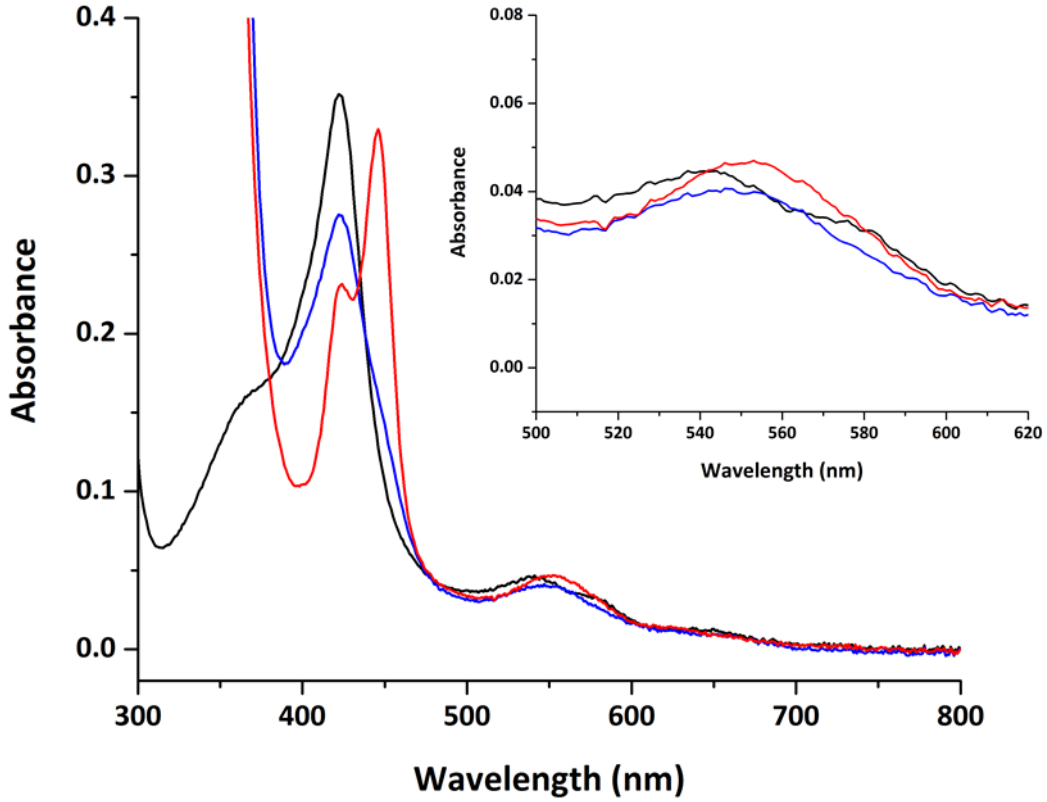

Figure 4.4 UV-visible spectroscopic features of P450 DC. UV-vis absorption spectra of P450 DC (~ 4 µM) in the substrate-free ferric (Fe^{II}) (black) with Soret maximum λ at 421 nm and β bands features at 541 nm and 578 nm, respectively. Sodium dithionite reduced ferrous form (Fe^{III}) which displays a diminished slightly blue shifted absorbance λ at 421 nm (blue), with a single asymmetric Q-band feature at 550 nm. The ferrous-carbon monoxide complex (red) with characteristic Soret λ maxima at 447 nm and Q-band feature at ~553 nm. A proportion of the inactive P420 form is observed due to presence of a cysteine-thiol coordinated heme. Insert shows magnification of the Q-band region.

4.4.4 Characterisation of P450 DC reaction products

To explore the product profiles of P450 DC, H_2O_2-dependent turnover reactions were undertaken using a range of saturated fatty acids (C10:0 – C18:0Turnover for all substrates tested was oberved, with production of C_{n-1} terminal alkenes and a mixture of Cα (2) and Cβ (3) hydroxylated fatty acid products as shown in **figure 4.5**. Under the conditions tested, P450 DC catalysed complete conversion to product with decanoic acid (C10:0), with ~38 % conversion to 1- nonene, 6% 2-hydroxy decanoic acid and 55% 3-hydroxy decanoic acid. These data suggest that DC is a more efficient catalyst of shorter chain fatty acid substrates than P450 KR, where ~22% total turnover of decanoic acid (1-nonene: 8%, 2-OH FA: 3% 3-OH FA: 12%) was reported (Andrews *et al.*, chapter 2). P450

DC displays an almost four-fold increase in alkene formation *cf*. P450 KR. Similar turnover product percentages are witnessed for lauric acid (C12:0) (Overall: 97%, C_{n-1} alkene: ~40% 2-OH FA: 5% and 3-OH: 52%). The highest alkene titre is observed with myristic acid (C14:0), with 1-tridecene constituting over 50% of the total products. These are similar conversion percentages as seen in P450 CE (total: 89%, 1-tridecene: 50.3% 2-OH FA: 14.5% and 3-OH FA: 24.1%) (Andrews *et al*., chapter 3). Hence, $OleT_{JE}$ still remains the most productive decarboxylase that has been characterised, with H_2O_2 dependent turnover of myristic acid yielding complete oxidation to 72 % 1-tridecene, 3.3% 2-OH myristic acid and 25% 3-OH myristic acid. Furthering this, $OleT_{JE}$-dependent turnover of arachidic acid (C20:0) only exhibits the alkene product (14% 1-nonene) (Belcher *et al.*, 2014; Matthews, Belcher, *et al.*, 2017).

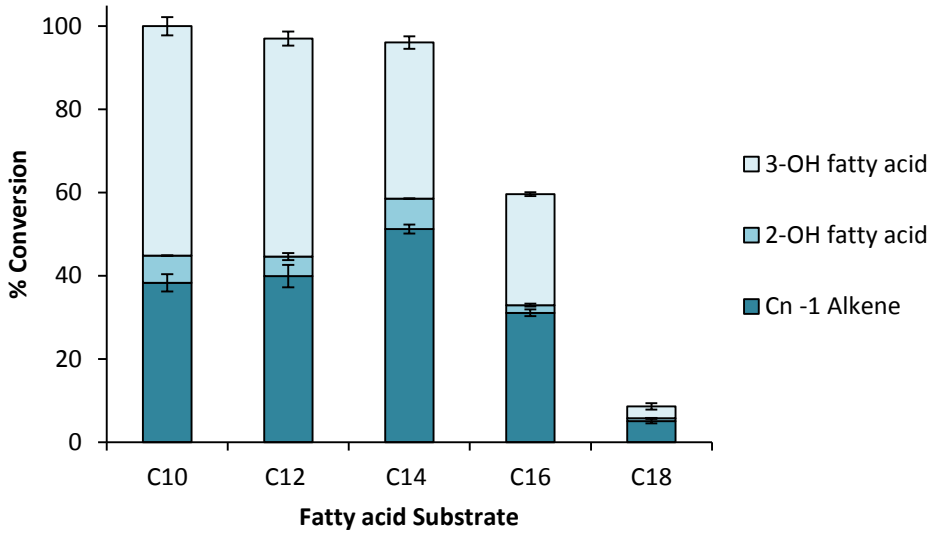

Figure 4.5 Percentage conversion of fatty acids by P450 DC. Bar chart represents the percentage conversion towards fatty acid substrates (C10:0 – C18:0) via H_2O_2-dependent turnover over 30 min reaction. Data shown are the average from three sets of the experiments with error bars representing the standard deviation between experiments.

Interestingly, we see that for the shorter mid-chain fatty acids tested (C10:0 – C12:0), hydroxylation is the dominant catalytic route. However, for C14:0 – C18:0 substrates, the ratio of alkene to hydroxylation changes, with the decarboxylation route becoming the preferred catalytic route. This change in alkene: hydroxylation ratio as the chain length increases is also observed in P450 CE. The opposite is observed in CYP-Sm46 (CYP152L2) from *Staphylococcus massiliensis*, an efficient decarboxylase and hydroxylase of fatty acids (C14 turnover: ~72% 1-tridecene). The ratio of products

changes across the substrate length, with hydroxylated long fatty acid (C18:0-C20:0) becoming the major reaction product with the longer chain fatty acids (Xu *et al.*, 2017).

Throughout all the fatty acids chain lengths tested, hydroxylation at the Cβ position is favoured over the Cα position for P450 DC. This preference towards β-hydroxylation is seen in CYP152 homologues 450 KR and P450 CE, as well as CYP-MP and $OleT_{JE}$ (Amaya, Rutland and Makris, 2016). Early studies highlighted an important active site histidine residue for alkene production. Rude and co-workers highlighted His85 in $OleT_{JE}$ and the equivalent residues are conserved in P450 KR (His89), CE (His91) and CYP-Sm46 (His86) which all are effective decarboxylases (Rude *et al.*, 2011). This histidine residue has been shown in multiple CYP152 structures (P450's $OleT_{JE}$, KR and CE) to extend the imidazole side chain into the active site with similar orientations. It was theorised that the histidine residue could act as a proton donor to compound I in the peroxygenase catalytic cycle, accompanying the reduction to compound II by electron abstraction from the fatty acid, then providing a further proton to restore the resting form Fe^{III}-OH_2 leading to the generation of the carbocation poised C−Cα cleavage to liberate the alkene and CO_2 (Belcher *et al.*, 2014).

There are characterised CYP152 members that do not display this histidine residue such as CYP-MP (Met96), as well as CYP152K6, SPα and BSβ that each contains a glutamine residue at the corresponding position. These enzymes seem to function predominantly as oxidative hydroxylases. Therefore, it was assumed that without the proton-donating histidine, the hydroxylation ●OH rebound mechanism would be prevalent leading to hydroxylation (refer to figure **1.7**). However, Rude and co-workers presented data to suggest that P450 BSβ can also function as a decarboxylase, with production of low levels of 1-pentadecene among hydroxylated palmitic acid. Formation of a P450 BSβ Q85H variant showed increased rates of decarboxylation of palmitic acid but also increased rate of β-hydroxylation (in comparison to WT BSβ). Furthering this research, CYP-MP (Met96) displays alkene formation for only stearic and palmitic acid with ~38 % and 24%, respectively (Amaya, Rutland and Makris, 2016). A Met96His variant, unlike the BSβ Q85H variant, did not restore alkene formation, but substantially reduced activity, with ~1% turnover to solely hydroxylated products. However, a H85Q mutation in $OleT_{JE}$ displayed 81% conversion to 1-tridecene, therefore suggesting that His85,

albeit important, is not crucial for proton transfer to iron-oxo species, or that another pathway may exist (Matthews, Belcher, *et al.*, 2017).

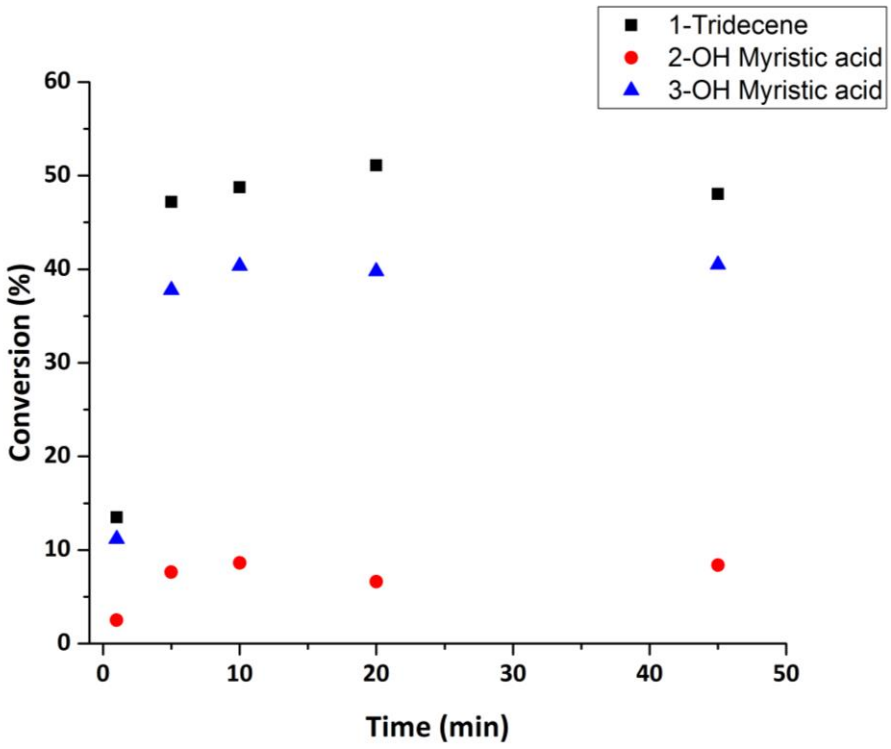

Figure 4.6 Time dependent conversion of myristic acid by P450 DC. Data obtained from reactions of 1 µM of P450 DC with 500 µM of myristic acid and initiated with 500 µM H_2O_2. Time points were collected at 1, 5, 10, 20, 30, 45 60 and 120 minutes. Data taken from GC-MS and represented by conversion percentage to 1-tridecene (black square), 2-hydroxy myristic acid (blue triangle) and 3-hydroxy myristic acid (red circle). Data were taken in triplicate.

Figure 4.6 shows the time dependent turnover of myristic acid (C14:0), following the addition of H_2O_2. Reactions proceeded for 1, 5, 10, 20 and 45 minutes. We see complete conversion within 10 minutes, with ~97% total conversion observed with ~50% conversion to 1-tridecene (C13 alkene) and ~8% 2-OH fatty acid and 40% to the 3-OH FA. This suggests a reaction rate in the order of ~1-10 s^{-1}.

4.5 Conclusions

In this study, we have characterised a new CYP152 peroxygenase belonging to the *Dietzia* genus, which has only been characterised fairly recently (Koerner, Goodfellow and Jones, 2009). Interestingly, some strains of *D. cinnamea* (strain P4) are capable of degrading petroleum hydrocarbon derivatives (von der Weid *et al.*, 2007). The components of the bacterial cell wall and cleavage of mycolic acids by pyrolysis releases fatty acids of C14:0, C15:0, C16:0, C17:0, C18:1 and C18:0 as the major products. The fatty acid profile mainly consists of straight-chain saturated, unsaturated and 10-methyl

branched fatty acids (Yassin, Hupfer and Schaal, 2006). A cytochrome P450 has been isolated from *Dietzia* sp. strain DQ12-45-1b belonging to a CYP153 family of cytochrome P450 genes that have typically have promoters induced by *n*-alkanes comprised of 8 to 14 carbon atoms (Liang *et al.*, 2016). The CYP153 enzymes are primarily alkane hydroxylases that perform ω-hydroxylations on their alkane substrates.

Our data suggest that P450 DC works as an efficient decarboxylase and hydroxylase. The native substrate is not known, however this study suggests that P450 DC prefers short to mid-chain length fatty acid chain lengths, from almost complete oxidation observed during turnover of decanoic acid. Although biophysical data suggest that DC has a propensity to aggregate, these aggregates are still catalytically active. This could suggest that P450 DC exists as in oligomeric state within solution. Further work is needed to fully explore these properties. With increased characterisation of further members of the CYP152 peroxygenase family it is becoming evident that many of these enzymes have dual functionalities, producing alkenes as well as hydroxylated products. Few of these members act as solely as decarboxylases ($OleT_{JE}$ towards C20:0) (Belcher *et al.*, 2014). Bioprospecting novel CYP152 enzymes provide a basis of understanding the catalytic and structural mechanisms underpinning these peroxygenases but perhaps laboratory evolution is needed to further improve the scope of these enzymes in terms of desirable products for their application as a viable catalytic platform. Although biophysical data suggest that DC has a propensity to aggregate, these aggregates are still catalytically active. This could suggest that P450 DC exists as in oligomeric state within solution; further work is needed to fully explore these properties.

4.6 References

Adams, P. D. *et al.* (2010) 'PHENIX: A comprehensive Python-based system for macromolecular structure solution', *Acta Crystallographica Section D: Biological Crystallography*. Acta Crystallogr D Biol Crystallogr, 66(2), pp. 213–221. doi: 10.1107/S0907444909052925.

Amaya, J. A., Rutland, C. D. and Makris, T. M. (2016) 'Mixed regiospecificity compromises alkene synthesis by a cytochrome P450 peroxygenase from Methylobacterium populi', *Journal of Inorganic Biochemistry*. Elsevier Inc., 158, pp. 11–16. doi: 10.1016/j.jinorgbio.2016.02.031.

Atsumi, S. and Liao, J. C. (2008) 'Metabolic engineering for advanced biofuels production from Escherichia coli', *Current Opinion in Biotechnology*, 19(5), pp. 414–419. doi: 10.1016/j.copbio.2008.08.008.

Barr, I. and Guo, F. (2015) 'Pyridine Hemochromagen Assay for Determining the Concentration of Heme in Purified Protein Solutions', *BIO-PROTOCOL*. Bio-Protocol, LLC, 5(18). doi: 10.21769/bioprotoc.1594.

Belcher, J. *et al.* (2014) 'Structure and biochemical properties of the alkene producing cytochrome p450 OleTJE (CYP152l1) from the jeotgalicoccus sp. 8456 bacterium', *Journal of Biological Chemistry*. American Society for Biochemistry and Molecular Biology, 289(10), pp. 6535–6550. doi: 10.1074/jbc.M113.527325.

Beller, H. R., Goh, E. B. and Keasling, J. D. (2010) 'Genes involved in long-chain alkene biosynthesis in micrococcus Luteus', *Applied and Environmental Microbiology*. American Society for Microbiology, 76(4), pp. 1212–1223. doi: 10.1128/AEM.02312-09.

Bernstein, S. L. *et al.* (2004) 'α-Synuclein: Stable compact and extended monomeric structures and pH dependence of dimer formation', *Journal of the American Society for Mass Spectrometry*. Springer New York LLC, 15(10), pp. 1435–1443. doi: 10.1016/j.jasms.2004.08.003.

Berry, E. A. and Trumpower, B. L. (1987) 'Simultaneous determination of hemes a, b, and c from pyridine hemochrome spectra', *Analytical Biochemistry*. Anal Biochem, 161(1), pp. 1–15. doi: 10.1016/0003-2697(87)90643-9.

Bharadwaj, V. S. *et al.* (2018) 'Different Behaviors of a Substrate in P450 Decarboxylase and Hydroxylase Reveal Reactivity-Enabling Actors', *Scientific Reports*. Nature Publishing Group, 8(1), p. 12826. doi: 10.1038/s41598-018-31237-4.

Brown, P. H. and Schuck, P. (2006) 'Macromolecular size-and-shape distributions by sedimentation velocity analytical ultracentrifugation', *Biophysical Journal*. Biophysical Society, 90(12), pp. 4651–4661. doi: 10.1529/biophysj.106.081372.

Bui, S. H. *et al.* (2012) 'Unusual spectroscopic and ligand binding properties of the cytochrome P450-flavodoxin fusion enzyme XplA', *Journal of Biological Chemistry*. American Society for Biochemistry and Molecular Biology, 287(23), pp. 19699–19714. doi: 10.1074/jbc.M111.319202.

Christenson, J. K. *et al.* (2017) 'OleB from Bacterial Hydrocarbon Biosynthesis Is a β-Lactone Decarboxylase That Shares Key Features with Haloalkane Dehalogenases', *Biochemistry*. American Chemical Society, 56(40), pp. 5278–5287. doi: 10.1021/acs.biochem.7b00667.

Clemmer, D. E. and Jarrold, M. F. (1997) 'Ion mobility measurements and their applications to clusters and biomolecules', *Journal of Mass Spectrometry*. John Wiley & Sons, Ltd, pp. 577–592. doi: 10.1002/(SICI)1096-9888(199706)32:6<577::AID-JMS530>3.0.CO;2-4.

Cole, J. L. *et al.* (2008) 'Analytical Ultracentrifugation: Sedimentation Velocity and Sedimentation Equilibrium', *Methods in Cell Biology*, pp. 143–179. doi: 10.1016/S0091-679X(07)84006-4.

Coleman, T. *et al.* (2020) 'Structural insights into the role of the acid-alcohol pair of residues required for dioxygen activation in cytochrome P450 enzymes', *Journal of Biological Inorganic Chemistry*. Springer, 25(4), pp. 583–596. doi: 10.1007/s00775-020-01781-4.

Coon, M. J. (2005) 'Cytochrome P450: Nature's most versatile biological catalyst', *Annual Review of Pharmacology and Toxicology*, pp. 1–25. doi: 10.1146/annurev.pharmtox.45.120403.100030.

Cryle, M. J. and De Voss, J. J. (2008) 'The role of the conserved threonine in P450BM3 oxygen activation: Substrate-determined hydroxylation activity of the Thr268Ala mutant', *ChemBioChem*, 9(2), pp. 261–266. doi: 10.1002/cbic.200700537.

Daff, S. N. *et al.* (1997) 'Redox control of the catalytic cycle of flavocytochrome P-450 BM3', *Biochemistry*. Biochemistry, 36(45), pp. 13816–13823. doi: 10.1021/bi971085s.

Das, A., Grinkova, Y. V. and Sligar, S. G. (2007) 'Redox potential control by drug binding to cytochrome P450 3A4', *Journal of the American Chemical Society*. NIH Public Access, 129(45), pp. 13778–13779. doi: 10.1021/ja074864x.

Dawson, J. H., Andersson, L. A. and Sono, M. (1982) 'Spectroscopic investigations of ferric cytochrome P-450-CAM ligand complexes. Identification of the ligand trans to cysteinate in the native enzyme.', *Journal of Biological Chemistry*, 257(7), pp. 3606–3617. doi: 10.1016/s0021-9258(18)34823-3.

Dawson, J. H., Anderssons, L. A. and Sono, M. (1982) *Spectroscopic investigations of ferric cytochrome P-450-CAM ligand complexes. Identification of the ligand trans to cysteinate in the native enzyme.*, *THE JOURNAL OF BIOLOGICAL CHEMISTRY*. doi: 10.1016/S0021-9258(18)34823-3.

Denisov, I. G. *et al.* (2005) *Structure and chemistry of cytochrome P450*, *Chemical Reviews*. American Chemical Society. doi: 10.1021/cr0307143.

Dennig, A. *et al.* (2015) 'Oxidative Decarboxylation of Short-Chain Fatty Acids to 1-Alkenes', *Angewandte Chemie - International Edition*, 54(30), pp. 8819–8822. doi: 10.1002/anie.201502925.

Driscoll, M. D. *et al.* (2011) 'Expression and characterization of Mycobacterium tuberculosis CYP144: Common themes and lessons learned in the M. tuberculosis P450 enzyme family', *Biochimica et Biophysica Acta - Proteins and Proteomics*. Biochim Biophys Acta, 1814(1), pp. 76–

87. doi: 10.1016/j.bbapap.2010.05.015.

Emsley, P. *et al.* (2010) 'Features and development of Coot', *Acta Crystallographica Section D: Biological Crystallography*. Acta Crystallogr D Biol Crystallogr, 66(4), pp. 486–501. doi: 10.1107/S0907444910007493.

Evans, P. R. and Murshudov, G. N. (2013) 'How good are my data and what is the resolution?', *Acta Crystallographica Section D: Biological Crystallography*. Acta Crystallogr D Biol Crystallogr, 69(7), pp. 1204–1214. doi: 10.1107/S0907444913000061.

Fu, W. J. *et al.* (2015) 'Hydrocarbons, the advanced biofuels produced by different organisms, the evidence that alkanes in petroleum can be renewable', *Applied Microbiology and Biotechnology*. Springer Verlag, pp. 7481–7494. doi: 10.1007/s00253-015-6840-6.

Fudou, R. *et al.* (2002) 'Corynebacterium efficiens sp. nov., a glutamic-acid-producing species from soil and vegetables', *International Journal of Systematic and Evolutionary Microbiology*. Microbiology Society, 52(4), pp. 1127–1131. doi: 10.1099/ijs.0.02086-0.

Fujishiro, T. *et al.* (2011) 'Crystal structure of H 2O 2-dependent cytochrome P450 SPαwith its bound fatty acid substrate: Insight into the regioselective hydroxylation of fatty acids at the α position', *Journal of Biological Chemistry*, 286(34), pp. 29941–29950. doi: 10.1074/jbc.M111.245225.

Gandomkar, S. *et al.* (2018) 'Biocatalytic Oxidative Cascade for the Conversion of Fatty Acids into α-Ketoacids via Internal H2O2 Recycling', *Angewandte Chemie - International Edition*. Wiley-VCH Verlag, 57(2), pp. 427–430. doi: 10.1002/anie.201710227.

Girvan, H. M. *et al.* (2004) 'Flavocytochrome P450 BM3 mutant A264E undergoes substrate-dependent formation of a novel heme iron ligand set', *Journal of Biological Chemistry*. J Biol Chem, 279(22), pp. 23274–23286. doi: 10.1074/jbc.M401716200.

Girvan, H. M. *et al.* (2018) 'Structural and catalytic properties of the peroxygenase P450 enzyme CYP152K6 from Bacillus methanolicus', *Journal of Inorganic Biochemistry*. Elsevier Inc., 188, pp. 18–28. doi: 10.1016/j.jinorgbio.2018.08.002.

Girvan, H. M. and Munro, A. W. (2016) 'Applications of microbial cytochrome P450 enzymes in biotechnology and synthetic biology', *Current Opinion in Chemical Biology*. Elsevier Ltd, pp. 136–145. doi: 10.1016/j.cbpa.2016.02.018.

Good, N. E. *et al.* (1966) 'Hydrogen Ion Buffers for Biological Research', *Biochemistry*. American Chemical Society, 5(2), pp. 467–477. doi: 10.1021/bi00866a011.

Grant, J. L., Hsieh, C. H. and Makris, T. M. (2015a) 'Decarboxylation of fatty acids to terminal alkenes by cytochrome P450 compound i', *Journal of the American Chemical Society*. American Chemical Society, 137(15), pp. 4940–4943. doi: 10.1021/jacs.5b01965.

Grant, J. L., Hsieh, C. H. and Makris, T. M. (2015b) 'Decarboxylation of fatty acids to terminal alkenes by cytochrome P450 compound I', *Journal of the American Chemical Society*, 137(15), pp. 4940–4943. doi: 10.1021/jacs.5b01965.

Grant, J. L., Mitchell, M. E. and Makris, T. M. (2016a) 'Catalytic strategy for carbon-carbon bond scission by the cytochrome p450 olet', *Proceedings of the National Academy of Sciences of the United States of America*, 113(36), pp. 10049–10054. doi: 10.1073/pnas.1606294113.

Grant, J. L., Mitchell, M. E. and Makris, T. M. (2016b) 'Catalytic strategy for carbon-carbon bond scission by the cytochrome P450 OleT', *Proceedings of the National Academy of Sciences of the United States of America*, 113(36), pp. 10049–10054. doi: 10.1073/pnas.1606294113.

Guengerich, F. P. and Munro, A. W. (2013) 'Unusual cytochrome p450 enzymes and reactions.', *The Journal of biological chemistry*. American Society for Biochemistry and Molecular Biology, 288(24), pp. 17065–73. doi: 10.1074/jbc.R113.462275.

Hagemans, D. *et al.* (2015) 'A script to highlight hydrophobicity and charge on protein surfaces', *Frontiers in Molecular Biosciences*. Frontiers Media S.A., 2(OCT), p. 56. doi: 10.3389/fmolb.2015.00056.

Hamdy, O. M. and Julian, R. R. (2012) 'Reflections on charge state distributions, protein structure, and the mystical mechanism of electrospray ionization', *Journal of the American Society for Mass Spectrometry*, 23(1), pp. 1–6. doi: 10.1007/s13361-011-0284-8.

Hannemann, F. *et al.* (2007) 'Cytochrome P450 systems—biological variations of electron transport chains', *Biochimica et Biophysica Acta (BBA) - General Subjects*, 1770(3), pp. 330–344. doi: 10.1016/j.bbagen.2006.07.017.

Van Hellemond, E. W. *et al.* (2009) 'Exploring the biocatalytic scope of alditol oxidase from Streptomyces coelicolor', *Advanced Synthesis and Catalysis*, 351(10), pp. 1523–1530. doi: 10.1002/adsc.200900176.

Howlett, G. J., Minton, A. P. and Rivas, G. (2006) 'Analytical ultracentrifugation for the study of protein association and assembly', *Current Opinion in Chemical Biology*. Curr Opin Chem Biol, pp. 430–436. doi: 10.1016/j.cbpa.2006.08.017.

Hsieh, C. H. *et al.* (2017) 'The Enigmatic P450 Decarboxylase OleT Is Capable of, but Evolved to

Frustrate, Oxygen Rebound Chemistry', *Biochemistry*. American Chemical Society, 56(26), pp. 3347–3357. doi: 10.1021/acs.biochem.7b00338.

Hsieh, C. H. and Makris, T. M. (2016) *Expanding the substrate scope and reactivity of cytochrome P450 OleT*, *Biochemical and Biophysical Research Communications*. doi: 10.1016/j.bbrc.2016.05.145.

Imai, Y. *et al.* (2000) 'Unique heme environment at the putative distal region of hydrogen peroxide-dependent fatty acid α-hydroxylase from Sphingomonas paucimobilis (peroxygenase P450(SPα))', *Journal of Biochemistry*, 128(2), pp. 189–194. doi: 10.1093/oxfordjournals.jbchem.a022740.

Isin, E. M. and Guengerich, F. P. (2008) 'Substrate binding to cytochromes P450', *Analytical and Bioanalytical Chemistry*. NIH Public Access, pp. 1019–1030. doi: 10.1007/s00216-008-2244-0.

Kabsch, W. (2010) 'Integration, scaling, space-group assignment and post-refinement', *Acta Crystallographica Section D: Biological Crystallography*. International Union of Crystallography, 66(2), pp. 133–144. doi: 10.1107/S0907444909047374.

Kang, M. K. and Nielsen, J. (2017) 'Biobased production of alkanes and alkenes through metabolic engineering of microorganisms', *Journal of Industrial Microbiology and Biotechnology*. Springer Verlag, pp. 613–622. doi: 10.1007/s10295-016-1814-y.

Kapust, R. B. *et al.* (2001) 'Tobacco etch virus protease: Mechanism of autolysis and rational design of stable mutants with wild-type catalytic proficiency', *Protein Engineering*. Oxford University Press, 14(12), pp. 993–1000. doi: 10.1093/protein/14.12.993.

Koerner, R. J., Goodfellow, M. and Jones, A. L. (2009) 'The genus Dietzia: A new home for some known and emerging opportunist pathogens', *FEMS Immunology and Medical Microbiology*. Oxford Academic, pp. 296–305. doi: 10.1111/j.1574-695X.2008.00513.x.

Köninger, K. *et al.* (2016) 'Light-driven enzymatic decarboxylation', *Journal of Visualized Experiments*. Journal of Visualized Experiments, 2016(111), p. 53439. doi: 10.3791/53439.

Korasick, D. A. and Tanner, J. J. (2018) 'Determination of protein oligomeric structure from small-angle X-ray scattering', *Protein Science*. Blackwell Publishing Ltd, pp. 814–824. doi: 10.1002/pro.3376.

Krissinel, E. and Henrick, K. (2004) 'Secondary-structure matching (SSM), a new tool for fast protein structure alignment in three dimensions', *Acta Crystallographica Section D: Biological Crystallography*. Acta Crystallogr D Biol Crystallogr, 60(12 I), pp. 2256–2268. doi:

10.1107/S0907444904026460.

Leadbeater, C. *et al.* (2000) 'Probing the NADPH-binding site of Escherichia coli flavodoxin oxidoreductase', *Biochemical Journal*. Portland Press Ltd, 352(2), pp. 257–266. doi: 10.1042/0264-6021:3520257.

Lee, D. S. *et al.* (2003) 'Substrate recognition and molecular mechanism of fatty acid hydroxylation by cytochrome P450 from Bacillus subtilis: Crystallographic, spectroscopic, and mutational studies', *Journal of Biological Chemistry*. American Society for Biochemistry and Molecular Biology, 278(11), pp. 9761–9767. doi: 10.1074/jbc.M211575200.

Leslie Dutton, P. (1978) 'Redox potentiometry: Determination of midpoint potentials of oxidation-reduction components of biological electron-transfer systems', *Methods in Enzymology*. Methods Enzymol, 54(C), pp. 411–435. doi: 10.1016/S0076-6879(78)54026-3.

Li, A. *et al.* (2017) 'A redox-mediated Kemp eliminase', *Nature Communications*. Nature Publishing Group, 8(1), pp. 1–8. doi: 10.1038/ncomms14876.

Li, H. and Poulos, T. L. (1997) 'The structure of the cytochrome p450BM-3 haem domain complexed with the fatty acid substrate, palmitoleic acid', *Nature Structural Biology*. Nature Publishing Group, 4(2), pp. 140–146. doi: 10.1038/nsb0297-140.

Li, N. *et al.* (2012) 'Evidence for only oxygenative cleavage of aldehydes to alk(a/e)nes and formate by cyanobacterial aldehyde decarbonylases', *Biochemistry*. Biochemistry, 51(40), pp. 7908–7916. doi: 10.1021/bi300912n.

Liang, J. L. *et al.* (2016) 'Regulation of the alkane hydroxylase CYP153 gene in a Gram-positive alkane-degrading bacterium, Dietzia sp. strain DQ12-45-1b', *Applied and Environmental Microbiology*. American Society for Microbiology, 82(2), pp. 608–619. doi: 10.1128/AEM.02811-15.

Lipscomb, J. D. (1980) 'Electron Paramagnetic Resonance Detectable States of Cytochrome P-450Cam', *Biochemistry*. American Chemical Society, 19(15), pp. 3590–3599. doi: 10.1021/bi00556a027.

Liu, H. *et al.* (2012) 'Production of extracellular fatty acid using engineered Escherichia coli', *Microbial Cell Factories*, 11(1), p. 41. doi: 10.1186/1475-2859-11-41.

Liu, Q. *et al.* (2015) 'Engineering an iterative polyketide pathway in Escherichia coli results in single-form alkene and alkane overproduction', *Metabolic Engineering*. Academic Press Inc., 28, pp. 82–90. doi: 10.1016/j.ymben.2014.12.004.

Liu, Y. *et al.* (2014) 'Hydrogen peroxide-independent production of α-alkenes by OleTJE P450 fatty acid decarboxylase.', *Biotechnology for biofuels*, 7(1), p. 28. doi: 10.1186/1754-6834-7-28.

Lu, C. *et al.* (2018) 'An Engineered Self-Sufficient Biocatalyst Enables Scalable Production of Linear α-Olefins from Carboxylic Acids', *ACS Catalysis*, 8(7), pp. 5794–5798. doi: 10.1021/acscatal.8b01313.

Luthra, A., Denisov, I. G. and Sligar, S. G. (2011) 'Spectroscopic features of cytochrome P450 reaction intermediates', *Archives of Biochemistry and Biophysics*. NIH Public Access, pp. 26–35. doi: 10.1016/j.abb.2010.12.008.

Matsunaga, I. *et al.* (1996) 'Direct involvement of hydrogen peroxide in bacterial α-hydroxylation of fatty acid', *FEBS Letters*. Elsevier B.V., 386(2–3), pp. 252–254. doi: 10.1016/0014-5793(96)00451-6.

Matsunaga, I. *et al.* (1997) 'Molecular cloning and expression of fatty acid α-hydroxylase from Sphingomonas paucimobilis', *Journal of Biological Chemistry*. American Society for Biochemistry and Molecular Biology, 272(38), pp. 23592–23596. doi: 10.1074/jbc.272.38.23592.

Matsunaga, I. *et al.* (1999) 'Characterization of the ybdT gene product of Bacillus subtilis: Novel fatty acid β-hydroxylating cytochrome P450', *Lipids*. John Wiley & Sons, Ltd, 34(8), pp. 841–846. doi: 10.1007/s11745-999-0431-3.

Matthews, S., Belcher, J. D., *et al.* (2017) 'Catalytic determinants of alkene production by the cytochrome P450 peroxygenase OleTJE', *Journal of Biological Chemistry*. American Society for Biochemistry and Molecular Biology, 292(12), pp. 5128–5143. doi: 10.1074/jbc.M116.762336.

Matthews, S., Tee, K. L., *et al.* (2017a) 'Production of alkenes and novel secondary products by P450 OleTJE using novel H2O2-generating fusion protein systems', *FEBS Letters*. Wiley Blackwell, 591(5), pp. 737–750. doi: 10.1002/1873-3468.12581.

Matthews, S., Tee, K. L., *et al.* (2017b) 'Production of alkenes and novel secondary products by P450 OleTJE using novel H2O2-generating fusion protein systems', *FEBS Letters*. Wiley Blackwell, 591(5), pp. 737–750. doi: 10.1002/1873-3468.12581.

Matthews, S., Tee, K. L., *et al.* (2017c) 'Production of alkenes and novel secondary products by P450 OleTJE using novel H2O2-generating fusion protein systems', *FEBS Letters*, 591(5), pp. 737–750. doi: 10.1002/1873-3468.12581.

McCoy, A. J. *et al.* (2007) 'Phaser crystallographic software', *Journal of Applied Crystallography*. International Union of Crystallography, 40(4), pp. 658–674. doi: 10.1107/S0021889807021206.

McIver, L. *et al.* (1998) 'Characterisation of flavodoxin NADP+ oxidoreductase and flavodoxin; key components of electron transfer in Escherichia coli', *European Journal of Biochemistry*. Blackwell Publishing Ltd., 257(3), pp. 577–585. doi: 10.1046/j.1432-1327.1998.2570577.x.

McKNIGHT, J. *et al.* (1993) 'Identification of charge-transfer transitions in the optical spectrum of low-spin ferric cytochrome P-450 Bacillus megaterium', *European Journal of Biochemistry*. Eur J Biochem, 213(2), pp. 683–687. doi: 10.1111/j.1432-1033.1993.tb17808.x.

McLean, K. J. *et al.* (2002) 'Expression, purification and spectroscopic characterization of the cytochrome P450 CYP121 from Mycobacterium tuberculosis', *Journal of Inorganic Biochemistry*. J Inorg Biochem, 91(4), pp. 527–541. doi: 10.1016/S0162-0134(02)00479-8.

McLean, K. J. *et al.* (2005) 'Biodiversity of cytochrome P450 redox systems', in *Biochemical Society Transactions*, pp. 796–801. doi: 10.1042/BST0330796.

McLean, K. J. *et al.* (2006) 'Biophysical characterization of the sterol demethylase P450 from Mycobacterium tuberculosis, its cognate ferredoxin, and their interactions', *Biochemistry*. Biochemistry, 45(27), pp. 8427–8443. doi: 10.1021/bi0601609.

McLean, K. J. *et al.* (2015) 'Biological diversity of cytochrome P450 redox partner systems', *Advances in Experimental Medicine and Biology*, 851, pp. 299–317. doi: 10.1007/978-3-319-16009-2_11.

Miles, J. S. *et al.* (1992) 'Domains of the catalytically self-sufficient cytochrome p-450 BM-3. Genetic construction, overexpression, purification and spectroscopic characterization', *Biochemical Journal*. Biochem J, 288(2), pp. 503–509. doi: 10.1042/bj2880503.

Monk, B. C. *et al.* (2014) 'Architecture of a single membrane spanning cytochrome P450 suggests constraints that orient the catalytic domain relative to a bilayer', *Proceedings of the National Academy of Sciences of the United States of America*. National Academy of Sciences, 111(10), pp. 3865–3870. doi: 10.1073/pnas.1324245111.

Munro, A. W. *et al.* (2002) 'P450 BM3: The very model of a modern flavocytochrome', *Trends in Biochemical Sciences*, pp. 250–257. doi: 10.1016/S0968-0004(02)02086-8.

Munro, A. W. *et al.* (2013) 'What makes a P450 tick?', *Trends in Biochemical Sciences*, 38(3), pp. 140–150. doi: 10.1016/j.tibs.2012.11.006.

Munro, A. W. *et al.* (2018) 'Structure and function of the cytochrome P450 peroxygenase enzymes', *Biochemical Society Transactions*. Portland Press Ltd, pp. 183–196. doi: 10.1042/BST20170218.

Munro, A. W., Girvan, H. M. and McLean, K. J. (2007) 'Variations on a (t)heme--novel mechanisms, redox partners and catalytic functions in the cytochrome P450 superfamily.', *Natural product reports*, 24(3), pp. 585–609. doi: 10.1039/b604190f.

Murugan, R. and Mazumdar, S. (2005) 'Structure and Redox Properties of the Haem Centre in the C357M Mutant of Cytochrome P450cam', *ChemBioChem*. John Wiley & Sons, Ltd, 6(7), pp. 1204–1211. doi: 10.1002/cbic.200400399.

Omura, T. and Sato, R. (1962) 'A new cytochrome in liver microsomes.', *The Journal of biological chemistry*, 237, pp. 1375–1376. Available at: http://www.ncbi.nlm.nih.gov/pubmed/14482007 (Accessed: 27 November 2016).

Perera, R. *et al.* (2003) 'Neutral thiol as a proximal ligand to ferrous heme iron: Implications for heme proteins that lose cysteine thiolate ligation on reduction', *Proceedings of the National Academy of Sciences of the United States of America*. National Academy of Sciences, 100(7), pp. 3641–3646. doi: 10.1073/pnas.0737142100.

Pickl, M. *et al.* (2019) 'Mechanistic Studies of Fatty Acid Activation by CYP152 Peroxygenases Reveal Unexpected Desaturase Activity', *ACS Catalysis*. American Chemical Society, 9(1), pp. 565–577. doi: 10.1021/acscatal.8b03733.

Pluschke, G. and Overath, P. (1981) 'Function of phospholipids in Escherichia coli. Influence of changes in polar head group composition on the lipid phase transition and characterization of a mutant containing only saturated phospholipid acyl chains', *Journal of Biological Chemistry*, 256(7), pp. 3207–3212. doi: 10.1016/s0021-9258(19)69590-6.

Podust, L. M. *et al.* (2001) 'Substrate recognition sites in 14α-sterol demethylase from comparative analysis of amino acid sequences and X-ray structure of Mycobacterium tuberculosis CYP51', *Journal of Inorganic Biochemistry*. Elsevier, 87(4), pp. 227–235. doi: 10.1016/S0162-0134(01)00388-9.

Poulos, T. L., Finzel, B. C. and Howard, A. J. (1987) 'High-resolution crystal structure of cytochrome P450cam', *Journal of Molecular Biology*, 195(3), pp. 687–700. doi: 10.1016/0022-2836(87)90190-2.

Presnell, S. R. and Cohen, F. E. (1989) 'Topological distribution of four-alpha-helix bundles.', *Proceedings of the National Academy of Sciences of the United States of America*. Proc Natl Acad Sci U S A, 86(17), pp. 6592–6596. doi: 10.1073/pnas.86.17.6592.

Prinz, H. (2010) 'Hill coefficients, dose–response curves and allosteric mechanisms', *Journal of*

Chemical Biology. Springer, 3(1), p. 37. doi: 10.1007/S12154-009-0029-3.

Qiu, Y. *et al.* (2012) 'An insect-specific P450 oxidative decarbonylase for cuticular hydrocarbon biosynthesis', *Proceedings of the National Academy of Sciences of the United States of America*. Proc Natl Acad Sci U S A, 109(37), pp. 14858–14863. doi: 10.1073/pnas.1208650109.

Raag, R. *et al.* (1991) 'Crystal Structure of the Cytochrome P-450CAM Active Site Mutant Thr252Ala', *Biochemistry*. American Chemical Society, 30(48), pp. 11420–11429. doi: 10.1021/bi00112a008.

Reinhard, F. G. C. *et al.* (2020) 'Bioengineering of Cytochrome P450 OleTJE: How Does Substrate Positioning Affect the Product Distributions?', *Molecules (Basel, Switzerland)*. NLM (Medline), 25(11). doi: 10.3390/molecules25112675.

Rittle, J. and Green, M. T. (2010) 'Cytochrome P450 compound I: Capture, characterization, and C-H bond activation kinetics', *Science*, 330(6006), pp. 933–937. doi: 10.1126/science.1193478.

Rude, M. A. *et al.* (2011) 'Terminal olefin (1-alkene) biosynthesis by a novel P450 fatty acid decarboxylase from Jeotgalicoccus species', *Applied and Environmental Microbiology*. American Society for Microbiology, 77(5), pp. 1718–1727. doi: 10.1128/AEM.02580-10.

Sabbadin, F. *et al.* (2009) 'The 1.5-Å structure of XplA-heme, an unusual cytochrome P450 heme domain that catalyzes reductive biotransformation of royal demolition explosive', *Journal of Biological Chemistry*. American Society for Biochemistry and Molecular Biology, 284(41), pp. 28467–28475. doi: 10.1074/jbc.M109.031559.

Sahin, E. and Roberts, C. J. (2012) 'Size-exclusion chromatography with multi-angle light scattering for elucidating protein aggregation mechanisms', *Methods in Molecular Biology*, 899, pp. 403–423. doi: 10.1007/978-1-61779-921-1_25.

Sayer, P., Gouterman, M. and Connell, C. R. (1982) 'Metalloid Porphyrins and Phthalocyanines', *Accounts of Chemical Research*, 15(3), pp. 73–79. doi: 10.1021/ar00075a002.

Schirmer, A. *et al.* (2010) 'Microbial biosynthesis of alkanes', *ScienceSchirmer, A. et al. (2010) 'Microbial biosynthesis of alkanes', Science, 329(5991), pp. 559–562. doi: 10.1126/science.1187936.*, 329(5991), pp. 559–562. doi: 10.1126/science.1187936.

Schlichting, I. *et al.* (2000) 'The catalytic pathway of cytochrome P450cam at atomic resolution', *Science*. American Association for the Advancement of Science, 287(5458), pp. 1615–1622. doi: 10.1126/science.287.5458.1615.

Schrödinger, L. (2015) 'The PyMOL Molecular Graphics System, Version 2.4.0a0'. Available at: https://www.schrodinger.com/products/pymol (Accessed: 14 March 2021).

Shaw, M. K. and Ingraham, J. L. (1965) 'Fatty Acid Composition of Escherichia coli as a Possible Controlling Factor of the Minimal Growth Temperature', *Journal of Bacteriology*, 90(1), pp. 141–146. doi: 10.1128/jb.90.1.141-146.1965.

Shimada, H. *et al.* (1991) 'The Role of Threonine 252 in the Oxygen Activation by Cytochrome P-450 cam: Mechanistic Studies by Site-directed Mutagenesis', *Studies in Surface Science and Catalysis*. Elsevier, 66(C), pp. 313–319. doi: 10.1016/S0167-2991(08)62847-5.

Shoji, O. and Watanabe, Y. (2014) 'Peroxygenase reactions catalyzed by cytochromes P450', *Journal of Biological Inorganic Chemistry*. Springer Verlag, pp. 529–539. doi: 10.1007/s00775-014-1106-9.

Singh, M. K. *et al.* (2017) 'Role of an N-terminal extension in stability and catalytic activity of a hyperthermostable α/β hydrolase fold esterase', *Protein Engineering, Design and Selection*. Oxford University Press, 30(8), pp. 559–570. doi: 10.1093/protein/gzx049.

Sligar, S. G. and Gunsalus, I. C. (1976) 'A thermodynamic model of regulation: modulation of redox equilibria in camphor monoxygenase', *Proceedings of the National Academy of Sciences of the United States of America*. National Academy of Sciences, 73(4), pp. 1078–1082. doi: 10.1073/pnas.73.4.1078.

Somvanshi, P. R. and Venkatesh, K. V. (2013) 'Hill Equation', in *Encyclopedia of Systems Biology*. Springer New York, pp. 892–895. doi: 10.1007/978-1-4419-9863-7_946.

'The CCP4 suite: Programs for protein crystallography' (1994) *Acta Crystallographica Section D: Biological Crystallography*. Acta Crystallogr D Biol Crystallogr, 50(5), pp. 760–763. doi: 10.1107/S0907444994003112.

Tyson, C. A., Lipscomb, J. D. and Gunsalus, I. C. (1972) 'The role of putidaredoxin and P450 cam in methylene hydroxylation.', *Journal of Biological Chemistry*, 247(18), pp. 5777–5784. doi: 10.1016/s0021-9258(19)44826-6.

Vagin, A. A. *et al.* (2004) 'REFMAC5 dictionary: Organization of prior chemical knowledge and guidelines for its use', *Acta Crystallographica Section D: Biological Crystallography*. International Union of Crystallography, 60(12 I), pp. 2184–2195. doi: 10.1107/S0907444904023510.

Wang, C. and Wamser, C. C. (2014) 'Hyperporphyrin effects in the spectroscopy of protonated porphyrins with 4-aminophenyl and 4-pyridyl meso substituents', *Journal of Physical Chemistry*

A. American Chemical Society, 118(20), pp. 3605–3615. doi: 10.1021/jp501398g.

Wang, S. *et al.* (2020) 'Directed evolution of a hydroxylase into a decarboxylase for synthesis of 1‐alkenes from fatty acids', *ACS Catalysis*. American Chemical Society, 10(24), pp. 14375–14379. doi: 10.1021/acscatal.0c04345.

Wang, Z. J. *et al.* (2014) 'Improved Cyclopropanation Activity of Histidine-Ligated Cytochrome P450 Enables the Enantioselective Formal Synthesis of Levomilnacipran', *Angewandte Chemie International Edition*. Wiley-VCH Verlag, 53(26), pp. 6810–6813. doi: 10.1002/anie.201402809.

von der Weid, I. *et al.* (2007) 'Identification and biodegradation potential of a novel strain of Dietzia cinnamea isolated from a petroleum-contaminated tropical soil', *Systematic and Applied Microbiology*. Elsevier GmbH, 30(4), pp. 331–339. doi: 10.1016/j.syapm.2006.11.001.

Wilson, G. S., Tsibris, J. C. M. and Gunsalus, I. C. (1973) 'Electrochemical studies of putidaredoxin and its selenium analog', *Journal of Biological Chemistry*. Elsevier, 248(17), pp. 6059–6061. doi: 10.1016/s0021-9258(19)43508-4.

Wise, C. E. *et al.* (2018) 'Dioxygen Activation by the Biofuel-Generating Cytochrome P450 OleT', *ACS Catalysis*. American Chemical Society, 8(10), pp. 9342–9352. doi: 10.1021/acscatal.8b02631.

Xu, H. *et al.* (2017) 'In vitro oxidative decarboxylation of free fatty acids to terminal alkenes by two new P450 peroxygenases', *Biotechnology for Biofuels*. BioMed Central Ltd., 10(1), p. 208. doi: 10.1186/s13068-017-0894-x.

Yassin, A. F., Hupfer, H. and Schaal, K. P. (2006) 'Dietzia cinnamea sp. nov., a novel species isolated from a perianal swab of a patient with a bone marrow transplant', *International Journal of Systematic and Evolutionary Microbiology*, 56(3), pp. 641–645. doi: 10.1099/ijs.0.63863-0.

5 Discussion

5.1 Summary and conclusions

This thesis describes the identification, cloning, expression, purification and characterisation of three novel members of the CYP152 peroxygenase family. The first discovery of this peroxygenase family was reported in the early 2000's with characterisation of the first two members P450 BSβ (CYP152A1) and P450 SPα (CYP152B1) from *Bacillus subtilis and Sphingomonas paucimobilis*, respectively (Matsunaga *et al.*, 1996, 1999). These peroxygenases are able to catalyse the hydroxylation of fatty acid substrates using H_2O_2 as a co-substrate. The isolation of $OleT_{JE}$ from *Jeotgalicoccus spp.* by Rude and co-workers in 2011 highlighted the true potential of the CYP152 family as a tool for biotechnological applications within the fuel industry. $OleT_{JE}$ displayed formation of 1-pentadecene and other alkenes. This study also highlighted several other organisms including *Kocuria rhizophila* and *Corynebacterium efficiens* which displays 29% and 27% sequence similarity towards $OleT_{JE}$, respectively and demonstrated the ability to produce 1-pentadecene *in vivo* (Rude *et al.*, 2011). However, *in vitro* data was not obtained during these studies due to the inability to produce and purify the associated *K. rhizophila* and *C. efficiens* enzymes.

In this thesis, the molecular characterisation and classification of the cytochrome P450 (KR) peroxygenase from *K. rhizophila* as CYP152T1 as well the peroxygenase (CE) from *C. efficiens* as CYP152T7 are reported for the first time. We identified another CYP152 peroxygenase through a BLAST search using the sequence of P450 KR, with a hit from *Dietzia cinnamea*. The novel peroxygenase P450 DC is formally classified as CYP152T8 and displays 62% and 55% similarity towards P450 KR and P450 CE, respectively.

Initial expression trials revealed that P450 KR overexpresses highly in C41 (DE3) *E. coli* cells following induction by IPTG. It was noted, similarly to $OleT_{JE}$, that P450 KR requires high salt concentrations (0.75 M NaCl) during the purification process to maintain high ionic conditions and evade protein aggregation (Belcher *et al.*, 2014). P450 KR was subsequently purified in a three step Ni-IDA chromatographic method. Expression and purification of P450 CE and P450 DC was also achieved by this method. However, P450 CE and P450 DC displayed a lower salt tolerance, as low (NaCl < 200 mM), for the purification buffers.

The UV-visible spectrum of P450 KR displayed a red-shifted Soret absorbance at 424 nm, with alpha and beta bands at 576 nm and 541 nm, respectively. A majority of P450 enzymes from a wide variety of organisms displays typical Soret maximas of 418 nm. It was originally thought that this unusual absorbance peak was due to retention of imidazole in the active site from the purification buffers. However, expression and purification of P450 KR using the Strep-tag/Step-Tactin system in the absence of any exogenous imidazole displayed the same Soret features. These shifted Soret features are unlike many other cytochromes P450 (e.g. $OleT_{JE}$ decarboxylase with major absorption features at 418, 566 and 535 nm) (Belcher *et al.*, 2014). In addition to P450 KR, P450 CE and P450 DC displays similar shifted absorbance; P450 CE: λ 424 nm, with smaller α- and β-bands in the visible region at 575 and 539 nm, respectively and P450 DC 421 nm with smaller α and β bands visible at 541 nm and 578 nm. Sodium dithionite reduction and addition of CO displayed the characteristic P450 spectrum with a Soret absorbance at 447 nm. Interestingly, a subset of recently characterised CYP152 peroxygenases also display this red-shifted Soret absorbance including CYP-MP from *Methylobacterium populi* (422, 545 and 575 nm) (Amaya, Rutland and Makris, 2016), and CYP-Sm46Δ29 from *Staphylococcus massiliensis* (424, 571 and 540 nm) (Xu *et al.*, 2017). Reduction of all three CYP152 orthologues with sodium dithionite resulted decreased blue-shifted Soret intensity with absorbance. Formation of the ferrous-CO complex resulted in the classic P450 spectrum with Soret absorbance for P450 KR, P450 CE and P450 DC at ~448 nm. These are consistent with the retention of cysteine thiolate proximal coordination to the ferrous heme iron for all three enzymes (Perera *et al.*, 2003).

Binding of substrates to P450 enzymes was assessed via spin-state shifts of the heme iron by UV-visible spectroscopy. A range of fatty acids (C10:0 – C18:0) induced Soret peak shifts from the low spin substrate-free state at 424 nm, towards the high spin substrate-bound state at 397 nm, usually through displacement of the water as the 6^{th} ligand to the heme. P450 KR undergoes extensive heme shift (100 – 90%) towards fatty acid chain length from C10:0 – C14:0. Less extensive heme shifts are observed for palmitic acid (C16:0) and stearic acid (C18:0). $OleT_{JE}$ displays increased spin-state change for longer chain fatty acids (C20:0) than for the shorter chain substrates (C12:0). P450 CE shows the most extensive heme accumulation for the C16:0 fatty acid and reduced

high spin accumulation as the chain length decreases. This extensive high spin heme accumulation is not witnessed in all CYP152 peroxygenases; P450 SPα, P450 BSβ and CYP152K6, display no spectral changes upon binding of fatty acid substrates, despite being able to perform hydroxylations on them (Fujishiro *et al.*, 2011; Girvan *et al.*, 2018). Binding dissociation constants were determined for the binding of fatty acids towards P450 CE and P450 KR. The K_d values for P450 KR for the fatty acids tested differ by >3 orders of magnitude, with the shortest chain length displaying K_d of 7.27 mM for decanoic acid to K_d of 1.95 μM for stearic acid. Binding of fatty acids (C10:0 – C16:0) towards P450 CE displayed K_d within the μM range.

Heme iron redox potentials were determined for substrate-free and decanoic acid bound P450 KR. Spectroelectrochemical titrations were undertaken, following the progressive conversion of the ferric enzyme to the ferrous state upon reduction by sodium dithionite. Determination of the midpoint potentials for the Fe^{III}/ Fe^{II} heme iron demonstrated both the substrate-free (-129 $\pm$ 3 mV vs. NHE) and decanoic acid-bound (-149 $\pm$ 4 mV vs. NHE) forms of P450 KR displayed relatively positive and similar midpoint potentials. $OleT_{JE}$ displayed similar positive heme redox potentials with substrate-free enzyme determined as -103 ± 6 mV vs. NHE. In typical redox-partner dependent P450 enzymes, substrate binding usually is linked to a change reduction potential e.g. P450 cam, the binding of camphor in the active site causes the heme iron redox potentials to change from 303 to -270 mV (substrate-free) to -173 to -163 mV (camphor-bound), which allows electron flow from the redox-partner and in turn progresses the P450 catalytic cycle. The positive redox potentials observed in these peroxygenases suggest an evolutionary divergence of these enzymes to harness H_2O_2-derived catalysis.

The structure of substrate-free P450 KR was solved to 3.0 Å. Overall, P450 KR displays many structural similarities towards $OleT_{JE}$ and other CYP152 peroxygenase members such as P450 SPα and P450 BSβ. However, the major structural difference in P450 KR lies within the N-terminal portion, with KR possessing an extended N-terminal alpha helix that protrudes out from the core and interacts in pseudo zipper-like interactions with another P450 KR monomer. These interactions are made by residues in the N-terminal helix Arg18, Tyr21 and Arg29 towards Phe300, Asp328 and Thr334 in the central domain, respectively. A Ser35 present at the end of the N-terminal helix makes hydrogen bonds with the equivalent serine from the other monomer. These interactions

are further stabilised via a disulphide bond between a cysteine (Cys39) residue located in the loop at the base of the N-terminal helix and cys residue present in the central domain of the same monomer (Cys317).

Disulphide bonds are uncommon in P450 enzymes with no physiological linkages observed in the PDB thus far. To explore this disulphide-linkage and oligomeric state of P450 KR, we probed the enzyme in solution in three states; (i) WT KR in oxidising conditions; (ii) KR in reducing conditions (1-2 mM of reducing agent such as TCEP or DTT) and (iii) P450 Δα35-KR variant (deletion of the N-terminal helix with the disulphide linkage still intact). WT P450 KR displayed a concentration dependent dimerisation using sedimentation velocity AUC, displaying a dimer dissociation constant of K_D of 8.6 ± 0.7 μM and estimated molecular weight of the dimer (MW) of 98.9 ± 5.8 kDa. Intact mass spectrometry techniques highlighted the global destabilising effect on the overall protein structure upon sustained reduction and destabilisation of the disulphide linkage in P450 KR. A 2 Da difference was observed between MW of oxidised and chemically-reduced samples of P450 KR by nanoESI-MS confirming the protonation of two cysteine residues and ensuring no excessive reduction of the heme/heme-thiolate. Although protein usually exhibit multiple charge states occurring from the ESI process, P450 KR samples that were treated with the reducing agent displayed an increase in the charge-state distributions in comparison to WT P450 samples. This shows that by breaking the disulphide linkage has a detrimental effect on the protein structure becoming partially unfolded and losing KR's compact core, accommodating the increase of charge. Furthering this, chemically reduced samples displayed an increase of free heme within the samples and mass corresponding to the apo-form of P450 KR. Reduction of the disulphide bond also resulted in a failure to dimerise, exhibiting monomer-like molecular weight (MW) of 53.7 KDa (± 0.8%) by SEC-MALS even at concentrations far beyond the dimer dissociation constant.

The role of the H-bonding network between residues in the N-terminal helix and the central domain was explored through the Δα35-KR variant that was designed to retain the disulphide linkage between Cys39 and Cys317 but with a deletion of 35 residues including those that form the N-terminal helix. Data showed that the removal of the N-helix prevents protein dimerisation with a monomeric weight of MW of 47.6 (± 2.1%)

kDa by SEC-MALS. Therefore both the interactions of the N-terminal helix as well as the stabilising effect on disulphide linkage are vital in the dimerisation of P450 KR.

P450 KR represents one of the first characterised CYP152 peroxygenases and P450 enzymes in general that exist in a dimeric state. Therefore, this led to investigations of the oligomeric states of additional CYP152 members (including P450 KR orthologues; P450 CE and P450 DC). The oligomerisation states of the CYP152 enzymes discussed in this thesis were explored by a variety of techniques including MALS and AUC. Solution data of P450 CE suggest that it exists solely as dimer, with SEC-MALS displaying a single peak with an average molecular weight of MW of 88.3 ± 5.8% kDa (monomer ~48 kDa). A dimer-dissociation constant could not be obtained as P450 CE remains a stable dimer even at very low protein concentrations. Oligomeric state studies of P450 DC using MALS was inconclusive due to its propensity to aggregate. However, initial purification data suggest that P450 DC does exist as oligomer, but further work is needed to elucidate the exact mechanism and size.

P450 CE was crystallised and analysed by X-ray crystallography, leading to the structure solved to 2.05 Å. Myristic acid was found in the active site of the P450 CE crystal, despite seeming ligand free spectroscopically. This crystallised ligand-bound state could likely be attributed to retention of the myristic acid ligand through expression in *E. coli* cells. The Arg248 residue in the I-helix interacts with carboxylate head group of the fatty acid substrate via H-bonding interactions. This interaction is conserved in the CYP152 peroxygenase family and has been observed with the other structurally characterised enzymes $OleT_{JE}$, P450 BSβ and SPα (Lee *et al.*, 2003; Fujishiro *et al.*, 2011; Belcher *et al.*, 2014).

Interestingly P450 CE is observed to crystallise in an unusual dimer formation with a distinct dimeric interface between the two monomers. Despite the homology towards P450 KR, the dimeric interface observed was very different between the two structures. In P450 CE a heme molecule is sandwiched between a His186 residues of each monomer, further interactions are made by the heme propionate group and a Phe179 residue. Intrestingly it seems that the substrate access channels are not involved with dimerisation. This is in stark contrast to P450 KR that displays a zipper-like helical interaction within its dimer interface.

Structural comparisons of the CE and KR dimers revealed a disulphide linkage present in P450 CE between Cys7 and Cys312, present in a structurally similar place to P450 KR. Initial experiments with P450 CE and reducing agent displaying some destabilisation of the enzyme. In oxidising conditions, both P450 CE and KR display increased thermal stability in comparison to $OleT_{JE}$ (T_m of P450 CE: 66°C, P450 KR: 52°C and $OleT_{JE}$: 48°C).

To probe whether this dimeric interface observed is the physiological dimer, two variants H186N and H186K were prepared. These CE mutant proteins both over-expressed and purified well, allowing investigation into the oligomeric state by SEC-MALS. Both variants showed that even when the His186/heme interaction is disrupted, the protein remains in the dimeric state as determined by their molecular masses. A crystal structure of the H186N variant was obtained with 2.06 Å resolution. Two copies were present in the asymmetric unit, with the dimeric structure found within the symmetry, retaining the dimeric interface as WT CE. Indeed, no heme was present at the interface due to disruption of the binding site, but hydrophobic interactions remained.

P450 KR, P450 CE and P450 DC, were shown to decarboxylate and hydroxylate C10:0 – C18:0 fatty acid substrates, producing Cn-1 terminal alkenes and α- and β-hydroxylated fatty acids. For clarity, these data with percentage conversions are summarised in **table 5.1**. For all three WT enzymes (KR, CE and DC) the highest alkene conversion for is observed with myristic acid.

Turnover of C14:0 by P450 KR produces 36% conversion to 1-tridecene, ~5% 2-OH myristic acid, and 48% to 3-OH myristic acid. P450 DC and CE are more efficient decarboxylases and display similar amounts of 1-tridecene formation (CE: 50 %, DC: 51%). P450 DC hydroxylation products comprise of 2-OH: 7.3%, 3-OH: 37.6, displaying decreased amount of α-hydroxylation in comparison to P450 CE (2-OH: 15%, 3-OH: 24%). These data indicate that P450 KR predominantly functions as a hydroxylase, with the 3-OH fatty acid as the favoured product. Whereas, although P450 CE and DC show preferences towards hydroxylation catalytic routes for the shorter chain fatty acids (C10:0 – C12:0), for longer chain substrates C14:0 – C18:0, the alkene product becomes the dominant product. As with all three CYP152 enzymes the Cβ hydroxylated fatty acid product is favoured over the Cα version, as seen for $OleT_{JE}$ and P450 BSβ.

Table 5.1 Summary of products formed with CYP152 peroxygenase enzymes. P450 KR (WT), CE (WT), CE variants (H186N and H186K) and P450 DC (WT) contained 1 µM enzyme, 500 µM substarte and 500 µM H_2O_2. Redox-partner dependent reactions with 1 µM P450 KR contained 20 µM *E. coli* flavodoxin (Fl) or 20 µM *S. oleracea* ferredoxin (Fx) and 5 µM *E. coli* flavodoxin reductase (FlR) as described in Materials and methods. The percentage conversions of each fatty acid towards their respective C_{n-1} terminal alkene, 2-OH fatty acid and 3-OH fatty acid are shown for each CYP152 member and variants to the nearest 0.1%. The data presented is the average of at least 3 sets of experiments.

Substrate	Products	CYP152 enzyme and % products formed						
		KR WT	KR Fld/FlR	KR Fx/FlR	CE WT	CE H186N	CE H186K	DC WT
C10:0	1-nonene	8.0	18.5	9.5	23.6	31.7	25.6	38.3
	2-OH decanoic acid	2.9	4.3	2.2	13.3	18.1	26.9	6.5
	3-OH decanoic acid	11.5	14.6	8.8	41	50.2	47.5	55.1
	total	**22.4**	**37.4**	**20.5**	**77.9**	**100.0**	**100.0**	**99.1**
C12:0	1-undecene	19.4	30.7	26.2	37.8	47.5	11.0	39.9
	2-OH lauric acid	11.8	6.5	11.3	19.4	11.4	13.1	4.7
	3-OH lauric acid	41.3	39.4	58.0	33.7	34.5	26.9	52.1
	total	**72.5**	**76.8**	**95.5**	**90.9**	**93.4**	**51.0**	**96.7**
C14:0	1-tridecene	35.9	28.4	47.2	50.3	44.5	28.2	51.2
	2-OH myristic acid	4.8	8.2	6.2	14.5	9.2	13.6	7.3
	3-OH myristic acid	48.4	50.2	35.9	24.1	26.4	24.6	37.6
	total	**89.1**	**86.6**	**89.2**	**88.9**	**80.1**	**66.4**	**96.1**
C16:0	1-pentadecene	14.0	11.5	22.3	48	39.9	22.9	31.1
	2-OH palmitic acid	7.7	7.8	4.6	2.8	3.1	3.1	1.9
	3-OH palmitic acid	18.9	23.8	20.4	10.5	9.7	10.1	26.7
	total	**40.5**	**43. 1**	**47.3**	**61.3**	**52.7**	**36.1**	**59.7**
C18:0	1-heptadecene	1.9	-/-	-/-	13.7	14.9	5.9	5.1
	2-OH stearic acid	1.4	-/-	-/-	0.8	1.1	0.9	0.7
	3-OH stearic acid	2.9	-/-	-/-	3.2	1.5	2.4	2.8
	Total	**6.2**	**-/-**	**-/-**	**17.7**	**17.5**	**9.2**	**8.6**

Additional hydroxylation reactions were also observed for P450 KR further than the Cβ position of the fatty acid chain. With palmitic acid, hydroxylation was observed in the δ- (5) position in addition to the β- (3), and to a lesser extent to the α- (2), hydroxy forms. When myristic acid was used as the substrate, hydroxylations in the γ- (4), δ- (5) and ε- (6) positions were observed. Furthermore, with lauric acid as substrate hydroxylation

products extend even further down the fatty acid chain with the δ-(5), ε- (6), ζ- (7) positions. This suggests multiple binding modes and flexibility afforded by these mid-length fatty acid substrates within the P450 KR active site to facilitate multiple oxidations. Unusually P450 KR does display almost full conversion to the HS state upon binding of shorter-chain (C10:0) fatty acids with relative weak binding (in comparison to longer chain fatty acids) in the mM range. Product analysis suggest relatively poor turnover of decanoic acid. However, in P450 CE limited decanoic acid induced spectroscopic changes to the HS state but almost 80% product conversion. Interestingly no extended hydroxylations are observed for the shorter chain decanoic acid or longer chain stearic acid. This extended hydroxylation further down the fatty acid chain has not been found to occur in P450 DC and P450 CE, suggesting possible alternative binding modes of the substrates and reduced substrate mobility within the active site. P450 CE and KR both display sigmoidal-type binding of fatty acid substrates appropriating most likely from their dimeric structure.

In addition to peroxygenase activity using H_2O_2 as the sole oxygen, hydride and electron donor related studies show P450 KR is also capable of performing oxidative decarboxylation and hydroxylation of fatty acids using *E.coli* and *S. oleracea* redox-partner proteins *in vitro*. An important study by Wise and co-workers highlighted that implementing a biological redox chain with additional redox partner proteins is also effective for driving catalysis in peroxygenase ($OleT_{JE}$) enzymes. However, oxidative decarboxylation still occurs in a H_2O_2-depedent manner as H_2O_2 can be generated via; (i) the autoxidation of the flavin group of the redox-donor: (ii) autoxidation from the oxy-ferrous complex or (iii) by the pyridine nucleotide itself (Wise *et al.*, 2018), but the $OleT_{JE}$ substate preferences and product profiles were found to differ. Therefore experiments implementing flavodoxin or ferredoxin, and flavodoxin reductase in conjunction with P450 KR to produce low levels of H_2O_2 were performed and displayed increases in the overall titer of alkene for all fatty acid lengths tested. These data suggest a more conservative addition of peroxide improves the decarboxylation activities of P450 KR, and something that would be interesting to explore *in vivo* with these peroxygenases.

The data in this thesis provides insight into an interesting subclass of peroxygenase family that exists in an oligomeric state and provide a basis to further understand the structural properties underlying their catalytic abilities.

5.2 Future work

This thesis describes the characterisation of three novel CYP152 peoxygenases with P450 KR and P450 CE displaying unique dimeric-forming abilities.

In *chapter 2*, the dimeric interface of P450 KR was described with a H-bonding network between residues in the N-terminal helix and the central domain of another monomer. Future research could examine the effect of mutating Arg21, Tyr24, Arg32, Phe303, Asp331 and Thr337 residues to fully assess the interface of the physiological dimer. Additionally enhancing these interactions and could have an overall stabilizing effect on the enzyme itself as well as promoting catalytic activity, and thus creating a more biotechnological stable catalyst.

We have shown that P450 KR displays increased conversion rates of alkene and overall turnover when paired with redox-partner proteins. Peroxygenase lack the important acid-alcohol pair that is present within typical O_2-depedent monooxygenases, therefore it seemed unlikely that P450 KR harnessing the typically P450 catalytic cycle. An important study by Wise and co-workers addressed these issues by showing H_2O_2 can be generated via; (i) the autoxidation of the flavin group of the redox-donor: (ii) autoxidation from the oxy-ferrous complex or (iii) by the pyridine nucleotide itself (Wise *et al.*, 2018). Therefore the advantageous production of H_2O_2 formed by these autoxidation pathways allows controlled and sustained of release of H_2O_2 which allows for the increase of turnover and reduced oxidative damage to the protein. Introducing an enzyme/system that could control the release of H_2O_2 could be harnessed with use in conjunction with the three CYP152 orthologues P450 CE, P450 DC and P450 KR. A study by Matthews and coworkers highlighted an enzyme from *Streptomyces coelicolor*, alditol oxidase that oxidises alditol (also glycerol and other polyols) to aldose and produced H_2O_2 as a co-product. This system can be used to drive decarboxylation in $OleT_{JE}$ by controlled peroxide concentration of measured alditol additions. These data suggests further research would be insightful into H_2O_2 co-producing enzymes and fusions of CYP152 enzymes. Alternatively, *In vivo* preparations in *E. coli* (or perhaps other organisms) that contain catalases to prevent excess H_2O_2 production and thus reducing unwanted oxidative damage to the catalysts.

In *chapter 3*, P450 CE was also shown to exist as a catalytically relevant dimer in solution and by X-ray crystallography studies. This enzyme has an unusual dimer interface and

retains the propensity to dimerise when this is disrupted by amino acid substitutions. To fully elucidate the dimeric interface of the physiological dimer crystallography and small angle X-ray scattering can be employed to determine the correct oligomer from several of our crystallographic assemblies (Korasick and Tanner, 2018). Addition of like-charged residues (or alanine) to each surface of P450 CE could provide an alternative method to elucidate the interface by creating a monomer.

A closer look into similarities the P450 CE and P450 KR structures revealed a disulphide linkage on the surface of P450 CE made by Cys7 and Cys312 placed in a similar position as P450 KR when the structures are superimposed (Cys39 and Cys317 in P450 KR). As discussed in *chapter 2*, the disulphide linkage seems to be vital in the stabilisation of the protein fold and formation of the dimer. Therefore, although the disulphide bond in P450 CE does not seem to play a role in the interface, it could have a noticeable effect on the ability of CE to form a dimer. Further research into how this disulphide bond functions in relation to P450 CE stability through cysteine labelling to explore dimerisation and folding. Addition of multiple surface disulphide linkages could be introduced to both proteins by mutagenesis to the see effect upon protein stability.

It would also be good to consider mutating the active site of all three orthologues. Directed evolution approaches could in introduced to make a "designer catalyst". This includes altering the substrate preference or changing the type of reaction (e.g. epoxidation). Product analysis of the P450 CE H186N and H186K variants displayed an increased overall turnover for C10:0 and C12:0 and increased formation of alkenes. This provides an interesting basis in creating P450 CE variants with more attractive attributes even with non active-site mutations.

Finally, in *chapter 4* we displayed the initial characterisation of P450 DC. Further research is required to optimise the stability of P450 DC to create a more viable catalyst for biotechnological applications. This would allow in the further structural characterisation and elucidation of the oligomeric state of the enzyme.

5.3 References

Adams, P. D. *et al.* (2010) 'PHENIX: A comprehensive Python-based system for macromolecular structure solution', *Acta Crystallographica Section D: Biological Crystallography*. Acta Crystallogr D Biol Crystallogr, 66(2), pp. 213–221. doi: 10.1107/S0907444909052925.

Amaya, J. A., Rutland, C. D. and Makris, T. M. (2016) 'Mixed regiospecificity compromises alkene synthesis by a cytochrome P450 peroxygenase from Methylobacterium populi', *Journal of Inorganic Biochemistry*. Elsevier Inc., 158, pp. 11–16. doi: 10.1016/j.jinorgbio.2016.02.031.

Atsumi, S. and Liao, J. C. (2008) 'Metabolic engineering for advanced biofuels production from Escherichia coli', *Current Opinion in Biotechnology*, 19(5), pp. 414–419. doi: 10.1016/j.copbio.2008.08.008.

Barr, I. and Guo, F. (2015) 'Pyridine Hemochromagen Assay for Determining the Concentration of Heme in Purified Protein Solutions', *BIO-PROTOCOL*. Bio-Protocol, LLC, 5(18). doi: 10.21769/bioprotoc.1594.

Belcher, J. *et al.* (2014) 'Structure and biochemical properties of the alkene producing cytochrome p450 OleTJE (CYP152l1) from the jeotgalicoccus sp. 8456 bacterium', *Journal of Biological Chemistry*. American Society for Biochemistry and Molecular Biology, 289(10), pp. 6535–6550. doi: 10.1074/jbc.M113.527325.

Beller, H. R., Goh, E. B. and Keasling, J. D. (2010) 'Genes involved in long-chain alkene biosynthesis in micrococcus Luteus', *Applied and Environmental Microbiology*. American Society for Microbiology, 76(4), pp. 1212–1223. doi: 10.1128/AEM.02312-09.

Bernstein, S. L. *et al.* (2004) 'α-Synuclein: Stable compact and extended monomeric structures and pH dependence of dimer formation', *Journal of the American Society for Mass Spectrometry*. Springer New York LLC, 15(10), pp. 1435–1443. doi: 10.1016/j.jasms.2004.08.003.

Berry, E. A. and Trumpower, B. L. (1987) 'Simultaneous determination of hemes a, b, and c from pyridine hemochrome spectra', *Analytical Biochemistry*. Anal Biochem, 161(1), pp. 1–15. doi: 10.1016/0003-2697(87)90643-9.

Bharadwaj, V. S. *et al.* (2018) 'Different Behaviors of a Substrate in P450 Decarboxylase and Hydroxylase Reveal Reactivity-Enabling Actors', *Scientific Reports*. Nature Publishing Group, 8(1), p. 12826. doi: 10.1038/s41598-018-31237-4.

Brown, P. H. and Schuck, P. (2006) 'Macromolecular size-and-shape distributions by sedimentation velocity analytical ultracentrifugation', *Biophysical Journal*. Biophysical Society, 90(12), pp. 4651–4661. doi: 10.1529/biophysj.106.081372.

Bui, S. H. *et al.* (2012) 'Unusual spectroscopic and ligand binding properties of the cytochrome P450-flavodoxin fusion enzyme XplA', *Journal of Biological Chemistry*. American Society for Biochemistry and Molecular Biology, 287(23), pp. 19699–19714. doi: 10.1074/jbc.M111.319202.

Christenson, J. K. *et al.* (2017) 'OleB from Bacterial Hydrocarbon Biosynthesis Is a β-Lactone Decarboxylase That Shares Key Features with Haloalkane Dehalogenases', *Biochemistry*. American Chemical Society, 56(40), pp. 5278–5287. doi: 10.1021/acs.biochem.7b00667.

Clemmer, D. E. and Jarrold, M. F. (1997) 'Ion mobility measurements and their applications to clusters and biomolecules', *Journal of Mass Spectrometry*. John Wiley & Sons, Ltd, pp. 577–592. doi: 10.1002/(SICI)1096-9888(199706)32:6<577::AID-JMS530>3.0.CO;2-4.

Cole, J. L. *et al.* (2008) 'Analytical Ultracentrifugation: Sedimentation Velocity and Sedimentation Equilibrium', *Methods in Cell Biology*, pp. 143–179. doi: 10.1016/S0091-679X(07)84006-4.

Coleman, T. *et al.* (2020) 'Structural insights into the role of the acid-alcohol pair of residues required for dioxygen activation in cytochrome P450 enzymes', *Journal of Biological Inorganic Chemistry*. Springer, 25(4), pp. 583–596. doi: 10.1007/s00775-020-01781-4.

Coon, M. J. (2005) 'Cytochrome P450: Nature's most versatile biological catalyst', *Annual Review of Pharmacology and Toxicology*, pp. 1–25. doi: 10.1146/annurev.pharmtox.45.120403.100030.

Cryle, M. J. and De Voss, J. J. (2008) 'The role of the conserved threonine in P450BM3 oxygen activation: Substrate-determined hydroxylation activity of the Thr268Ala mutant', *ChemBioChem*, 9(2), pp. 261–266. doi: 10.1002/cbic.200700537.

Daff, S. N. *et al.* (1997) 'Redox control of the catalytic cycle of flavocytochrome P-450 BM3', *Biochemistry*. Biochemistry, 36(45), pp. 13816–13823. doi: 10.1021/bi971085s.

Das, A., Grinkova, Y. V. and Sligar, S. G. (2007) 'Redox potential control by drug binding to cytochrome P450 3A4', *Journal of the American Chemical Society*. NIH Public Access, 129(45), pp. 13778–13779. doi: 10.1021/ja074864x.

Dawson, J. H., Andersson, L. A. and Sono, M. (1982) 'Spectroscopic investigations of ferric cytochrome P-450-CAM ligand complexes. Identification of the ligand trans to cysteinate in the native enzyme.', *Journal of Biological Chemistry*, 257(7), pp. 3606–3617. doi: 10.1016/s0021-9258(18)34823-3.

Dawson, J. H., Anderssons, L. A. and Sono, M. (1982) *Spectroscopic investigations of ferric cytochrome P-450-CAM ligand complexes. Identification of the ligand trans to cysteinate in the native enzyme.*, *THE JOURNAL OF BIOLOGICAL CHEMISTRY*. doi: 10.1016/S0021-9258(18)34823-3.

Denisov, I. G. *et al.* (2005) *Structure and chemistry of cytochrome P450*, *Chemical Reviews*. American Chemical Society. doi: 10.1021/cr0307143.

Dennig, A. *et al.* (2015) 'Oxidative Decarboxylation of Short-Chain Fatty Acids to 1-Alkenes', *Angewandte Chemie - International Edition*, 54(30), pp. 8819–8822. doi: 10.1002/anie.201502925.

Driscoll, M. D. *et al.* (2011) 'Expression and characterization of Mycobacterium tuberculosis CYP144: Common themes and lessons learned in the M. tuberculosis P450 enzyme family', *Biochimica et Biophysica Acta - Proteins and Proteomics*. Biochim Biophys Acta, 1814(1), pp. 76–87. doi: 10.1016/j.bbapap.2010.05.015.

Emsley, P. *et al.* (2010) 'Features and development of Coot', *Acta Crystallographica Section D: Biological Crystallography*. Acta Crystallogr D Biol Crystallogr, 66(4), pp. 486–501. doi: 10.1107/S0907444910007493.

Evans, P. R. and Murshudov, G. N. (2013) 'How good are my data and what is the resolution?', *Acta Crystallographica Section D: Biological Crystallography*. Acta Crystallogr D Biol Crystallogr, 69(7), pp. 1204–1214. doi: 10.1107/S0907444913000061.

Fu, W. J. *et al.* (2015) 'Hydrocarbons, the advanced biofuels produced by different organisms, the evidence that alkanes in petroleum can be renewable', *Applied Microbiology and Biotechnology*. Springer Verlag, pp. 7481–7494. doi: 10.1007/s00253-015-6840-6.

Fudou, R. *et al.* (2002) 'Corynebacterium efficiens sp. nov., a glutamic-acid-producing species from soil and vegetables', *International Journal of Systematic and Evolutionary Microbiology*. Microbiology Society, 52(4), pp. 1127–1131. doi: 10.1099/ijs.0.02086-0.

Fujishiro, T. *et al.* (2011) 'Crystal structure of H 2O 2-dependent cytochrome P450 SPαwith its bound fatty acid substrate: Insight into the regioselective hydroxylation of fatty acids at the α position', *Journal of Biological Chemistry*, 286(34), pp. 29941–29950. doi: 10.1074/jbc.M111.245225.

Gandomkar, S. *et al.* (2018) 'Biocatalytic Oxidative Cascade for the Conversion of Fatty Acids into α-Ketoacids via Internal H2O2 Recycling', *Angewandte Chemie - International Edition*. Wiley-VCH Verlag, 57(2), pp. 427–430. doi: 10.1002/anie.201710227.

Girvan, H. M. *et al.* (2004) 'Flavocytochrome P450 BM3 mutant A264E undergoes substrate-dependent formation of a novel heme iron ligand set', *Journal of Biological Chemistry*. J Biol Chem, 279(22), pp. 23274–23286. doi: 10.1074/jbc.M401716200.

Girvan, H. M. *et al.* (2018) 'Structural and catalytic properties of the peroxygenase P450 enzyme CYP152K6 from Bacillus methanolicus', *Journal of Inorganic Biochemistry*. Elsevier Inc., 188, pp.

18–28. doi: 10.1016/j.jinorgbio.2018.08.002.

Girvan, H. M. and Munro, A. W. (2016) 'Applications of microbial cytochrome P450 enzymes in biotechnology and synthetic biology', *Current Opinion in Chemical Biology*. Elsevier Ltd, pp. 136–145. doi: 10.1016/j.cbpa.2016.02.018.

Good, N. E. *et al.* (1966) 'Hydrogen Ion Buffers for Biological Research', *Biochemistry*. American Chemical Society, 5(2), pp. 467–477. doi: 10.1021/bi00866a011.

Grant, J. L., Hsieh, C. H. and Makris, T. M. (2015a) 'Decarboxylation of fatty acids to terminal alkenes by cytochrome P450 compound i', *Journal of the American Chemical Society*. American Chemical Society, 137(15), pp. 4940–4943. doi: 10.1021/jacs.5b01965.

Grant, J. L., Hsieh, C. H. and Makris, T. M. (2015b) 'Decarboxylation of fatty acids to terminal alkenes by cytochrome P450 compound I', *Journal of the American Chemical Society*, 137(15), pp. 4940–4943. doi: 10.1021/jacs.5b01965.

Grant, J. L., Mitchell, M. E. and Makris, T. M. (2016a) 'Catalytic strategy for carbon-carbon bond scission by the cytochrome p450 olet', *Proceedings of the National Academy of Sciences of the United States of America*, 113(36), pp. 10049–10054. doi: 10.1073/pnas.1606294113.

Grant, J. L., Mitchell, M. E. and Makris, T. M. (2016b) 'Catalytic strategy for carbon-carbon bond scission by the cytochrome P450 OleT', *Proceedings of the National Academy of Sciences of the United States of America*, 113(36), pp. 10049–10054. doi: 10.1073/pnas.1606294113.

Guengerich, F. P. and Munro, A. W. (2013) 'Unusual cytochrome p450 enzymes and reactions.', *The Journal of biological chemistry*. American Society for Biochemistry and Molecular Biology, 288(24), pp. 17065–73. doi: 10.1074/jbc.R113.462275.

Hagemans, D. *et al.* (2015) 'A script to highlight hydrophobicity and charge on protein surfaces', *Frontiers in Molecular Biosciences*. Frontiers Media S.A., 2(OCT), p. 56. doi: 10.3389/fmolb.2015.00056.

Hamdy, O. M. and Julian, R. R. (2012) 'Reflections on charge state distributions, protein structure, and the mystical mechanism of electrospray ionization', *Journal of the American Society for Mass Spectrometry*, 23(1), pp. 1–6. doi: 10.1007/s13361-011-0284-8.

Hannemann, F. *et al.* (2007) 'Cytochrome P450 systems—biological variations of electron transport chains', *Biochimica et Biophysica Acta (BBA) - General Subjects*, 1770(3), pp. 330–344. doi: 10.1016/j.bbagen.2006.07.017.

Van Hellemond, E. W. *et al.* (2009) 'Exploring the biocatalytic scope of alditol oxidase from Streptomyces coelicolor', *Advanced Synthesis and Catalysis*, 351(10), pp. 1523–1530. doi: 10.1002/adsc.200900176.

Howlett, G. J., Minton, A. P. and Rivas, G. (2006) 'Analytical ultracentrifugation for the study of protein association and assembly', *Current Opinion in Chemical Biology*. Curr Opin Chem Biol, pp. 430–436. doi: 10.1016/j.cbpa.2006.08.017.

Hsieh, C. H. *et al.* (2017) 'The Enigmatic P450 Decarboxylase OleT Is Capable of, but Evolved to Frustrate, Oxygen Rebound Chemistry', *Biochemistry*. American Chemical Society, 56(26), pp. 3347–3357. doi: 10.1021/acs.biochem.7b00338.

Hsieh, C. H. and Makris, T. M. (2016) *Expanding the substrate scope and reactivity of cytochrome P450 OleT*, *Biochemical and Biophysical Research Communications*. doi: 10.1016/j.bbrc.2016.05.145.

Imai, Y. *et al.* (2000) 'Unique heme environment at the putative distal region of hydrogen peroxide-dependent fatty acid α-hydroxylase from Sphingomonas paucimobilis (peroxygenase P450(SPα))', *Journal of Biochemistry*, 128(2), pp. 189–194. doi: 10.1093/oxfordjournals.jbchem.a022740.

Isin, E. M. and Guengerich, F. P. (2008) 'Substrate binding to cytochromes P450', *Analytical and Bioanalytical Chemistry*. NIH Public Access, pp. 1019–1030. doi: 10.1007/s00216-008-2244-0.

Kabsch, W. (2010) 'Integration, scaling, space-group assignment and post-refinement', *Acta Crystallographica Section D: Biological Crystallography*. International Union of Crystallography, 66(2), pp. 133–144. doi: 10.1107/S0907444909047374.

Kang, M. K. and Nielsen, J. (2017) 'Biobased production of alkanes and alkenes through metabolic engineering of microorganisms', *Journal of Industrial Microbiology and Biotechnology*. Springer Verlag, pp. 613–622. doi: 10.1007/s10295-016-1814-y.

Kapust, R. B. *et al.* (2001) 'Tobacco etch virus protease: Mechanism of autolysis and rational design of stable mutants with wild-type catalytic proficiency', *Protein Engineering*. Oxford University Press, 14(12), pp. 993–1000. doi: 10.1093/protein/14.12.993.

Koerner, R. J., Goodfellow, M. and Jones, A. L. (2009) 'The genus Dietzia: A new home for some known and emerging opportunist pathogens', *FEMS Immunology and Medical Microbiology*. Oxford Academic, pp. 296–305. doi: 10.1111/j.1574-695X.2008.00513.x.

Köninger, K. *et al.* (2016) 'Light-driven enzymatic decarboxylation', *Journal of Visualized*

Experiments. Journal of Visualized Experiments, 2016(111), p. 53439. doi: 10.3791/53439.

Korasick, D. A. and Tanner, J. J. (2018) 'Determination of protein oligomeric structure from small-angle X-ray scattering', *Protein Science*. Blackwell Publishing Ltd, pp. 814–824. doi: 10.1002/pro.3376.

Krissinel, E. and Henrick, K. (2004) 'Secondary-structure matching (SSM), a new tool for fast protein structure alignment in three dimensions', *Acta Crystallographica Section D: Biological Crystallography*. Acta Crystallogr D Biol Crystallogr, 60(12 I), pp. 2256–2268. doi: 10.1107/S0907444904026460.

Leadbeater, C. *et al.* (2000) 'Probing the NADPH-binding site of Escherichia coli flavodoxin oxidoreductase', *Biochemical Journal*. Portland Press Ltd, 352(2), pp. 257–266. doi: 10.1042/0264-6021:3520257.

Lee, D. S. *et al.* (2003) 'Substrate recognition and molecular mechanism of fatty acid hydroxylation by cytochrome P450 from Bacillus subtilis: Crystallographic, spectroscopic, and mutational studies', *Journal of Biological Chemistry*. American Society for Biochemistry and Molecular Biology, 278(11), pp. 9761–9767. doi: 10.1074/jbc.M211575200.

Leslie Dutton, P. (1978) 'Redox potentiometry: Determination of midpoint potentials of oxidation-reduction components of biological electron-transfer systems', *Methods in Enzymology*. Methods Enzymol, 54(C), pp. 411–435. doi: 10.1016/S0076-6879(78)54026-3.

Li, A. *et al.* (2017) 'A redox-mediated Kemp eliminase', *Nature Communications*. Nature Publishing Group, 8(1), pp. 1–8. doi: 10.1038/ncomms14876.

Li, H. and Poulos, T. L. (1997) 'The structure of the cytochrome p450BM-3 haem domain complexed with the fatty acid substrate, palmitoleic acid', *Nature Structural Biology*. Nature Publishing Group, 4(2), pp. 140–146. doi: 10.1038/nsb0297-140.

Li, N. *et al.* (2012) 'Evidence for only oxygenative cleavage of aldehydes to alk(a/e)nes and formate by cyanobacterial aldehyde decarbonylases', *Biochemistry*. Biochemistry, 51(40), pp. 7908–7916. doi: 10.1021/bi300912n.

Liang, J. L. *et al.* (2016) 'Regulation of the alkane hydroxylase CYP153 gene in a Gram-positive alkane-degrading bacterium, Dietzia sp. strain DQ12-45-1b', *Applied and Environmental Microbiology*. American Society for Microbiology, 82(2), pp. 608–619. doi: 10.1128/AEM.02811-15.

Lipscomb, J. D. (1980) 'Electron Paramagnetic Resonance Detectable States of Cytochrome P-

450Cam', *Biochemistry*. American Chemical Society, 19(15), pp. 3590–3599. doi: 10.1021/bi00556a027.

Liu, H. *et al.* (2012) 'Production of extracellular fatty acid using engineered Escherichia coli', *Microbial Cell Factories*, 11(1), p. 41. doi: 10.1186/1475-2859-11-41.

Liu, Q. *et al.* (2015) 'Engineering an iterative polyketide pathway in Escherichia coli results in single-form alkene and alkane overproduction', *Metabolic Engineering*. Academic Press Inc., 28, pp. 82–90. doi: 10.1016/j.ymben.2014.12.004.

Liu, Y. *et al.* (2014) 'Hydrogen peroxide-independent production of α-alkenes by OleTJE P450 fatty acid decarboxylase.', *Biotechnology for biofuels*, 7(1), p. 28. doi: 10.1186/1754-6834-7-28.

Lu, C. *et al.* (2018) 'An Engineered Self-Sufficient Biocatalyst Enables Scalable Production of Linear α-Olefins from Carboxylic Acids', *ACS Catalysis*, 8(7), pp. 5794–5798. doi: 10.1021/acscatal.8b01313.

Luthra, A., Denisov, I. G. and Sligar, S. G. (2011) 'Spectroscopic features of cytochrome P450 reaction intermediates', *Archives of Biochemistry and Biophysics*. NIH Public Access, pp. 26–35. doi: 10.1016/j.abb.2010.12.008.

Matsunaga, I. *et al.* (1996) 'Direct involvement of hydrogen peroxide in bacterial α-hydroxylation of fatty acid', *FEBS Letters*. Elsevier B.V., 386(2–3), pp. 252–254. doi: 10.1016/0014-5793(96)00451-6.

Matsunaga, I. *et al.* (1997) 'Molecular cloning and expression of fatty acid α-hydroxylase from Sphingomonas paucimobilis', *Journal of Biological Chemistry*. American Society for Biochemistry and Molecular Biology, 272(38), pp. 23592–23596. doi: 10.1074/jbc.272.38.23592.

Matsunaga, I. *et al.* (1999) 'Characterization of the ybdT gene product of Bacillus subtilis: Novel fatty acid β-hydroxylating cytochrome P450', *Lipids*. John Wiley & Sons, Ltd, 34(8), pp. 841–846. doi: 10.1007/s11745-999-0431-3.

Matthews, S., Belcher, J. D., *et al.* (2017) 'Catalytic determinants of alkene production by the cytochrome P450 peroxygenase OleTJE', *Journal of Biological Chemistry*. American Society for Biochemistry and Molecular Biology, 292(12), pp. 5128–5143. doi: 10.1074/jbc.M116.762336.

Matthews, S., Tee, K. L., *et al.* (2017a) 'Production of alkenes and novel secondary products by P450 OleTJE using novel H2O2-generating fusion protein systems', *FEBS Letters*. Wiley Blackwell, 591(5), pp. 737–750. doi: 10.1002/1873-3468.12581.

Matthews, S., Tee, K. L., *et al.* (2017b) 'Production of alkenes and novel secondary products by P450 OleTJE using novel H2O2-generating fusion protein systems', *FEBS Letters*. Wiley Blackwell, 591(5), pp. 737–750. doi: 10.1002/1873-3468.12581.

Matthews, S., Tee, K. L., *et al.* (2017c) 'Production of alkenes and novel secondary products by P450 OleTJE using novel H2O2-generating fusion protein systems', *FEBS Letters*, 591(5), pp. 737–750. doi: 10.1002/1873-3468.12581.

McCoy, A. J. *et al.* (2007) 'Phaser crystallographic software', *Journal of Applied Crystallography*. International Union of Crystallography, 40(4), pp. 658–674. doi: 10.1107/S0021889807021206.

McIver, L. *et al.* (1998) 'Characterisation of flavodoxin NADP+ oxidoreductase and flavodoxin; key components of electron transfer in Escherichia coli', *European Journal of Biochemistry*. Blackwell Publishing Ltd., 257(3), pp. 577–585. doi: 10.1046/j.1432-1327.1998.2570577.x.

McKNIGHT, J. *et al.* (1993) 'Identification of charge-transfer transitions in the optical spectrum of low-spin ferric cytochrome P-450 Bacillus megaterium', *European Journal of Biochemistry*. Eur J Biochem, 213(2), pp. 683–687. doi: 10.1111/j.1432-1033.1993.tb17808.x.

McLean, K. J. *et al.* (2002) 'Expression, purification and spectroscopic characterization of the cytochrome P450 CYP121 from Mycobacterium tuberculosis', *Journal of Inorganic Biochemistry*. J Inorg Biochem, 91(4), pp. 527–541. doi: 10.1016/S0162-0134(02)00479-8.

McLean, K. J. *et al.* (2005) 'Biodiversity of cytochrome P450 redox systems', in *Biochemical Society Transactions*, pp. 796–801. doi: 10.1042/BST0330796.

McLean, K. J. *et al.* (2006) 'Biophysical characterization of the sterol demethylase P450 from Mycobacterium tuberculosis, its cognate ferredoxin, and their interactions', *Biochemistry*. Biochemistry, 45(27), pp. 8427–8443. doi: 10.1021/bi0601609.

McLean, K. J. *et al.* (2015) 'Biological diversity of cytochrome P450 redox partner systems', *Advances in Experimental Medicine and Biology*, 851, pp. 299–317. doi: 10.1007/978-3-319-16009-2_11.

Miles, J. S. *et al.* (1992) 'Domains of the catalytically self-sufficient cytochrome p-450 BM-3. Genetic construction, overexpression, purification and spectroscopic characterization', *Biochemical Journal*. Biochem J, 288(2), pp. 503–509. doi: 10.1042/bj2880503.

Monk, B. C. *et al.* (2014) 'Architecture of a single membrane spanning cytochrome P450 suggests constraints that orient the catalytic domain relative to a bilayer', *Proceedings of the National Academy of Sciences of the United States of America*. National Academy of Sciences, 111(10),

pp. 3865–3870. doi: 10.1073/pnas.1324245111.

Munro, A. W. *et al.* (2002) 'P450 BM3: The very model of a modern flavocytochrome', *Trends in Biochemical Sciences*, pp. 250–257. doi: 10.1016/S0968-0004(02)02086-8.

Munro, A. W. *et al.* (2013) 'What makes a P450 tick?', *Trends in Biochemical Sciences*, 38(3), pp. 140–150. doi: 10.1016/j.tibs.2012.11.006.

Munro, A. W. *et al.* (2018) 'Structure and function of the cytochrome P450 peroxygenase enzymes', *Biochemical Society Transactions*. Portland Press Ltd, pp. 183–196. doi: 10.1042/BST20170218.

Munro, A. W., Girvan, H. M. and McLean, K. J. (2007) 'Variations on a (t)heme--novel mechanisms, redox partners and catalytic functions in the cytochrome P450 superfamily.', *Natural product reports*, 24(3), pp. 585–609. doi: 10.1039/b604190f.

Murugan, R. and Mazumdar, S. (2005) 'Structure and Redox Properties of the Haem Centre in the C357M Mutant of Cytochrome P450cam', *ChemBioChem*. John Wiley & Sons, Ltd, 6(7), pp. 1204–1211. doi: 10.1002/cbic.200400399.

Omura, T. and Sato, R. (1962) 'A new cytochrome in liver microsomes.', *The Journal of biological chemistry*, 237, pp. 1375–1376. Available at: http://www.ncbi.nlm.nih.gov/pubmed/14482007 (Accessed: 27 November 2016).

Perera, R. *et al.* (2003) 'Neutral thiol as a proximal ligand to ferrous heme iron: Implications for heme proteins that lose cysteine thiolate ligation on reduction', *Proceedings of the National Academy of Sciences of the United States of America*. National Academy of Sciences, 100(7), pp. 3641–3646. doi: 10.1073/pnas.0737142100.

Pickl, M. *et al.* (2019) 'Mechanistic Studies of Fatty Acid Activation by CYP152 Peroxygenases Reveal Unexpected Desaturase Activity', *ACS Catalysis*. American Chemical Society, 9(1), pp. 565–577. doi: 10.1021/acscatal.8b03733.

Pluschke, G. and Overath, P. (1981) 'Function of phospholipids in Escherichia coli. Influence of changes in polar head group composition on the lipid phase transition and characterization of a mutant containing only saturated phospholipid acyl chains', *Journal of Biological Chemistry*, 256(7), pp. 3207–3212. doi: 10.1016/s0021-9258(19)69590-6.

Podust, L. M. *et al.* (2001) 'Substrate recognition sites in 14α-sterol demethylase from comparative analysis of amino acid sequences and X-ray structure of Mycobacterium tuberculosis CYP51', *Journal of Inorganic Biochemistry*. Elsevier, 87(4), pp. 227–235. doi:

10.1016/S0162-0134(01)00388-9.

Poulos, T. L., Finzel, B. C. and Howard, A. J. (1987) 'High-resolution crystal structure of cytochrome P450cam', *Journal of Molecular Biology*, 195(3), pp. 687–700. doi: 10.1016/0022-2836(87)90190-2.

Presnell, S. R. and Cohen, F. E. (1989) 'Topological distribution of four-alpha-helix bundles.', *Proceedings of the National Academy of Sciences of the United States of America*. Proc Natl Acad Sci U S A, 86(17), pp. 6592–6596. doi: 10.1073/pnas.86.17.6592.

Prinz, H. (2010) 'Hill coefficients, dose–response curves and allosteric mechanisms', *Journal of Chemical Biology*. Springer, 3(1), p. 37. doi: 10.1007/S12154-009-0029-3.

Qiu, Y. *et al.* (2012) 'An insect-specific P450 oxidative decarbonylase for cuticular hydrocarbon biosynthesis', *Proceedings of the National Academy of Sciences of the United States of America*. Proc Natl Acad Sci U S A, 109(37), pp. 14858–14863. doi: 10.1073/pnas.1208650109.

Raag, R. *et al.* (1991) 'Crystal Structure of the Cytochrome P-450CAM Active Site Mutant Thr252Ala', *Biochemistry*. American Chemical Society, 30(48), pp. 11420–11429. doi: 10.1021/bi00112a008.

Reinhard, F. G. C. *et al.* (2020) 'Bioengineering of Cytochrome P450 OleTJE: How Does Substrate Positioning Affect the Product Distributions?', *Molecules (Basel, Switzerland)*. NLM (Medline), 25(11). doi: 10.3390/molecules25112675.

Rittle, J. and Green, M. T. (2010) 'Cytochrome P450 compound I: Capture, characterization, and C-H bond activation kinetics', *Science*, 330(6006), pp. 933–937. doi: 10.1126/science.1193478.

Rude, M. A. *et al.* (2011) 'Terminal olefin (1-alkene) biosynthesis by a novel P450 fatty acid decarboxylase from Jeotgalicoccus species', *Applied and Environmental Microbiology*. American Society for Microbiology, 77(5), pp. 1718–1727. doi: 10.1128/AEM.02580-10.

Sabbadin, F. *et al.* (2009) 'The 1.5-Å structure of XplA-heme, an unusual cytochrome P450 heme domain that catalyzes reductive biotransformation of royal demolition explosive', *Journal of Biological Chemistry*. American Society for Biochemistry and Molecular Biology, 284(41), pp. 28467–28475. doi: 10.1074/jbc.M109.031559.

Sahin, E. and Roberts, C. J. (2012) 'Size-exclusion chromatography with multi-angle light scattering for elucidating protein aggregation mechanisms', *Methods in Molecular Biology*, 899, pp. 403–423. doi: 10.1007/978-1-61779-921-1_25.

Sayer, P., Gouterman, M. and Connell, C. R. (1982) 'Metalloid Porphyrins and Phthalocyanines', *Accounts of Chemical Research*, 15(3), pp. 73–79. doi: 10.1021/ar00075a002.

Schirmer, A. *et al.* (2010) 'Microbial biosynthesis of alkanes', *ScienceSchirmer, A. et al. (2010) 'Microbial biosynthesis of alkanes', Science, 329(5991), pp. 559–562. doi: 10.1126/science.1187936.*, 329(5991), pp. 559–562. doi: 10.1126/science.1187936.

Schlichting, I. *et al.* (2000) 'The catalytic pathway of cytochrome P450cam at atomic resolution', *Science*. American Association for the Advancement of Science, 287(5458), pp. 1615–1622. doi: 10.1126/science.287.5458.1615.

Schrödinger, L. (2015) 'The PyMOL Molecular Graphics System, Version 2.4.0a0'. Available at: https://www.schrodinger.com/products/pymol (Accessed: 14 March 2021).

Shaw, M. K. and Ingraham, J. L. (1965) 'Fatty Acid Composition of Escherichia coli as a Possible Controlling Factor of the Minimal Growth Temperature', *Journal of Bacteriology*, 90(1), pp. 141–146. doi: 10.1128/jb.90.1.141-146.1965.

Shimada, H. *et al.* (1991) 'The Role of Threonine 252 in the Oxygen Activation by Cytochrome P-450 cam: Mechanistic Studies by Site-directed Mutagenesis', *Studies in Surface Science and Catalysis*. Elsevier, 66(C), pp. 313–319. doi: 10.1016/S0167-2991(08)62847-5.

Shoji, O. and Watanabe, Y. (2014) 'Peroxygenase reactions catalyzed by cytochromes P450', *Journal of Biological Inorganic Chemistry*. Springer Verlag, pp. 529–539. doi: 10.1007/s00775-014-1106-9.

Singh, M. K. *et al.* (2017) 'Role of an N-terminal extension in stability and catalytic activity of a hyperthermostable α/β hydrolase fold esterase', *Protein Engineering, Design and Selection*. Oxford University Press, 30(8), pp. 559–570. doi: 10.1093/protein/gzx049.

Sligar, S. G. and Gunsalus, I. C. (1976) 'A thermodynamic model of regulation: modulation of redox equilibria in camphor monoxygenase', *Proceedings of the National Academy of Sciences of the United States of America*. National Academy of Sciences, 73(4), pp. 1078–1082. doi: 10.1073/pnas.73.4.1078.

Somvanshi, P. R. and Venkatesh, K. V. (2013) 'Hill Equation', in *Encyclopedia of Systems Biology*. Springer New York, pp. 892–895. doi: 10.1007/978-1-4419-9863-7_946.

'The CCP4 suite: Programs for protein crystallography' (1994) *Acta Crystallographica Section D: Biological Crystallography*. Acta Crystallogr D Biol Crystallogr, 50(5), pp. 760–763. doi: 10.1107/S0907444994003112.

Tyson, C. A., Lipscomb, J. D. and Gunsalus, I. C. (1972) 'The role of putidaredoxin and P450 cam in methylene hydroxylation.', *Journal of Biological Chemistry*, 247(18), pp. 5777–5784. doi: 10.1016/s0021-9258(19)44826-6.

Vagin, A. A. *et al.* (2004) 'REFMAC5 dictionary: Organization of prior chemical knowledge and guidelines for its use', *Acta Crystallographica Section D: Biological Crystallography*. International Union of Crystallography, 60(12 I), pp. 2184–2195. doi: 10.1107/S0907444904023510.

Wang, C. and Wamser, C. C. (2014) 'Hyperporphyrin effects in the spectroscopy of protonated porphyrins with 4-aminophenyl and 4-pyridyl meso substituents', *Journal of Physical Chemistry A*. American Chemical Society, 118(20), pp. 3605–3615. doi: 10.1021/jp501398g.

Wang, S. *et al.* (2020) 'Directed evolution of a hydroxylase into a decarboxylase for synthesis of 1‑alkenes from fatty acids', *ACS Catalysis*. American Chemical Society, 10(24), pp. 14375–14379. doi: 10.1021/acscatal.0c04345.

Wang, Z. J. *et al.* (2014) 'Improved Cyclopropanation Activity of Histidine-Ligated Cytochrome P450 Enables the Enantioselective Formal Synthesis of Levomilnacipran', *Angewandte Chemie International Edition*. Wiley-VCH Verlag, 53(26), pp. 6810–6813. doi: 10.1002/anie.201402809.

von der Weid, I. *et al.* (2007) 'Identification and biodegradation potential of a novel strain of Dietzia cinnamea isolated from a petroleum-contaminated tropical soil', *Systematic and Applied Microbiology*. Elsevier GmbH, 30(4), pp. 331–339. doi: 10.1016/j.syapm.2006.11.001.

Wilson, G. S., Tsibris, J. C. M. and Gunsalus, I. C. (1973) 'Electrochemical studies of putidaredoxin and its selenium analog', *Journal of Biological Chemistry*. Elsevier, 248(17), pp. 6059–6061. doi: 10.1016/s0021-9258(19)43508-4.

Wise, C. E. *et al.* (2018) 'Dioxygen Activation by the Biofuel-Generating Cytochrome P450 OleT', *ACS Catalysis*. American Chemical Society, 8(10), pp. 9342–9352. doi: 10.1021/acscatal.8b02631.

Xu, H. *et al.* (2017) 'In vitro oxidative decarboxylation of free fatty acids to terminal alkenes by two new P450 peroxygenases', *Biotechnology for Biofuels*. BioMed Central Ltd., 10(1), p. 208. doi: 10.1186/s13068-017-0894-x.

Yassin, A. F., Hupfer, H. and Schaal, K. P. (2006) 'Dietzia cinnamea sp. nov., a novel species isolated from a perianal swab of a patient with a bone marrow transplant', *International Journal of Systematic and Evolutionary Microbiology*, 56(3), pp. 641–645. doi: 10.1099/ijs.0.63863-0.